IUTAM

Theoretical and Numerical Developments in Cellular Mechanobiology

PROGRAMME

Sevilla, 3-5 June 2024


Theoretical and Numerical Developments
in Cellular Mechanobiology

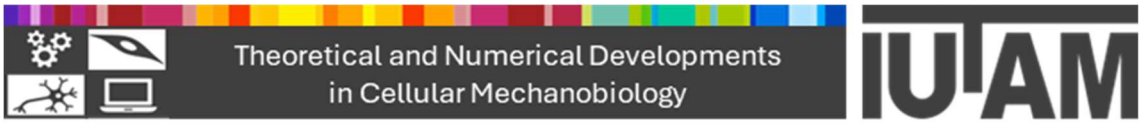

SYMPOSIUM PROGRAMME

Theoretical and Numerical Developments in Cellular Mechanobiology

Seville, June 3-5, 2024

VII Plan Propio de Investigación y Transferencia.
Vicerrectorado de Investigación, Universidad de Sevilla

CONTENTS

WELCOME MESSAGE

Dear Colleagues,

Welcome to Seville to the "Theoretical and numerical developments in cellular mechanobiology" symposium, an international scientific meeting supported by IUTAM and organized by the University of Seville (Spain). During three days, world-renowned experts will review state-of-the-art theoretical and numerical methods as well as experimental methods in cellular mechanobiology. The event will be an excellent opportunity for researchers to discuss open problems and questions in mechanobiology, to share novel methods, findings and views, and to create synergies between theory, computations and experiments. We strongly believe that such synergies are needed to advance our understanding on fundamental mechanobiological mechanisms that govern cell and tissue behaviour in health and disease.

We wish you an enriching and pleasant stay in Seville.

On behalf of the Organizing Committee

José A. Sanz-Herrera.
University of Seville, Seville, Spain.

Hans Van Oosterwyck
KU Leuven, Leuven, Belgium

SYMPOSIUM ORGANIZATION

Organizer:

José A. Sanz-Herrera	University of Seville (Spain)

Co-organizer:

Hans Van Oosterwyck	KU Leuven (Belgium)

International Organizing Committee

Aurélie Carlier	University of Maastricht (Netherlands)
Ben Fabry	University of Erlangen-Nuremberg (Germany)
Roger Kamm	MIT (USA)
Gijsje Koenderink	TU Delft (Netherlands)
Corey Neu	University of Colorado Boulder (USA)
José A. Sanz-Herrera	University of Seville (Spain)
Hans Van Oosterwyck	KU Leuven (Belgium)

Local Organizing Committee

Alejandro Apolinar Fernández
Jorge Barrasa Fano
Pablo Blázquez Carmona
Ana Carrasco Mantis
Jaime Domínguez Abascal
Juan Mora Macías
Elías Núñez Ortega
Esther Reina Romo
Fernando Rubio Iglesias
Raquel Ruiz-Mateos Brea
José Antonio Sanz Herrera
Juan José Toscano Angulo

Symposium secretariat: iutam24@us.es

INFORMATION

The scientific part of the symposium will take place in the 2nd floor of the venue. Both keynote and short oral presentations will be held in the main room *(Salon de Grados)*. Poster sessions will be available in the room *Sala Juan Larrañeta*.

Coffee breaks will be served in the 2nd floor of the venue, either in the main corridor or the terrace. On the other hand, lunches will be placed in the ground floor of the venue.

There will be a Welcome Reception social event on Monday at 19h. It will be served in the terrace (2nd floor of the venue).

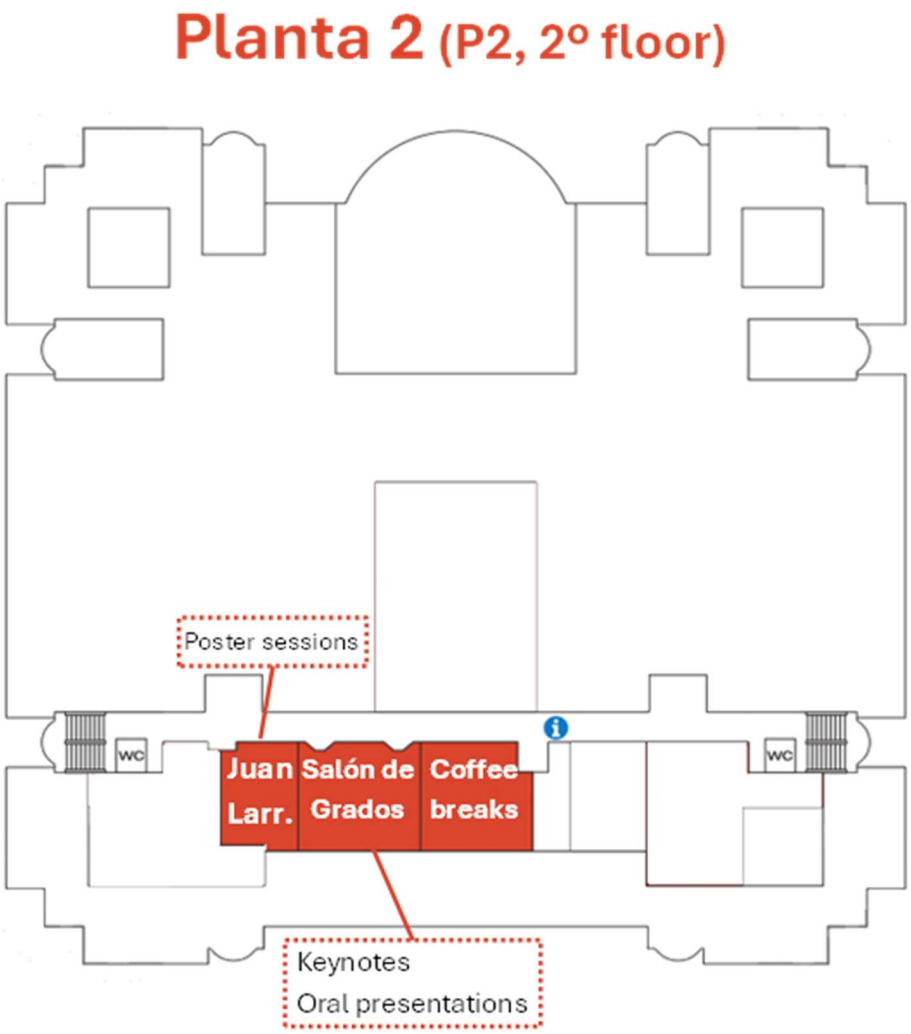

GALA DINNER

Date: Tuesday, June 4th, from 9 to 11:30 p.m.

Venue: Abades Triana Restaurante, C. Betis, 69, 41010 Seville.




In the Sevillian district of Triana, in the presence of the Guadalquivir River, the Torre del Oro and the Triana Bridge, is located the Abades Triana restaurant, a unique place that allows you to enjoy an unparalleled culinary experience. The Andalusian cuisine presented here combines traditional flavors with innovative touches, creating dishes that surprise and delight diners. With the Sevillian sunset and a beautiful panoramic view of the city, it is the perfect place to savor the culinary richness of Andalusia in a unique and memorable atmosphere.

WIFI CONNECTION

1. Search for the network with SSID “reinus-web” and connect to it.

2. Once the connection is active, the following webpage will appear when first trying to navigate the internet:

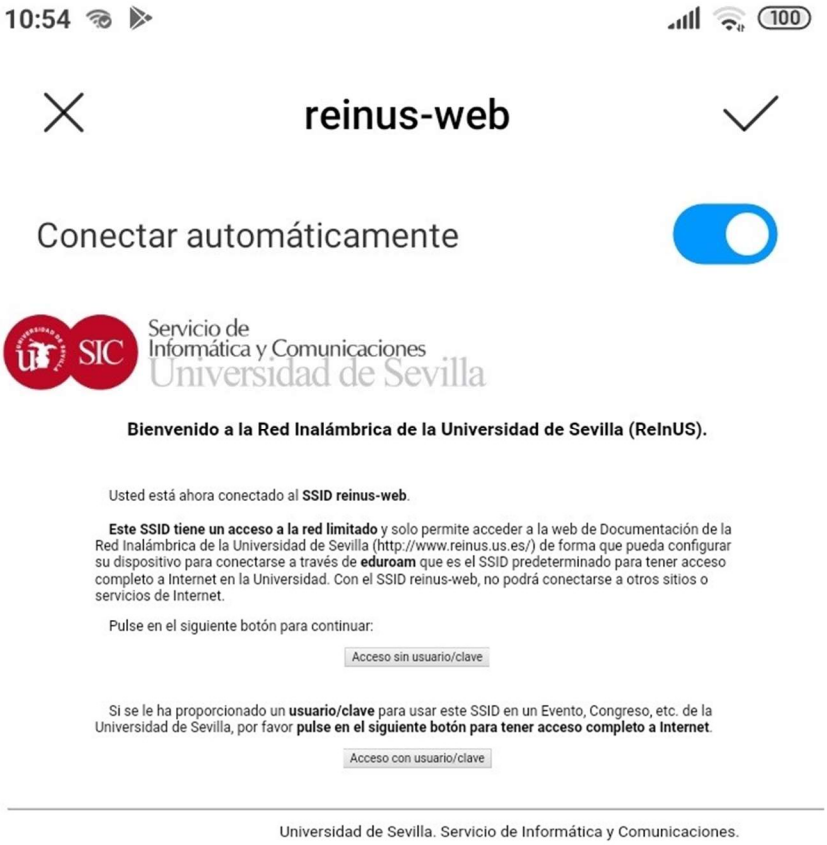

3. In this webpage, select the second option *“Acceso con usuario/clave”*, and the following window will appear:

4. Introduce the following data, taking into account that the data entry form is case sensitive:

   - **Usuario (User):** Eventos_IUTAM_SYM
   - **Clave (Password):** NUMERICAL.2024

5. Once entered the identification data, the following window indicating the successful log in will appear and you will be able to navigate the internet normally:

PROGRAMME AT A GLANCE

	Monday 03/06	Tuesday 04/06	Wednesday 05/06	
09:00 - 09:25	REGISTRATION	KS 9 DISCHER	KS 17 GOMEZ	09:00 - 09:40
09:25 - 09:40	OPENING			
09:40 -10:20	KS 1 CAMBI	KS 10 SHENOY	KS 18 FISCHER-FRIEDRICH	09:40 -10:20
10:20 -11:00	KS 2 SCHWARZ	KS 11 CHARRAS	KS 19 GENIN	10:20 -11:00
11:00 -11:30	COFFEE & POSTER SESSION	COFFEE & POSTER SESSION	COFFEE & POSTER SESSION	11:00 -11:30
11:30 - 12:10	KS 3 SANZ-HERRERA	KS 12 CYRON	KS 20 ARROYO	11:30 - 12:10
12:10 - 12:20	OP 1 - MIETKE	OP 13 - BORGIANI	KS 21 SMEETS	12:10 - 12:50
12:20 - 12:30	OP 2 - GIANNOPOULOS	OP 14 - PEÑA		
12:30 - 12:40	OP 3 - BLAWZDZIEWICZ	OP 15 - AYENSA JIMENEZ		
12:40 - 12:50	OP 4 - SANCHEZ RENDON	OP 16 - MAES		
12:50 - 13:00	OP 5 - POZZI	OP 17 - SARRATE	OP 24 - SARAVANAN	12:50 - 13:00
13:00 - 13:10	OP 6 - UCLA	OP 18 - FAMAEY	OP 25 - HUNDSDORFER	13:00 - 13:10
13:10 - 13:20	OP 7 - SUH	OP 19 - KULKARNI	OP 26 - ABDEL-RAOUF	13:10 - 13:20
13:20 - 13:30	OP 8 - BAGRIANTSEV	OP 20 - VILLETE	CLOSURE	13:20 - 13:30
13:30 - 14:30	LUNCH & POSTER SESSION	LUNCH & POSTER SESSION	LUNCH & POSTER SESSION	13:30 - 14:30
14:30 - 15:10	KS 4 VAN OOSTERWYCK	KS 13 CHAUDHURI	14:30 - 15:10	
15:10 - 15:50	KS 5 NEU	KS 14 FABRY	15:10 - 15:50	
15:50 - 16:30	KS 6 AVRIL	KS 15 LOERAKKER	15:50 - 16:30	
16:30 -17:00	COFFEE & POSTER SESSION	COFFEE & POSTER SESSION	16:30 -17:00	
17:00 - 17:40	KS 7 DING	KS 16 MONEGO	17:00 - 17:40	
17:40 - 18:20	KS 8 McGARRY	OP 21 - TRAVASSO	17:40 - 17:50	
		OP 22 - CARLIN	17:50 - 18:00	
		OP 23 - MUKHERJEE	18:00 - 18:10	
18:20 - 18:30	OP 9 - MUÑOZ			
18:30 - 18:40	OP 10 - MUENKEL			
18:40 - 18:50	OP 11 - ARROYO VAZQUEZ			
18:50 - 19:00	OP 12 - TSINGOS			
19:00 - 20:00	WELCOME COCKTAIL			
21:00 - 23:30		GALA DINNER		

PROGRAMME OVERVIEW

Monday 03/06. Session 1 9:40-11:00

(Chairman: Ovijit Chaudhuri)

KS-1. Alessandra Cambi, Radboud University (The Netherlands). *Mechanobiology of immune cells: how stiffness and geometry of the extracellular environment influence myeloid cell properties.*

KS-2. Ulrich Schwarz, Heidelberg University (Germany). *Controlling cell contraction by optogenetics.*

Coffee	**-**	***2nd Floor***
Poster session	**-**	***Sala (Room) Juan Larrañeta***

Monday 03/06. Session 2 11:30-13:30

(Chairman: Stéphane Avril)

KS-3. José A. Sanz-Herrera, University of Seville (Spain). *Monitoring the mechanical activity of cancer cells under normal, hypoxic and chemotherapeutic conditions.*

OP-1. Alexander Mietke, Rui Ma. *Emergent Morphologies of Active Surfaces*.

OP-2. Dimosthenis Giannopoulos, Maja Schlittler, Marzia De Bortoli, Raffaele Coppini, Mina Petrovic, Elisabetta Cerbai, Gerhard Schütz, Philipp J. Thurner, Alessandra Rossini, Orestis G. Andriotis. *Micromechanics of cardiac* spheroids.

OP-3. Redowan A. Niloy, Guo–Jie J. Gao, Michael C. Holcomb, Jeffrey H. Thomas, **Jerzy Blawzdziewicz**. *The role of tensile stress in the initiation and coordination of cephalic furrow formation in the drosophila embryo*.

OP-4. Julio César Sánchez-Rendón, Annalena Reuss, Effie E. Bastounis. *Apical shear stress impacts cell dynamics, kinematics and transcriptomic profile of three different endothelial cell types*.

OP-5. Giulia Pozzi, Pasquale Ciarletta. *Geometric control by active mechanics of epithelial gap closure*.

OP-6. Pierre Ucla, Xingming Ju, Joanne Le Chesnais, Henri Ver Hulst, Ludovic Leconte, Jean Salamero, Catherine Monnot, Hélène Moreau, Jessem Landoulsi, Vincent Semetey, Sylvie Coscoy. *Photopolymerization of 3D fiber networks to study the dynamics of cell-matrix interaction*.

OP-7. Young Joon Suh, Mrinal Pandey, Alan T Li, Bangguo Zhu, Chung-Yuen Hui, Jeffrey E Segall, Mingming Wu. *Tumor spheroid mechanics and invasion revealed by a microfluidic rheometer*.

OP-8. Slav N. Bagriantsev, Elena O. Gracheva. *3D architecture and mechanism of touch detection by mechanosensory corpuscles*.

Lunch	**-**	***Ground Floor***
Poster session	**-**	***Sala (Room) Juan Larrañeta***

Monday 03/06. Session 3 14:30-16:30

(Chairman: Christian Cyron)

KS-4. Hans Van Oosterwyck, KU Leuven (Belgium). *Measuring cellular forces in 3D and application to microvascular disease.*

KS-5. Corey Neu, University of Colorado Boulder (USA). *Inverse modeling to map heterogeneous properties of the cell nucleus.*

KS-6. Stéphane Avril, Ecole des Mines de Saint-Etienne (France). *Bridging the gap between mechanobiology of aortic smooth muscle cells and biomechanics of aortic aneurysms.*

Coffee	**->**	***2nd Floor***
Poster session	**->**	***Sala (Room) Juan Larrañeta***

Monday 03/06. Session 4 17:00-19:00

(Chairman: Slav Bagriantsev)

KS-7. Xiaoyun Ding, University of Colorado Boulder (USA). *High throughput mechanical disruption of plasma membrane and nuclear envelope for repair dynamics study.*

KS-8. Patrick McGarry, NUI Galway (Ireland). *Active contractility and remodelling of stress fibres and sarcomeres.*

OP-9. Jose Muñoz, Shafaq Zahra, Andrea Malandrino. *Inference of cytoskeletal contractility from TFM data*.

OP-10. Marie Muenkel, Erva Keskin, Aylin Balmes, Tilman Schäffer, Marco Lebtig, Dorothee Kretschmer, Kathryn Wright, Serge Mostowy, Effie Bastounis. *Biomechanical alterations of endothelial cells exposed to bacterially-infected immune cells.*

OP-11. Raquel B. Arroyo Vázquez, Marina Pérez-Aliacar, Jacobo Ayensa-Jiménez, Manuel Doblaré. *Simulation of glioblastoma evolution in microfluidic devices with an agent-based model*.

OP-12. Saber Shakibi, **Erika Tsingos**. *Modeling the Impact of Cell-Matrix Mechanics on Migratory Heterogeneity in Cancer Metastasis*.

Welcome Reception	**->**	***2nd Floor***

Tuesday 04/06. Session 1 09:00-11:00

(Chairman: Hans Van Oosterwyck)

KS-9. Dennis Discher, University of Pennsylvania (USA). *Pan-tissue scaling of mechanoregulated genes and heritable genetic changes in cancer.*

KS-10. Vivek Shenoy, University of Pennsylvania (USA). *How do forces from the cell's environment affect DNA organization?*

KS-11. Guillaume Charras, University College London (UK). *The rupture strength of living cell sheets.*

Coffee	**->**	***2nd Floor***
Poster session	**->**	***Sala (Room) Juan Larrañeta***

Tuesday 04/06. Session 2 11:30-13:30

(Chairman: Héctor Gómez)

KS-12. Christian J. Cyron, TU Hamburg (Germany). *What mechanical quantity do cells regulate in soft tissues?*

OP-13. Edoardo Borgiani, Gabriele Nasello, Liesbet Geris. *A novel in silico approach to investigate mechano-regulation of macrophages during bone fracture inflammatory stage.*

OP-14. Ricardo Caballero, Miguel A. Martínez, **Estefanía Peña**. *Hybrid approach for in-silico modelling of atherosclerosis: combining continuous and agent-based methods.*

OP-15. Marina Pérez-Aliacar, **Jacobo Ayensa-Jiménez**, Manuel Doblaré. *A continuum mathematical framework for modelling cellular adaptation and phenotypic plasticity in glioblastoma*.

OP-16. Lauranne Maes, Thibault Vervenne, Amber Hendrickx, Ana C. Estrada, Lucas Van Hoof, Peter Verbrugghe, Filip Rega, Elizabeth A.V. Jones, Jay D. Humphrey, Nele Famaey. *A computational study of pharmacological treatment after the ross procedure*.

OP-17. J. Sarrate, E. Sala–Lardies, M. Pérez–Aliacar, J. Ayensa–Jiménez, M. Doblaré. *Efficient numerical solution of a model for the evolution of glioblastoma cells*.

OP-18. Maïté Marie Pétré, Greet Kerckhofs, Lauranne Maes, **Nele Famaey**. *Meso-scale modelling of the arterial vessel wall*.

OP-19. Shardool Kulkarni, Pablo Saez. *Competing signaling pathways control electrotaxis*.

OP-20. Claire C. Villette, Liesbet Geris. *Modelling the influence of mechanical loading on the development of bone metastases using a hybrid cellular automaton*.

Lunch	**->**	***Ground Floor***
Poster session	**->**	***Sala (Room) Juan Larrañeta***

Tuesday 04/06. Session 3: 14:30-16:30

(Chairwoman: Elisabeth Fischer-Friedrich)

KS-13. Ovijit Chaudhuri, Stanford (USA). *Cell migration and morphogenesis in viscoelastic matrices*

KS-14. Ben Fabry, Univ Erlangen-Nuremberg (Germany). *High-throughput measurements of viscoelastic cell properties: Potential and limitations.*

KS-15. Sandra Loerakker, TU Eindhoven (The Netherlands). *Computational models to understand and advance the regeneration of engineered cardiovascular tissues.*

Coffee	**-**	***2nd Floor***
Poster session	**-**	***Sala (Room) Juan Larrañeta***

Tuesday 04/06. Session 4 17:00-18:10

(Chairman: Ben Fabry)

KS-16. Debora Monego, Uni-Heidelberg (Germany). *Exploring the evolutionary mechanisms of collagen as a protein Material.*

OP-21. Rui DM Travasso, Soraia Melo, Pilar Guerrero, Maurício Moreira-Soares, José Rafael Bordin, Fátima Carneiro, João Carvalho, Joana Figueiredo, Raquel Seruca. *The ECM and tissue architecture are major determinants of early invasion mediated by e-cadherin dysfunction*.

OP-22. Gildas Carlin, Ian Manifacier, Jean-Louis Milan. *Persistent random walk model of cell migration over curved surface.*

OP-23. Satanik Mukherjee, Raphaelle Lesage, Laurens Spoelstra, Thanh Le, Carolina Serrano Larrea, Carlo Alberto Paggi, Jorge Barrasa Fano, Hans van Oosterwyck, Marcel Karperien, Liesbet Geris. *A combinatorial in silico and in vitro approach to study cartilage mechanobiology using a cartilage-on-chip setup*.

Gala Dinner -> Abades Triana. C/ Betis 69

Wednesday 05/06. Session 1 09:00-11:00

(Chairman: Vivek Shenoy)

KS-17. Héctor Gómez, Purdue University (USA). *Computational modeling of collective chemotaxis*.
KS-18. Elisabeth Fischer-Friedrich, TU Dresden (Germany). *Twofold mechanosensitivity ensures actin cortex reinforcement upon peaks in mechanical tension*.
KS-19. Guy M. Genin. Washington University (USA). *Recursive Cell-Matrix Feedback in Fibroblasts*.

Coffee	**-**	***2nd Floor***
Poster session	**-**	***Sala (Room) Juan Larrañeta***

Wednesday 05/06. Session 2 11:30-13:30

(Chairwoman: Sandra Loerakker)

KS-20. Marino Arroyo, UPC (Spain). *Collective invasion in strain-stiffening matrices by durolysis*.

KS-21. Bart Smeets, KU Leuven (Belgium). *Computational modeling of active foam dynamics in 3D tissues*.

OP-24. Yogesh Saravanan, Sudiksha Mishra, Ramray Bhat, Claire Valotteau, Felix Rico. *A semi automatised pipeline to measure the nano mechanics of complex samples*.

OP-25. Lara Hundsdorfer, David Jaworski, Marie Muenkel, Julio César Sánchez Rendón, Iordania Constantinou, Effie Bastounis. *A live-cell imaging-compatible strteching device to study the influence of biomechanics on the interaction between bacterial pathogens and epithelia*.

OP-26. Yousof MA Abdel-Raouf, Lauranne Maes, Mathias Peirlinck, Nele Famaey, Patrick Sips, Julie De Backer, Jonathan Weissmann, Jay D Humphrey, Patrick Segers. *Mechanisms of maladaptation and the constrained mixture model*.

Lunch	**->**	***Ground Floor***
Poster session	**->**	***Sala (Room) Juan Larrañeta***

Poster Sessions

P-1. Alejandro Apolinar-Fernández, Pablo Blázquez-Carmona, Raquel Ruíz-Mateos Brea, Jorge Barrasa-Fano, Hans Van Oosterwyck, Esther Reina-Romo, José Antonio Sanz-Herrera. *Inverse traction reconstruction in 3D TFM: regularized and non-regularized methods*.

P-2. Amlan Barai, Matis Soleilhac, Wang Xi, Shao-Zen Lin, Marc Karnat, Elsa Bazellières, Sylvie Richelme, Manuel Théry, Jean-François Rupprecht, Delphine Delacour. *The emergence of "actin stars" for epithelium coordination and tissue patterning*.

P-3. Jorge Barrasa-Fano, Alejandro Apolinar-Fernández, Laurens Kimps, Iain Muntz, Gijsje Koenderink, José Antonio Sanz-Herrera, Hans Van Oosterwyck. *Novel data-driven method to measure cell forces in fibrillar hydrogels*.

P-4. Chandini Bhaskar Naidu, Bruno Goud, Stéphanie Miserey, Jean-Baptiste Manneville. *Mechanotransduction at the golgi apparatus*.

P-5. Pablo Blázquez-Carmona, Fernando Rubio-Iglesias, Elisa Bevilacqua, Israel Valverde, Gorka Gómez-Ciriza, Ignacio González-Loscertales, Tarik Smani, Antonio Ordoñez, Esther Reina-Romo. *Mechanical evaluation of 3d-printed vascular patches for congenital heart treatments*.

P-6. Ana Carrasco Mantis, Esther Reina-Romo, José Antonio Sanz-Herrera. *An in silico study of a flow-enhanced vascularized organoid*.

P-7. Lucie Jadrrna, Jaromir Gumulec, Jiri Bursa. *Role of cytoskeleton in cancer cells under a variety of mechanical stimuli: a computational study*.

P-8. Erva Keskin, Mai Wang, Effie Bastounis. *Apically applied fluid shear stresses are vasoprotective, decreasing the susceptibility of endothelial cells to infection with Listeria monocytogenes*.

P-9. Alice Perucca, Andrea Gómez Llonin, Oriol Mañe Benach, Clement Hallopeau, Elisa I. Rivas, Jenniffer Linares, Marta Garrido, Anna Sallent-Aragay, Tom Golde, Julien Colombelli, Elena Dalaka, Judith Linacero, Marina Cazorla, Teresa Galan, Jordi Pastor Viel, Xavier Badenas, Alba Recort-Bascuas, Laura Comerma, Pere Roca-Cusachs, Joan Albanell, Xavier Trepat, Alexandre Calon, **Anna Labernadie**. *Micro immune response on-chip (MIRO) model to study the spatial repartition of Immune cells in Tumor driven by Stromal Mechanosensing*.

P-10. Lucía López-de Abajo, Luis Saucedo-Mora, Francisco J. Montáns, José Mª Benítez. *Influence of some genotypic parameters on the formation of necrotic cores in glioblastoma multiforme*.

P-11. Audrey Ntadambanya, Julien Pernier, Violaine David, Kimihiro Susumu, Igor L. Medintz, Mayeul Collot, A. Klymchenko, I. Le Potier, Niko Hildebrandt, Christophe Le Clainche, Marcelina Cardoso Dos Santos. *Quantum-dot based nanosensors to study focal adhesion assembly and mechanosensing*.

P-12. Jyotsana Priyadarshani, Apeksha Shapeti, Jorge Barrasa Fano, Eva Faurobert, Hans Van Oosterwyck. *Engineering ccm-associated mechanics on a microfluidic chip*.

P-13. Raquel Ruiz-Mateos, Pablo Blázquez-Carmona, Jorge Barrasa-Fano, Apeksha Shapeti, José Enrique Martín-Alfonso, Jaime Domínguez, Hans Van Oosterwyck, Esther

Reina-Romo, José Antonio Sanz-Herrera. *Hydrogels with tuneable collagen density regulate breast cancer cell mechanical activity.*

P-14. **Beatrice Senigagliesi**, Nassim Haffiane, Julien Sage, Pierre Nassoy, Rémi Galland, Grégory Giannone. *Role of cell adhesion and cytoskeleton structures in three dimensional aggregates of small cell lung cancer cells*.

P-15. **Apeksha Shapeti**, Jorge Barrasa-Fano, Abdel Rahman Abdel Fattah, Janne de Jong, José Antonio Sanz-Herrera, Mylène Pezet, Said Assou, Emilie de Vet, Seyed Ali Elahi, Adrian Ranga, Eva Faurobert, Hans Van Oosterwyck. *Force-mediated angiogenesis – a mechanism for vascular lesion growth*.

P-16. **Juan José Toscano-Angulo**, Juan Mora-Macías, Pablo Blázquez-Carmona, Juan Morgaz, Rocío Navarrete-Calvo, Jaime Domínguez, Esther Reina-Romo. *BMD evolution during bone regeneration in osteoporotic bone*.

P-17. **Nele Vaes**, Maxim Vovchenko, Rocío Castro Viñuelas, Jorge Barrasa-Fano, Apeksha Shapeti, Ilse Jonkers, Hans Van Oosterwyck. *Unraveling the mechanisms of traction force generation by chondrocytes and the effect of osteoarthritis*.

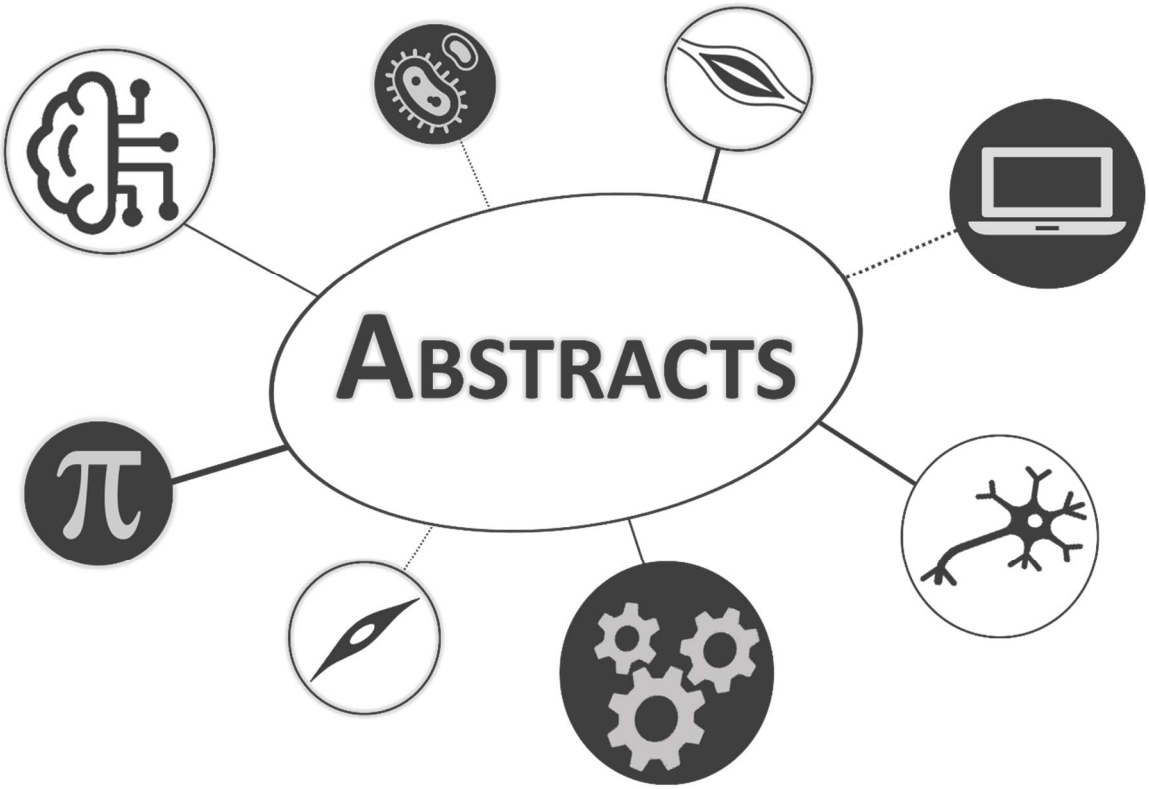

(by alphabetical order by name as shown in the programme)

Mechanisms of Maladaptation and the Constrained Mixture Model

Yousof MA Abdel-Raouf[1], Lauranne Maes[2], Mathias Peirlinck[3], Nele Famaey[2], Patrick Sips[4], Julie De Backer[4,5], Jonathan Weissmann[6], Jay D Humphrey[6,7], Patrick Segers[1*]

1. IBiTech-BioMMedA, UGent, Belgium; 2. BMe, KU Leuven, Belgium; 3. BMechE, TU Delft, Netherlands; 4. CMGG, UGent, Belgium; 5. Department of Cardiology, UZ Gent, Belgium; 6. Department of Biomedical Engineering, Yale University, USA; 7. Vascular Biology and Therapeutics Program, Yale School of Medicine, USA

INTRODUCTION

The extracellular matrix (ECM) provides vital support to soft tissues, influencing their mechanical properties and aiding in cell signalling. Advances in microscopy allow closer scrutiny of the ECM in elastic arteries, particularly the remodelling activities of stress-sensing smooth muscle cells (SMCs) in the arterial media. Aligned within elastin lamellae, SMCs exhibit differential glycosaminoglycan (GAG) deposition, causing Donnan Swelling in response to mechanical cues [1]. Since SMCs also grow in number as a response to stress changes in their environment, these two adaptive mechanisms can have an effect on their immediate ECM integrity [2]. In advanced aging models, SMCs in Hutchinson-Guilford Progeria mice undergo phenotypic changes into "myochondrocytic" cells, producing excessive GAGs due to elastin degeneration, triggering a positive feedback loop of GAG production and ECM damage [3][4]. Recognizing the importance of the correlation between elastin damage, GAG deposition, and aortic dilatation, we aim to mathematically describe these relationships. Building upon previous work by Roccabianca et al. [5] on swollen arteries, our study utilizes this framework to simulate the behaviour of arteries experiencing elastin damage and Donnan Swelling. We observe the model's behaviour in the context of elastin integrity loss, attempting to characterize the accompanying swelling. Acknowledging suggestions that interlamellar distance and medial thickness are somewhat preserved with elastin damage and dilatation [6], we incorporate these factors into our model to maintain radially sensed stresses by SMCs. Stress-driven growth of SMCs is implemented, as well as compensatory swelling to maintain interlamellar distance (represented in our model as medial thickness).

MATERIALS AND METHODS

Identical to [5], the framework of the constrained mixture model is used to describe the constitutive behaviour of four constituents in the bilayered modelled arteries (namely elastin, collagen. SMCs and GAGs). The cylindrically shaped layers are an inner layer (comprising approximately 38% of the total thickness) representing the media, and an outer one representing the adventitia. Relevant to our investigation in this article is a configuration that deviates from homeostatically hydrated (swollen) homeostatic conditions $(\kappa_h{}^*)$ conditions previously reported in [5]. The configuration (κ_γ^*) corresponds to the carotid artery dimensions at an elevated internal pressure but with a compromised elastin integrity, that we implement by multiplying the elastin mass fraction in the media (φ^e) by a gain parameter representing stress-driven, time evolving damage (γ) bounded between 0% and 100%. Evolution of elastin is shown in Eq. (1a) while damage is shown in Eq. (1b).

$$\varphi^e = (1-\gamma) * \varphi^e{}_{max}\,; \tag{1a}$$

$$\dot{\gamma} = k_{gamma} * \Delta\sigma * \gamma * (1-\gamma)\,; \tag{1b}$$

$$\dot{\varphi^{smc}} = k_{smc} * \Delta\sigma * \varphi^{smc} - k_{transition} * f(\varphi^{smc}, \varphi^{chondro}, \gamma)\,; \tag{1c}$$

$$\dot{\varphi^{chondro}} = k_{transition} * f(\varphi^{smc}, \varphi^{chondro}, \gamma) - k_{anoikis} * g(\varphi^{chondro}); \tag{1d}$$

where the gain parameters k_{gamma}, k_{smc}, $k_{transition}$, and $k_{anoikis}$ represent susceptibility to damage due to stress, cell-growth rate due to stress, likelihood to modulate due to damage and likelihood to enter cell-death protocol due to anoikis, respectively. We model the effect of anoikis here since cells that sustain excessive damage to their environments often enter programmed cell death. The stress stimulus ($\Delta\sigma$) is calculated in the SMC constituent as $\Delta\sigma = (\sigma - \sigma_{homeo})/\sigma_{homeo}$. Finally, φ^e, φ^{smc}, and $\varphi^{chondro}$ represent elastin, SMC and mycochondrocyte mass fractions. It is important to note that the latter is not added to the constrained mixture as an elastic load-bearing constituent, and the mass evolution plays no role in stress or energy storage. The change in stress due to elevated pressure drives both the elastin damage, and SMC production, as well as SMC modulation, and as elastin degrades, the artery must dilate to accommodate the homeostatic load, leading to a decrease in the interlamellar distance which is then reestablished with compensatory swelling.

* Corresponding author. Email: **Patrick.segers@ugent.be**

RESULTS & DISCUSSION

The model presents a versatile tool to explore different scenarios, and replicates results that satisfy trends in those scenarios. Some of such studies are shown here, but most interestingly, we find that the scenario in which we apply an elevated pressure of 120 mmHg, the initial values of damage (of 0.1%) does not cause maladaptation and excessive dilatation (Fig.1 solid blue). Higher initial values (0.5%, 1%) do trigger maladaptation and damage (Fig1. solid red, solid green). That is to say, patients with prolonged hypertensive pressure, who may also have more elastin damage due to ageing or connective tissue disease, are more susceptible to enter this maladaptive regime where aneurysmal dilatation takes place. It is interesting to note that at that aneurysmal equilibrium, the model also shows key hallmarks such as loss of total energy due to damage (and total stiffness), as well as an average elevated number of SMCs and GAGs [7]. While there is an evident loss in elastic energy, the total circumferential stress is lower in cases where we assumed compensatory swelling compared to cases where we forgo this constraint [5]. The parameter of susceptibility also shows that low values of initial damage will always trigger high elastin damage and maladaptation at elevated pressures (Fig 1. Dashed Lines). Additionally, we find that collagen compromise that replicates lost mechanostrasduction and disrupted x-linking of newly turned-over collagen does show a loss in the adventitial rescue [3][8]. This also increases susceptibility to dilatation and damage, and can be interpreted in the understanding that collagen in the adventitia (which otherwise bears most of the load at elevated pressure, can no longer store enough energy when compromised, and the compensatory swelling and SMC recruitment must then bear the load.

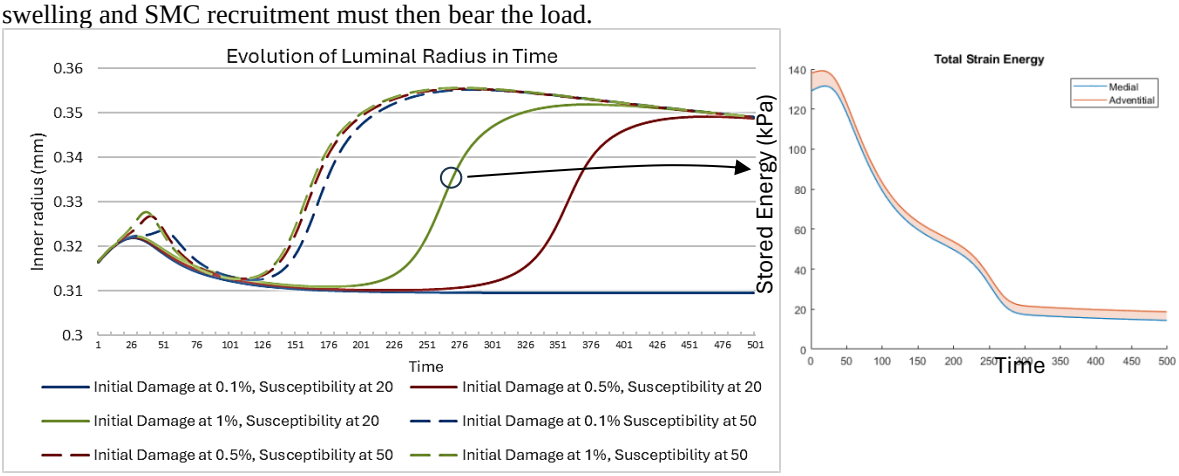

Figure 1 Evolution of Artery radius predicted by our maladaptaion model. Right panel demonstrates energy loss in media (blue) and adventitia (red) from approximately 120 kPa to 20 kPa during maladaptation

CONCLUSIONS

We presented here a model that employs the constrained mixture theory, as well as growth laws that can then replicate different profiles of aneurysmal arteries, satisfying trends seen in patients or animal models of disease. It becomes clear that our model takes into account the sustained temporal effect of the presence of damage, excess stress and compromised constituents, and the prolonged co-incidence of these confounding factors leads to excessive aneurysmal dilatation and phenotype. It is therefore reassuring that this approach to expanding on existing well-established research in arterial modelling can offer additional versatility when integrating phenotypic behaviour and modelling acute disease on one hand, or minor deviation from homeostasis on another.

ACKNOWLEDGEMENTS

This research was funded by the **Concerted Action Program** of Ghent University Special Research Fund (GOA019-21BOF). We would also like to thank Dr. Sara Roccabianca for sharing relevant material with us.

References

[1] Glagov S. Morphology of collagen and elastin fibers in atherosclerotic lesions. Adv Exp Med Biol. 1977;82:767-73. doi: 10.1007/978-1-4613-4220-5_154. PMID: 920431.

[2] Humphrey, J., Dufresne, E. & Schwartz, M. Mechanotransduction and extracellular matrix homeostasis. Nat Rev Mol Cell Biol 15, 802–812 (2014). https://doi.org/10.1038/nrm3896Seifried, R.; Schiehlen, W.: *Computational Analysis and Experimental Investigations of Impacts in Multibody Systems.* In P. Eberhard (Ed.) IUTAM Symposium on Multiscale Problems in Multibody System Contacts, pp. 269-280, Springer 2007.

[3] Weiss, D., et al. "Biomechanical consequences of compromised elastic fiber integrity and matrix cross-linking on abdominal aortic aneurysmal enlargement." Acta Biomaterialia, vol. 134, Oct. 2021, pp. 422–434, https://doi.org/10.1016/j.actbio.2021.07.059.

[4] Kawamura, Y., et al. "Adventitial remodeling protects against aortic rupture following late smooth muscle-specific disruption of TGFB signaling." Journal of the Mechanical Behavior of Biomedical Materials, vol. 116, Apr. 2021, p. 104264, https://doi.org/10.1016/j.jmbbm.2020.104264.

[5] Roccabianca S., Bellini C. and Humphrey J. D. 2014 Computational modelling suggests good, bad and ugly roles of glycosaminoglycans in arterial wall mechanics and mechanobiology J. R. Soc. Interface.11201403972014039 7

[6] Yousef, S., Matsumoto, N., Dabe, I. et al. Quantitative not qualitative histology differentiates aneurysmal from nondilated ascending aortas and reveals a net gain of medial components. Sci Rep 11, 13185 (2021). https://doi.org/10.1038/s41598-021-92659-1

[7] Cavinato, Cristina, et al. "Evolving structure-function relations during aortic maturation and aging revealed by Multiphoton Microscopy." Mechanisms of Ageing and Development, vol. 196, June 2021, p. 111471, https://doi.org/10.1016/j.mad.2021.111471.

[8] Li David S., Cavinato Cristina, Latorre Marcos and Humphrey Jay D. 2023Computational modelling distinguishes diverse contributors to aneurysmal progression in the Marfan aorta Proc. R. Soc. A.4792023011620230116

INVERSE TRACTION RECONSTRUCTION IN 3DTFM: REGULARIZED AND NON-REGULARIZED METHODS

Alejandro Apolinar-Fernández[1,2,*],Pablo Blázquez-Carmona[1,2], Raquel Ruiz-Mateos Brea[1,2], Jorge Barrasa-Fano[3], Hans Van Oosterwyck[3,4], Esther Reina-Romo[1,2], José Antonio Sanz-Herrera[1,2]

1. Escuela Técnica Superior de Ingeniería, Universidad de Sevilla, Spain; 2. Instituto de Biomedicina de Sevilla (IBIS), Spain; 3. Biomechanics section, Department of Mechanical Engineering, KU Leuven, Belgium 4. Prometheus division of Skeletal Tissue Engineering, KU Leuven, Belgium

INTRODUCTION

3D Traction Force Microscopy (3DTFM) epitomizes an advanced approach that successfully integrates experimental and computational frameworks with the aim of studying the tractions exerted by cells during their interactions with the extracellular matrix (ECM). Through sophisticated microscopic image acquisition protocols, displacements induced by cellular activity in a collagen hydrogel that mimics the ECM's features are captured. The computational part of 3DTFM is performed mainly through two distinct approaches: the forward and inverse methods for traction reconstruction. The forward method entails little computational complexity since measured displacement data are introduced directly into the constitutive law describing the hydrogel behaviour for the computation of tractions. However, numerical differentiation of noisy measurements of the displacement field involves the presence of considerable errors on the results, rendering its efficacy rather limited. The inverse method is formulated around the concept of finding new displacements that, while fulfilling a certain condition, remain as similar as possible to the measured ones. In general, inverse methods provide considerably better traction reconstructions than the forward method, and thus research about different variations of the inverse method and their performance is justified. Implementations of these methodologies are diverse, spanning from moderate to highly complex computational schemes. Each approach comes with its own set of advantages and disadvantages, and careful consideration of the expected result accuracy and computational efficiency is needed. The aim of this work is to establish a comparison between a constrained inverse method (constrained optimization) without regularization developed by the authors and the standard unconstrained regularized formulation of the inverse problem (zero-order Tikhonov regularization) that reveals which methodology yields better traction reconstructions, while at the same time taking into account time of execution and complexity of implementation.

MATERIALS AND METHODS

There is a great variety of inverse method formulations. Particularly, when dealing with 3D nonlinear scenarios, the solution to the inverse problem will require the inversion of the matrix associated to the corresponding system of equations. The noise present in the measured displacements will be amplified by said inversion and the results will contain inacceptable errors. To circumvent this problem, zero-order Tikhonov regularization is often employed for inverse traction reconstruction, as it penalizes high norm values of the computed tractions, acting as a low-pass filter on the input displacements. The authors in [2] and [3] present mathematical frameworks for solving the constrained inverse problem with Tikhonov regularization, both formulated in the context of the Finite Element Method. Previously, we designed a constrained inverse method called Physics-Based Nonlinear Inverse Method (PBNIM) [1], which enforces the nullity of nodal forces at nodes interior to the hydrogel via the weak form of the Principle of Virtual Work. This method does not include regularization. In this study, we distiguish between two unconstrained regularized scenarios: only nodes at cell surface are regularized (Unconstrained 1 method, UC1), and all nodes in the problem domain are regularized (Unconstrained 2 method, UC2). The general method formulation for a regularized constrained case is the following,

$$\min_{\mathbf{u}} \left(\frac{1}{2} ||\mathbf{u} - \mathbf{u}^*||_2^2 + \frac{\alpha}{2} \left[\int_\Gamma ||\mathcal{T}_t \cdot \mathbf{t}||_2^2 \, ds + \int_\Omega ||\mathcal{T}_b \cdot \mathbf{b}||_2^2 \, dv \right] \right), \qquad \text{s.t.} \qquad \Theta = 0 \tag{1}$$

in which $\mathbf{u}$ and $\mathbf{u}^*$ correspond to the recovered and measured displacements, respectively; α is the regularization parameter, $\mathbf{t}$ denotes the surface forces acting on surface Γ, $\mathbf{b}$ are the body forces acting on the interior domain Ω and $\mathcal{T}_t$ and $\mathcal{T}_b$ are scalar weight fields. Θ represents the equilibrium condition equation, formulated in terms of the Principle of Virtual Work. In the case of PBNIM, $\alpha = 0$. For the unconstrained methods (UC1 and UC2), $\alpha \neq 0$ while $\Theta = 0$ is not enforced. In order to obtain the accuracy of traction reconstruction of each method, we define error metrics for both tractions and displacements in the following way,

$$T_{\text{e}}^{\text{method}} = 100 \cdot \frac{\|\mathbf{t}^{\text{method}} - \mathbf{t}^{\text{GT}}\|}{\|\mathbf{t}^{GT}\|} \qquad\qquad U_{\text{e}}^{\text{method}} = 100 \cdot \frac{\|\mathbf{u}^{\text{method}} - \mathbf{u}^{\text{GT}}\|}{\|\mathbf{u}^{GT}\|} \tag{2}$$

* Corresponding author. E-mail: apolinar@us.es

where $\mathbf{t}^{\text{method}}$ and $\mathbf{u}^{\text{method}}$ represent the arrays containing the list of components of the traction and displacement vectors associated respectively to the boundary nodes of the cell and all nodes of the domain for a certain method solution, and $\mathbf{t}^{GT}$ and $\mathbf{u}^{GT}$ are defined analogously for the ground truth solution.

RESULTS

We performed 3DTFM simulations using synthetic displacement data generated from a ground truch reference case built from the morphology of an actual cell studied in the laboratory. Noise is added to the ground truth displacements to produce the displacement input data that would correspond to in vivo measured displacements. Three levels of noise are considered: low (0.0625%), medium (1.25%) and high (1.875%). Figure 1 shows the traction magnitude field on the cell surface for each of the methods implemented in the study in the high noise case. Table 1 shows the values of the traction and displacement error metrics for the assessed methods for the three considered noise levels.

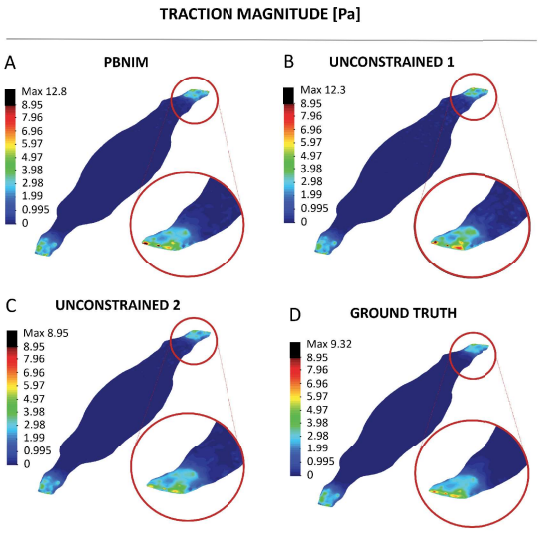

Figure 1. Traction fields recovered by each method showcased together with that of the ground truth scenario for the high noise case.

PBNIM

	α	T_e	U_e
Low noise	-	0.179	0.00432
Medium noise	-	0.242	0.00868
High noise	-	0.314	0.0130

Unconstrained 1

	α	T_e	U_e
Low noise	5e-5	0.202	0.00590
Medium noise	5e-5	0.282	0.0116
High noise	1e-5	0.413	0.0181

Unconstrained 2

	α	T_e	U_e
Low noise	1e-5	0.181	0.00518
Medium noise	5e-5	0.250	0.00879
High noise	5e-5	0.292	0.0130

Table 1. Values of the defined error metrics (tractions and displacements) for each method and for each noise level case.

DISCUSSION AND CONCLUSIONS

We find that both PBNIM and UC2 methods offer similar degrees of accuracy at the time of reconstructing the overall traction field on the cell surface, although UC2 gives a closer estimate of the maximum traction featured in the ground truth scenario. UC1 shows the worst performance of the three in every case. We also conclude that, in the case of unconstrained methods, applying regularization to all nodes in the cell and hydrogel domain (UC2) gives the best traction reconstruction while at the same time ensuring a good estimate of the maximum traction. Nonetheless, the consideration of regularization involves the calibration of the regularization parameter, which is done typically through ad-hoc procedures that are non-conclusive in terms of the optimality of the selected value. This can be a deciding factor at the time of selecting an inverse method, and in this particular case, the constrained non-regularized inverse method (PBNIM) is the most adequate if regularization parameter calibration is omitted, given that the estimated maximum tractions provide acceptable values with errors of the order of magnitude of the best inverse approach. The conclusions underline the importance on considering not only accuracy of traction recovery but complexity of computational implementation of each method.

ACKNOWLEDGEMENTS

A.A.-F. and J.A.S.-H. gratefully acknowledge the Financial support from project PID2021-126051OB-C42 by the Ministerio de Ciencia e Innovación (MCI), Agencia Estatal de Investigación (AEI) and Fondo Europeo de Desarrollo Regional (FEDER).

References

[1] Sanz-Herrera, J.A. et al.: *Inverse method based on 3D nonlinear physically constrained minimisation in the framework of traction force microscopy*. Soft Matter, 2021,17, 10210-10222.

[2] Dong, L., Oberai, A. A..: *Recovery of cellular traction in three-dimensional nonlinear hyperelastic matrices*. Computer Methods in Applied Mechanics and Engineering, 2017, Vol. 314, pp. 296-313.

[3] Michel, R. et al.: *Mathematical framework for Traction Force Microscopy*. ESAIM Proceedings, 2013.

SIMULATION OF GLIOBLASTOMA EVOLUTION IN MICROFLUIDIC DEVICES WITH AN AGENT-BASED MODEL

Raquel B. Arroyo-Vázquez[1*], Marina Pérez-Aliacar[1], Jacobo Ayensa-Jiménez[1,2], Manuel Doblaré[1,2,3]

1. Aragón Institute for Engineering Research (I3A), University of Zaragoza, Spain;
2. Institute for Health Research Aragón (IISAragón), Spain;
3. Nanjing Tech university, China

INTRODUCTION

Mathematical models and simulation are useful tools in cancer research since they allow to test biological hypotheses, propose new ones as well as optimize experimental protocols or design experimental campaigns. Overall, in combination with *in vivo* or *in vitro* experiments, they enable a greater understanding of this disease and help design new successful treatment strategies [1].

Among the wide variety of existent models, Agent-Based Models (ABMs) have gained attention in recent years, as they model directly at the cell scale and hence permit a straightforward comparison with the biological reality. Besides, they have other advantages such as the inherent inclusion of stochastic phenomena or the easy implementation of important cancer features such as angiogenesis or mechanical interactions between cells.

We present here an ABM of the evolution of glioblastoma (GBM), the most common and lethal brain tumour, and one of the cancers with worst prognosis, with a 5-year survival rate below 7% [2]. GBM is highly aggressive and invasive and it has been proved that the lack of oxygen or hypoxia is one of the causes of this behaviour. GBM cells exhibit a dual behaviour, known as go-or-grow, proliferating when the oxygen level is high and turning into a migratory phenotype when the oxygen level falls below a certain hypoxia threshold [3]. Hence, we focus on the interaction between GBM cells and the oxygen present in their microenvironment.

The main aim is to reproduce GBM evolution in hypoxic environments within microfluidic devices. These devices are 3D culture platforms able to recreate the gradients and structure of the *in vivo* tumour microenvironment, being nowadays the most biomimetic technique [4]. In particular, GBM culture in microfluidic devices has been able to reproduce the formation of necrotic cores (areas of dead cells caused by necrosis due to extreme lack of oxygen) and pseudopalisades (migrating cell waves towards more oxygenated areas), the main histopathological features of this tumour [5,6]. Moreover, microfluidic devices allow easy visualisation and tracking of cells, so they data for model calibration can be easily obtained.

With this purpose, we define a hybrid model, with an ABM for GBM cells, including their proliferation, migration, death, oxygen uptake and cell-cell interactions, and a continuum phase consisting on a partial differential equation for the evolution of the oxygen concentration. The model as well as the methodology followed to calibrate it is further detailed in the Materials and Methods section, followed by the first results and the main conclusions of the work.

MATERIALS AND METHODS

The model is developed using the open-source modelling framework PhysiCell, which incorporates a finite volume library, named BioFVM, for simulating the substances in the microenvironment [7]. The developed model considers two cell populations, alive and dead GBM cells together with oxygen concentration, the chemical species acting as moderator of the phenomena. The main hypotheses implemented to reproduce GBM behaviour are:

- Migration and proliferation depend on the oxygen concentration, following the go-or-grow paradigm.
- Migration and proliferation are also dependent on the availability of space and nutrients, that is, the phenomena cannot occur in saturated environments.
- Death comprises necrosis (due to lack of oxygen) and apoptosis (stochastic), so it depends also on the oxygen concentration. Dead cells cannot migrate, proliferate and do not consume oxygen.
- Oxygen consumption follows Michaelis-Menten kinetics.
- Cells undergo adhesion and repulsion forces in presence of other cells, due to cell's ligands interactions.

The parameter calibration process is typically complicated in ABMs, since they include a high number of parameters, requiring high amounts of time and computational resources. Besides, optimisation problems in large dimensional spaces yields slow convergence, with many local minima that can lead to incorrect outputs. To avoid these problems, we take advantage of a previously developed and calibrated continuum model for the evolution of GBM in microfluidic devices [8]. We define mathematical relationships between the parameters in the continuum model and the functions defining cell evolution in the ABM. This methodology avoids the parametric fitting in the space of the ABM parameters in a first step.

* Corresponding author. Email: **rbarroyo@unizar.es**

However, continuum mathematical models do not incorporate phenomena at the cellular scale such as cell-cell interactions. This phenomenon is included in a second step, and a fitting process can be carried out now to fit the newly defined parameters to the experimental data, having a space of reduced dimensionality since some parameters that have been previously fitted. In summary, this methodology allows to obtain a first model derived from a calibrated continuum model and then refine the model to incorporate aspects at the individual level.

RESULTS

The calibrated ABM model allows to accurately reproduce the experimental results obtained in the experiments. To capture the stochastic nature of the problem, present in both the initial cell configuration and the random nature of some phenomena, 30 replicates of each simulation are carried out, ensuring convergence of the solution, and the mean and confidence interval of the solution are computed. Figure 1 shows the formation of a necrotic core both *in vitro* in a microfluidic device and *in silico* with the proposed ABM. It can be seen that cells die in the central part of the chamber due to lack of oxygen, and the surviving ones migrate towards the lateral channels where there is oxygen enough to proliferate.

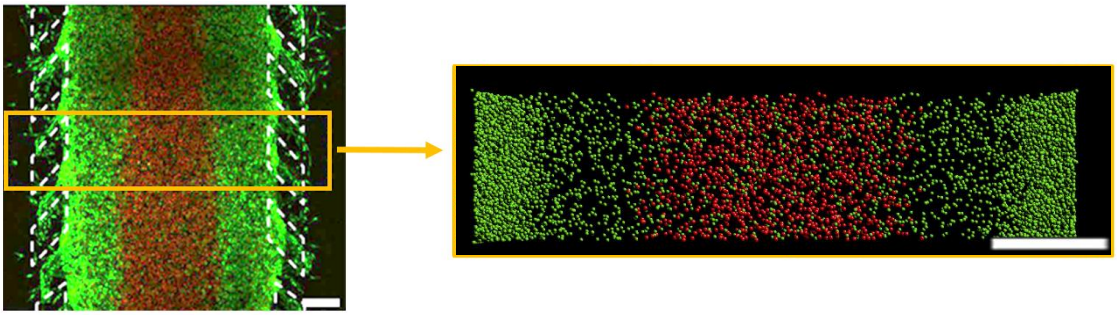

Figure 1. Necrotic core formation. The left figure, adapted from [5], shows a fluorescence image of a necrotic core within a microfluidic device (scale bar 400 µm), and the right figure shows the ABM simulation of cell evolution in the central part of the chamber (scale bar 400 µm). Alive cells are displayed in green and dead cells in red.

DISCUSSION AND CONCLUSIONS

In this work we have presented an ABM for the simulation of GBM evolution under hypoxic conditions in microfluidic devices. To avoid the cumbersome calibration process, characteristic of ABMs, we first obtained analytical expressions that relate the parameters of the ABM and a continuum model. Then, we extend the ABM to incorporate cell-cell interactions, which cannot be implemented in a straightforward manner in continuum models. The resulting ABM model is able to reproduce the experimental results as good as the continuum model, incorporating the inherent uncertainty of the predictions. Moreover, the derived relationships bridge the gap between continuum and discrete models, allowing an interplay where the former can be used for the initial fitting and/or for large scale simulations and the latter for detailed simulations of the evolution at the cellular scale.

ACKNOWLEDGEMENTS

The authors would like to thank the financial support from the **Spanish Ministry of Science and Innovation** (MICINN), the State Research Agency (AEI), and FEDER, UE through the GBM_IMMUNE project (PID2021-126051OB-C41:/AEI/10.13039/501100011033/FEDER, UE) and the FPI grant (PRE2022-102428).

References

[1] Bull, J.A., Byrne, H.M.: *The Hallmarks of Mathematical Oncology*. Proceedings of the IEEE Vol 110, pp. 523-540, 2022.

[2] Batash, R., Asna, N., Schaffer, P., Francis, N., Schaffer, M.: *Glioblastoma multiforme, diagnosis and treatment; recent literature review.* Current medicinal chemistry Vol 24, pp. 3002-3009, 2017.

[3] Hatzikirou, H., Basanta, D., Simon, M., Schaller, K., Deutsch, A.: *'Go or grow': the key to the emergence of invasion in tumour progression?.* Mathematical medicine and biology: a journal of the IMA Vol 29, pp. 49-65, 2012.

[4] Wlodkowic, D., Cooper, J. M.: *Tumors on chips: oncology meets microfluidics.* Current opinion in chemical biology Vol 14, pp. 556-567, 2010.

[5] Ayuso, J. M., Virumbrales-Muñoz, M., Lacueva, A., Lanuza, P. M., et al.: *Development and characterization of a microfluidic model of the tumour microenvironment.* Scientific reports Vol 6, pp. 36086, 2016.

[6] Ayuso, J. M., Monge, R., Martínez-González, A., Virumbrales-Muñoz, M., et al.: *Glioblastoma on a microfluidic chip: Generating pseudopalisades and enhancing aggressiveness through blood vessel obstruction events.* Neuro-oncology Vol , pp. 503-513, 2017.

[7] Ghaffarizadeh, A., Heiland, R., Friedman, S. H., Mumenthaler, S. M., Macklin, P.: *PhysiCell: An open source physics-based cell simulator for 3-D multicellular systems.* PLoS computational biology Vol 14, pp. 1005991, 2018.

[8] Ayensa-Jiménez, J., Pérez-Aliacar, M., Randelovic, T., Oliván, S., et al: *Mathematical formulation and parametric analysis of in vitro cell models in microfluidic devices: application to different stages of glioblastoma evolution.* Scientific Reports Vol 10, pp. 21193, 2020.

FROM MECHANOBIOLOGY OF AORTIC SMOOTH MUSCLE CELLS TO IMPROVED PROGNOSIS OF THORACIC AORTIC ANEURYSMS

Stéphane Avril

Sainbiose, Mines Saint-Etienne, INSERM, France

Abstract

The media of the aorta consists primarily of smooth muscle cells (SMCs) embedded in a highly structured matrix of collagen fibrils and elastin lamellae. Thanks to their phenotypic plasticity [1], SMCs normally maintain a certain mechanical homeostasis through variations of their active tone (contractile phenotype, short-term adaptation) and through synthesis and remodeling of the extracellular matrix (ECM) (synthetic phenotype, long-term adaptation). However, missensing of mechanical stimuli by SMCs (stress, strain, or stiffness) can alter the maintenance of mechanical homeostasis and induce impaired adaptations that are responsible for thoracic aortic aneurysm (TAA) [2]. Accordingly, there is a pressing need to investigate and model how SMC biomechanics participate in the development of TAAs.

Our recent contributions on this topic were both computational and experimental:

- using a finite-element model of growth and remodelling based on the constrained mixture theory, we showed that cell mechanosensitivity plays a critical role in TAA progression and remodelling [3].
- using traction force microscopy (TFM) on primary SMCs (Fig. 1), we recently found that SMCs of aneurysmal aortas apply larger traction forces than SMCs of healthy aortas [4]. We explained this result by the increased abundance of hypertrophic SMCs in aneurysmal aortas. Our experimental results also confirmed that SMCs modulate their traction forces according to the stiffness two regimes. We even found that SMCs apply optimal traction forces for a substrate stiffness of 12 kPa [5].

It is now unanimously acknowledged that before catastrophic events such as rupture or dissections, TAAs enter a vicious circle combining phenotypic modulation/loss of SMCs and compromised biomechanical properties of the wall. Improvements in clinical care and prognosis will require that we are able to couple cell models informed by our recent experimental results with tissue level models of arterial mechanobiology [6]. About mechanoregulation, the motor–clutch-based model [7] may be the way to put forward, as it can also relate stiffness increase of the aortic wall to the increase of aortic failure.

References

1. Lacolley et al, Cardiovasc. Res. 95(2), 194-204, 2012.
2. Humphrey et al, Circ. Res. 116(8), 1448-1461, 2015.
3. Mousavi et al, Comp. M. Prg. Biomed. 205, 106107, 2021.
4. Petit et al, Biomech. Model. Mechanobiol. 20(2), 717-731, 2021.
5. Petit et al, Mol. Cell. Biomech., 2019.
6. Irons and Humphrey, PLoS comp. biol. 16(8), e1008161, 2020.
7. Chan and Odde, Sci. 322(5908), 1687-1691, 2008.

A CONTINUUM MATHEMATICAL FRAMEWORK FOR MODELLING CELLULAR ADAPTATION AND PHENOTYPIC PLASTICITY IN GLIOBLASTOMA

Marina Pérez-Aliacar[1], Jacobo Ayensa-Jiménez[1,2*], Manuel Doblaré[1,2,3]

1. Aragon Institute for Engineering Research, Spain; 2. Institute for Health Research Aragón, Spain; 3. Nanjing Tech University, China

INTRODUCTION

Cells are in constant interaction with their environment and adapt their behavior in response to different stimuli and environmental conditions. This adaptation takes place through epigenetic changes (changes in gene expression that are not caused by alterations in the DNA sequence), giving rise to phenotypic plasticity. Phenotypic plasticity plays a fundamental role in the development and progression of cancer. Indeed, in 2022 it was included among the Hallmarks of Cancer [1].

One example of cancer in which phenotypic heterogeneity and plasticity is paramount is glioblastoma (GBM). GBM is the most common and lethal primary brain tumor, with a 5-year survival ratio of only 6.8% [2]. The main causes explaining this poor prognosis are its aggressiveness and its intrinsic resistance to treatment. Even though there is a standard treatment for GBM, consisting in maximal safe resection by surgery followed by radiotherapy with concomitant and adjuvant chemotherapy with temozolomide (TMZ), there have been no significant advances in the treatment or the survival rate of this tumour [3]. This is mainly due to the fact that GBM adaptation to hypoxia triggers the transition toward stem-like phenotypes, with enhanced aggressiveness, as well as to the tumor cellular adaptation to the treatment itself. Indeed, even if cells initially respond to TMZ, they eventually develop resistance and recurrence is almost inevitable. Therefore, when developing mathematical models for *in silico* cancer research, cellular adaptation is a key feature to take into account.

The aim of this work is to establish a mathematical framework to model and simulate the cells' phenotypic plasticity and epigenetic mechanisms, that can be used both to analyse GBM adaptation to hypoxia or TMZ resistance development. Even if some mathematical works have already study phenotypic plasticity using a multiphenotypic approach [4] or an epigenetic state coordinate [5], we propose a novel approach in which cell state is identified with an internal variable attached to each material point. This approach considers cell state as a continuum macroscopic representation of the epigenetic changes that a cell has undergone, allowing for an easy interpretation of the internal variables and to directly relate them to the environment and the functions governing cell behaviour.

The proposed framework allows both for the study of homogeneous scalar problems (such as spheroid cell cultures) and spatially dependent evolving fields. The former case is illustrated with the analysis of GBM spheroid growth and adaptation in response to TMZ and the latter with the study of GBM cell migration and proliferation enhancement in microfluidic platforms.

MATERIALS AND METHODS

Our approach considers a set of cell population variables $C_i,\ i = 1, \dots, n$, whose evolution is defined via a set of Ordinary Differential Equations (ODEs) or Partial Differential Equations (PDEs), involving also the effect some chemical moderation fields (such as TMZ or oxygen), represented by $S_j,\ j = 1, \dots, m$.

Homogeneous problems

For the spatially homogeneous problem, the cell evolution law is expressed in terms of the available microenvironment nutrient and chemical cues S_j, and also some extra scalar properties $V_k,\ k = 1, \dots r$, related to the cell internal state, whose evolution has also to be prescribed. Hence, the evolution equations can be expressed as:

$$\frac{\mathrm{d}C_i}{\mathrm{d}t} = F_i(\boldsymbol{C}, \boldsymbol{S}, \boldsymbol{V}), i = 1, \dots, n, \tag{1a}$$

$$\frac{\mathrm{d}S_j}{\mathrm{d}t} = G_j(\boldsymbol{C}, \boldsymbol{S}, \boldsymbol{V}), j = 1, \dots, m, \tag{1b}$$

$$\frac{\mathrm{d}V_k}{\mathrm{d}t} = H_k(\boldsymbol{C}, \boldsymbol{S}, \boldsymbol{V}), k = 1, \dots, r, \tag{1c}$$

where $\boldsymbol{C} = (C_1, \dots, C_n)$, $\boldsymbol{S} = (S_1, \dots, S_m)$ and $\boldsymbol{V} = (V_1, \dots, V_k)$ are the unknown fields of the problem that has to be determined by solving the system of ODEs. The explicit expression of the functions F, G and H is problem dependent and defines the system dynamics.

* Corresponding author. Email: **jacoboaj@unizar.es**

Spatial dependent fields

The framework is adapted to spatially dependent problems using standard transport equations, so that the equations of the problem are now:

$$\frac{\partial c_i}{\partial t} = \nabla \cdot \boldsymbol{U}_i + F_i(\boldsymbol{C}, \boldsymbol{S}, \boldsymbol{V}), i = 1, \dots, n, \tag{2a}$$

$$\frac{\partial s_j}{\partial t} = \nabla \cdot \boldsymbol{V}_j + G_j(\boldsymbol{C}, \boldsymbol{S}, \boldsymbol{V}), j = 1, \dots, m, \tag{2b}$$

$$\frac{\partial v_k}{\partial t} = \nabla \cdot \boldsymbol{W}_k + H_k(\boldsymbol{C}, \boldsymbol{S}, \boldsymbol{V}),\ k = 1, \dots, r, \tag{2c}$$

where $\boldsymbol{U}_i$ and $\boldsymbol{V}_j$ are the fluxes of cells and chemical species in the microenvironment and $\boldsymbol{W}_k$ is the flux associated with the internal variable V_k, which has to be considered as the state of each cell is a material property and, therefore, must be carried along with the cell flow. Although $\boldsymbol{U}_i$ and $\boldsymbol{V}_j$ are, as in the previous case context-dependent, $\boldsymbol{W}_k$ is directly inherited from $\boldsymbol{U}_i$ such that, if V_p is associated with cell phenotype C_q:

$$\frac{\mathrm{d}}{\mathrm{dt}} \int_{\delta \mathcal{V}} \boldsymbol{C_q}\, V_p \, \mathrm{d}V = R_{pq}, \tag{3}$$

being R_{pq} the p-stress state acquisition by the cell phenotype C_q in a reference volume $\delta \mathcal{V}$.

RESULTS

We particularize our framework to the two previously commented relevant cases: the study of GBM resistance to TMZ using spheroid cell cultures and the effect of hypoxia preconditioning in GBM aggressiveness. For the first study, we are able to recreate spheroid response to TMZ for two different cell populations (TMZ – resistant and TMZ – sensitive) of U-251 cell line, which have been subjected to two cycles of the clinical treatment pattern (Fig. 1). In the second study, we demonstrate that tumors whose phenotype is more sensitive to hypoxia, undergoing epigenetic changes, are more likely to survive under cyclic hypoxia conditions than those whose phenotype is insensitive to these changes (Table 1), when varying the oxygenation conditions of the tumors. That is, adaptation to hypoxia confers GBM tumors increased resilience.

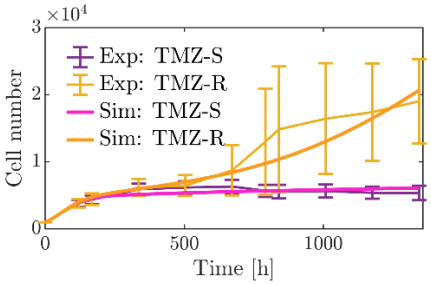

Figure 1. experimental vs. simulated results for TMZ-sensitive (TMZ-S) and TMZ-resistant (TMZ-R) spheroids.

Tumor	Remission	Shrinkage	Growth
Sensitive	9 %	12 %	79 %
Insensitive	14 %	7 %	79 %

Table 1. Summary of the tumor evolution under different scenarios involving hypoxic conditions.

DISCUSSION AND CONCLUSIONS

The computational studies carried out with the presented model are able to reproduce many biological features of epigenetic adaptation, particularly of GBM, such as the development of TMZ resistance or hypoxia-mediated GBM enhancement of aggressiveness. Even if the adoption of mathematical models for the study of epigenetics mechanism requires an extensive validation, especially if they are going to be used as pre-clinical decision making tools, they can be used for testing different biological mechanisms or hypotheses or for the design of revealing experiments. This, at the end of the day, is key for reducing time and resources in any pre-clinical platform.

ACKNOWLEDGEMENTS

The authors would like to thank the financial support from the **Spanish Ministry of Science and Innovation** (MICINN), the State Research Agency (AEI), and FEDER, UE through the GBM_IMMUNE project (PID2021-126051OB-C41:/AEI/10.13039/501100011033/FEDER, UE).

References

[1] Hanahan, D. *Hallmarks of cancer: new dimensions.* Cancer discovery, Vol 12(1), pp. 31-46, AACR 2021.

[2] Stanković, Tijana, et al. *In vitro biomimetic models for glioblastoma-a promising tool for drug response studies*. Drug Resistance Updates. Vol 55, p 100753, Elsevier 2021.

[3] McCutcheon, Ian E., and Mark C. Preul. *Historical perspective on surgery and survival with glioblastoma: how far have we come?* World neurosurgery, Vol 149, pp 148-168, Elsevier 2021.

[4] Greene, James M., et al. *Mathematical approach to differentiate spontaneous and induced evolution to drug resistance during cancer treatment.* JCO clinical cancer informatics, Vol 3 pp. 1 – 20, ASCO 2019.

[5] Hodgkinson, Arran, et al. *Spatio-Genetic and phenotypic modelling elucidates resistance and re-sensitisation to treatment in heterogeneous melanoma.* Journal of theoretical biology, Vol 466, pp. 84-105, Elsevier 2019.

3D ARCHITECTURE AND MECHANISM OF TOUCH DETECTION BY MECHANOSENSORY CORPUSCLES

Slav N. Bagriantsev[1,*], Elena O. Gracheva[1]

1. Department of Cellular & Molecular Physiology, Yale University, USA

INTRODUCTION

Meissner corpuscles are mechanosensory end-organs which detect transient touch and vibration in the skin of vertebrates, enabling precise sensation of the physical environment, handling objects and tools, foraging, and forming social bonds. In all studied organisms, including birds, rodents and primates, Meissner corpuscles are tuned to detect small, micrometer-deep indentations and low-frequency (30-100Hz) vibration. The sensory core of corpuscles is composed of a mechanoreceptor afferent surrounded by terminal Schwann cell-derived lamellar cells (LCs). Despite their fundamental importance for biology, the mechanism of touch detection in Meissner corpuscles remains poorly understood. The afferent is thought to be the sole touch-sensing element within corpuscles, whereas the role of LCs cells is obscure. Because detailed architecture of corpuscles is unknown, the role of the afferent and LCs in touch detection remains speculative in the absence of structural insight into the relationship between LC and sensory afferents.

MATERIALS AND METHODS

To understand the mechanoelectrical conversion events in the sensory core of Meissner, we used single-corpuscle *ex vivo* electrophysiology in the skin from tactile specialist duck (*Anas platyrhynchos*). To obtain 3D architecture of entire duck Meissner corpuscles, we used focused ion beam scanning electron microscopy (FIB-SEM) and machine learning based segmentation. We used transmission electron microscopy and electron tomography to obtain a high-resolution of a segment of LC-afferent contact in corpuscles. For detailed methods, see references [1-3].

RESULTS

We report the 3D architecture of Meissner corpuscle at acquired using FIB-SEM and machine learning based segmentation. The corpuscle comprises a stack of LCs interdigitated with terminal endings from two afferents (Figure 1). Transmission electron microscopy and electron tomography revealed that LCs form tethered connections with the afferent membrane and contain dense core vesicles which release their content onto the afferent [1]. Using a preparation of duck bill skin, we performed direct electrophysiological recordings from LC and terminal afferents of Meissner corpuscles. We show that mechanical stimulation evokes mechanically activated (MA) current in the afferent with fast kinetics of activation and inactivation during the ON and OFF dynamic phases of the mechanical stimulus [3]. These responses trigger Na^+ channel-dependent, rapidly adapting firing in the afferent detected at the terminal and in the afferent fiber outside of the corpuscle. Mechanical stimulation of LCs evokes MA current only during the ON phase of the stimulus, leading to a Ca^{2+}-dependent action potential firing [2]. Simultaneous electrophysiological recordings from the afferent and LC revealed that mechanosensitive LCs use Ca^{2+} influx to trigger action potentials in the afferent and thus serve as physiological touch sensors in the skin (Figure 2) [1].

DISCUSSION AND CONCLUSIONS

Our findings determine a high-resolution Meissner corpuscle structure and elucidate the initial electrogenic events in LCs and mechanoreceptor nerve terminal. These are, to our knowledge, the first direct electrophysiological recordings of mechanotransduction events at the physiological site of touch detection. Our findings that activation of a single LC is sufficient to induce action potential firing in the afferent provide support for a new model of touch detection in Meissner corpuscles. The elaborate architecture and bi-cellular sensory mechanism in the corpuscles, which comprises the afferents and LCs, create the capacity for more nuanced encoding of the submodalities of touch.

ACKNOWLEDGEMENTS

The authors would like to thank **National Science Foundation** (grants 1923127, 2114084) and **National Institutes of Health** (1R01NS097547, R01NS126277) for providing financial support to this project".

References

1. Nikolaev, Y.A., et al., *3D architecture and a bicellular mechanism of touch detection in mechanosensory corpuscle.* Science Advances, 2023. **9**(37): p. eadi4147.
2. Nikolaev, Y.A., et al., *Lamellar cells in Pacinian and Meissner corpuscles are touch sensors.* Sci Adv, 2020. **6**(51).
3. Ziolkowski, L.H., E.O. Gracheva, and S.N. Bagriantsev, *Mechanotransduction events at the physiological site of touch detection.* eLife, 2023. **12**: p. e84179.

* Corresponding author. Email: slav.bagriantsev@yale.edu

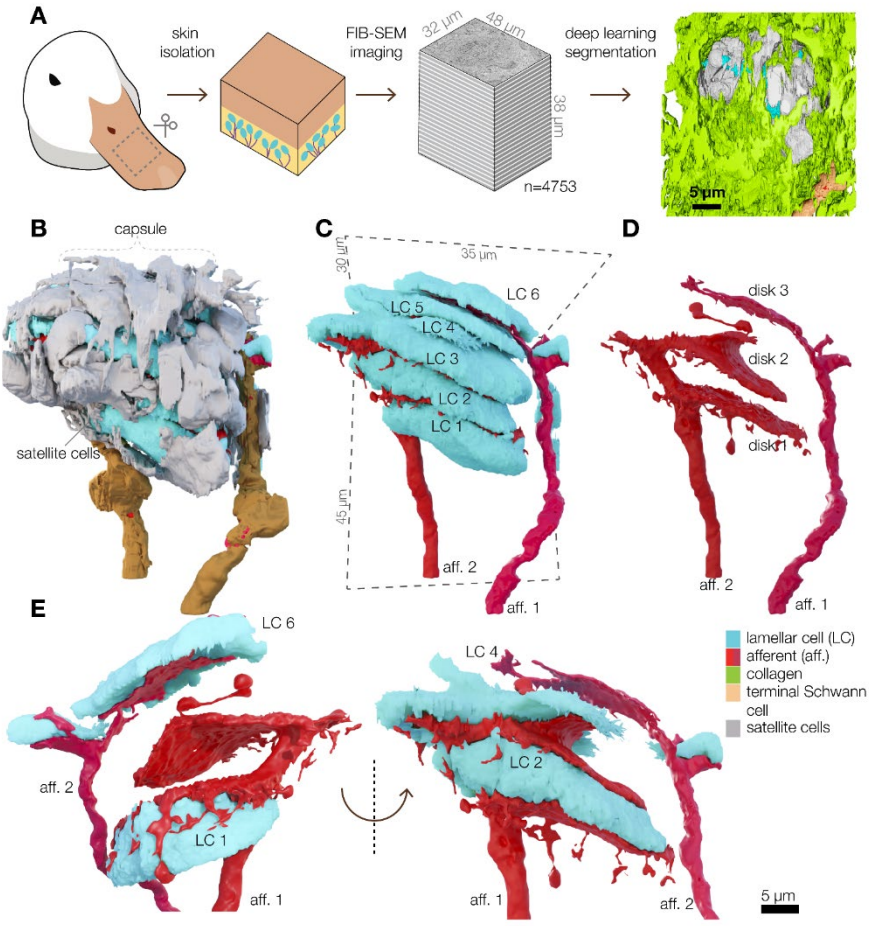

Figure 1. Meissner corpuscles comprise a stack of LCs interdigitated with terminal afferent disks. (A) FIB-SEM workflow for automated segmentation and machine learning-based 3D reconstruction of a Meissner corpuscle in duck bill skin. (B—D) 3D architecture of a Meissner corpuscle (B), corpuscle without outer capsule (C), isolated afferents (E). (E) 3D architecture of a section of afferent 1 and afferent 2 and associated LCs.

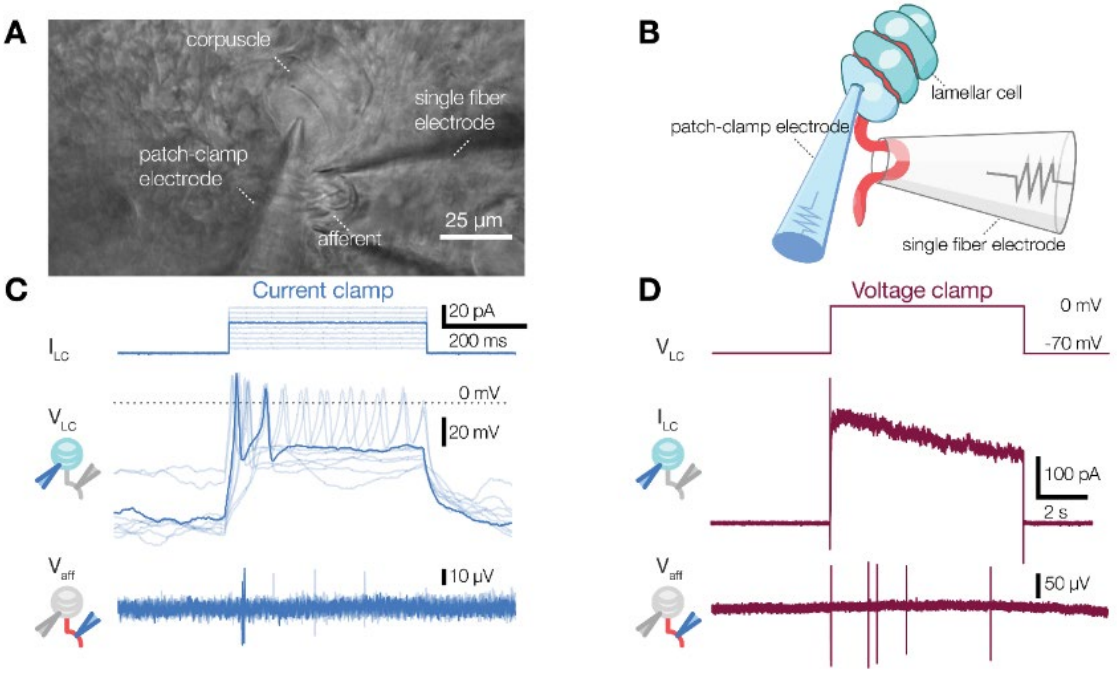

Figure 2. Activation of a single LC is sufficient to drive afferent firing via a Ca-dependent mechanism. (A) Bright-field image of the experimental setup. (B) Schematic representation of the experimental setup. (C) Current injection applied to the LC (ILC, top), voltage response and APs in the LC (VLC, middle), and extracellular voltage and APs in the afferent (Vaff, bottom). (D) Voltage step stimulus applied to the LC (VLC, top), current response with potassium-based internal in the LC (ILC, middle), and extracellular voltage and APs in the afferent (Vaff, bottom).

THE EMERGENCE OF "ACTIN STARS" FOR EPITHELIUM COORDINATION AND TISSUE PATTERNING

Amlan Barai[1,2,&], Matis Soleilhac[1,2,&], Wang Xi[2], Shao-Zen Lin[3], Marc Karnat[3], Elsa Bazellières[1], Sylvie Richelme[1], Manuel Théry[4], Jean-François Rupprecht[3], Delphine Delacour[1,*]

1. Aix Marseille Univ, CNRS, IBDM (UMR 7288), Turing Center for Living Systems, Marseille, France; 2. Univ. Paris Cité, CNRS, Institut Jacques Monod, F-75013 Paris, France; 3. Aix Marseille Univ, Université de Toulon, CNRS, CPT (UMR 7332), Turing Centre for Living systems, Marseille, France; 4. Univ. Paris, INSERM, CEA, UMRS1160, Institut de Recherche Saint Louis, CytoMorpho Lab, Hôpital Saint Louis, Paris, France

ABSTRACT

Faithful epithelial morphogenesis is crucial during development and tissue homeostasis. The dynamic intestinal epithelium is an appropriate model to study this field of research. Constant epithelium regeneration is one of the main characteristics of intestinal homeostasis mediated by finely controlled balance between intestinal stem cell proliferation and differentiation. Therefore, studying mechanisms controlling intestinal organization to understand tissue homeostasis and function is instrumental.

Recently, by using intestinal organoids as a working model, we have discovered a unique multicellular actin assembly specifically located in the basal domain of the columnar differentiated epithelium, and absent from the crypt domain. This network is characterized by 6-branched star-shaped actin clusters, thus termed "actin stars" (AcSs), with each AcS located at the centroid of the basal side of each epithelial cell. Each branch of the AcS orthoradially connects plasma membrane at cell-cell contacts and mirrors a corresponding branch from a neighboring cell. Importantly, we could confirm the presence of such actin structures in vivo, along villi in the mouse small intestine. Thus, the AcS network represents a large-scale interconnecting meshwork in the differentiated epithelial domain.

Collectively, the AcS network, because of its highly regular multicellular architecture, "crystallize" or freeze cell packing and lock epithelial order in the differentiated domain during intestinal morphogenesis. As a consequence, it likely limits changes in cell shape, intercalation, and migratory events. In addition, the existence of such a cytoskeletal scaffold in the differentiated domain could establish a physical barrier to prevent expansion of the proliferative compartment and ultimately control cryptogenesis.

We anticipate that our results will have a significant impact on understanding the role of AcSs in epithelial differentiation, tissue homeostasis in physiological and pathological conditions.

* Corresponding author. E-mail: delphine.delacour@univ-amu.fr

& Authors participated equivalently.

NOVEL DATA-DRIVEN METHOD TO MEASURE CELL FORCES IN FIBRILLAR HYDROGELS

Jorge Barrasa-Fano[1], Alejandro Apolinar-Fernández[2], Laurens Kimps[1], Iain Muntz[3], Gijsje Koenderink[3], José Antonio Sanz-Herrera[2], Hans Van Oosterwyck[1,4,*]

1. *Biomechanics Section, Dept. of Mechanical Engineering, KU Leuven, Belgium*
2. *Escuela Técnica Superior de Ingeniería, Univ. Sevilla, Spain*
3. *Dep. of Bionanoscience, Kavli Institute of Nanoscience Delft, TU Delft, The Netherlands*
4. *Prometheus division of Skeletal Tissue Engineering, KU Leuven, Belgium*

INTRODUCTION

Many diseases are intricately linked to the mechanical interactions between cells and the extracellular matrix (ECM) [1] or are directly influenced by them. Traction Force Microscopy (TFM) is a methodology for quantifying these interactions within in vitro cultures, often using collagen hydrogels to replicate the three-dimensional ECM environment. However, traditional 3D TFM methods treat the ECM as a homogeneous continuum, failing to capture local remodeling near cells and imposing limitations on force recovery resolution. In response, this work proposes a novel 3D data-driven TFM approach founded on a discrete fiber model, leveraging geometric insights extracted from microscopy images of the collagen network. Unlike conventional methodologies reliant on single constitutive models to describe ECM behavior, our approach matches the mechanical response of collagen hydrogels to the specific geometric features of the fiber network. Furthermore, we integrate this method with a previously developed nonlinear inverse TFM method, ensuring accurate computation of cellular forces[2,3].

MATERIALS AND METHODS

Development of an image-based collagen discrete fiber computational model. We have developed an image analysis routine that automatically segments collagen fibers from second harmonic generation (SHG) images of real collagen hydrogels. This segmentations allow us to translate from image voxels to coordinates of a fiber computational model, in which fibers of a given diameter and stiffness are discretized using nonlinear beam elements[4]. We then performed shear rheology measurements of several collagen specimens providing us with experimental curves of the strain-stress response of our hydrogels. Then, by using a real geometry of a collagen hydrogel in our model, we found the optimal value for the elastic modulus and the diameter of the fiber. The result is a system that can model the fiber structure (based on SHG images) and its bulk mechanical properties (based on fitting the shear rheology curves).

In silico ground truth simulations. First, we segmented a real confocal microscopy image of a cell that was embedded in a collagen hydrogel. Then, we embedded the relaxed state of the cell geometry in the synthetically generated matrix and we prescribed a 7 μm displacement at the closest point to the protrusion tip and obtained a ground truth matrix displacement field and a ground truth nodal force of around 540 pN. To analyze the performance of our traction recovery methods we added different levels of white Gaussian noise to the ground truth displacements. We tested the traction recovery accuracy of two different methods: a forward method, which computes forces directly from the measured (noisy) displacements, and our physics-based inverse method (PBIM) which imposes equilibrium of forces in the hydrogel domain.

Acquisition and Analysis of TFM Data: Experimental validation involved performing TFM experiments with single human umbilical vein endothelial cells (HUVECs) embedded in collagen gels, measuring fiber displacements around these cells using the open-source toolbox TFMLAB[5]. Our ongoing efforts focus on applying these displacements to our fiber models to quantify cell forces corresponding to measured displacements.

RESULTS

Fig.1A shows an example of the segmentation and construction of the computational model of a fiber structure taken from a second harmonic generation (SHG) image of a collagen hydrogel. Each fiber is modeled as a series of connected beams with a certain stiffness and diameter. These two parameters are fitted from experimental measurements of shear rheology on real collagen hydrogels and the optimal values of E=186.34MPa and d=70nm were obtained (see Fig. 1B). Fig 1C shows a segmentation of a real geometry of an endothelial cell embedded in a collagen hydrogel. The collagen network was segmented and a computational model was created using the above mentioned mechanical parameters to generate ground truth forces and matrix displacements. We then perturbed these ground truth displacements with different levels of noise to quantify the error of our inverse method, which

remains below 10% for all cases (Fig. 1D). Fig 1E shows matrix displacements measured around a real endothelial cell by means of TFM.

* Corresponding author. Email: **hans.vanoosterwyck@kuleuven.be**

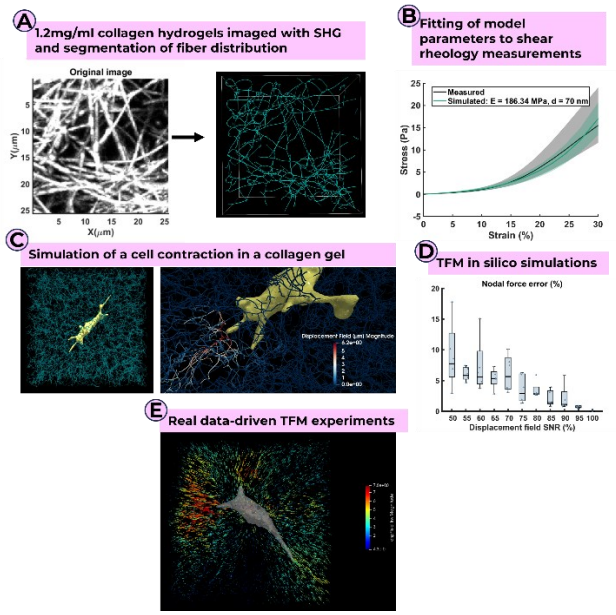

Figure 1.Summary of the results.

DISCUSSION AND CONCLUSIONS

In this work, we presented a novel data-driven 3D TFM approach and validated its accuracy and viability by means of in silico ground truth simulations. These preliminary results lay the foundations of our future work, which will focus on applying this framework to real experiments with cells to obtain multiscale cell force information at length scales closer to the length scale of mechanotransduction.

ACKNOWLEDGEMENTS

Financial support: JBF (FWO:1259223N), HVO (KUL:IBOF-21-083), AAF & JSH (PID2021-126051OB-C42), GHK & IM (Convergence programme Syn-Cells for Health).

References

1 Hall, M. S. *et al. Proc Natl Acad Sci U S A* 113, 14043–14048 (2016)
2 Sanz-Herrera, J. A. *et al. Soft Matter* (2020)
3 Barrasa-Fano, J. *et al. Acta Biomater* 126, 326–338 (2021)
4 Sanz-Herrera, J. A. *et al. bioRxiv* 2024.01.09.574800 (2024)
5 Barrasa-Fano, J. *et al. SoftwareX* 15, 100723 (2021)

-

MECHANOTRANSDUCTION AT THE GOLGI APPARATUS

Chandini BHASKAR NAIDU[1], Bruno GOUD[1], Stéphanie MISEREY[1], Jean-Baptiste MANNEVILLE[2]

1-Institut Curie, UMR144 CNRS, 12 rue Lhomond, Paris, France

2- Laboratoire Matière et Systèmes Complexes (MSC), Université Paris Cité, CNRS, UMR7057, Paris, France

INTRODUCTION

Cells can sense and respond to external forces and mechanotransduction events appear to be critical for most cellular functions. While mechanotransduction has been extensively studied at the plasma membrane and at the nucleus, the impact of forces on other organelles is still poorly known. Our project focuses on the study of mechanotransduction at the Golgi apparatus (GA), a central organelle regulating intracellular transport pathways. We aim to answer the following questions: 1) Can external and internal forces propagate to the GA and impact its tension? 2) Is the tension of the GA regulated by actin dynamics and/or the composition of Golgi membranes and the Golgi matrix? 3) Do post-Golgi trafficking and polarized secretion depend on the tension of the GA?

Our findings suggest that the GA is mechanosensitive and can modulate its membrane tension in response to external or internal constraints. Cytoskeletal protein disruption/modifications effectively modulate Golgi membrane tension. Furthermore, we have shown that external constraints such as substrate stiffness has a strong impact on the function of the GA as it affects the trafficking kinetics of some selected cargoes. Our results should provide new fundamental insights in the role played by mechanical tension in force transduction at the level of the GA

MATERIALS AND METHODS

To achieve these aims, we use specific experimental techniques:

1) We apply internal forces directly on the GA by manipulating a bead with optical tweezers (1). 2) We apply external constraints by modulating substrate stiffness.

2) We monitor the effects of internal and external forces on membrane tension at the GA using fluorescent HaloFlipper probes (2).

3) We follow post-Golgi trafficking of synchronously secreted cargoes using the RUSH assay (3).

RESULTS

SUBSTRATE STIFFNESS MODULATES THE TENSION OF THE GOLGI MEMBRANES

Halo Flipper probes are a general tool for imaging membrane tension changes in living cells (4). Tension changes are monitored by FLIM (fluorescence lifetime imaging) of the Flipper probe (5). I have established stable RPE1 cell lines in which the Halo Flipper probes are targeted to the GA via Golgi resident enzymes (Mannosidase and Sialyl transferase). To validate their sensitivity to membrane tension, I performed FLIM measurements on cells exposed to hypoosmotic shocks and reported a transient increase in fluorescence lifetime compared to isotonic conditions, which reflects an increase in GA membrane tension. Next, I measured the fluorescence lifetime of Halo Flipper probes in cells plated substrates of varying stiffness. These experiments show a significant difference in the fluorescence lifetime of the Halo Flipper probes at the GA in cells on different substrate stiffness, suggesting that substrate stiffness influences the tension of Golgi membranes and that forces are transmitted from focal adhesions (FAs) to the GA. In addition, I investigated the influence of substrate stiffness on the rigidity of the GA (data not shown). My results show that the rigidity index of the GA, a phenomenological measurement of the Golgi rigidity (6) is comparatively higher in cells plated on both soft substrates (2 kPa) and stiff substrates (30 kPa), whereas a reduction in the rigidity index of the GA was observed for cells plated on substrates of intermediate stiffness (11 kPa). Although the trend is not linear, these results show that the mechanical properties of the GA depend on that of the substrate.

I used the 'Retention Using Selective Hooks' (RUSH) synchronized transport system to investigate the influence of substrate stiffness on the kinetics of vesicular trafficking and secretion (7). To achieve this, I continuously monitor and record the time points of cargo arrival and exit from the GA. Our results indicate that substrate stiffness influences the kinetics of post-Golgi trafficking. We are currently repeating these experiments with different types of cargoes (such as CD59 a GPI-anchor proteins) which are available in the lab. In parallel, we monitor the arrival of cargoes at the plasma membrane using surface staining and a fluorescence-activated cell sorting-based assay called surface sensing of translation (SUnSET assay) which allows the monitoring and quantification of global protein synthesis and transport in individual mammalian cells to confirm that transport is modulated based on substrates (8,9). Our results should provide new fundamental insights in the role played by mechanical tension in force transduction at the level of the GA.

ACKNOWLEDGEMENTS

The authors would like to thank "Institut Curie- EuReCa PhD - European Horizon 2020 MSCA COFUND" for providing financial support to this project.

REFERENCES

1) Guet D, Mandal K, Pinot M, Hoffmann J, Abidine Y, Sigaut W, Bardin S, Schauer K, Goud B, Manneville JB. Mechanical role of actin dynamics in the rheology of the Golgi complex and in Golgi-associated trafficking events. Curr Biol. 2014 Aug 4;24(15):1700-11. doi: 10.1016/j.cub.2014.06.048. Epub 2014 Jul 17. PMID: 25042587.
2) Straková K, López-Andarias J, Jiménez-Rojo N, Chambers JE, Marciniak SJ, Riezman H, Sakai N, Matile S. HaloFlippers: A General Tool for the Fluorescence Imaging of Precisely Localized Membrane Tension Changes in Living Cells. ACS Cent Sci. 2020 Aug 26;6(8):1376-1385. doi: 10.1021/acscentsci.0c00666. Epub 2020 Jul 20. PMID: 32875078; PMCID: PMC7453570.
3) Fourriere L, Kasri A, Gareil N, Bardin S, Bousquet H, Pereira D, Perez F, Goud B, Boncompain G, Miserey-Lenkei S. RAB6 and microtubules restrict protein secretion to focal adhesions. J Cell Biol. 2019 Jul 1;218(7):2215-2231. doi: 10.1083/jcb.201805002. Epub 2019 May 29. PMID: 31142554; PMCID: PMC6605799.
4) Straková K, López-Andarias J, Jiménez-Rojo N, Chambers JE, Marciniak SJ, Riezman H, Sakai N, Matile S. HaloFlippers: A General Tool for the Fluorescence Imaging of Precisely Localized Membrane Tension Changes in Living Cells. ACS Cent Sci. 2020 Aug 26;6(8):1376-1385.
5) Colom A, Derivery E, Soleimanpour S, Tomba C, Molin MD, Sakai N, González-Gaitán M, Matile S, Roux A. A fluorescent membrane tension probe. Nat Chem. 2018 Nov;10(11):1118-1125.
6) Guet D, Mandal K, Pinot M, Hoffmann J, Abidine Y, Sigaut W, Bardin S, Schauer K, Goud B, Manneville JB. Mechanical role of actin dynamics in the rheology of the Golgi complex and in Golgi-associated trafficking events. Curr Biol. 2014 Aug 4;24(15):1700-11.
7) Boncompain G, Divoux S, Gareil N, de Forges H, Lescure A, Latreche L, Mercanti V, Jollivet F, Raposo G, Perez F. Synchronization of secretory protein traffic in populations of cells. Nat Methods. 2012 Mar 11;9(5):493-8.
8) Schmidt EK, Clavarino G, Ceppi M, Pierre P. SUnSET, a nonradioactive method to monitor protein synthesis. Nat Methods. 2009 Apr;6(4):275-7.
9) Fourriere L, Kasri A, Gareil N, Bardin S, Bousquet H, Pereira D, Perez F, Goud B, Boncompain G, Miserey-Lenkei S. RAB6 and microtubules restrict protein secretion to focal adhesions. J Cell Biol. 2019 Jul 1;218(7):2215-2231.

THE ROLE OF TENSILE STRESS IN THE INITIATION AND COORDINATION OF CEPHALIC FURROW FORMATION IN THE *DROSOPHILA* EMBRYO

Redowan A. Niloy[1], Guo–Jie J. Gao[2], Michael C. Holcomb[3], Jeffrey H. Thomas[4], Jerzy Blawzdziewicz[1,5,*]

1. Department of Mechanical Engineering, Texas Tech University, U.S.A.; 2. Department of Mathematical and Systems Engineering, Shizuoka University, Hamamatsu, Japan; 3. Department of Physics and Geosciences, Angelo State University, U.S.A.; 4. Department of Cell Biology and Biochemistry, Texas Tech University Health Sciences Center, U.S.A.; 5. Department of Physics and Astronomy, Texas Tech University, U.S.A.

INTRODUCTION

Morphogenetic movements that occur during gastrulation of the *Drosophila* embryo involve complex sequences of cell shape changes and embryo-scale cellular flows that generate embryonic architecture. One of the major morphogenetic movements is the cephalic furrow formation (CFF), which gives rise to a deep epithelial invagination. Unlike ventral furrow and midgut invaginations, cephalic furrow (CF) is transitory and does not contribute to formation of germ layers. However, it has been hypothesized that its role is to mechanically separate the head and trunk morphogenetic regions.

In our recent work [1], we studied mechanical forces driving the progression stage of CFF, in which the already formed furrow continuously increases its depth. The furrow geometry was determined from confocal fixed embryo images that were analyzed using our advanced vertex model in which curvatures of lateral membranes allowed us to quantify cell-to-cell pressure differences. We found that high-pressure cells that are already incorporated into the furrow provide a firm support that helps pull new (low-pressure) invaginating cells over the CF cleft.

The above mechanism is not available during the initiation stage of CFF, and we demonstrate here that the CF initiation cannot occur merely as a result of the interplay of membrane tensions and cell pressures alone. We furnish evidence that the tension developing along the furrow is the key factor in the initiation process. First, this longitudinal tension in a narrow band along the curved embryo surface provides an inward force that helps push the initiator cells toward the yolk sac. Second, this tension is also a source of mechanical signals that coordinate coherent furrow expansion and ensure its robustness.

MATERIALS AND METHODS

We have designed an advanced multi-node lateral vertex model (MNLVM) and an en-face force-center model to analyze a set of *Drosophila* embryo images (previously collected by our group) to infer key mechanical processes that govern the initiation of CFF. Our numerical and experimental techniques are described below.

Multi-node lateral vertex model with membrane curvature

Our MNLVM allows us to study in detail the apical, lateral, and basal cortical tensions as well as cell pressures during the invagination processes. The model is based on a multi-node membrane representation that enables inferring cellular pressure differences from the membrane tensions and curvatures [1]. Our new expanded version of this model includes an explicit representation of the perivitelline fluid region at the CF cleft.

En-face force-center model of a cellular-constriction process with tensile-stress feedback

The force-center model, previously developed by our group to describe constriction-chain formation at the onset of ventral furrow formation [2], is used here to analyze how a chain of initiator cells that carries tensile stress propagating along the furrow is generated. The tensile-stress feedback effect is incorporated into the model by increasing the constriction probability for the cells subject to mechanical tension.

Experimental techniques

Our techniques for collecting Spider-GFP time-lapse images and for imaging fixed and stained embryos are described in [1]. The previously collected images have been reused here under Elsevier's author rights.

RESULTS

The key results of our study are summarized in Figure 1. The image of the expanding furrow depicted in panel (*a*) and the blowup in panel (*b*) show the initiation of CF and its expansion in the ventral and dorsal directions. Popkova *et al.* [4] suggested that the expansion occurs as a result of a triggering wave generated by apicobasal shortening of initiator cells. According to their model, shortening of a cell at the expansion front causes length reduction of the lateral membrane of the adjacent initiator cell. This shortening provides a triggering signal for apicobasal shortening of the adjacent cell.

* Corresponding author. E-mail: jerzy.blawzdziewicz@ttu.edu

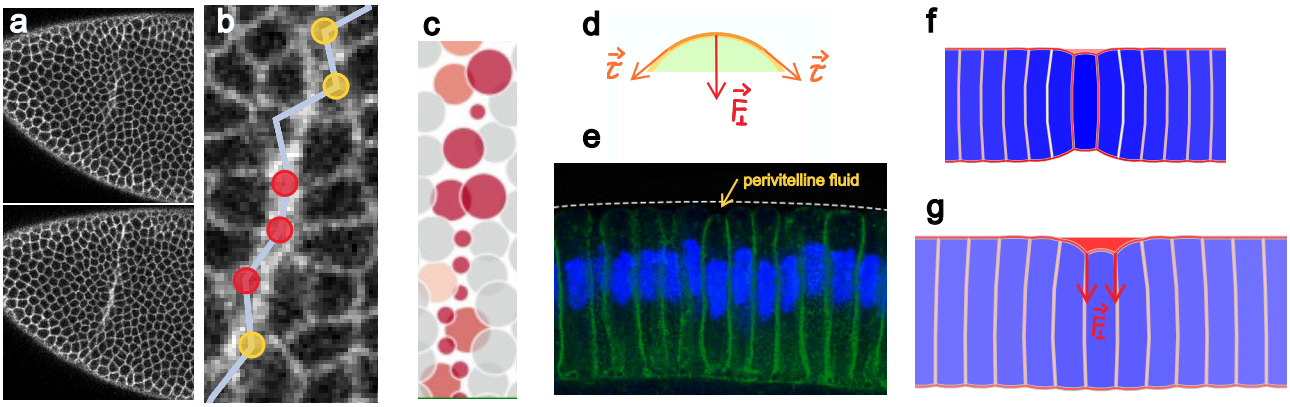

Figure 1. The mechanics of CF initiation. (*a*) The CF cleft first appears on the lateral sides of the embryo and then expands in the ventral and dorsal directions. (*b*) The line of the activated initiator cells (marked with circles) is discontinuous, with one-cell or two-cell gaps associated with cells with delayed activation. (*c*) The non-monotonic initiation of CF is explained by our tensile-stress-feedback model, in which the reduction of the apical ends of initiator cells generates tensile stress that propagates along the furrow and coordinates further constrictions. Constricted cells are marked by small circles. Cells with enhanced tensile stress are marked in red. (*d*) Tension $\vec{\tau}$ propagating along the CF cleft produces inward force $\vec{F}_\perp$ pushing the initiator cells toward the yolk sac. (*e*) Confocal image of a fixed embryo reveals formation of a perivitelline fluid region between the vitelline membrane (indicated by the dashed line) and the apical end of the initiator cell. (*f*) Our MNLVM shows that without the line-tension-generated inward force $\vec{F}_\perp$, the apico-basal shortening of the initiator cell does not initiate the invagination but instead results in formation of a basal indentation not observed in experiments. (*g*) In contrast, the MNLVM shows that with the inward force $\vec{F}_\perp$ included, the geometry of the CF initiation is faithfully reproduced.

The mechanism described in [4] relies on near-neighbor cell interactions. Our experimental results, however, reveal that the chain of activated initiator cells is discontinuous (Figure 1(*b*)), which contradicts the concept of the nearest-neighbor-triggered expansion front. Here we show an alternative explanation based on a tensile-stress triggering mechanism. Since the development of tensile stress propagating along the furrow has recently been demonstrated [3], we propose that the expansion of the stress chain is coordinated by tensile-stress feedback, similar to the case of constriction chains in the ventral furrow field [2]. Because of nonlocal stress propagation, such feedback can produce a discontinuous chain of activated initiator cells, as evidenced by our force-center model (Figure 1(*c*)).

The line tension τ along the CF cleft on the curved embryo surface produces an inward force $F_\perp = \tau\kappa\delta l$ (Figure 1(*d*)). This force acts on each line segment of length δl in the direction of the yolk sac and is proportional to the line tension τ and surface curvature κ along the cleft. Our simulations using MNLVM show that the inward force $\vec{F}_\perp$ is necessary for the initiation of the invagination (Figure 1(*d–g*)). Our additional simulations demonstrate that the entire invagination process can be described using the cell pressures, apical, lateral, and basal cortical tensions, and the inward force $\vec{F}_\perp$.

DISCUSSION AND CONCLUSIONS

Building on our present investigations of the CF initiation and on recently published our and others' results [1–4], we propose the following scenario. The most active initiator cells in a small lateral region produce actomyosin contractions that initiate generation of either intercellular cables or a less rigid meshwork that run along the apices of the invaginating cells. A coherent development of such structures is aided by tensile-stress feedback. The tensile-stress stripe along the developing CF cleft generates the curvature-associated inward force that pushes the initiator cells toward the yolk sac. Most likely, this force also provides a mechanical signal that triggers apico-basal shortening of the cell. The associated increase of the apical tension oriented across the furrow produces further mechanical signals, resulting in the observed shape changes of subsequent invaginating cells. If this proposed sequence of mechanical signaling events is corroborated by further studies, it will demonstrate the paramount role of mechanical feedback control in morphogenetic movements.

References

[1] R. A. Niloy, M. C. Holcomb, J. H. Thomas, and J. Blawzdziewicz: *The mechanics of cephalic furrow formation in the Drosophila embryo*. Biophys. J., Vol. 122, pp. 3843–3859, 2023.

[2] M. C. Holcomb, G.-J. J. Gao, M. Servati, D. Schneider, P. K. McNeely, J. H. Thomas, and J. Blawzdziewicz. *Mechanical feedback and robustness of apical constrictions in Drosophila embryo ventral furrow formation*. PLOS Comput. Biol. Vol. 17, e1009173, 2021.

[3] A. S. Eritano, C. L. Bromley, A. B. Albero, L. S. Utz, F.-L. Wen, M. Takeda, T. Fukaya, M. M. Sami, T. Shibata, S. Lemke, and Y.-C. Wang. *Tissue-scale mechanical coupling reduces morphogenetic noise to ensure precision during epithelial folding*. Dev. Cell, Vol. 53, pp. 212+, 2020.

[4] A. Popkova, U. Andrenšek, S. Pagnotta, P. Ziherl, M. Krajnc, and M. Rauzi. *A mechanical wave travels along a genetic guide to drive the formation of an epithelial furrow during Drosophila gastrulation.* Dev. Cell, Vol. 59, pp. 400-414, 2024.

MECHANICAL EVALUATION OF 3D-PRINTED VASCULAR PATCHES FOR CONGENITAL HEART TREATMENTS

Pablo Blázquez-Carmona[1,2,3,*], Fernando Rubio-Iglesias[1], Elisa Bevilacqua[2], Israel Valverde[2], Gorka Gómez-Ciriza[2], Ignacio González-Loscertales[4], Tarik Smani[2], Antonio Ordoñez[2], Esther Reina-Romo[2,3]

1. Escuela Superior de Ingeniería, Universidad de Cádiz, Spain; 2. Instituto de Biomedicina de Sevilla, Spain; 3. Escuela Técnica Superior de Ingeniería, Universidad de Sevilla, Spain; 4. Escuela de Ingenierías Industriales, Universidad de Málaga, Spain.

INTRODUCTION

As of now, patients diagnosed with aortic arch hypoplasia or coarctation are reported to experience heightened cardiovascular morbidity, notwithstanding the effective surgical correction of the disease during childhood [1]. Recent vascular grafting aims to reduce recoarctation rates (11-37%) [2]. Nevertheless, they generally lead to long-term complications, including turbulent flow, decreased ejection fraction, or inability to accommodate patient growth [3,4]. As an alternative, tissue engineering for vascular applications investigates the combination of porous 3D-printed biocompatible patches with cells to mimic the interstitial matrix and restore damaged tissue. Moreover, using biodegradable base material leads to its progressive replacement by the naïve cardiovascular tissue [5]. Despite this biological advantage, evaluating the mechanical properties of these novel patches is crucial to ensure their suitability to withstand the pressures and deformations imposed by blood flow *in vivo*.

In this line, this study aims to mechanically characterize tissue-engineered vascular grafts (TEVG) for surgical treatments in neonates, assessing parameters including burst pressure, burst stress, and the apparent elastic modulus. Mechanical alterations following the seeding and maturation of multipotent mesenchymal cells (MSC) into vascular smooth cells were also investigated using a novel device and inflation protocol.

MATERIALS AND METHODS

Manufacture of the vascular patches and cell culture

Patches for the TEVG and cultured TVEG groups were manufactured using a Prusa MK3S printer (Prusa Research, Prague, Czech Republic), PCL 100 filament, and a nozzle diameter of 1.75 mm. Printing layers were 0.1 mm with a 3D honeycomb filling and 25% of porosity. For the cultured patches, Poietics human adipose-derived stem cells ADSC-PT-5006 (Lonza, Switzerland) were employed. After at least 1 week in culture, around 2.5 x 10^5 cells were seeded per patch, which was again cultured for 20 days. Inflation tests with cultured TEVG were performed immediately after culture to avoid the detachment of cells from patches.

Design of the inflation tests

The designed device comprised a customized mechanized cylindrical aluminium chamber pierced with a circular top opening measuring 25 mm in diameter and two concentric constraining plates. The first plate featured an attached latex membrane, simulating cardiovascular tissue during the inflation test. The patches were positioned between the two plates and secured to the container via screwed joints (Figure 1A). Below, the chamber was linked to a closed water circuit. A syringe pump (IPS 12-R, Inovenso Pump Systems, Inovenso, MA, USA) regulated fluid entry into the chamber at a constant flow rate (0.5 ml/min). The closed water circuit incorporated a manometer (Testo 549i, Testo, Titisee-Neustadt, Germany) to monitor pressure changes at the container inlet. Pressure variations corresponded to resulting deformations (vertical displacement) in the patch, measured by focusing a central reference point of the patch using a microscope, as shown in Figure 1A. In total, 18 patches were characterized, comprising an isolated TEVGs (n=12) and cultured TEVGs (n=6) groups.

Mechanical characterization of the patches

The deformation of the patches (ε) during the inflation tests were calculated using Eq. (1).

$$\varepsilon = \frac{L-D}{D} = \frac{1}{D}\left(h - \frac{D^2}{4h}\right) asin\left(\frac{D}{h+{D^2}/{4h}}\right) - 1 \quad (1)$$

where D is the inflation diameter (25 mm), L is the length of arch formed by the patch after inflation, and h is the height of the reference point measured by microscopy. The burst stress (σ_b) was estimated using the law of Laplace for a thin-walled sphere:

$$\sigma_b = \frac{p_b - r}{2t} \quad (2)$$

where p_b is the burst pressure, t is the thickness of the patches (0.225 ± 0.029 mm), and r is the characteristic radius of the deformed patch.

RESULTS

Figure 1B displays the pressure-strain curves from the inflation tests conducted on the PEVG (blue points) and cultured PEVG (red points). Overall, both groups demonstrated substantial resistance to pressure (>750 mmHg) and deformation (>10%) before reaching burst. Specifically, the PEVG exhibited a burst pressure of 1254.31 ± 219.22 mmHg, whereas the cultured group failed at a pressure of 963.82 ± 222.74 mmHg. Additionally, the burst stress was higher in the PEVG group, measuring 7.59 ± 1.65 MPa compared to 4.53 ± 1.48 MPa in the cultured patches. Finally, as shown in Figure 1C, the patches typically failed through a cross crack near their center of inflation.

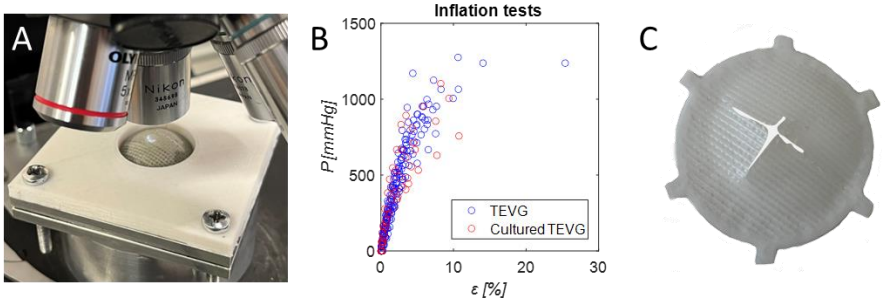

Figure 1. A) Designed device and patch during an inflation test; B) Evolution of the pressure measured by the manometer with the deformation of the TEVG (blue data) and cultured TEVG patches (red data) during inflation; C) Cross fracture in the patch at the end of the inflation test.

DISCUSSION AND CONCLUSIONS

The designed equipment and inflation protocol have been shown to provide an estimation of burst pressure and stress, critical properties for ensuring the proper *in vivo* mechanical performance of the scaffold. Both groups of these novel patches were able to withstand pressures exceeding those encountered *in vivo* in the adult aorta (~120 mmHg), including in neonates (~60 mmHg) and in the most critical cases of hypertension (~180 mmHg) [6,7]. However, the cultured patches were found to reduce their deformation limit and resistance to the mechanical boundary conditions imposed by the vascular tissue, possibly due to structural stiffening following a decrease in porosity.

ACKNOWLEDGEMENTS

This publication is part of the R+D project PID2020-113790RB-I00, financed by MCIN/AEI/10.13039/501100011033.

References

[1] Vigneswaran T.V., Sinha, M. D., Valverde, I., Simpson, J.M., Charakida, M.: *Hypertension in Coarctation of the Aorta: Challenges in Diagnosis in Children*. Pediatric Cardiology Vol. 39, pp. 1-10, Springer 2017.

[2] Dong L., et al.: *Impact of Re-Coarctation Following the Norwood Operation on Survival in the Balloon Angioplasty Era*. Journal of the American College of Cardiology Vol. 45, pp. 1844-1848, Elsevier 2005.

[3] Itatani K., et al.: *Influence of surgical arch reconstruction methods on single ventricle workload in the Norwood procedure*. The Journal of Thoracic and Cardiovascular Surgery Vol. 144, pp. 130-138, Elsevier 2012.

[4] Bouten C.V.C., et al.: *Substrates for cardiovascular tissue engineering.* Advanced Drug Delivery Reviews Vol. 63, pp. 221-241, Elsevier 2011.

[5] Mayoral I., et al.: *Tissue engineered in-vitro vascular patch fabrication using hybrid 3D printing and electrospinning*. Materials Today Bio Vol. 14, pp. 100252, Elsevier 2022.

[6] Vigneswaran T.V., et al.: *Hypertension in Coarctation of the Aorta: Challenges in Diagnosis in Children.* Pediatric Cardiology Vol. 39, pp. 1-10. Springer 2017.

[7] Lyes, E.K. et al.: *Aortic Stenosis and Systemic Hypertension: What is worse? Introduction to Hypertensive Equivalent Effective Orifice Area*. World Congress on Medical Physics and Biomedical Engineering Vol. 14, pp. 3390-3394, Springer 2006.

A NOVEL *IN SILICO* APPROACH TO INVESTIGATE MECHANO-REGULATION OF MACROPHAGES DURING BONE FRACTURE INFLAMMATORY STAGE

Edoardo Borgiani[1,2,3,*], Gabriele Nasello[2], Liesbet Geris[1,2,3]

1. Biomechanics Research Unit, GIGA-In Silico Medicine, University of Liège, Liège, Belgium;
2. Prometheus, Division of Skeletal Tissue Engineering, KU Leuven, Leuven, Belgium;
3. Division of Biomechanics, Department of Mechanical Engineering, KU Leuven, Leuven, Belgium

INTRODUCTION

Bone fracture healing is a convoluted process that spans multiple time- and length-scales. For example, it is known that mechanical cues sensed at the tissue level control how mechanosensitive cells trigger alternative pathways at the molecular level [1]. Therefore, due to its convoluted nature, the experimental investigation of the bone healing dynamics might be challenging when the many hidden inter-level interactions need to be explored.

For this reason, in the last decades, numerous computer models have been developed to simulate the multiscale dynamics of bone fracture healing at the repair and remodeling stage. However, most of the computational work in the literature does not investigate the early inflammatory stage of bone healing, which could strongly benefit from the multiscale computational approach to explore the mechano-biology of the immune cells [2]. Macrophages are known to be mechanosensitive [3] and their capacity to tune the inflammatory response is essential to promote a successful healing. Therefore, we propose a new computational multiscale model to explore the mechanoregulatory rules that characterize bone marrow-derived macrophages and their role in the overall healing process. An initial model for the biological characterization of the inflammatory stage of bone healing has been already developed and validated in mice [4]. An additional mechanical module has recently been integrated to evaluate the role of mechanical stimulation in the regulation of inflammatory response.

The mechanobiological model is expected to characterize a validated predictive tool to investigate the role of mechanical supports (e.g. external fixator, scaffolds) combined with biochemical therapies (e.g. exogenous growth factors, anti-inflammatory drugs) in enhancing bone healing success rate since its early immune response, with a dedicated spotlight to critical healing conditions (e.g. segmental defects, aging).

MATERIALS AND METHODS

The biological model has been developed with agent-based methods to simulate the dynamics of the immune cell populations within the callus domain. The employment of agents to identify each single cell as a discrete entity introduces stochasticity to the cellular dynamics, agreeing with the intrinsic nature of the process. The biological model has been coupled with a subcellular environment, to simulate the dynamics of cytokines and other inflammatory molecules. The coupling of the cellular and subcellular level generated COMMBINI (COmputational Model of Macrophage dynamics in the Bone INjury Immunoresponse) [4]. Recently the model has been extended to the third dimension (Fig. 1A) and further coupled with a mechanical model to simulate the distribution of mechanical stresses and strains within the tissues that characterize the fracture region (Fig. 1B). The mechanical model has been created as a finite element model, reproducing the geometry of the fracture simulated with COMMBINI. Mechanical properties have been assigned to the different parts of the bone. To simulate murine gait, loadings and boundary conditions have been applied to the extremities of the bone. For mechanical characterization, two different external fixation strategies have been used (rigid vs flexible).

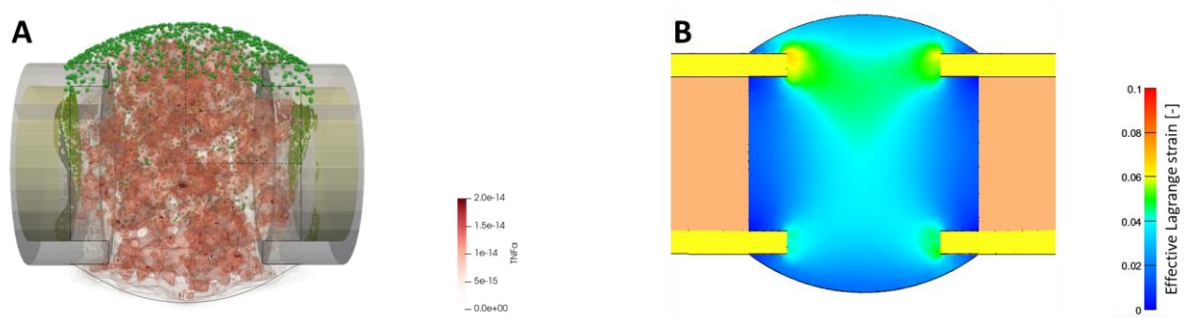

Figure 1. (A) Biological agent-based model of bone fracture healing to simulate the immune cell populations as agents (spheres with different colors, according to phenotypes) and molecular distribution (TNFα concentration, ng/mL) within the healing region. (B) Finite element model to simulate effective Lagrange strain distribution within the same region of interest. Both models are three-dimensional and have been sliced for visualization purposes.

* Corresponding author. Email: **edoardo.borgiani@uliege.be**

The mechanobiological rules that regulate macrophage behavior have been derived from *in vitro* experimental data found in literature [5,6] (Fig. 2). Nevertheless, for a more reliable calibration of the model, on-chip experiments will be performed with macrophage population in our laboratory. Each model iteratively runs for a virtual time of three days to simulate the full development of the inflammatory stage, including the triggering of the inflammation and its subsequent buffer (anti-inflammatory response).

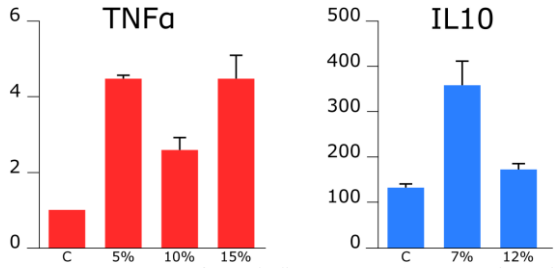

Figure 2. *In vitro* macrophage relative expression of pro-inflammatory (TNFα, adapted from [5]) and anti-inflammatory cytokines (IL10, adapted from [6]) according to the sensed mechanical strain. C: static control.

RESULTS

From the preliminary results obtained from the model after the integration of the mechanical model, a stronger inflammatory response is predicted within the fracture, if compared with static conditions: 5% more pro-inflammatory macrophages are predicted on Day 1 (Fig. 3), followed by a reduction of 4% of the anti-inflammatory macrophage population on Day 3 post-fracture.

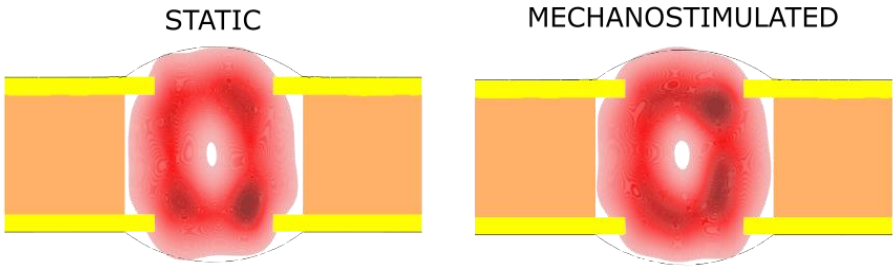

Figure 3. Predicted concentration of pro-inflammatory macrophages within the bone fracture in static and stimulated conditions at Day 1 post-fracture. The darker shade of red indicates a higher concentration of pro-inflammatory macrophages.

DISCUSSION AND CONCLUSIONS

The computational model provides a novel point of view in the exploration of bone healing mechano-regulation. The preliminary results highlight how a proper mechanical environment is essential for successful fracture repair since the first hours post-injury, during the inflammatory response. In particular, the macrophages are susceptible to changes in mechanical stimulation, which might lead to a prolonged acute inflammation state, compromising the healing process. The multiscale approach proposed with this model is essential to evaluate how fracture stabilization strategies can have a primary role in enhancing the healing process at cellular and molecular levels. Nevertheless, the proposed mechanobiological model has still a margin for improvement and additional mechanically driven rules will be implemented in future versions of the computer model. Moreover, microfluidic experiments on mechano-stimulated macrophage cultures are planned by us to extend the investigation to further mechano-regulated cell activities.

References

[1] Augat, P., Hollensteiner, M., von Rüden, C.: *The role of mechanical stimulation in the enhancement of bone healing*. Injury 52 Suppl 2:S78-S83, 2021.

[2] Lafuente-Gracia, L., Borgiani, E., Nasello, G., Geris, L.: *Towards in silico Models of the Inflammatory Response in Bone Fracture Healing.* Front Bioeng Biotechnol. 9:703725, 2021.

[3] Adams, S., Wuescher, L.M., Worth, R., Yildirim-Ayan, E.: *Mechano-Immunomodulation: Mechanoresponsive Changes in Macrophage Activity and Polarization*. Ann Biomed Eng. 47(11):2213-2231, 2019.

[4] Borgiani, E., Nasello, G., Ory, L., et al.: *COMMBINI: an experimentally-informed COmputational Model of Macrophage dynamics in the Bone INjury Immunoresponse.* Front Immunol. 14:1231329, 2023.

[5] Shan, S., Fang, B., Zhang, Y., et al.: *Mechanical stretch promotes tumoricidal M1 polarization via the FAK/NF-κB signaling pathway.* FASEB J 33(12):13254-13266, 2019.

[6] Ballotta, V., Driessen-Mol, A., Bouten, C.V., Baaijens, F.P.: *Strain-dependent modulation of macrophage polarization within scaffolds.* Biomaterials 35(18):4919-4928, 2014.

MECHANOBIOLOGY OF IMMUNE CELLS: HOW STIFFNESS AND GEOMETRY OF THE EXTRACELLULAR ENVIRONMENT INFLUENCE MYELOID CELL PROPERTIES.

Alessandra Cambi*

Department of Medical BioSciences, Radboud university medical center, Geert Grooteplein Zuid 26-28, 6525 GA Nijmegen, The Netherlands

INTRODUCTION

Tissue stiffness alteration, resulting in disrupted homeostasis of mechanical forces, is involved in many pathologies including pulmonary fibrosis, atherosclerosis and cancer. Dendritic cells (DCs) are specialized leukocytes involved in these pathologies. In tissues, DCs patrol for pathogens or aberrant cells. Upon danger recognition, DCs migrate to lymph nodes to initiate immune responses. DCs experience multiple, elastically diverse extracellular environments both in healthy and in diseased tissues. Yet, little is known about how mechanical forces in these microenvironments contribute to the regulation of DC immunobiology. DCs use podosomes, mechanosensitive actin-rich protrusions, to generate forces, migrate, and ingest large foreign antigens (Fig. 1). Individual podosomes probe their microenvironment through periodic protrusion and retraction cycles (vertical oscillations), while oscillations of multiple podosomes in a cluster are coordinated in a wave-like fashion. The molecular mechanisms orchestrating this complex dynamic behavior are poorly understood.

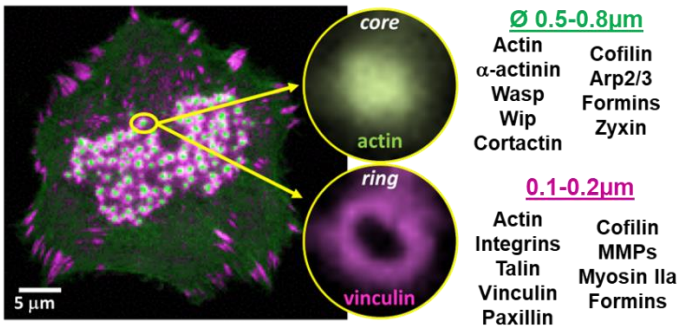

Figure 1. Podosomes are actin-rich protrusion formed by dendritic cells adhering onto a substrate. Representative image of one dendritic cell with a large cluster of podosomes that were stained for actin (green) and vinculin (magenta). To note, several molecules compose the core and the ring of each individual podosome.

MATERIALS AND METHODS

We integrated advanced quantitative bioimaging, 2D and 3D biomimetic substrates of variable stiffness, immunological assays and a chemo-mechanical model.

RESULTS

We demonstrated that collective wave dynamics arise from the coupling between chemo-mechanical signaling and actin diffusion, proving the role of podosome clusters in DC mechanosensing [1]. By perturbing the septin network, which is considered the fourth type of cytoskeletal filaments, we altered podosome architecture and cluster dynamics, identifying a novel interplay among septins, myosin IIa and actin (Fig. 2).

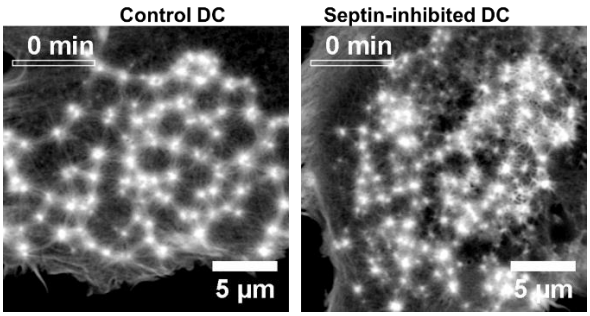

Figure 2. Septin inhibition affects podosome appearance and tunrover. DCs expressing GFP_tagged LifeAct (to stain actin) were treated or not with a peptide that blocks all septins, resulting in many smaller podosomes with higher turnover (dynamics not shown).

Finally, preliminary observations by superresolution microscopy of DCs migrating on collagen bundles in decellularized dermis reveal for the first time podosome nanoscale architecture and dynamics in a semi-physiological 3D environment (Fig. 3).

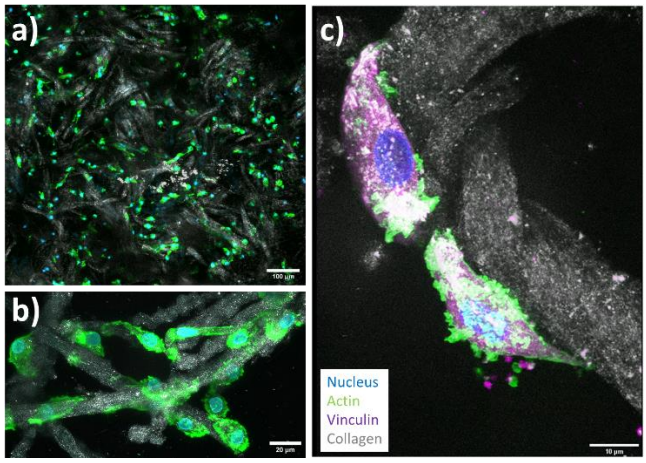

Figure 3. Dendritic cells seeded into decellularized dermal matrices. a)-b) DDMs were used as physiological 3D environments to seed DCs and study whether the cells would form podosomes on the large collagen fibers. Images were taken by confocal microscopy. c) To check for podosome formation, cells were stained with DAPI (nucleus), phalloidin (actin) and an anti-vinculin antibody. Collagen is imaged using reflection.

DISCUSSION AND CONCLUSIONS

These novel observations emphasize the need to develop dedicated image analysis tools and more sophisticated mathematical models that take the complexity of the 3D environment into account. Tissue-resident DCs are the orchestrators of immune responses in pathologies associated with changes in extracellular matrix mechanical properties and are the first cells to respond to implanted biomaterials, playing a role in persistent implant infection and subsequent biofilm growth. A better understanding of the mechanisms regulating DC mechanoimmunology will foster the development of new immunotherapeutic approaches aimed at targeting aberrant extracellular matrix and for medical interventions to reduce implant rejection.

ACKNOWLEDGEMENTS

The authors would like to thank **Radboudumc** for providing intramural financial support to this project".

References

[1] Gong Z, van den Dries K, Migueles-Ramírez RA, Wiseman PW, Cambi A, Shenoy VB. *Chemo-mechanical diffusion waves explain collective dynamics of immune cell podosomes.*. Nat Commun, 2023.

* Corresponding author. Email: **Alessandra.cambi@radboudumc.nl**

PERSISTENT RANDOM WALK MODEL OF CELL MIGRATION OVER CURVED SURFACE

Gildas Carlin[1,2,*], Ian Manifacier[1,2], Jean-Louis Milan[1,2]

1. Aix Marseille Univ, CNRS, ISM, 13009 Marseille, France

2. Aix Marseille Univ, APHM, CNRS, ISM, Sainte-Marguerite Hospital, Institute for Locomotion, Department of Orthopaedics and Traumatology, 13009 Marseille, France

INTRODUCTION

Cell migration is a key process in tissue formation which occurs during embryo development or regeneration. Among the numerous factors that impact cell behavior, substrate cell-scale curvature redirects cells toward concave areas [1] (Fig.1). Yet, the mechanism driving this directional change remains elusive-whether it emerges from signal pathway activation induced by curvature and/or mechanical constraints imposed by curvature.

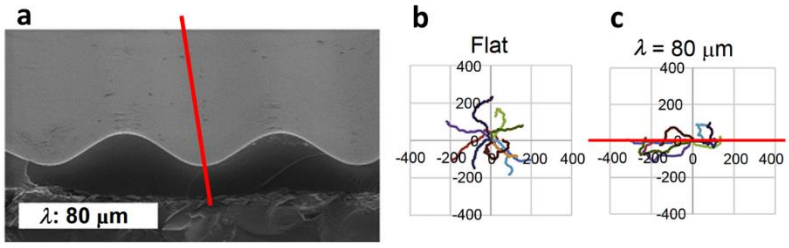

Figure 1: a. Sinusoidal wavy substrate with a wavelength (distance between two consecutive peaks) of $80\mu m$. b, c. Trajectories of T-cells cultivated on flat and wavy substrates. Cells predominantly migrate along the valleys (indicated by red axes) on the wavy substrate. Images reproduced from [1].

MATERIALS AND METHODS

Here, a persistent random walk (PRW) model [2] has been developed in order to assess the mechano-sensitivity of cells to substrate curvature. A parameter $\beta \in [0,1]$ regulates whether curvature activates signal pathways (β close to 1) or not (β close to 0). Sensibility to curvature may arise from a local gradient measurement at the cell's position or a cell-scale measurement at the periphery. Our study aims to test all these hypotheses.

RESULTS

Simulations were conducted for 10 hours on a sinusoidal wavy surface with an amplitude of $10\mu m$ and a wavelength $\lambda = 80\mu m$ (Fig. 2).

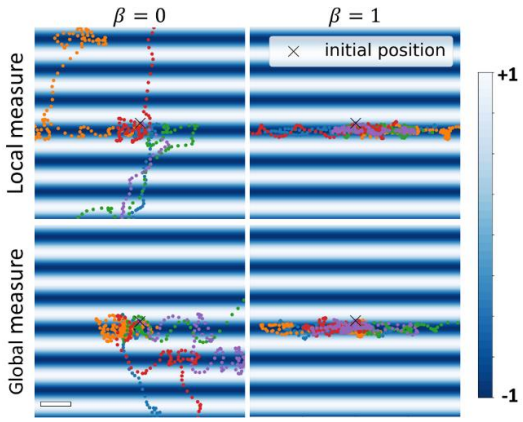

Figure 2: Trajectories of five cells under different parameters conditions. Scale bar is $80\mu m$ and color bar is the normalized height of the substrate (+1 is peaks and -1 is valleys).

* Corresponding author. **gildas.carlin@univ-amu.fr**

Preliminary results, when compared with experiments (Fig. 1c), suggest that cells change of directionality is mostly caused by signal pathway activation (β close to 1).

DISCUSSION AND CONCLUSIONS

The PRW model reproduces cell trajectories on curved surface. A numerical study [3] showed that dynamic surfaces can guide cell migration in a given direction. Adapting the PRW model to dynamic substrates can reinforce the development of methods to guide cell migration.

References

[1] Song, K. H., Park, S. J., Kim, D. S., Doh, J.: *Sinusoidal wavy surfaces for curvature-guided migration of T lymphocytes*. Biomaterials, 2015.

[2] Wu, P. H., Giri, A., Sun, S. X., Wirtz, D.: *Three-dimensional cell migration does not follow a random walk*. PNAS, 2014.

[3] Manifacier, I., Carlin, G., Dongshu, L., Vassaux, M., Pieuchot, L., Luchnikov, V., Anselme, K., Milan, J. L.: *In silico analysis shows that dynamic changes in curvature guide cell migration over long distances.* Biomechanics and Modeling Mechanobiology, 2023.

AN *IN SILICO* STUDY OF A FLOW-ENHANCED VASCULARIZED ORGANOID

Ana Carrasco-Mantis*, Esther Reina-Romo, José A. Sanz-Herrera

Escuela Técnica Superior de Ingeniería, Universidad de Sevilla, 41092 Seville, Spain

INTRODUCTION

Organoids are widely used as 3D *in vitro* models of cell groups that mimic certain characteristics of living tissues and organs [1]. They represent a good platform for the study of *ex vivo* morphogenesis, diagnosis and treatment of diseases [2]. An organoid may originate from pluripotent, tissue resident stem cells or differentiated cells [3]. When an organoid grows to a considerable size, a necrotic core may appear since the cells located further inside have more difficulty to access nutrients and oxygen. One of the possible solutions to prevent the appearance of this core and to achieve a more mature organoid is vascularization [4]. In this work, we have developed a 3D hybrid *in silico* model to analyze the evolution of an organoid partially embedded in an extracellular matrix (ECM) and exposed to a stationary laminar flow. The aim of the study is analyzing how the fluid induced shear stress promotes enhanced differentiation of cells within the organoid into endothelial cells, thus increasing vascularization within the organoid.

MATERIALS AND METHODS

Our hybrid model combines an agent-based (discrete) framework to simulate the vascularized organoid, coupled with continuum models.

Discrete model

The evolution of the organoid is based on a previous study of spheroids [5]. We consider two types of agents, cells of the organoid (*o*) and ECM particles. The interactions between cells and between cells and particles are modeled as follows (Eq. (1)):

$$\mu_o \frac{d\boldsymbol{x}_o}{dt} = \boldsymbol{F}_o^{m,o} + \boldsymbol{F}_o^r + \boldsymbol{F}_o^s + \boldsymbol{F}_o^{CFD} + \boldsymbol{F}_o^H \quad in \quad \Omega_O(\boldsymbol{x},t) \quad (1)$$

where $\boldsymbol{F}_o^{m,o}$ is the mechanical force between organoid cells, $\boldsymbol{F}_o^r$ is the cell random force to account for the heterogeneity of the medium, $\boldsymbol{F}_o^s$ is the surface tension force applied on the contour cells to maintain the spherical morphology, $\boldsymbol{F}_o^{CFD}$ is the tangential force exerted by the fluid on the organoid boundary cells and $\boldsymbol{F}_o^H$ is the mechanical force of interaction between an organoid cell and ECM particles. In Eq. (1), $\boldsymbol{x}_o$ is the position of an organoid cell and μ_o is the damping coefficient between organoid cells. $\Omega_O(\boldsymbol{x},t)$ is an evolutionary domain in which the organoid develops.

When an organoid boundary cell subjected to the laminar flow exceeds a certain threshold of the tangential force, it differentiates into an endothelial cell, representing the initiation of a new blood vessel, as described in Ref. [6]. In a similar way, we have two types of endothelial cells: (i) tips (*t*), that sense the chemotactic gradient and (ii) stalks (*s*), that proliferate after completion of their cell cycle. Their respective equations of motion are:

$$\mu_e \frac{d\boldsymbol{x}_t}{dt} = \boldsymbol{F}_t^{m,e} + \boldsymbol{F}_t^{m,eo} + \boldsymbol{F}_t^{m,eh} + \boldsymbol{F}_t^c \quad in \quad \Omega_O(\boldsymbol{x},t) \quad (2)$$

$$\mu_e \frac{d\boldsymbol{x}_s}{dt} = \boldsymbol{F}_s^{m,e} + \boldsymbol{F}_s^{m,eo} + \boldsymbol{F}_s^{m,eh} + \boldsymbol{F}_s^a \quad in \quad \Omega_O(\boldsymbol{x},t) \quad (3)$$

where $\boldsymbol{F}^{m,e}$ is the mechanical force between endothelial cells, $\boldsymbol{F}^{m,eo}$ is the mechanical force between an endothelial cell and the organoid cells, $\boldsymbol{F}^{m,eh}$ is the mechanical force between an endothelial cell and the ECM particles, $\boldsymbol{F}^c$ is the chemotactic force and $\boldsymbol{F}^a$ is the angular force whereby a daughter cell is incorporated into the blood vessel of the parent cell. In Eqs. (2) and (3), $\boldsymbol{x}$ is the endothelial cell position and μ_e is the damping coefficient between endothelial cells.

Continuum models

The Computational Fluid Dynamics (CFD) equations, for a laminar, stationary and Newtonian flow, are employed to simulate the fluid flow over the top surface of the organoid (Eqs. (4-6)):

$$\rho(\boldsymbol{u}\cdot\nabla)\boldsymbol{u} = \nabla\cdot[-p\boldsymbol{I} + \mu(\nabla\boldsymbol{u} + (\nabla\boldsymbol{u})^T)] + \boldsymbol{F} \quad in \quad \Omega_F(\boldsymbol{x},t) \quad (4)$$

$$\boldsymbol{\sigma} = -p\boldsymbol{I} + \mu(\nabla\boldsymbol{u} + (\nabla\boldsymbol{u})^T) \quad in \quad \Omega_F(\boldsymbol{x},t) \quad (5)$$

$$\tau = \sqrt[2]{|\boldsymbol{t}|^2 - \sigma^2} \quad in \quad \Omega_F(\boldsymbol{x},t) \quad (6)$$

* Corresponding author. Email: **acmantis@us.es**

where, ρ is the density of the fluid (medium), $\boldsymbol{u}$ its velocity, μ its dynamic viscosity, p its pressure and $\boldsymbol{F}$ the volumetric force vector. $\boldsymbol{\sigma}$ is the Cauchy stress tensor and $\boldsymbol{t}$ the traction vector, with normal, σ, and tangential, τ, components. $\Omega_F(\boldsymbol{x}, t)$ is the evolutionary domain of the fluid flow. The obtained shear stress, τ, is then interpolated to a tangential force on the organoid cells.
To model the distribution of oxygen and nutrients, ω, a Fickean diffusion-reaction equation is used (Eq. (7)):

$$\frac{\partial \omega}{\partial t} = D_\omega \nabla^2 \omega - \kappa \omega \sum_i \delta\,(\boldsymbol{x} - \boldsymbol{x}_i) \quad in \quad \Omega_O(\boldsymbol{x}, t)\; U\; \Omega_H(\boldsymbol{x}, t) \qquad (7)$$

where the first term of the right hand side of Eq. (7), represents the Fickean diffusion and the second the organoid cell consumption. Cells are classified into proliferative, quiescent, hypoxic or necrotic layers, in the organoid domain, depending on the value of ω.

RESULTS

We analyze how the fluid inlet velocity and the rate of consumption of the organoid cells affect the maturation of endothelial cells, as shown in Figure 1.

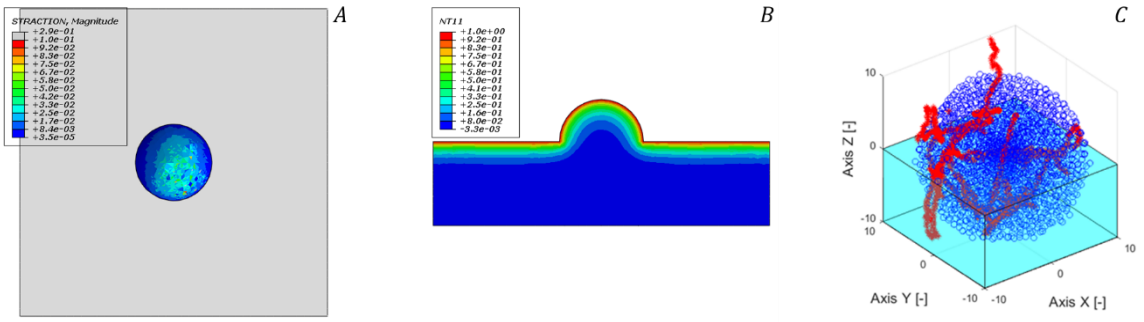

Figure 1. *A*: Top view of the Z = 0 plane of the shear stress distribution on the organoid boundary. *B*: Diffusion of oxygen and nutrients from the medium into the organoid and ECM *C*: Agent-based simulation showing the vascularized organoid.

DISCUSSION AND CONCLUSIONS

In this work, we have combined continuum and discrete models to reproduce how organoids evolve and vascularize when exposed to a controlled fluid flow. Our model successfully replicates the development of vasculature within the organoid, by integrating a CFD problem, nutrient and oxygen diffusion and organoid and blood vessel evolution into a numerical framework. Simulations highlight the role of fluid inlet velocity and nutrient consumption rate in the vascularization formation. Moreover, the mechanical interactions of the organoid with the ECM are considered. The results of the simulations qualitatively agree with *in vitro* results [7].

ACKNOWLEDGEMENTS

The authors gratefully acknowledge the financial support from project PID2021-126051OB-C42 by the Ministerio de Ciencia e Innovación (MCI), Agencia Estatal de Investigación (AEI) and Fondo Europeo de Desarrollo Regional (FEDER). Ana Carrasco-Mantis was supported by grant PRE2019-090391.

References

[1] Zhang, S., et al. Vascularized organoids on a chip: strategies for engineering organoids with functional vasculature. Lab on a Chip, 2021.
[2] LeSavage, B. L., et al. Next-generation cancer organoids. Nature materials, 2022.
[3] Bar-Ephraim, Y. E., et al. Organoids in immunological research. Nature Reviews Immunology, 2020.
[4] Salewskij, K., et al. Blood vessel organoids for development and disease. Circulation Research, 2023.
[5] Bull, J. A., et al. Mathematical modelling reveals cellular dynamics within tumour spheroids. PLoS computational biology, 2020.
[6] Carrasco-Mantis, A., et al. An *in silico* study on the influence of extracellular matrix mechanics on vasculogenesis. Computer Methods and Programs in Biomedicine, 2023.
[7] Homan, K. A., et al. Flow-enhanced vascularization and maturation of kidney organoids *in vitro* (2019).

RUPTURE STRENGTH IN LIVING CELL MONOLAYERS

Julia Duque[1], Alessandra Bonfanti[2], Jonathan Fouchard[3], Lucia Baldauf[1], Sara Azenha[4], Emma Ferber[1], Andrew Harris[5], Elias Barriga[6], Alexandre Kabla[7], Guillaume Charras[1,*]

1. University College London, UK; 2. Politecnico di Milano, Italy; 3. Institut de Biologie Paris Seine, France ; 4. Gulbenkian Institute of Science, Portugal ; 5. Carleton university, Canada; 6. TU Dresden, Germany; 7. University of Cambridge, UK

ABSTRACT

The ability of tissues to sustain mechanical stress and avoid rupture is a fundamental pillar of their function. Rupture in response to physiological levels of stress can be undesired, for example resulting from disease or genetic mutations, or be an integral part of developmental processes, such as during blastocoel formation in mouse or leg eversion in flies. Despite its importance, we know very little about rupture in cellularised tissues because it is a multi-scale phenomenon that necessitates comprehension of the interplay between mechanical forces and biological processes at the molecular and cellular scales.

Using a combination of mechanical measurements, live imaging and computational modelling, we characterise rupture in epithelial monolayers. We show that, despite consisting of only a single layer of cells, monolayers can withstand surprisingly large deformations, often accommodating several-fold increases in their length before rupture. At large deformation, epithelia increase their stiffness multiple-fold in a process controlled by a supracellular network of keratin filaments. Perturbing keratin organisation fragilised monolayers and prevented strain stiffening. Using computational approaches, we show that, although the kinetics of adhesive bond rupture ultimately control tissue strength, tissue rheology and the history of deformation prior to failure set the strain and stress that the tissue reaches at the onset of fracture.

Our data paint a picture of epithelia as versatile materials that combine resistance to shocks with deformability when subjected to low strain rates.

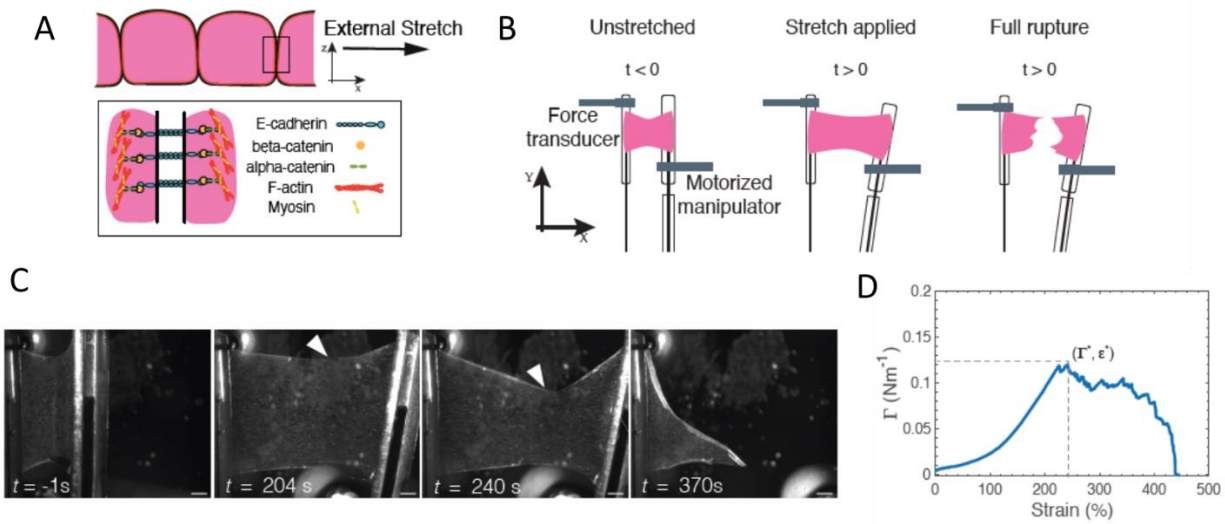

Figure 1: Epithelial monolayers rupture in response to excessive stretch. (**A**) Cellular-scale diagram of the epithelial monolayer. Top: profile view of the monolayer. Cells are linked to one another via specialized protein junctions. Bottom: zoom of an adherens junctions linking the F-actin cytoskeleton of neighbouring cells. The ectodomain of E-cadherin links cells to one another while its intracellular domain binds to the F-actin cytoskeleton via beta- and alpha-catenin. Myosin motor proteins bind F-actin to generate a cellular surface tension which results in a pre-tension in the monolayer. (**B**) Diagram of the experiment. Monolayers in pink are subjected to a ramp in deformation applied via displacement of one of the test rods. Stretch starts at time 0 and continues at a constant rate until full rupture of the monolayer. (**C**) Bright-field microscopy time series of an MDCK monolayer subjected to a ramp in deformation performed at 1% s^{-1}. Arrowheads indicate the crack tip. Time is indicated in the bottom left corner. Scale bar = 500 μm. (**D**) Evolution of monolayer tension as a function of applied strain for the monolayer shown in C. Dashed lines show the maximum tension Γ^* and strain ϵ^* coinciding with the appearance of the first defects. Full rupture of the monolayer takes place for ϵ=450%.

* Corresponding author. Email: **g.charras@ucl.ac.uk**

ACKNOWLEDGEMENTS

The authors would like to thank **the European Research Council (ERC), the British Biotechnology and Biological Sciences Research council (BBSRC), Politecnico di Milano, The European Molecular Biology Organisation (EMBO), La Caixa, Instituto Gulbenkian, Fundacao Calouste Gulbenkian, Deustsche Forschung Gemeinschaft (DFG)** for providing financial support to this project.

Cell migration and morphogenesis in viscoelastic matrices

Ovijit, Chaudhuri[1,*]

1. Department of Mechanical Engineering, Stanford University, USA

The extracellular matrix (ECM) is a complex assembly of structural proteins that provides physical support and biochemical signaling to cells in tissues. Over the last two decades, studies have revealed the important role that ECM elasticity plays in regulating a variety of biological processes in cells, including stem cell differentiation and cancer progression. However, tissues and ECM are often viscoelastic, displaying stress relaxation over time in response to a deformation, and viscoplastic, exhibiting irreversible deformations in response to mechanical stress. In this talk, I will discuss our recent findings on how matrix viscoelasticity regulates various biological processes, including collective invasion by cancer cells, morphogenesis of pluripotent stem cells, and monocyte migration.

WHAT MECHANICAL QUANTITY DO CELLS REGULATE IN SOFT TISSUES?

Christian J. Cyron[1,2,*], Daniel Paukner[1,2], Roland C. Aydin[1,2], Jay D. Humphrey[3]

1. Hamburg University of Technology, Germany; 2. Helmholtz-Zentrum Hereon, Germany; 3. Yale University, USA

INTRODUCTION

In soft biological tissues, cells seek to establish and maintain a preferred mechanical state, the so-called homeostatic state. This state is marked by a specific (non-zero) tensile stress. However, so far, it remains controversial whether cells directly regulate stress or whether they primarily control some other target quantity from which tensile stress results as a consequence [1]. Understanding what target quantity cells are primarily regulating in soft tissues and how they are doing this is one of the key questions of currrent soft tissue biomechanics and mechanobiology. Answering it will be an important step towards predictive computer simulations of growth and remodeling in soft tissues, which play key roles in various areas ranging from tissue engineering to clinical healthcare (e.g., aneurysms).

MATERIALS AND METHODS

We have developed a combined experimental [2] and computational framework [3] to study the micromechanical and mathematical foundations of mechanical homeostasis in soft biological tissues (Fig. 1). Our experimental setup allows well-controlled biaxial stress and strain states in tissue equivalents. Our computational framework models soft tissues as networks of discrete fibers and cells. The interactions between both are represented by a detailed model of focal adhesions.

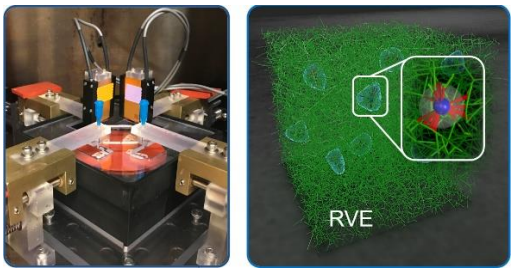

Figure 1. Combined experimental (left) and computational (right) framework to study interactions between cells and extracellular matrix (ECM)

RESULTS

We carefully validated our model and demonstrated an excellent agreement between the experimental and computational results, for example, for the scaling relation between fiber density and homeostatic stress level (Fig. 2, left). Subsequently, we developed a simple mechanical analog model to understand our results in a mechanistic sense (Fig. 2, center) and confirmed that our computational model could reproduce also advanced phenomena such as durotaxis (Fig. 2, right).

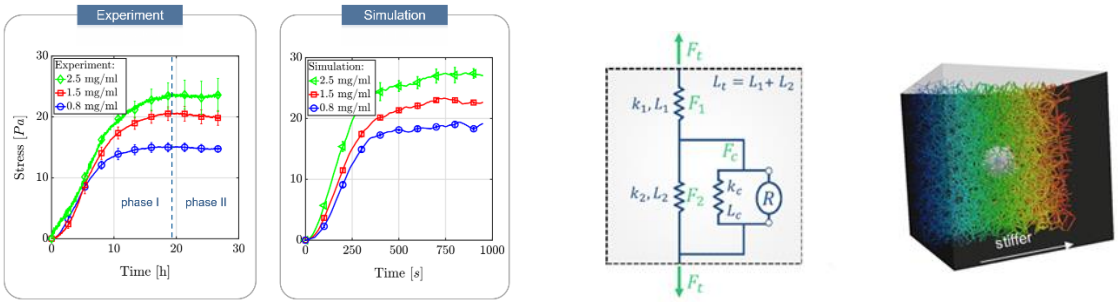

Figure 2. Agreement between homeostatic stress in experiments and simulation model for different collagen fiber densities (left); mechanical analog model developed to understand and interpret experimental and computational results (center); simulation of durotaxis (right)

* Corresponding author. Email: **christian.cyron@tuhh.de**

DISCUSSION AND CONCLUSIONS

Combining and interpreting extensive experimental and computational studies with our mechanical analog model, we were able to identify the key factors and processes in the homeostasis of soft tissues, in particular the target quantity that cells regulate [4]. On the micro-scale and on short time scales, this target quantity appears to be the forces exerted by the cells on the surrounding extra-cellular matrix (ECM). Future work may focus on the question whether this observation can be expressed in the form of a simple continuum mechanical target quantity or conservation law and how to leverage this understanding for developing a new generation of continuum-scale models of growth and remodeling in soft biological tissues.

ACKNOWLEDGEMENTS

The authors would like to thank the International Graduate School for Science and Engineering (IGSSE) of the Technical University of Munich as well as Hamburg University of Technology and Helmholtz-Zentrum Hereon for providing financial support to this project.

References

[1] Ambrosi et al.: *Growth and remodelling of living tissues: perspectives, challenges and opportunities.* Journal of the Royal Society Interface Vol. 16, p. 20190233, The royal society publishing 2019.

[2] Eichinger et al.: *Computer-controlled biaxial bioreactor for investigating cell-mediated homeostasis in tissue equivalents*. Journal of biomechanical engineering Vol. 142, p. 071011, ASME 2020

[3] Eichinger et al.: *A computational framework for modeling cell–matrix interactions in soft biological tissues.* Biomechanics and modeling in mechanobiology Vol. 20, pp. 1851-1870, Springer 2021

[4] Eichinger et al.: *What do cells regulate in soft tissues on short time scales?.* Acta biomaterialia Vol. 134, pp. 348-356, Elsevier 2021

HIGH THROUGHPUT MECHANICAL DISRUPTION OF PLASMA MEMBRANE AND NUCLEAR ENVELOP FOR REPAIR DYNAMIC STUDY

Apresio K. Fajrial[1], Leyla Akh[2], and Xiaoyun Ding[1,2,3,*]

1 Paul M. Rady Department of Mechanical Engineering, University of Colorado, Boulder, CO 80309, USA.
2 Biomedical Engineering Program, University of Colorado, Boulder, CO 80309, USA.
3 BioFrontiers Institute, University of Colorado, Boulder, CO 80309, USA.

INTRODUCTION

Understanding the dynamics of mechanical disruption at plasma membrane and nuclear envelope as well as how they maintain the integrity are invaluable for gaining insights into health disorders [1]. Moreover, controlling the disruption of the plasma membrane and nuclear envelope can be used as a promising strategy for intracellular delivery [2]. Here we report a new technique that could help address the challenge of inadequate understanding of plasma membrane, particularly nuclear envelope, mechanical disruption and recovery response through our proposed novel NEST microfluidic platform which can precisely disrupt both plasma and nuclear membranes homogeneously at high throughput. To study membrane repair dynamics, we monitor the endosomal sorting complexes required for transport (ESCRT) machinery after mechanoporation. The ESCRT complexes play an essential role in plasma membrane and nuclear envelope repair [3,4]. We show that the CHMP4B protein, a component of the ESCRT complex, aggregates mainly at the nucleus-cytoplasm boundary, with tenfold higher intensity than untreated cells. We investigate the spatial localization of the ESCRT protein, indicating that the major wound location is only in a single spot. Our platform is a useful tool to study biological processes related to wound repair on the plasma membrane and nuclear envelope by creating precise and controlled membrane disruption.

MATERIALS AND METHODS

The working mechanism of the nanostructured microfluidics platform is illustrated in Figure 1A. Figure 1B shows the fabricated device and electron micrograph of the parallel microchannel with integrated sharp tip nanostructures for high-throughput deterministic mechanoporation. HeLa cells expressing CHMP4B-GFP protein were maintained in culture media with geneticin. Before the experiment, the HeLa CHMP4B-GFP cells were stained with Hoechst 33342 to observe the nucleus. After treatment, cells were fixed at time points 5, 15, and 30 minutes. Fixed cells were observed in a laser scanning confocal microscope and analyzed using Fiji ImageJ and Python with the scikit-image library.

RESULTS AND DISCUSSION

We compared the distribution of CHMP4B protein between untreated and mechanoporated samples. The CHMP4B protein in the untreated sample is distributed throughout the cell cytosol, with strong localization in the nucleus (Figure 2A). After nanostructured microfluidics treatment, the CHMP4B protein aggregated outside the nucleus envelope (Figure 2B). Notably, the cell allocates most of the resources to the wound site, vacating CHMP4B from the nucleus. We quantified the fluorescence intensity of the CHMP4B protein from the confocal images (Figure 2C and Figure 2D). Figure 2E shows the CHMP4B aggregation dynamics after mechanoporation. At 5 minutes, the CHMP4B protein showed maximum localization intensity (Figure 2F). The CHMP4B protein profile returned to before treatment after 15 minutes. Our confocal imaging also showed that the NEST device was able to generate a rupture of 6-10 um at plasma membrane while only penetrating a pore of 1-2 um at nuclear envelope, indicating a very different disruption dynamics on those two membrane systems. To assess the spatial distribution of the CHMP4B, we analyzed multiple cell images using stacking workflow. We created a probability density distribution of the CHMP4B protein within the cells at different time points. This analysis revealed that mechanoporation treatment triggered CHMP4B aggregation in a single spot with the highest density near the nuclear envelope. Altogether, our device serves as a powerful tool in controlling the disruption of the plasma membrane and nuclear envelope to millions of cells in seconds.

ACKNOWLEDGEMENTS

The authors would like to thank financial support to this project from the NIH MIRA Award 1R35GM142817, W. M. Keck Foundation Research Grant, and the University of Colorado Boulder Research & Innovation Seed Grant. Part of the microfabrication of the devices was performed in the Utah Nanofabrication facility at the University of Utah.

* Corresponding author. Email: **Xiaoyun.Ding@colorado.edu**

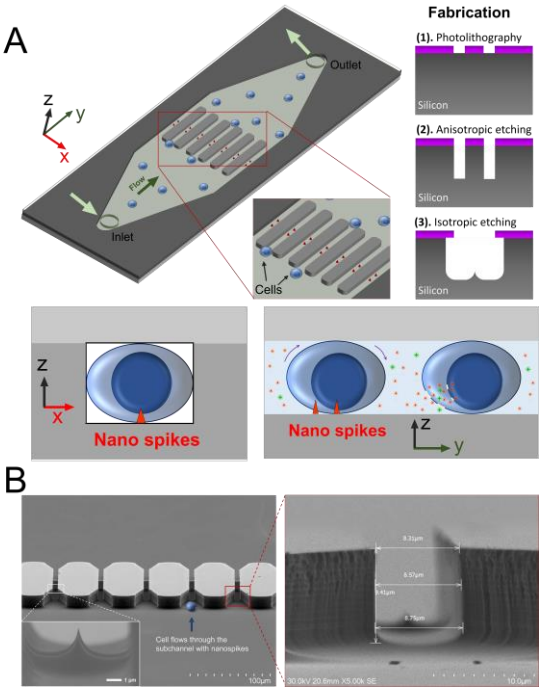

Figure 1 | Working mechanism of nanoengineered surface technology. (**a**) Schematic of the NEST microfluidic device. A simple and standard microfabrication is needed for device manufacturing. Each subchannel is smaller than cell size to enable a hard contact between cell and nano spikes. The number and size of pores is determined by the number and geometry of nanospikes fabricated in each subchannel. (**b**) SEM images of nanospikes (**a**) in silicon microchannel. Each microchannel has 1 or more nanospikes as desired and has a height of 8 um – 25 um and a width of 8 um – 12 um, to be adjusted to fit target cells.

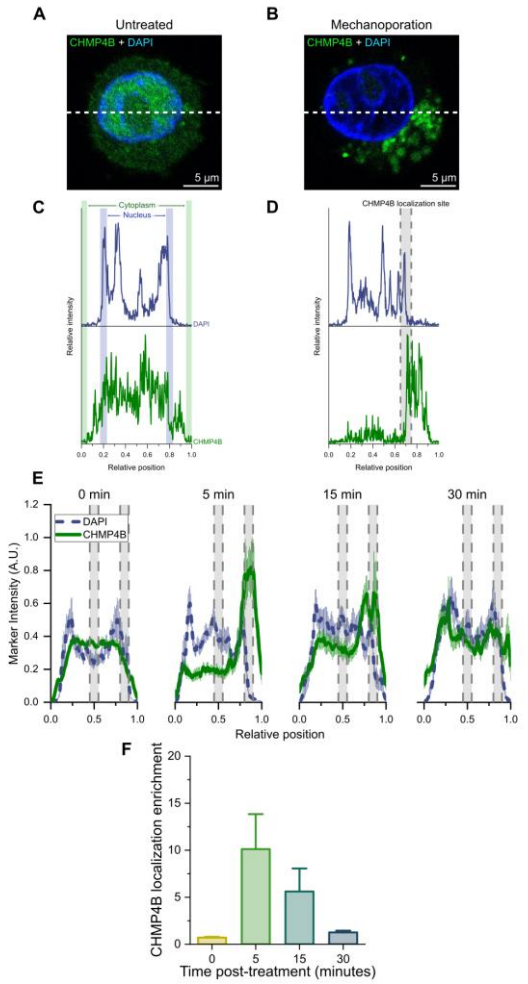

Figure 2 | Figure 2: CHMP4B protein localization analysis in HeLa cells. A. CHMP4B protein distribution in untreated control cells. B. CHMP4B protein distribution of cells after nuclear mechanoporation. C, D. Fluorescence intensity profile from dashed white lines in A and B, respectively. E. Fluorescence intensity profile of HeLa CHMP4B-GFP at time point 0, 5, 15, and 40 minutes after treatment. F. Localization enrichment of CHMP4B at aggregation site by calculating the ratio of fluorescence intensity between the edge gray band and the center gray band in E. n = 12-15. Error bars represent SEM.

References

[1] Hatch, E & Hetzer, M "Breaching the nuclear envelope in development and disease," J Cell Biol, 2014

[2] Stewart, MP, et al. "Intracellular Delivery by Membrane Disruption: Mechanisms, Strategies, and Concepts," Chem Rev, 2018

[3] Denais, C. M. et al. "Nuclear envelope rupture and repair during cancer cell migration," Science, 2016

[4] Raab, M. et al. "ESCRT III repairs nuclear envelope ruptures during cell migration to limit DNA damage and cell death," Science, 2016

PAN-TISSUE SCALING OF MECHANOREGULATED GENES AND HERITABLE GENETIC CHANGES IN CANCER

Dennis Discher[1*]

1. Molecular Cell Biophysics Lab, University of Pennsylvania, Philadelphia, USA

INTRODUCTION

Scaling relations are foundational to physical science and potentially apply to the mechanobiology of some genes across tissues and species. We showed previously that the levels of Lamin-A nuclear filaments and Collagen-1 matrix fibers exhibit power laws versus tissue stiffness, from soft brain to stiffer muscle and bone [1,2].

MATERIALS AND METHODS

Pan-tissue public data shows Piezo1 and YAP1/TAZ exhibit similar trends and define a 'mechanoregulated' supercluster in whole genome genescapes. Focused experiments fit use-it-or-lose-it models of stress-stabilized protein with transcriptional feedback, whereas related genes such as Lamin-B1 and Piezo2 are only mechanosensitive in function.

RESULTS

Lamin-B1 particularly responds to high Gaussian curvature, with nuclear indentation – even by small lipid droplets – causing local dilution and nuclear rupture. Chromatin breaching from rupture sites sometimes occurs, which raises possibilities of chromosome loss. A novel fluorescence 'ChReporter' was therefore developed based on Lamin-B1 and other constitutive genes in order to visualize heritable chromosome losses, particularly after strong confinement of cells relevant to solid tissues and tumors.

DISCUSSION AND CONCLUSIONS

Our results suggest mechanoregulation of pervasive genetic changes in cancer and explain why such changes are more frequent and variable in solid tumors compared to soft or liquid tumors.

ACKNOWLEDGEMENTS

The author would like to thank NIH and NSF for providing financial support to this project.

References

[1] Swift J, Ivanovska IL, Buxboim A, Harada T, Dingal PC, Pinter J, Pajerowski JD, Spinler KR, Shin JW, Tewari M, Rehfeldt F, Speicher DW, Discher DE**.** *Nuclear lamin-A scales with tissue stiffness and enhances matrix-directed differentiation.* Science. Vol.341(6149):1240104. 2013.

[2] Cho Cho S, Vashisth M, Abbas A, Majkut S, Vogel K, Xia Y, Ivanovska IL, Irianto J, Tewari M, Zhu K, Tichy ED, Mourkioti F, Tang HY, Greenberg RA, Prosser BL, Discher DE. *Mechanosensing by the Lamina Protects against Nuclear Rupture, DNA Damage, and Cell-Cycle Arrest.* Developmental Cell. Vol. 49(6):920-935.e5. 2019.

High-throughput measurements of viscoelastic cell properties: Potential and limitations

Ben Fabry*

Department of Physics, University of Erlangen-Nuremberg, Erlangen, Germany

INTRODUCTION

Many cell functions are accompanied by phenotypic changes in viscoelastic properties, and their measurement can help elucidate higher-level cellular functions in health and disease. However, measurements of cell mechanical properties based on the relationship between applied forces and measured cell deformations face numerous challenges:

1) The forces and deformations are very small, on the order or even below the nano-Newton and micrometer range. This requires dedicated, highly specialized equipment, and experimental skill.

2) Cell-to-cell variability is very high, typically showing a log-normal distribution. For example, as cells spread on a substrate, cell stiffness typically increases. Moreover, cells are anisotropic, and mechanical properties of different organelles or cell regions (e.g. the nucleus versus the cell periphery) can differ by more than one order in magnitude. As different techniques for measuring cell mechanics have different probe sizes (e.g. AFM tip ~ 10 nm, magnetic bead ~ 1-5 μm), this too influences the results.

3) Cells display complex, frequency-dependent visco-elastic and visco-plastic properties [1]. As cell mechanical properties are typically expressed within the framework of a model, any discrepancies between the data and the model, e.g. regarding frequency dependence and linearity, lead to erroneous results and interpretations.

4) Cell mechanical properties fluctuate over time and change in a time-dependent manner after interventions, e.g. after trypsinization, after attaching magnetic beads etc.

5) Most active techniques to measure cell mechanics involve probing the cell with a defined force and subsequently measuring the deformation responses. However, cells are often mechano-sensitive, and hence can respond to the applied forces with altered mechanical properties.

Taken together, techniques for measuring cell mechanics should therefore be technically simple, have a high throughput, and allow researchers to probe cell mechanics over a range of frequencies or time scales, and deformation amplitudes. A technique that fulfils these criteria is shear flow deformation cytometry [2].

MATERIALS AND METHODS

Shear flow deformation cytometry is a quantitative, low-cost, high-throughput, and simple method to measure the viscoelastic properties of cells, specifically the storage modulus G', and the loss modulus G", as a function of frequency. The cells are suspended in a high-viscosity (0.5–10 Pa s) fluid (e.g. a 2% alginate solution) and are pumped at pressures of typically between 50–300 kPa through a several cm long microfluidic channel with a square cross section (200x200 μm). The fluid shear stress induces large cell deformations that are imaged using a CCD camera at frame rates of up to 500 frames/s to achieve a measurement throughput of up to 100 cells/s.

The method takes advantage of two physical principles: First, the shear stress profile inside a long microfluidic channel depends only on the pressure gradient along the channel, which can be precisely controlled, and the channel geometry, which is fixed. Importantly, the shear stress profile does not depend on the viscosity of the cell suspension medium and smoothly increases from zero at the channel center to a maximum value at the channel walls. Accordingly, cells appear circular near the channel center and become increasingly elongated near the channel walls. As the width of the channel is significantly larger than the cell diameter, fluid shear stresses remain approximately constant across the cell surface, which considerably simplifies the fluid dynamics computations [3]. From the stress-strain relationship, we estimate the storage modulus of the cell, which characterizes its elastic behavior.

Second, depending on the flow speed profile inside the channel, the cells rotate in a tank-treading manner. Tank-treading in combination with the cell's viscous properties leads to energy dissipation, which limits the increase of cell strain at higher stresses near the channel walls. From this behavior, we extract the loss modulus of the cell, which characterizes its viscous behavior [3]. Since the microfluidic channel is several centimeters long, cell deformations are in a steady state, which greatly simplifies the calculation of viscoelastic cell parameters.

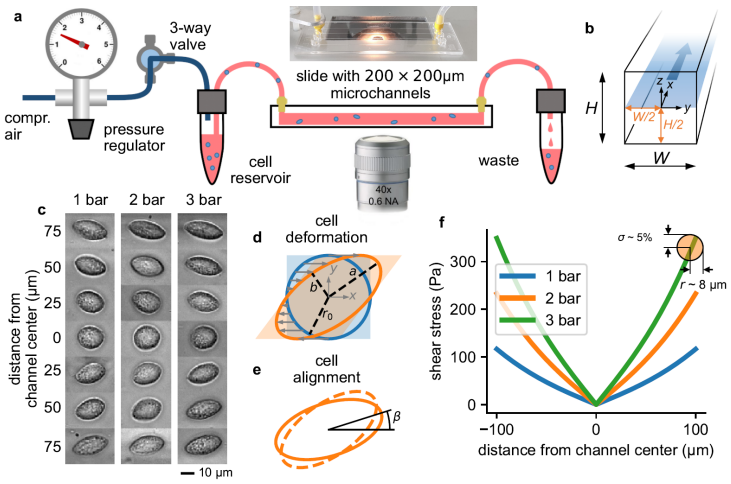

Measurement setup and principle [2]. **a**) Schematic of the microfluidic device. **b**) Cross section through the microchannel with dimensions $W = H = 200$ µm. The focal plane of the microscope at a height of $H/2 = 100$ µm is indicated by the blue shaded area. Fluid flow is in x direction. **c**) Bright field images of NIH-3T3 cells under control conditions at different y-positions in a microchannel at a pressure of 1, 2, and 3 bar. Cells appear round in the channel center and become more elongated near the walls. **d**) Illustration of cell deformations under fluid shear. The circular cell with radius r_0 (blue) is transformed to an elliptical shape (orange) with semi-major axis a and semi-minor axis b depending on the ratio of fluid shear stress and the cell's shear modulus. **e**) The sheared cell (dashed outline) will partially align in flow direction (solid outline), characterized by an alignment angle β. This angle depends on the ratio of cell viscosity and suspension fluid viscosity . a, b and β are measured from the segmented cell shapes. **f**) Fluid shear stress versus distance from the channel center in y-direction for three different pressures of 1, 2 and 3 bar. The shear stress varies by 5% across the cell surface for a typical cell with a radius of 8 µm (indicated by the orange circle).

RESULTS

Using cell lines and calibrated polyacrylamide beads, we verify that our method provides accurate quantitative measurements of viscoelastic properties. Measurement results are not or only marginally influenced by experimental details such as the viscosity of the suspension fluid or the time point after suspending the cells. We demonstrate that the cell's viscoelastic properties measured with our method conform to soft glassy power-law rheology that has been reported for a wide range of cells measured with different methods [4]. We also show that our method can be used for dose-response measurements of drugs that induce actin cytoskeleton disassembly, and that these responses are modulated by the cell cycle and the intermediate filament network of the cells.

Although the method meets all of the criteria listed in Introduction, there are several inherent limitations. Cells must be in suspension, which requires that adherent cells are detached from the substrate to which they normally adhere. This harvesting step triggers a major reorganization of the cytoskeleton, in a time-dependent manner. Currently, it is impossible to extrapolate from the measurements of suspended cells to their mechanical properties prior to detachment from the substrate. Moreover, each cell can only be measured at a given shear stress and tank treading frequency, both of which are determined by the (fixed) position of the cell relative to the channel center. Any shear stress or frequency dependency can therefore only be measured across different cells to obtain a population average. Also, the theoretical framework to extract the cell's visco-elastic properties assumes linearity and homogeneity. All of this requires researchers using this or related techniques to exercise caution when interpreting the results.

References

[1] N. Bonakdar, R. Gerum, M. Kuhn, M. Sporrer, A. Lippert, W. Schneider, K.E. Aifantis, B. Fabry, Mechanical plasticity of cells, Nat Mater 15(10) (2016) 1090-4.

[2] R. Gerum, E. Mirzahossein, M. Eroles, J. Elsterer, A. Mainka, A. Bauer, S. Sonntag, A. Winterl, J. Bartl, L. Fischer, S. Abuhattum, R. Goswami, S. Girardo, J. Guck, S. Schrüfer, N. Ströhlein, M. Nosratlo, H. Herrmann, D. Schultheis, F. Rico, S.J. Müller, S. Gekle, B. Fabry, Viscoelastic properties of suspended cells measured with shear flow deformation cytometry, eLife 11 (2022) e78823.

[3] R. Roscoe, On the rheology of a suspension of viscoelastic spheres in a viscous liquid, J.Fluid Mechanik (1967) 21.

[4] B. Fabry, G.N. Maksym, J.P. Butler, M. Glogauer, D. Navajas, J.J. Fredberg, Scaling the microrheology of living cells, Phys Rev Lett 87(14) (2001) 148102.

MESO-SCALE MODELLING OF THE ARTERIAL VESSEL WALL

Maïté Marie Pétré[1,2], Greet Kerckhofs[1,3], Lauranne Maes[2], Nele Famaey[2*]

[1]Institute of Mechanics, Materials and Civil Engineering (iMMC), UCLouvain, Belgium; [2]Department of Mechanical Engineering, KU Leuven, Belgium; [3]Department of Materials Engineering, KU Leuven, Belgium

INTRODUCTION

Multiscale modelling is increasingly used to link mechanobiological pathways at the cellular and subcellular level to the tissue scale level [1]. However, accurate calculation of load transfer to the cells and extracellular matrix is challenging in biological tissues with a complex and heterogeneous microstructure. Also conversely, the translation of cellular activity to mechanical changes at the tissue scale requires a number of assumptions regarding homogenization. Representative volume element (RVE) models at the meso-scale can bridge this gap, whereby the challenge is to populate these RVE's with microstructurally informed constituents and reliably model their interactions. For arterial tissue for example, Dalbosco et al. defined a RVE that incorporates two collagen fiber families by embedding truss elements in a solid matrix to capture their orientation and dispersion [2]. In this study, we investigate how to include other constituents into the RVE.

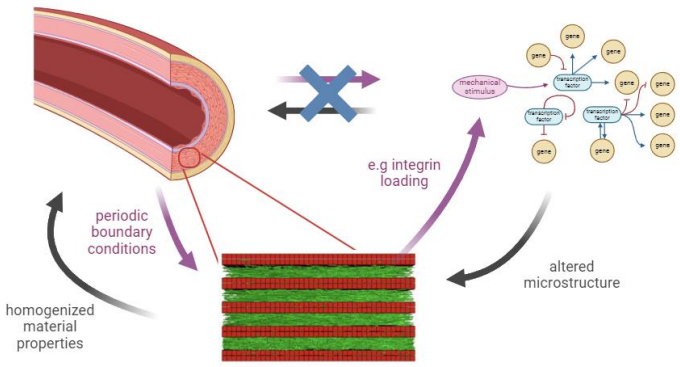

Figure 1. Inserting a meso-scale RVE to enable proper translation from the tissue scale to the cellular scale. The purple arrows are considered in this abstract. *(image partially generated using biorender.com)*

MATERIALS AND METHODS

An RVE of 120 x 120 x 65 μm³ was created using PyVista, comprising five elastic lamellae with 15μm thickness, arranged at regular separation intervals. Elastin struts and interlamellar elastin fibers (IEFs) link the lamellae, connecting the respective lower and upper planes. Also between these lamellae, collagen fibers are deposited, according to a preferred orientation and dispersion dictated by probability density functions [2]. Finally, smooth muscle cells are included as spheroids with their long axis parallel to the lamellae. These constituents are embedded in a ground matrix, which can be considered as the interstitial fluid. All microstructural parameters in terms of volume fraction, geometry, orientation, length and thickness were derived from 3D contrast-enhanced computed tomography (CECT) scans of the medial layer of porcine aorta [3] and relevant literature using scanning electron microscopy, second harmonic generation microscopy and histology [4], [5], [6], [7], [8].
Collagen fibers, elastin struts, and IEFs are represented by truss elements (T3D2), elastic lamellae by shell elements (S4R), and the ground matrix and SMCs by solid elements (C3D8RH and C3D4RH), as illustrated in Fig. 2. The elastin constituents, SMCs and ground matrix are represented by a neo-Hookean material model, whereas the collagen fibers have a strain energy density function implemented into a user-defined material model (UMAT) as

$$\Psi_{c_i}(\lambda) = \begin{cases} 0, if\ 0 < \lambda < \lambda_{r_i} \\ \frac{E_f}{2}\left(\lambda - \lambda_{r_i}\right)^2, if\ \lambda \geq \lambda_{r_i} \end{cases} \quad (1)$$

in which the fiber recruitment stretch of each individual fiber λ_{r_i} is given by a β distribution, with mean value 1.31 [2]. All mechanical model parameters were estimated from literature [2], [6], [8], [9].
For model validation, periodic boundary conditions are assigned to replicate a uniaxial tensile test. The results in terms of macroscopic stress-strain behaviour are compared to actual uniaxial tensile tests of porcine aorta performed at FIBEr, KU Leuven Core Facility for Biomechanical Experimentation. Next, periodic boundary conditions are assigned to replicate *in vivo* loading conditions. Virtual strain gauges are placed at the location of the integrins which link the cortex of the SMCs to neighbouring extracellular matrix.

* Corresponding author. Email: **nele.famaey@kuleuven.be**

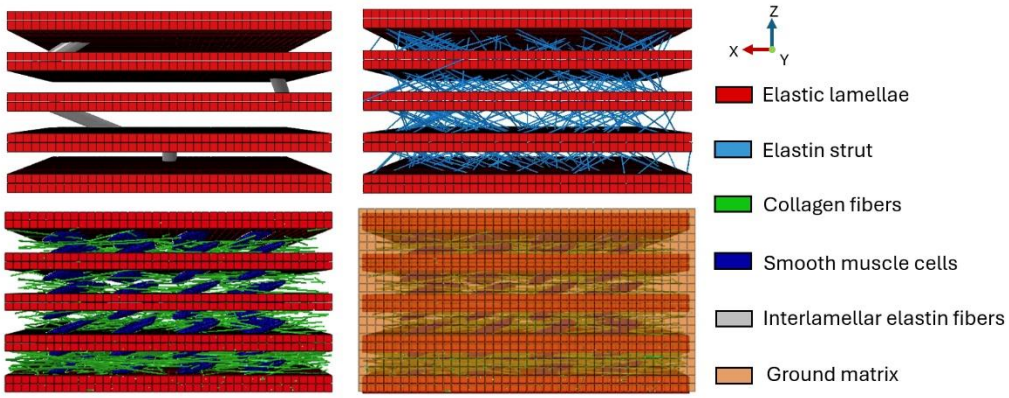

Figure 2. The different constituents of the RVE of the medial layer of a porcine aorta, all constituents are included into the ground matrix of the RVE using the 'embedding' option in Abaqus.

RESULTS

Figure 3 shows the results of the model validation, in casu the homogenized response of the RVE and experimental data on porcine aorta, as well as the SMC contribution to the total stress.

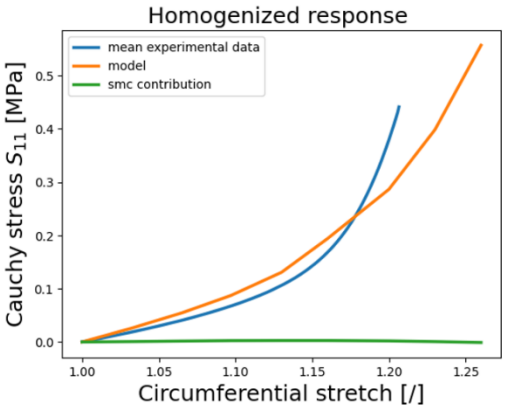

Figure 3. Results of model validation

DISCUSSION AND CONCLUSIONS

Rather than directly linking a macro-scale tissue model to a cellular scale regulatory model, an RVE was developed to allow for a more accurate representation of load transfer. The model shows a relatively good correlation with actual experimental results. However, the contribution of the SMC to the total stress appears low which might be due to the method with which the constituents are embedded into the ground matrix. Future work should be aimed at further optimizing connection methods between the different constituents, as well as the coupling of the three scales in both directions to enable simulation of growth & remodeling due to e.g. elevated mechanical loading.

ACKNOWLEDGEMENTS

This research was supported by the Research Foundation Flanders (SB/1S64923N and G088020N)

References

[1] L. Maes *et al.*, "Cell signaling and tissue remodeling in the pulmonary autograft after the Ross procedure: a computational study," *J Biomech*, Submitted, 2024.

[2] M. Dalbosco, T. A. Carniel, E. A. Fancello, and G. A. Holzapfel, "Multiscale numerical analyses of arterial tissue with embedded elements in the finite strain regime," *Comput Methods Appl Mech Eng*, vol. 381, p. 113844, Aug. 2021, doi: 10.1016/j.cma.2021.113844.

[3] L. Leyssens *et al.*, "Non-destructive 3D characterization of the blood vessel wall microstructure in different species and blood vessel types using contrast-enhanced microCT and comparison with synthetic vascular grafts.," *Acta Biomater*, vol. 164, pp. 303–316, Jul. 2023, doi: 10.1016/j.actbio.2023.04.013.

[4] M. OCONNELL *et al.*, "The three-dimensional micro- and nanostructure of the aortic medial lamellar unit measured using 3D confocal and electron microscopy imaging☆," *Matrix Biology*, vol. 27, no. 3, pp. 171–181, Apr. 2008, doi: 10.1016/j.matbio.2007.10.008.

[5] A. Giudici, I. B. Wilkinson, and A. W. Khir, "Review of the Techniques Used for Investigating the Role Elastin and Collagen Play in Arterial Wall Mechanics," *IEEE Rev Biomed Eng*, vol. 14, pp. 256–269, 2021, doi: 10.1109/RBME.2020.3005448.

[6] C. Morin, W. Krasny, and S. Avril, "Multiscale Mechanical Behavior of Large Arteries," Dec. 2019, doi: 10.1016/B978-0-12-801238-3.99934-3.

[7] Y. Zhu *et al.*, "Temporal analysis of vascular smooth muscle cell elasticity and adhesion reveals oscillation waveforms that differ with aging," *Aging Cell*, vol. 11, no. 5, pp. 741–750, Oct. 2012, doi: 10.1111/j.1474-9726.2012.00840.x.

[8] H. Mozafari, C. Zhou, and L. Gu, "Mechanical contribution of vascular smooth muscle cells in the tunica media of artery," *Nanotechnol Rev*, vol. 8, no. 1, pp. 50–60, May 2019, doi: 10.1515/ntrev-2019-0005.

[9] J. Gosline, M. Lillie, E. Carrington, P. Guerette, C. Ortlepp, and K. Savage, "Elastic proteins: biological roles and mechanical properties," *Philos Trans R Soc Lond B Biol Sci*, vol. 357, no. 1418, pp. 121–132, Feb. 2002, doi: 10.1098/rstb.2001.1022.

TWOFOLD MECHANOSENSITIVITY ENSURES ACTIN CORTEX REINFORCEMENT UPON PEAKS IN MECHANICAL TENSION

Elisabeth Fischer-Friedrich[1,*]

1. Physics of Life, Technische Universität Dresden, Dresden, Germany

ABSTRACT

The actin cortex is an active biopolymer network underneath the plasma membrane at the periphery of mammalian cells. It is a major regulator of cell shape through the generation of active cortical tension. In addition, the cortex constitutes a mechanical shield that protects the cell during mechanical agitation. Cortical mechanics is tightly controlled by the presence of actin cross-linking proteins that dynamically bind and unbind actin filaments. Cross-linker actin bonds are weak non-covalent bonds whose bond lifetime is likely affected by mechanical tension in the actin cortex making cortical composition inherently mechanosensitive. Here, we present a quantitative study of changes in cortex composition and turnover dynamics upon short-lived peaks in active and passive mechanical tension in mitotic HeLa cells. Our findings disclose a twofold mechanical reinforcement strategy of the cortex upon tension peaks entailing i) a direct catch-bond mechanosensitivity of cross-linkers filamin and α-actinin and ii) an indirect cortical mechanosensitivity that triggers actin cortex reinforcement via enhanced polymerization of actin. We thereby disclose a 'molecular safety belt' mechanism that protects the cortex from injury upon mechanical challenges.

* Corresponding author. E-mail: elisabeth.fischer-friedrich@tu-dresden.de

RECURSIVE CELL-MATRIX FEEDBACK IN FIBROBLASTS

Xiangjun Peng[1],Ziyao Jia[1], Wenlong Xiao[2], Yuxuan Huang[3], Elliot L. Elson[3], Guy M. Genin[3,*], Xi-Qiao Feng[1,*]

1. Department of Engineering Mechanics, Applied Mechanics Laboratory, Institute of Biomechanics and Medical Engineering, Tsinghua University, Beijing, China; 2. Department of Equipment, Xiangyang Central Hospital, Affiliated Hospital of Hubei University of Arts and Science, Xiangyang, China; 3. NSF Science and Technology Center for Engineering Mechanobiology, Dept. of Mechanical Engineering and Materials Science, Washington University, St. Louis, MO, USA

INTRODUCTION

Most animal cells reside within a 3D fibrous extracellular matrix (ECM), and interact with these fibers via integrin proteins on their surfaces. Tissue-level mechanical forces that travel through the fibers can reach cells, and transmit through the integrins to reach the cytoskeleton and nucleus. Nuclear deformation can affect gene expression, which can upregulate cell contractility and stiffening of the ECM by fiber remodeling via modulation of molecular motors like myosin and stress fibers. This cell-ECM feedback drives physiological and pathological processes, including wound healing, fibrosis, and development.

The ECM and its constituent fibers behave differently from most continua in that mechanical forces cause the fibers to become aligned and stiffened, in a way that is often irreversible. Cells harness these behaviors to remodel their surroundings in a way that can change the way that can, in turn, change the way that the cells themselves subsequently respond to force, initiating a positive feedback loop between cells and the ECM. Properties of the ECM such as fiber diameter, concentration, stiffness, and pore size affect the nonlinear properties of the ECM, which affects cell contractility. Increasing the ECM shear modulus increases tensile strains and stiffness in the vicinity of poles of the cell, which further increases cell contractility, actin alignment, and polarization. Cell contractility increases as well with ECM stiffness and collagen concentration.

Our goal was to formulate an integrated model of this cell-ECM feedback whose governing equations could be solved to develop closed form scaling laws for this behavior.

MATERIALS AND METHODS

Cell model: Myosin II motors in elongated cells interact with actin filaments to form force dipoles that can respond actively to mechanical factors in the external cellular microenvironment. These active forces increase as levels of F-actin and phosphorylated myosin light chain (p-MLC) rise in response to extrinsic tension, and work against passive resistance from cytoskeletal protein networks including the actin, microtubule and intermediate filament networks (Fig. 1). These forces were modeled with a coarse-grained contractility tensor of Shenoy and co-workers [1]. This model contains three parameters: a cell modulus E_c, a chemo-mechanical feedback parameter, α, and a chemical stiffness, β.

Matrix model: The strain-stiffening, transverse bucking ECM model based upon that of Ban, et al. [2-3] was used. This model was characterized by three parameters: a background stiffness, E_b , a strain-stiffening parameter, χ , and a critical tensile strain, ε_c beyond which fiber straightening begins.

Approach: We studied an isolated cell in a fibrous ECM that was approximated by the continuum matrix model (Fig. 1). The cell underwent active contraction, and reacted to changes in ECM stiffness via a number of mechanisms (Fig. 1c). These changes modulated the active contractility of the cell. Modulation of this active contractility was studied as a function of the active contraction and the six parameters of the combined model.

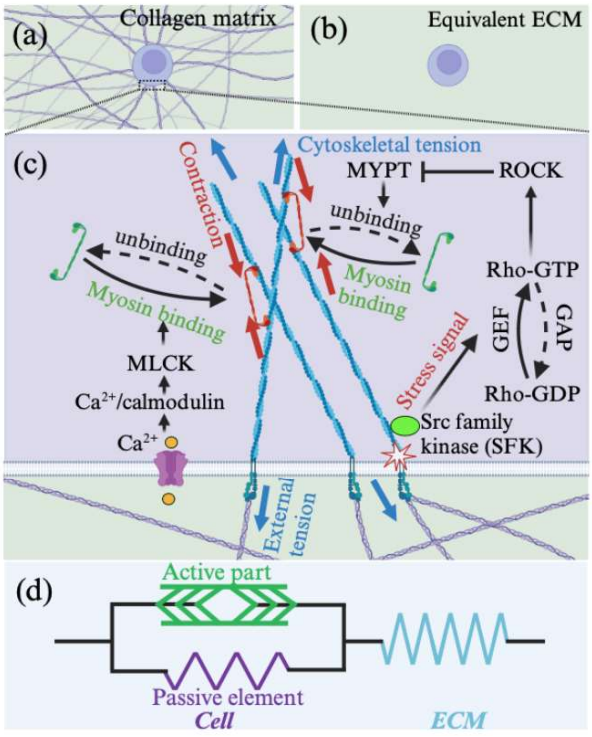

Figure 1. Traction fields recovered by each method showcased together with that of the ground truth scenario for the high noise case.

* Corresponding author. E-mail: genin@wustl.edu, fengxq@tsinghua.edu.cn

RESULTS

ECM stiffness and bio-chemo-mechanical feedback synergistically contribute to cell contraction. While the fact that cells perceive ECM stiffness is well known, the role of bio-chemo-mechanical coupling between the cell and ECM system is difficult to separate. Our model captures how cell-ECM coupling relates to stiffness (Fig. 2(a)). Cell-generated stress increases with increased ECM stiffness. The cell responded actively to this tensile stress by augmenting the concentration of phosphorylated myosin motors, resulting in heightened cell contractility as ECM stiffness increases (Fig. 2(b)). Despite the stress exhibiting linear decay in a linear elastic ECM following the scaling of the Eshelby solution, a stiffer ECM allows for longer stress transmission due to higher contractility activated by the more rigid matrix. However, it is important to note that such contractility is insufficient to cause noticeable deformation in the ECM. Consequently, the displacement field transmits over longer distances in the softer matrix.

Figure 2 highlights the impact of increasing the chemo-mechanical feedback parameter and the chemical stiffness parameter on the cell's response to its surrounding stiffness. A higher value of the chemo-mechanical feedback parameter α fortifies the stress-dependent feedback mechanism in our model, as the cell enhances myosin phosphorylation in response to matrix stiffness. This augmentation in the overall density of phosphorylated myosin motors subsequently amplifies the cell's generated active stress σ cell and cell contractility ρ. The radial displacement and stress in the ECM due to cell contraction extend further. In contrast to α, an elevated value of the chemical stiffness parameter β weakens the stress-dependent feedback mechanism of the cell by complicating motor recruitment. Consequently, an increase in β leads to a reduction in active stress and cell contractility. As a result, the displacement and stress in the ECM due to cell contraction transmit over shorter distances.

One of the most intrinsic characteristics of the collagen matrix is its limited capacity to withstand compression loads, leading to buckling. This phenomenon prompts an exploration into the buckling behavior of collagen fibers within the context of ECM interactions. As the softening parameter χ increases, indicating improved resilience of collagen fibers against compression, the displacement, and stress in the ECM due to cell contraction demonstrate extended transmission capacity (Fig. 3). This extension arises because the cell can exert greater contraction when the collagen fibers are more adept at bearing compression loads, resulting in higher cell stress and displacement at the cell-ECM interface. Normalizing the radial displacement to that of the cell-ECM interface displacement reveals a faster decay increasing χ (see Fig. 3(b)). This suggests that the compression softening property of collagen fibers enhances the transmission of force within the collagen matrix. The reason behind this enhancement lies in the reduction of resistance caused by the buckling of collagen fibers in the circumferential direction. This decrease results in diminished circumferential compression stress, making a smaller contribution to balancing the inward stress. Consequently, this promotes a higher radial stress and a slower ratio of displacement and stress decay. However, it is noteworthy that this property of compression softening may not be sufficient to trigger chemo-mechanical feedback within the cell, resulting in shorter force transmission in practical scenarios.

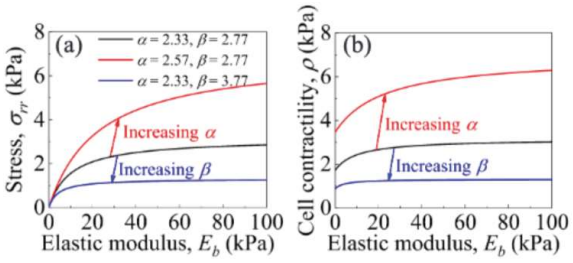

Figure 2. Traction fields recovered by each method showcased together with that of the ground truth scenario for the high noise case.

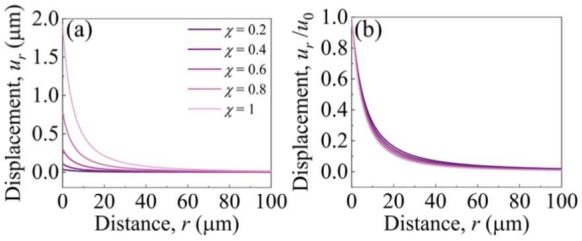

Figure 3. Traction fields recovered by each method showcased together with that of the ground truth scenario for the high noise case.

DISCUSSION AND CONCLUSIONS

In conclusion, this study developed an integrated cell-ECM model to characterize the feedback between cell contractility and ECM mechanics. It was found that ECM stiffness and cell contractility synergistically increase due to biochemical signaling and mechanical feedback. This positive feedback loop between cells and the ECM matrix has important implications in physiological and pathological processes like development, wound healing, and fibrosis.

References

[1] M. S. Hall, F. Alisafaei, E. Ban, X. Feng, C.-Y. Hui, V. B. Shenoy, and M. Wu, Fibrous nonlinear elasticity enables positive mechanical feedback between cells and ECMs, Proceedings of the National Academy of Sciences 113, 14043 (2016).

[2] E. Ban, H. Wang, J. M. Franklin, J. T. Liphardt, P. A. Janmey, and V. B. Shenoy, Strong triaxial coupling and anomalous poisson effect in collagen networks, Proceedings of the National Academy of Sciences 116, 6790 (2019).

[3] D. Shakiba, F. Alisafaei, A. Savadipour, R. A. Rowe, Z. Liu, K. M. Pryse, V. B. Shenoy, E. L. Elson, and G. M. Genin, The balance between actomyosin contractility and microtubule polymerization regulates hierarchical protrusions that govern efficient fibroblast–collagen interactions, ACS nano 14, 7868 (2020).

MICROMECHANICS OF CARDIAC SPHEROIDS

Dimosthenis Giannopoulos[1], Maja Schlittler[2], Marzia De Bortoli[2], Raffaele Coppini[3], Mina Petrovic[4], Elisabetta Cerbai[3], Gerhard Schütz[5], Philipp J. Thurner[1], Alessandra Rossini[2], Orestis G. Andriotis[1,*]

1. Institute of Lightweight Design and Structural Biomechanics, TU Wien, Austria;
2. Institute for Biomedicine, Eurac Research, Italy;
3. Department of Neuroscience, Psychology, Drug Sciences & Child Health, University of Florence, Italy;
4. Institute of Materials Science and Technology, TU Wien, Austria;
5. Institute of Applied Physics, TU Wien, Austria

INTRODUCTION

Uncontrolled cell growth and scar tissue formation, known as fibrosis, are hallmarks of hypertrophic cardiomyopathy (HCM) [1]. Cardiac fibroblasts (CF), responsible for tissue fibrosis, are mechanosensitive cells, and increased extracellular matrix (ECM) stiffness may contribute to fibrotic pathways leading to disease progression. TGF-β signalling plays a pivotal role in mediating fibrosis by activating CF. State-of-the-art cell culture techniques allow the development of 3D cellular spheroids that can be mechanically tested and characterized. Current analysis methods are often limited to Hertzian theory and its modifications, that only account for small deformations. However, spheroids exhibit low stiffness, thus undergoing large deformations at small external forces, and therefore current contact mechanics models fail to describe such behavior [2,3]. Here, we employ a hyperelastic model for large deformations to assess the mechanics of cell spheroids. As a case study, we compared the stiffness of HCM spheroids to that of control healthy ones and tested the effect of TGF-β treatment on the mechanics of both of these groups.

MATERIALS AND METHODS

Four groups of cell spheroids (Table 1), consisting of primary human fibroblasts cultured for two days (ethical approval, Nr. 5/2018 Ethical Committee of the Province of Alto Adige/South Tyrol & Nr. 19337_bio Regional Ethical Committee for the clinical experimentation of Tuscany), were subjected to parallel-plate compression testing (MicroSquisher, CellScale) fitted with a round tungsten cantilever and accompanying SquisherJoy V5.23 software (CellScale, Ontario, Canada). The fluid bath test chamber was filled with sterile phosphate buffered saline (pH=7.4). Stage and optics were calibrated according to manufacturer's instructions. Samples were compressed up to 50% apparent linear strain at different displacement rates. F–ε data was fitted using linear least squares regression on the Hertz and Tatara model and its extended version (custom MATLAB code) with fully constrained contact points (F=0, δ=0) [2,3]. During compression, images were captured via two digital cameras to determine lateral expansion of cell spheroids over a range of deformations. The effect of TGF-β on the collagen concentration was studied using the Zeiss LSM800 confocal microscope. The cell spheroids were stained with Picrosirius red solution.

Code name	Description
CU (n=50)	Control
CT (n=40)	Control + TGF-β
HCMU (n=25)	HCM
HCMT (n=17)	HCM + TGF-β

Table 1. Groups of cell spheroids tested.

RESULTS

Figure 1a shows the non-linear force response of a cell spheroid compressed up to 50% strain. Transition from softer behavior at small strains to a stiffer one at larger strains is observed. Hertzian theory can be applied from 10% to 30% compressive strain depending on the displacement rate. However, at larger strains, where the force follows the third and fifth power of the displacement, the Tatara model was successfully applied. This model was used to extract the stiffness of different cell spheroids and results are presented in Figure 1b. HCM spheroids exhibit a nearly three-fold higher stiffness compared to control (healthy) ones. Additionally, stiffness of cell spheroids treated with TGF-β is approximately twice that of the untreated groups, in both HCM and control spheroids.

* Corresponding author. Email: **orestis.andriotis@tuwien.ac.at**

This can be attributed to the increased collagen production in the treated spheroids (Figure 1c). Another advantage of the Tatara model is its capability to compute the deformed shape of the spheroid. The compression modulus was calculated for the new Poisson's ratio obtained from image analysis, showing 40% increase (Figure 1d).

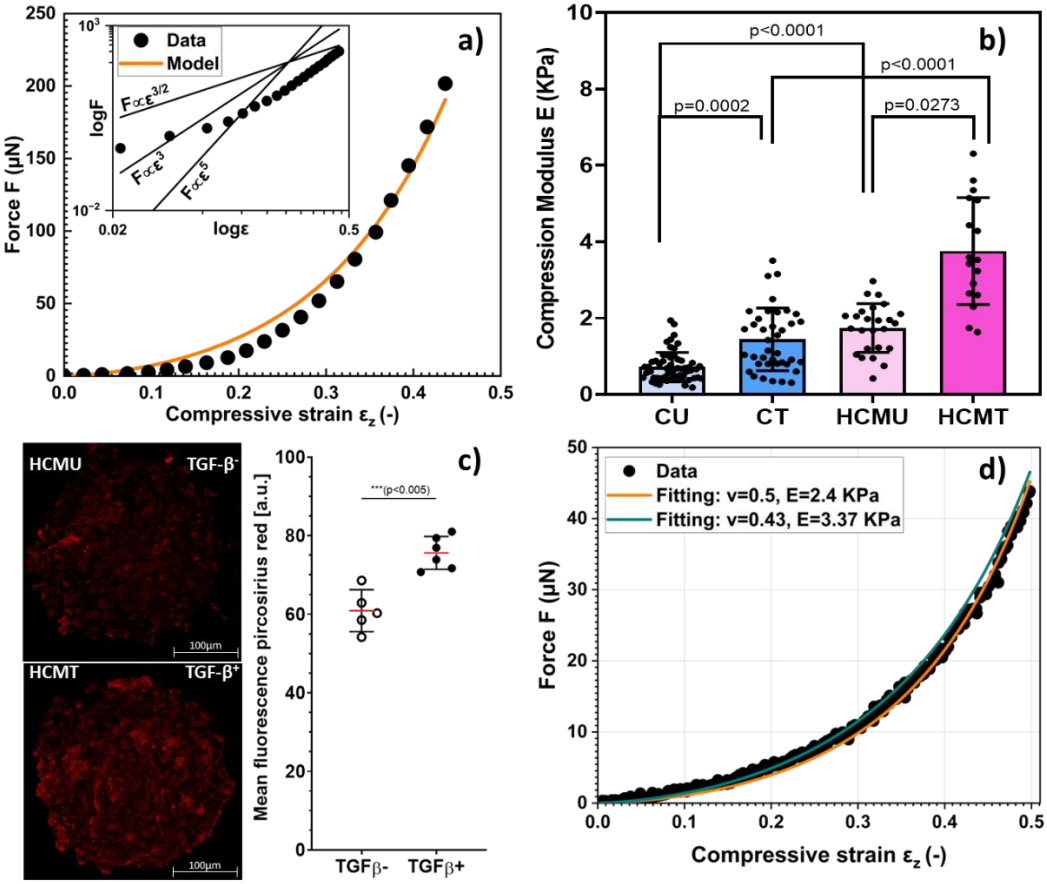

Figure 1. α) F-ε data of a spheroid fitted with the Tatara extended model, b) Compression modulus of samples tested, c) Confocal microscopy reveals accumulation of ECM in treated spheroids, d) Compression modulus correction via geometrical analysis.

DISCUSSION AND CONCLUSIONS

Linear elastic continuum mechanics with some important modifications can be applied to the case of large deformations. Beyond the effect of HCM on stiffening of cell spheroids, our results show that also TGF-β treatment noticeably influences spheroid stiffness. Possible mechanisms of this effect could be increased ECM production, crosslinking changes and enhanced cell contractility [4, 5]. HCM pathogenesis of cardiac fibrosis is yet to be fully understood and multiple mechanisms could contribute to tissue stiffening and disease progression, which can be studied with the models presented in a patient-specific manner.

ACKNOWLEDGEMENTS

This project has been funded by the Marie Skłodowska-Curie COFUND program under the EU Horizon 2020 research and innovation programme and the Autonomous Province of Bolzano/ Bozen South Tyrol in the framework of the Programme "International Mobility of Researchers 18021/2020" awarded to M.S.

References

[1] Schlittler, M., Pramstaller, P. P., Rossini, A., De Bortoli, M..: *Myocardial Fibrosis in Hypertrophic Cardiomyopathy: A Perspective from Fibroblasts.* International Journal of Molecular Sciences Vol. 24, pp. 14845, Oct. 2023, MDPI 2023

[2] Tatara, Y..: *Large Deformations of a Rubber Sphere under Diametral Compression : Part 1 : Theoretical Analysis of Press Approach, Contact Radius and Lateral Extension.*" JSME International Journal Series A Solid Mechanics and Material Engineering Vol. 36, pp. 190–196, J-STAGE 1993.

[3] Liu, K., Williams, D. R., Briscoe, B. J..: *The large deformation of a single micro-elastomeric sphere.* Journal of Physics D: Applied Physics Vol. 31, pp. 294–303, IOPscience 1998.

[4] Vallée, A., Lecarpentier, Y..: *TGF-β in fibrosis by acting as a conductor for contractile properties of myofibroblasts.* Cell and Bioscience Vol. 9, pp. 1–15, BMC 2019.

[5] Ma, Z. G., Yuan, Y. P., Wu, H. M., Zhang, X., Tang, Q. Z..: *Cardiac fibrosis: New insights into the pathogenesis.* International Journal of Biological Sciences Vol. 14, pp. 1645–1657, Ivyspring International 2018.

COMPUTATIONAL MODELING OF COLLECTIVE CHEMOTAXIS

Aditya Paspunurwar[1], Adrian Moure[2], Hector Gomez [1,*]

1. Purdue University, USA; 2. California Institute of Technology, USA

ABSTRACT

Eukaryotic cell motion is a fundamental process influencing several biological processes, including embryogenesis, wound healing, tissue growth, or metastatic disease. External stimuli such as physical and chemical cues generally guide cell migration. Chemotaxis is cell migration in response to a chemical gradient.The study of chemotaxis has been primarily focused on the notion of a cell moving along a pre-defined and fixed chemoattractant gradient [1]. This is insufficient because cell motion through the extracellular matrix modifies the spatial distribution of the chemoattractant in various ways. For example, some cells secrete chemoattractant; some cells uptake chemoattractant through their membrane receptors, and the motion of any cell changes the extracellular space continuously where the chemoattractant diffuses and reacts with other chemicals. However, the literature indicates a lack of experimental tools to visualize the activity of the guiding signal [2]. Thus, unveiling key mechanisms of cell motion can benefit from computational tools to understand the complex interactions between cells, chemoattractant, and extracellular matrix.

The phase-field method [3, 4] is an emerging modeling technique used to formulate problems involving cell motion that accounts for the interactions between the cytosolic, membrane, and extracellular compounds [5, 6]. We recently proposed a phase-field model for amoeboid cells undergoing chemotaxis [5]. In our model, the motion of the cell is guided by a chemotactic gradient and driven by the actin filament network, which is assumed to be a Newtonian fluid subjected to forces such as surface tension of the membrane, cell-substrate adhesion, actin-driven protrusion, and myosin contraction caused by the cell motion machinery. The phase-field method facilitates the incorporation of classical models of membrane mechanics and permits solving the partial-differential equations posed on the different domains (i.e., the cytosol, the membrane, and the time-evolving extracellular medium) by using a fixed mesh only. Our model focuses on the chemotaxis of amoeboid cells and captures the interactions between the extracellular chemoattractant, membrane-bound proteins, and the cytosolic components involved in the signaling pathway. The results reproduce the main features of chemotactic motion and unveil a complicated interplay between the geometry of the cell's environment and the chemoattractant dynamics that tightly regulate cell motility.

In most cases, cells do not migrate in isolation but collectively. In collective cell migration interactions among multiple cells, and the chemoattractant in their surroundings become even more significant [2]. Understanding collective chemotaxis poses challenges for experimental, theoretical, and computational scientists because cells are sensitive to minute chemoattractant gradients, significantly influenced by cell-cell interactions and the regulation of the chemoattractant distribution by the cells.

Over recent years, the phase-field model for individual cell migration has been extended to account for collective cell dynamics. However, efforts to extend these high-fidelity models to collective cell migration have been limited by high computational cost. The reason is that predicting the motion of N cells using phase-field methods requires solving at least N coupled PDEs, which has only been done in the literature for $N \sim 15$; see [6]. As an alternative, researchers have often resorted to homogenized phenomenological models which do not resolve the individual position of the cells but give an estimate of the average cell density. While these models have been successful in predicting cell migration patterns, they fail to provide accurate distribution of the chemoattractant in the extracellular spaces around cell clusters, Also, they possess a limited ability to provide a mechanistic understanding of collective chemotaxis.

Here, we present Dynamic cluster field (DCF) modeling, a novel computational method capable of predicting the chemotactic migration of $N = \mathcal{O}(1000)$ cells accounting for cell-cell and cell-chemoattractant interactions

* Corresponding author. E-mail: hectorgomez@purdue.edu

and high-resolution transport dynamics of the chemoattractant in the time-evolving extracellular space. The DCF approach uses fundamental properties of the phase-field theory to solve the transport dynamics of the chemoattractant on the extracellular space and specifically designed algorithms to dynamically allocate and de-allocate multiple cells to a *cluster field*, thus reducing the number of PDEs to be solved and enabling us to achieve a 60-fold increase in the number of simulated cells compared to existing algorithms that use the same level of fidelity. We compare our numerical simulations with experimental data in various scenarios involving the production and uptake of chemoattractant by migrating cells, the impact of cell movement on chemoattractant distribution, and the interactions between the chemoattractant and specific enzymes. Our results demonstrate the predictive capabilities of the proposed algorithm and highlight the importance of solving the transport dynamics of chemoattractant in extracellular space, an essential aspect of the DCF approach. Furthermore, we showcase the application of the DCF approach in predicting the migration patterns of tumor cells in extracellular matrix influenced by interstitial flow. The proposed algorithm opens new avenues for exploring outstanding problems that involve collective cell migration in the central nervous system, immune response, and cancer metastasis.

ACKNOWLEDGEMENTS

This work is supported by the National Science Foundation (Award CMMI 1952912). This work uses the Bridges-2 system at the Pittsburgh Supercomputing Center (PSC) through allocation MCH220014 from the Advanced Cyberinfrastructure Coordination Ecosystem: Services and Support (ACCESS) program, which is supported by the National Science Foundation, grants 2138259, 2138286, 2138307, 2137603, and 2138296.

References

[1] P. Rørth, Whence directionality: guidance mechanisms in solitary and collective cell migration, Developmental cell 20 (1) (2011) 9–18.

[2] E. Donà, J. D. Barry, G. Valentin, C. Quirin, A. Khmelinskii, A. Kunze, S. Durdu, L. R. Newton, A. Fernandez-Minan, W. Huber, et al., Directional tissue migration through a self-generated chemokine gradient, Nature 503 (7475) (2013) 285–289.

[3] H. Levine, D. A. Kessler, W.-J. Rappel, Directional sensing in eukaryotic chemotaxis: a balanced inactivation model, Proceedings of the National Academy of Sciences 103 (26) (2006) 9761–9766.

[4] H. Gomez, K. G. Van der Zee, Computational phase-field modeling, Encyclopedia of computational mechanics (2017) 1–35.

[5] A. Moure, H. Gomez, Three-dimensional simulation of obstacle-mediated chemotaxis, Biomechanics and modeling in mechanobiology 17 (2018) 1243–1268.

[6] A. Moure, H. Gomez, Phase-field modeling of individual and collective cell migration, Archives of Computational Methods in Engineering 28 (2021) 311–344.

A LIVE-CELL IMAGING-COMPATIBLE STRTECHING DEVICE TO STUDY THE INFLUENCE OF BIOMECHANICS ON THE INTERACTION BETWEEN BACTERIAL PATHOGENS AND EPITHELIA

Lara Hundsdorfer[1], David Jaworski[2], Marie Muenkel[1], Julio César Sánchez Rendón[1], Iordania Constantinou[2], Effie Bastounis[1,*]

1. IMIT, CMFI, University of Tübingen, Germany; 2. IMT, TU Braunschweig, Germany

INTRODUCTION

Bacterial infections are a serious health concern being a significant cause of death worldwide. Yet we do not fully understand how bacteria infect and spread throughout the human body and how hosts counteract this spread. In the vulnerable site of the intestine, foodborne, facultative intracellular bacterial pathogens like *Listeria monocytogenes* (LM) have to overcome the epithelial cell (EC) barrier to be able to spread systemically. The integrity of the EC barrier is dynamically regulated in response to mechanical cues, like fluid flow-induced shear stresses or stretching-induced strain due to peristalsis, to enable nutrient uptake. Accordingly, pathologies associated with changed mechanical cues, such as inflammatory bowel disease, undermine the EC barrier function and increase the risk of infections [1]. We are interested in understanding the impact of mechanical cues, such as stretching, on EC monolayers and on their interactions with bacterial pathogens like LM.
It is known that during late LM infection of EC monolayers, a mechanical competition takes place between ECs whereby stiffer and elongated uninfected surrounder cells squeeze, extrude and drive the collective onslaught of softer and less contractile infected cells [2]. To identify the intracellular signaling pathway behind collective infected cell extrusion, we investigated the possible involvement of the extracellular-signal regulated kinase (ERK), which is activated by cell stretching and by other types of infection [3,4].

MATERIALS AND METHODS

In our experimental design we mimicked physiologically relevant conditions by e.g., exposing cells to cyclic mechanical stretch by stretching their underlying substrate. To elucidate the behavior of EC monolayers upon mechanical stretch we analyzed kinematics and dynamics on the multicellular level. For that purpose, we built and successfully implemented a cell stretching device (Fig. 1A) that combines cyclic cell stretching of a PDMS membrane with high-resolution live-cell imaging, infection assays, and biomechanical measurements like traction force microscopy (TFM). Single-cell morphometrics like cell shape and area over time (Fig. 1C) were extracted with automated image segmentation (in FiJi, Fig. 1B) followed by data processing in Matlab.
To decipher the involvement of ERK in the process of LM-infected cell extrusion in stationary conditions, we performed a phosphoproteomic analysis of EC monolayers before, 8 h and 24 h post LM-infection, in the presence or absence of ERK inhibition by PD0325901 (50 μm). To monitor the spatiotemporal ERK activity in EC monolayers we combined infections assays with live-cell imaging of cells containing FRET based ERK activity biosensors. Additionally, we measured the cell stiffness, epithelial resistance and traction stresses with atomic force microscopy, trans epithelial electrical resistance (TEER) measurement and TFM, respectively.

RESULTS

We found that EC monolayers responded to cyclic mechanical stretch by decreased cellular migration, and enhanced pericellular localization of the cell-cell junction protein E-cadherin. Furthermore, the cell area but not the shape factor (perimeter divided by the square root of the area) changed cyclically with stretch. Thus, mechanical cues caused adaptations in ECs, which might influence host-pathogen interactions.
In stationary conditions the EC monolayers reacted to LM-infection with increased coordinated cell migration, cell polarization and increased traction stresses in cells surrounding the infection focus, which led to the extrusion of infected cells. This mechanism limits bacterial spread and depends on ERK activity waves in the EC monolayer, which we observed by imaging cells with the FRET based ERK activity biosensor. Disrupting periodic ERK activity via pharmacologically induced inhibition or constitutive activation of ERK increased bacterial spread, and decreased infected cell extrusion as well as coordinated cell migration in LM-infected cell monolayers.
In the future, we plan to investigate the effect of cyclic mechanical stretch on LM-infection of EC monolayers and on extrusion of LM-infected cells.

* Corresponding author. Email: **effie.bastounis@uni-tuebingen.de**

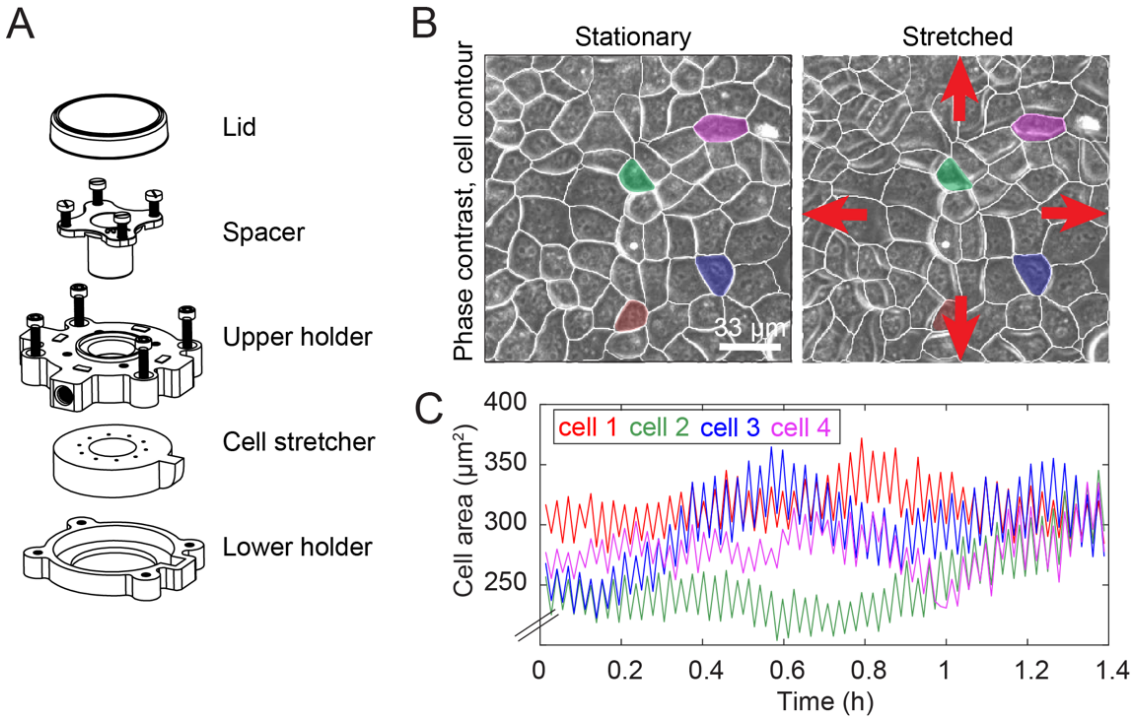

Figure 1. A) Schematic drawing of components of our automated, high-resolution, live-cell imaging compatible cell stretch device. B) Representative phase contrast images of an epithelial MDCK cell monolayer in the stationary state (left) and subjected to 6% radial stretch (right), with segmented cell borders indicated by the overlayed white contour of the stationary cells. Color-coded cells tracked over time to extract morphometric parameters. C) Cell area (μm^2) over time of four tracked cells (shown in panel B) subjected to 6% radial strain with a period of T = 20 s, images were taken every 50 s.

DISCUSSION AND CONCLUSIONS

The extrusion of LM-infected cells serves to limit bacterial dissemination and depends on intercellular communication via ERK activity waves. Interestingly, the stretching of cells has also been shown to activate ERK. Thus, we expect cyclic mechanical stretch to alter – possibly increase – the extrusion of LM-infected cells from EC monolayers via changes in ERK signalling. Cyclic mechanical stretch could also alter bacterial dissemination within EC monolayers. Our interdisciplinary approach combining engineering with cell- and microbiology promises to reveal novel mechanisms used by bacteria and host cells to facilitate or conversely obstruct infection spread.

ACKNOWLEDGEMENTS

The authors would like to thank the Cluster of Excellence - Controlling Microbes to Fight Infections (CMFI), the University hospital Tübingen (UKT), and the German Research foundation (DFG) for providing financial support to this project. We want to thank Tsuyoshi Hirashima for his advice and providing the ERK activity biosensors. Furthermore, we want to acknowledge the support from Libera Lo Presti.

References

[1] Ghoshal, U.C., Ghoshal, U.: *Small Intestinal Bacterial Overgrowth and Other Intestinal Disorders*. Gastroenterology Clinics Vol 46.1, pp. 103–120, Elsevier 2017.

[2] Bastounis, E., et al.: *Mechanical competition triggered by innate immune signaling drives the collective extrusion of bacterially infected epithelial cells.* Developmental cell Vol. 56.4, pp. 443-460, Cell Press 2021.

[3] Hino, N., et al.: *ERK-mediated mechanochemical waves direct collective cell polarization.* Developmental cell Vol. 53.6, pp. 646-660, Cell Press 2020.

[4] Beerli, Corina, et al.: *Vaccinia virus hijacks EGFR signalling to enhance virus spread through rapid and directed infected cell motility.* Nature microbiology Vol 4.2, pp. 216-225, Nature Publishing Group 2019.

ROLE OF CYTOSKELETON IN CANCER CELLS UNDER A VARIETY OF MECHANICAL STIMULI: A COMPUTATIONAL STUDY

Lucie Jadrrna[1,*], Jaromir Gumulec[2], Jiri Bursa[1,*]

1. Department of Biomechanics, Brno University of Technology, Czechia;
2. Department of Pathophysiology, Masaryk University, Czechia

INTRODUCTION

Cancer progression frequently causes alterations in cellular mechanics as well as inner and outer morphology characteristics. These alterations together with changes in cellular metabolism occur, among other reasons, to deal with increased demands on motility. As a result, the stiffness change is observed and is oftentimes tied to the level of cancer aggressivity. This study intends to uncover the mechanisms underlying such stiffness alterations focusing primarily on evaluating the role of cytoskeletal changes and their prominence under different loading setups, both on a local and global level.

MATERIALS AND METHODS

To assess the differences in the cellular stiffness across two different model cell lines (22Rv1 and PC-3 cells, both prostate cancer cell lines), the cells were subjected to several stiffness screening setups, Atomic Force Microscopy (AFM) to probe the cellular mechanics on a local level as it is a well-established method for cancer cell stiffness measurements, and two methods for assessing the global mechanical response: Real-Time Deformability Cytometry (RT-DC), and shear flow-induced cell deformation.

Evaluating the protein profile uncovered significant changes in cytoskeleton-associated proteins: vimentin and actin. Corroborating the experimental findings, we employed a structural Finite Element Model that accounts for the nucleus, cellular membrane, cytoplasm as well as cytoskeletal components: actin cortex and actin bundles to which the actin protein content was attributed, microtubules (tubulin content) and intermediate filaments (vimentin content) (Fig. 1(a), further details on the modeling in Bansod, 2018). The aim was to reflect the observed changes in the protein content in the computational setup under the loading conditions mimicking the experimental setup and uncover, to what extent is the cytoskeletal inner reorganization capable of capturing the scale of the observed stiffness change.

RESULTS

Transitioning between experimental measurements and their computational assessment (as in Fig. 1(b) and (c)) has brought an insight into the role of cytoskeleton in the cellular stiffness. Even though the stiffness of selected cancer cell lines is prominently different, it has been established that the cytoskeleton itself is capable only of capturing roughly a third of overall cellular stiffness.

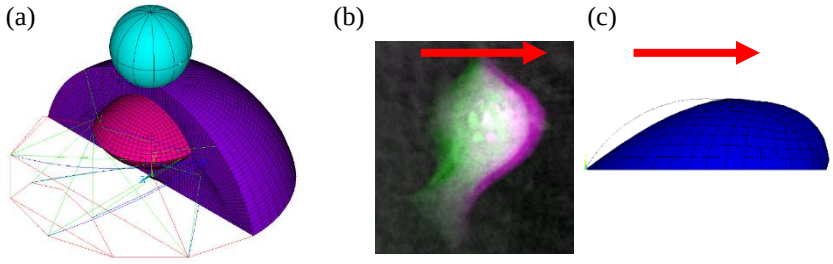

Figure 1. Computational setup mimicking the experimental loading environment: (a) detailed hybrid computational model in AFM setup with spherical tip in central position, a depiction of shear loading in a direction indicated by a red arrow using holographic microscopy images (b) and deformed computational model (c).

DISCUSSION AND CONCLUSIONS

The role of the cytoskeleton has been exploited using computational modeling based on experimental data measured using various loading conditions. The role of a “deep cytoskeleton” (i.e. actin filaments, microtubules, and especially of the wavy microfilaments) has been only subtle for AFM, which reflects mainly the stiffness contribution of superficial structures such as membrane and actin cortex. On the other hand, the contribution of the inner fibrous structures has been more pronounced in methods of deforming the cell on a global scale.

Nonetheless, we expect another underlying mechanism to be bound to play a crucial role in the mechanical response. Even though the cytoskeleton has been given more attention in computational cellular mechanics than other organelles, it is not entirely ruled out that there are other contributing factors such as bonds between organelles. For instance, the reorganization in the cancer cell cytoplasm also includes changes in the architecture of mitochondria, which is responsible for generating energy for the cell. Thus, the attention will be directed toward the mitochondrial organization within the cytoskeleton together with their mutual interactions and how it impacts cancer cell mechanics.

ACKNOWLEDGEMENTS

This work was supported by the Ministry of Health of the Czech Republic NU22J-08-00062.

References

[1] Bansod YD, Matsumoto T, Nagayama K, Bursa J. 2018. A Finite Element Bendo-Tensegrity Model of Eukaryotic Cell. J Biomech Eng 140. doi:10.1115/1.4040246

[2] Vicar T, Chmelik J, Navratil J, Kolar R, Chmelikova L, Cmiel V, Jagos J, Provaznik I, Masarik M, Gumulec J. 2022. Cancer cell viscoelasticity measurement by quantitative phase and flow stress induction. Biophys J 121:1632–1642. doi:10.1016/j.bpj.2022.04.002

Apically applied fluid shear stresses are vasoprotective, decreasing the susceptibility of endothelial cells to infection with *Listeria monocytogenes*

Erva Keskin[1], Mai Wang[1], Effie Bastounis[1,*]

1. *Interfaculty Institute of Microbiology and Infection Medicine, Cluster of Excellence "Controlling Microbes to Fight Infections" (CMFI, EXC 2124) University of Tübingen, Germany*

INTRODUCTION

Endothelial cells (ECs) line the lumen of blood vessels, forming a single cell monolayer that acts as a protective barrier against different insults, including bacterial pathogens. The barrier integrity is maintained through a synergy of several elements at the cell surface including focal adhesions, adherens junctions and surface receptors. In ECs, these components play a crucial role in the response to fluid shear stresses (SS) and gradients (SSG), which vary in space, time and (patho)physiological conditions (e.g., arteriosclerosis). Although EC responses to SS and SSG have been studied to some extent, how they modulate EC biomechanics and thus interactions with bacterial pathogens, has not been explored previously.

MATERIALS AND METHODS

To study the effects of fluid SS and SSG on infections with intracellular bacterial pathogens we exposed ECs to flow for 20 h or not (stationary conditions) and immediately after, we infected human microvascular endothelial cells (HMEC-1) with *Listeria monocytogenes (Lm)*, an enteric pathogen that can spread to distant organs, by interacting with different types of vascular ECs, where it can cause fatalities.

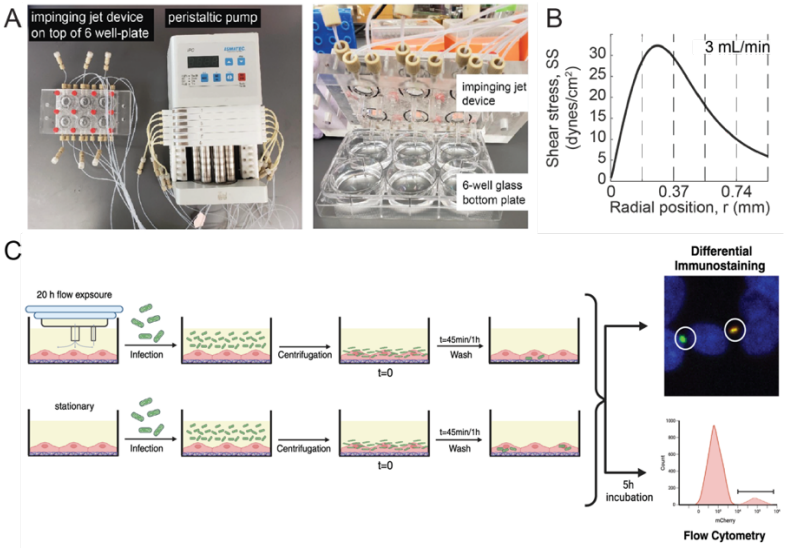

Figure 1. A) Image of multiplex impinging flow jet device designed by Gerald Fuller and Alexander Dunn. B) Shear stress profile from jet center outwards at a flow rate of 3 mL/min. C) Workflow of infection assay: after flow exposure the cells (in pink) were infected with *Lm* (in green) and the infection rate was assessed by flow cytometry, while adhesion vs invasion was discriminated by differential immunostaining.

Multiplex Impinging Flow Jet Device

For flow exposure we used a multiplex impinging flow jet device developed by Gerald Fuller and Alexander Dunn at the Stanford University. The Reynolds numbers for the device are in the laminar flow regime as experienced by ECs in blood vessels. The impinging flow chamber fits onto a 6-well plate and contains vertical posts extending into each well of the cell culture dish up until 1 mm between the flow exit and the cells. Fluid is pumped into each well with a 9-roller dampened peristaltic pump through the central orifice and is pumped up through a second orifice located near the side of the well and 13 mm away from the inlet post. The inner diameter of the inlet port is 0.7 mm, while the exit port has a diameter of 2 mm and is 4 mm away from the polystyrene bottom of the well, hence the cells do not experience the effects of fluid exit velocity and shear stresses apart from the flow of interest [1]. The flow rate in all experiments was 3 mL/min, corresponding to a peak SS of 34 dynes/cm^2.

*Corresponding author. Email: effie.bastounis@uni-tuebingen.de

Infection Assay and Analysis

Directly after 20 h exposure to flow or stationary conditions HMEC-1 were incubated in culture medium containing 40-50 bacteria per cell of a *Lm* strain that expresses RFP once inside the cytosol of the host cells and is unable to spread from cell to cell. After 45 min incubation, HMEC-1 were washed 3 times, incubated in fresh medium containing gentamycin at 37°C for 5 hours and then analysed by flow cytometry. For an orthogonal analysis differential immunostaining was used. Therefore, HMEC-1 were incubated with culture medium containing 50-70 bacteria per cell of a *Lm* strain that constitutively expresses GFP. After 1h incubation, the samples were fixed – but not permeabilized – for immunostaining. This enabled us to stain extracellular bacteria, i.e. on the cell surface, with a second fluorophore and discriminate them from intracellular, GFP-positive bacteria. The analysis of differential immunostaining was performed using quantitative microscopy.

RESULTS

We observed a 25% decrease in the infection rate of HMEC-1 previously exposed to shear flow as compared to HMEC-1 under stationary conditions. To determine whether decreased infection is caused by decreased bacterial adhesion onto EC surface, decreased invasion efficiency of *Lm* into ECs; or a combination of both, differential immunostaining was performed. The results show that while there were no differences in adhesion of *Lm* onto ECs, ECs that were exposed to shear flow were significantly less susceptible to invasion as compared to ECs under stationary conditions.

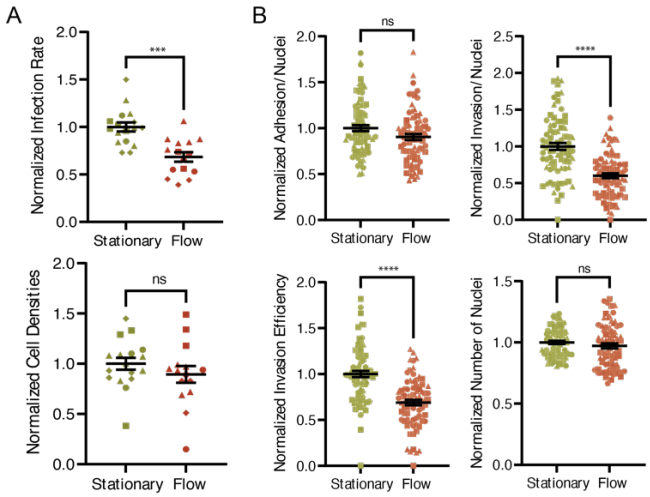

Figure 2. A) Normalized infection rates and cell densities under static or flow conditions. B) Differential immunostaining analysis shows no significant difference in adhesion but significant difference in invasion and invasion efficiency at comparable cell densities between flow and static conditions. Statistical analysis was conducted with nonparametric unpaired Mann-Whitney U test. Error bars indicate standard error of the mean (SEM). Data was normalized to the mean of stationary condition. If $p \leq 0.05$ = *; if $p \leq 0.01$ = **; if $p \leq 0.001$ = ***; if $p \leq 0.0001$ = ****.

DISCUSSION AND CONCLUSIONS

The findings of our study so far suggest that shear flow might serve as a vasoprotective mechanism against *Lm* infection. The underlying cause has not yet been investigated, but we plan to analyse potential molecular and/or physical mechanisms responsible for the SS-dependent decrease in *Lm* invasion. Our main hypothesis is that this decrease is receptor-mediated, which is partially supported by our transcriptomics screen. Another hypothesis in this regard is that SS induced changes in biophysical properties of ECs (e.g., cortical stiffness) could underlie the differential susceptibility of flow- vs non-exposed ECs to infection. To assess whether potential stiffness-changes impact *Lm* infection, we will perform atomic force microscopy (AFM). Another possibility might be changes in EC membrane tension and thus endocytic trafficking which will be tested using Flipper-TR system.

ACKNOWLEDGEMENTS

We would like to thank **the German Research Foundation (DFG) and CMFI** for providing financial support to this project.

References

[1] Ostrowski MA, Huang EY, Surya VN, Poplawski C, Barakat JM, Lin GL, Fuller GG, Dunn AR. Multiplexed Fluid Flow Device to Study Cellular Response to Tunable Shear Stress Gradients. Ann Biomed Eng. 2016 Jul;44(7):2261-72. doi: 10.1007/s10439-015-1500-7. Epub 2015 Nov 20. PMID: 26589597; PMCID: PMC4874920.

COMPETING SIGNALING PATHWAYS CONTROL ELECTROTAXIS

Shardool Kulkarni[1,*], Pablo Saez[1,2]

1. LaCaN, Universitat Politecnica de Catalunya-BarcelonaTech,Barcelona, Spain;
2. IMTech (Institute of Mathematics), Universitat Politecnica de Catalunya-BarcelonaTech., Barcelona, Spain

INTRODUCTION

How cells migrate following exogenous cues is one of the most fundamental questions for biology and medicine. Cell migration is involved in tissue regeneration and cancer invasion, among many other biological processes [1]. Growing evidence suggests that electrotaxis, the directed cell migration toward electric potential gradients, represents a precise and programmable method approach to control cell migration. Most data suggest that the polarization of membrane components [2] and the following downstream signalling are central to electrotaxis. Unfortunately, how these multiple mechanisms coordinate with the motile machinery of the cell to respond to an electric field is still poorly understood, hindering the engineering control of electrotaxis. In this study, we provide a mechanistic model that explains and reproduces electrotaxis across different cell types. We show that the ζ-potential of the cell controls electro-motility of charged membrane components, which effects competing intracellular signalling pathways, which then further polarizes the intracellular acto-myosin network leading to cell migration. We show that ζ-potential uniquely determines the migration direction and that the degree of polarization of these motile forces establishes the speed of migrating cells. Furthermore, revealing how to control cell migration would allow us not only to promote tissue regeneration or arrest tumour progression but also to design better biomimetic-engineered tissue constructs.

MATERIALS AND METHODS

To model the cascade of events toward electrotaxis, we consider a one-dimensional Finite Element Method based computational model. For modelling the electrotaxis, we first look to model the redistribution of Charge Membrane Proteins (CMPs) in the presence of an electric field (EF). This redistribution is then responsible for the downstream polarization of intracellular signals [3]. Finally, we use our previous active gel models of cell migration to computationally analyze the coupling of GTPases with the migration forces of the cell under the effect of EF. We model the redistribution of CMPs, the downstream polarization of signaling molecules, and the subsequent repolarization of the contractile actomyosin networks. The moving of both cell ends will depend on the velocity of the contractile actomyosin network and the velocity of actin polymerization at the cell front, which will eventually dictate the migration direction and velocity of the cell.

Polarization of Signalling Cues

To model cell signalling we follow a Local Excitation Global Inhibition model (LEGI) [4] which represents a comprehensive mathematical model for cell signalling. It proposes PI3K and PTEN are activator (A) and inhibitor (I) of the response element (R), which represents the small GTPases (Rac and CDC42). The fast-acting local activator and the slow global inhibitor are activated in direct proportion The LEGI model is described by the following system of PDEs:

$$\partial_t A = k_A \rho_\pm - k_{-A} A \tag{1}$$

$$\partial_t I = D_I \partial_x^2 + k_I \rho_\pm - k_{-I} I \tag{2}$$

$$\partial_t R = k_R A - k_{-R} I R \tag{3}$$

here k_i and k_{-i} are the on/off rates for each variable and D_I is the diffusion parameter for the inhibition process. Following the hypothesis that redistribution of CMPs is responsible for electrotaxis, we take the CMP density, $\rho_\pm$, which varies as a convection-diffusion equation with zero Neumann boundary condition, as the stimuli for cell polarization. Transport of the acto-myosin network is modelled using similar coupled convection-diffusion equations.

RESULTS

To analyze electrotxis, we initially define an unpolarized state of the cell which means the density of CMPs, actin, myosin and intracellular signals are uniformly distributed along the cell. When we impose an Electric Field of 120 mv/mm at t= 180s. We first measure the velocity of redistribution of CMPs using the difference in Zeta Potentials (ζ) between cell surface and CMP. The polarization of the CMPs (EGFR in this case) induces a cascade of intracellular signals. Firstly the PI3K path ways are activated, which leads to the increase in actin polymerization velocity in those regions. This further leads to myosin activity at the rear of the cell and consequently a backward retrograde flow. The balance between actin polymerization velocity and the retrograde flow velocity leads to directed migration of the cell.

* Corresponding author. E-mail: shardool.kulkarni@upc.edu

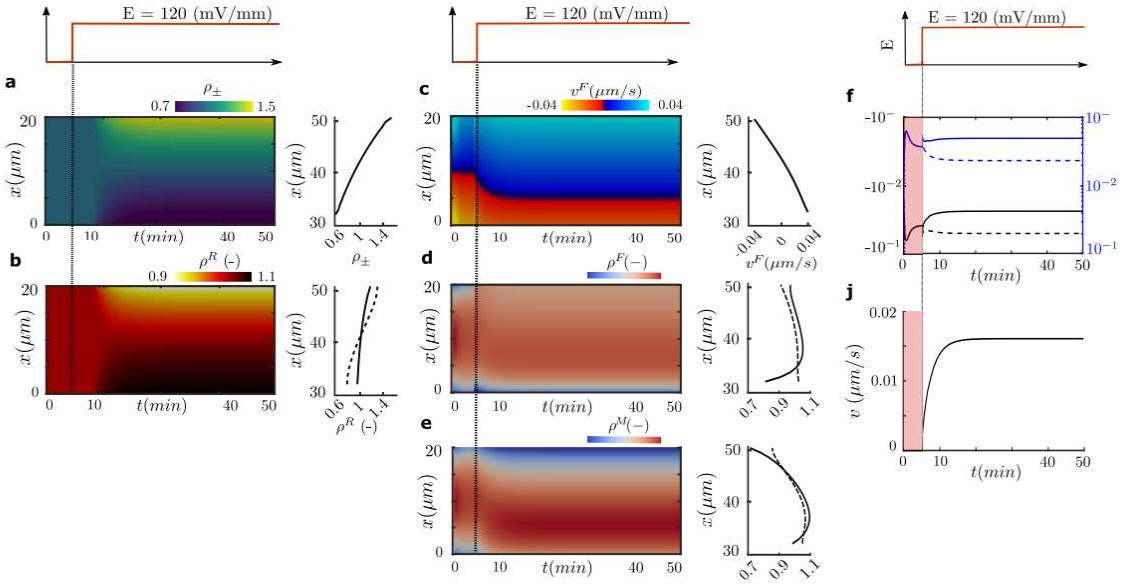

Figure 1. Kymograph of the CMPs polarization (a) and intracellular signals (b). At a steady state (right), the CMPs and the intracellular signals (activator, solid line, and responder, dash line) are shown; Kymographs of the retrograde flow (c), actin (d), and myosin (e) densities. At steady state, the retrograde flow and actin (F-actin, solid line, G-actin, dash line) and myosin densities (bound, solid line, unbound, dash line) are shown on the right; Retrograde flow (solid) and polymerization velocity (dash) at the front and rear of the cell (f). Blue and black represent positive and negative velocities, respectively. Migration velocity of the cell (j).

We also show the ζ potential differences (magnitude and sign) directly influence the cell migration velocity at steady state. This can be used to estimate the probable cell migration velocities of CMPs with different physical properties. We also study a database of proteins from the study of proteome of zebrafish keratocytes. From this we can estimate which CMP will move to cathode or anode in presence of an applied EF. Finally, we take a closer look at the downstream signalling pathways that affect electrotaxis. We model a slightly complex signalling model [6] which includes small GTPases of the rho family (Rac, Rho and CDC42) and also include the phosphoinositides (PIs), their kinases/phosphatases (PI3K,PI5K). Based on our analysis, differences in cellular responses, such as migration velocities,direction or time to respond to an electric stimulus, should respond to differences in activation strengths and the feedback loops between GTPases and PIPs.

DISCUSSION AND CONCLUSIONS

After adopting a minimal model of cell migration in our previous work [5], and extending it with electromigration of cell membrane receptors and signalling pathways implicated in cell motility, we have proposed a complete computational model of electrotaxis. We have shown how all layers involved in the electrotaxis process interact to control the active forces involved in cell migration and, consequently, to induce an electrotactic response.

ACKNOWLEDGEMENTS

The authors would like to thank **the Spanish Ministry of Science and Innovation (Grant PID2022-142178NB-I00 funded by MCIN/ AEI/10.13039/501100011033/ FEDER, UE)** for providing financial support to this project.

References

[1] Friedl P, Gilmour D. *Collective cell migration in morphogenesis, regeneration and cancer.* Nature reviews Molecular cell biology. 2009 Jul;10(7):445-57.

[2] Zhao M, Pu J, Forrester JV, McCaig CD. *Membrane lipids, EGF receptors, and intracellular signals colocalize and are polarized in epithelial cells moving directionally in a physiological electric field.* The FASEB Journal. 2002 Jun;16(8):857-9.

[3] Jilkine A, Edelstein-Keshet L. *A comparison of mathematical models for polarization of single eukaryotic cells in response to guided cues*. PLoS computational biology. 2011 Apr 28;7(4):e1001121.

[4] Levchenko A, Iglesias PA. *Models of eukaryotic gradient sensing: application to chemotaxis of amoebae and neutrophils.* Biophysical journal. 2002 Jan 1;82(1):50-63.

[5] Betorz J, Bokil GR, Deshpande SM, Kulkarni S, Araya DR, Venturini C, Sáez P. *A computational model for early cell spreading, migration, and competing taxis.* Journal of the Mechanics and Physics of Solids. 2023 Oct 1;179:105390.

[6] Dawes AT, Edelstein-Keshet L. *Phosphoinositides and Rho proteins spatially regulate actin polymerization to initiate and maintain directed movement in a one-dimensional model of a motile cell.* Biophysical journal. 2007 Feb 1;92(3):744-68.

MICRO IMMUNE RESPONSE ON-CHIP (MIRO) MODEL TO STUDY THE SPATIAL REPARTITION OF IMMUNE CELLS IN TUMOR DRIVEN BY STROMAL MECHANOSENSING

Alice Perucca[†,1], Andrea Gómez Llonin[†,2], Oriol Mañe Benach[†,1], Clement Hallopeau[1], Elisa I. Rivas[2], Jenniffer Linares[2], Marta Garrido[2], Anna Sallent-Aragay[2], Tom Golde[1], Julien Colombelli[3], Elena Dalaka[1], Judith Linacero[1], Marina Cazorla[1], Teresa Galan[1], Jordi Pastor Viel[4], Xavier Badenas[4], Alba Recort-Bascuas[2], Laura Comerma[9], Pere Roca-Cusachs[1,5], Joan Albanell[2,10,11,12], Xavier Trepat[1,5,6,7,*], Alexandre Calon[2,*], Anna Labernadie[1,8,*]

1. Institute for Bioengineering of Catalonia (IBEC), The Barcelona Institute for Science and Technology (BIST), 08028 Barcelona, Spain; 2. Cancer Research Program, Hospital del Mar Medical Research Institute (IMIM), 08003 Barcelona, Spain; 3. Institute for Research in Biomedicine (IRB) Barcelona, Barcelona Institute of Science and Technology (BIST), 08028 Barcelona, Spain; 4. Unitat de Tecnologia Mecànica, Centres Científics i Tecnològics, Universitat de Barcelona, 08028 Barcelona, Spain; 5. Unitat de Biofisica i Bioenginyeria, Facultat de Medicina, Universitat de Barcelona, 08036 Barcelona, Spain; 6. Institucio Catalana de Recerca i Estudis Avancats (ICREA), 08010 Barcelona, Spain; 7. Center for Networked Biomedical Research on Bioengineering, Biomaterials and Nanomedicine (CIBER-BBN), 08028 Barcelona, Spain; 8. Centro de Investigacion Principe Felipe, 46012 Valencia, Spain; 9. Pathology Department, Hospital del Mar, 08003 Barcelona, Spain; 10. Universitat Pompeu Fabra, 08003 Barcelona, Spain; 11. Centro de Investigación Biomédica en Red de Oncología (CIBERONC-ISCIII), 28029 Madrid, Spain; 12. Medical Oncology Department, Hospital del Mar, 08003 Barcelona, Spain

ABSTRACT

Understanding cellular interactions occuring at the tumor/stroma boundary is one of the main challenges for anti-cancer immunotherapies as the efficacy of those treatments tightly depends on the capacity of immune cells to reach the tumoral compartment. Increasing evidence reports that within the TME, the spatial repartition, density, and physical properties of the extracellular matrix (ECM) and Cancer-Associated-Fibroblast (CAF) shape the tumoral immune landscape that predict patient's response to treatment. Yet, the mechanical and architectural properties of the TME modulating immune cells trafficking and activation state are still poorly understood. To uncover how spatial architecture of the TME influence immune infiltration in tumor we recently created a Micro Immunotherapy Response On-chip (MIRO), an immunocompetent in vitro model that recapitulates a tumor/stroma interface for immunotherapy testing. We show that this model can offers a versatile tool to unveil how stromal mechanosensing could spatially shape the TME and impact immune cell repartition in tumors.

* Corresponding author. E-mail: alabernadie@cipf.es

COMPUTATIONAL MODELS TO UNDERSTAND AND ADVANCE THE REGENERATION OF ENGINEERED CARDIOVASCULAR TISSUES

Sandra Loerakker[1,2,*]

1. Department of Biomedical Engineering, Eindhoven University of Technology, The Netherlands;
2. Institute for Complex Molecular Systems, Eindhoven University of Technology, The Netherlands.

ABSTRACT

Engineered cardiovascular tissues have the intrinsic ability to grow and adapt to changes in their hemodynamic environment. This fascinating adaptive capacity gives these tissues the potential to overcome the limitations of current cardiovascular replacements that are unable to accommodate changes in the recipient's demands. For cardiovascular tissue engineering to be successful, however, we need to thoroughly understand the responsible growth and remodeling mechanisms of (engineered) cardiovascular tissues, and be able to steer tissue development towards establishing a physiological tissue organization and long-term tissue functionality. In this talk, I will discuss how computational modeling, particularly when integrated with experimental research, can aid in addressing both challenges. I will give a conceptual overview of the computational models that we developed to analyze the growth and remodeling of cardiovascular tissues, with a primary focus on heart valves. Specifically, I will show how we used our models to understand postnatal human heart valve development and adaptation [1-2], to predict and steer the in vivo remodeling of tissue-engineered heart valves [3-5], and to understand the role of cell-cell communication in directing vascular adaptation [6-8].

ACKNOWLEDGEMENTS

Funding from the European Union's Seventh Framework Program (FP7/2007-2013; grant agreement no. 242008) and the European Research Council (ERC) under the European Union's Horizon 2020 research and innovation program (ERC Starting Grant 'MechanoSignaling'; grant agreement no. 802967) is gratefully acknowledged.

References

[1] Ristori T, Bouten CVC, Baaijens FPT, Loerakker S. Predicting and understanding collagen remodeling in human native heart valves during early development. **Acta Biomater** 80:203-216, 2018.

[2] Middendorp E, Braeu F, Baaijens FPT, Humphrey JD, Cyron CJ, Loerakker S. Computational analysis of heart valve growth and remodeling after the Ross procedure. *In revision*.

[3] Loerakker S, Argento G, Oomens CWJ, Baaijens FPT. Effects of valve geometry and tissue anisotropy on the radial stretch and coaptation area of tissue-engineered heart valves. **J Biomech** 46:1792-1800, 2013.

[4] Sanders B, Loerakker S, Fioretta ES, Bax DJP, Driessen-Mol A, Hoerstrup SP, Baaijens FPT. Improved geometry of decellularized tissue engineered heart valves to prevent leaflet retraction. **Ann Biomed Eng** 44:1061-1071, 2016.

[5] Emmert MY, Schmitt BA, Loerakker S, Sanders B, Spriestersbach H, Fioretta E, Bruder L, Brakmann K, Motta S, Lintas V, Dijkman P, Frese L, Berger F, Baaijens FPT, Hoerstrup SP. Computational modeling guides tissue-engineered heart valve design for long-term in vivo performance in a translational sheep model. **Sci Transl Med** 10:eaan4587, 2018.

[6] Loerakker S, Stassen OMJA, Ter Huurne FM, Boareto M, Bouten CVC, Sahlgren CM. Mechanosensitivity of Jagged-Notch signaling can induce a switch-type behavior in vascular homeostasis. **PNAS** 115:E3682-3691, 2018.

[7] Karakaya C, Van Turnhout MC, Visser VL, Ristori T, Bouten CVC, Sahlgren CM, Loerakker S. Notch signaling regulates strain-mediated phenotypic switching of vascular smooth muscle cells. **Front Cell Dev Biol** 10:910503, 2022.

[8] Van Asten JGM, Latorre M, Karakaya C, Baaijens FPT, Sahlgren CM, Ristori T, Humphrey JD, Loerakker S. A multiscale computational model of arterial growth and remodeling including Notch signaling. **Biomech Model Mechanobiol** 22:1569-1588, 2023.

* Corresponding author. Email: **s.loerakker@tue.nl**

INFLUENCE OF SOME GENOTYPIC PARAMETERS ON THE FORMATION OF NECROTIC CORES IN GLIOBLASTOMA MULTIFORME

Lucía López-de Abajo[1], Luis Saucedo-Mora[1,2,3], Francisco J. Montáns[1,4], José Mª Benítez[1*]

1. E.T.S. de Ingeniería Aeronáutica y del Espacio, Universidad Politécnica de Madrid, Spain; 2. Department of Materials, University of Oxford, UK; 3. Department of Nuclear Science and Engineering. M.I.T., USA; 4. Department of Mechanical and Aerospace Engineering, University of Florida, USA.

INTRODUCTION

Glioblastoma multiforme (GBM) is one of the most aggressive cancers of the central nervous system. GBM hallmarks can be summarized in the great mitotic and invasive capabilities of the GBM cells, the formation of necrotic cores and neovascularization. Based on an agent-based hybrid model recently published by the authors, in this contribution they perform a sensitivity analysis to study which biological parameters are determinant to simulate the formation of necrotic cores. The model reproduces the evolution of the oxygen field during cellular migration and the phenotypic plasticity considering five phenotypes: migratory (individually or collectively), necrotic, quiescent, proliferative, and hypoxic.

MATERIALS AND METHODS

The phenotypic plasticity of the GBM cells is formulated as the result of the interaction between every single GBM cell and its microenvironment. The interaction is simulated by the continuous interplay between the discrete layer of the model and the continuum one. In the discrete part, cells are considered as individual agents that take decisions according to their micro-environment conditions. The cell microenvironment is mimicked by the oxygen concentration evolution, calculated through a finite element model (FEM) implemented in the continuum layer, and the cell density, obtained in the discrete one. Cells are considered as sinks in the FEM and a steady state is adopted due to the different characteristic times of the oxygen evolution and cell events. Equations that reproduce the cell behavior are formulated in terms of genotypic parameters, namely: the minimum oxygen concentration that a cell needs to be in normoxia conditions, i.e. switch between normoxia and anoxia (C_{O2}), the maximum time that a cell can be in anoxia (t_a), the oxygen consumption rate of the cell (O_2), the optimum cell density (ρ_{op}) and the cell velocity during migration (v). ρ_{op} represents the volume of cells within the volume of an element of the FEM mesh. Three different values, based on the ones available in the literature [1], have been adopted for each parameter, Table 1.

Parameter	Minimum value	Medium value	Maximum value
C_{O2} [mmHg]	1.0	1.8	2.6
t_a [days]	0	1	15
O_2 [mmHg/s]	10^{-14}	10^{-9}	10^{-5}
ρ_{op} [-]	0.2	0.7	1
v [mm/s]	10^{-10}	10^{-6}	$2x10^{-6}$

Table 1. Values of the main genotypic parameters adopted.

Collective behavior is modelled through a flocking parameter ($0 < f \leq 1$) that represents the tendency of a cell to adopt a quiescent phenotype if it is alone. Flocking is formulated so that cells will migrate in groups with a density equal to ρ_{op}. Thus, when f=1 a cell will not migrate looking for other cells to reach the optimum density and therefore, no collective behavior is given. For the cases at hand, f=0.4 to reproduce a collective behavior. For more detail about the formulation see reference [1].

A population of 1000 cells arranged in the perimeter of a circumference with a diameter of 1mm was considered. The initial oxygen field was constant with a concentration of 1mmHg. The domain consisted of a square of 5.5x5.5 mm^2 with a constant oxygen supply of 7 mmHg through the four borders.

* Corresponding author. Email: **josemaria.benitez@upm.es**

RESULTS

Figure 1 shows the results of the analysis in terms of dead and alive cells, respectively. The summation of them and the subtraction of the initial 1000 cells turn out the number of mitotic events. According to these results, and as was expected, when the minimum oxygen concentration needed by a cell to be in normoxia (C_{O2}) is increased, the number of dead cells is also increased, whereas the number of alive cells is reduced. A similar thing happens with the consumption of oxygen (O_2), depicted in yellow. Relative to the maximum time in apnea (t_a), all the cells die when t_a=0, whereas the number of dead cells is reduced, and therefore more cells proliferate, as t_a is increased. The most significant results are found for cases of the migration velocity (v) and the optimum density to flock (ρ_{op}). In the first case, a low migration velocity induces cell proliferation in a restricted area up to the depletion of the oxygen available. Both events trigger an increment of the death cells. From a threshold velocity, this parameter does not influence the number of necrotic cells. However, the number of alive cells drops not because other cells die but because they do not proliferate. The same thing happens in the case of ρ_{op}. Furthermore, the influence of ρ_{op} on the number of necrotic cells is negligible.

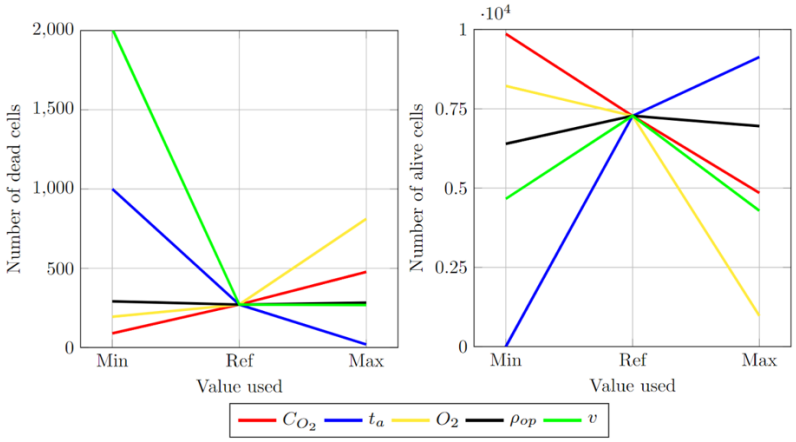

Figure 1. Number of dead and alive cells after 10 days.

DISCUSSION AND CONCLUSIONS

In the collective migration, the survival of the group prevails over the cell proliferation regardless of the size of the clusters, directly related to the optimum density, or the velocity, as long as it is greater than a minimum. This implies more resources available, since the cell population reduces its mitotic activity, and delays the formation of necrotic cores.

ACKNOWLEDGEMENTS

Grant PID2021-126051OB-C43 funded by MCIN/AEI/10.13039/501100011033 and "ERDF A way of making Europe"

References

[1] Saucedo-Mora, L. Sanz, M.A. Montáns, F.J. Benítez J.M. *A simple agent-based hybrid model to simulate the biophysics of glioblastoma multiforme cells and the concomitant evolution of the oxygen field* in Computer Methods and Programs in Biomedicine. Vol. 246, pp. 108046, Elsevier 2024.

A COMPUTATIONAL STUDY OF PHARMACOLOGICAL TREATMENT AFTER THE ROSS PROCEDURE

Lauranne Maes[1,*], Thibault Vervenne[1], Amber Hendrickx[2], Ana C. Estrada[3], Lucas Van Hoof[2], Peter Verbrugghe[2], Filip Rega[2], Elizabeth A.V. Jones[2,4], Jay D. Humphrey[3], Nele Famaey[1]

1. Department of Mechanical Engineering, KU Leuven, Belgium; 2. Department of Cardiovascular Sciences, KU Leuven, Belgium; 3. Department of Biomedical Engineering, Yale University, USA; 4. Department of Cardiology, Maastricht University, Netherlands

INTRODUCTION

An excellent alternative to the treatment of aortic valve disease through mechanical or biological valve replacement, is the Ross procedure, where the pulmonary valve is transplanted into aortic position [1]. After the surgery, this pulmonary autograft is suddenly exposed to systemic hemodynamic conditions, including an often more than five-fold pressure increase. Reintervention occurs in about 10% of the adult patients [2], and is often needed due to excessive dilatation of the autograft over time, leading to valve dysfunction. The failure mechanism, related to the inability of the tissue to adapt to its new mechanical environment, has been studied through various animal [3] and computational [4] models. The aim of the present study is to explore pharmacological treatment in order to reduce autograft failure risk through computational modeling.

METHODS

Multiscale model

We use our previously developed multiscale model, that predicts autograft dilatation after the Ross procedure, alternating at every time step between a tissue-scale growth and remodeling model and a cell-scale network model [5]. A schematic overview of the model in shown in figure 1.

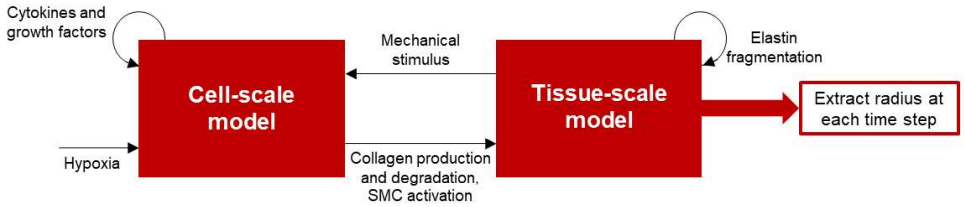

Figure 1. Schematic overview of the multiscale model.

The cell-scale model is a network composed of protein interactions and interactions between transcription factors and their targets. The activity scores of the nodes in the network take a continuous value in a range from 0 to 1. A node's score is calculated as a weighted sum of its upstream node activities, where activation interactions have a positive contribution and inhibition interactions a negative contribution. The cell-scale model takes as main inputs the cytokine and growth factor activity, the current level of hypoxia and the current mechanical state of the tissue. The main outputs are the activity levels of genes relevant for the mechanical properties of the tissue, such as genes coding for collagen, extracellular matrix degrading proteins and smooth muscle cell contractile apparatus proteins.

At the tissue-scale, the autograft is modeled as a pressurized perfect cylinder. The axial stretch is fixed, while the circumferential stretch at each time point is calculated with Laplace's law. The material properties are updated at every time point using a homogenized constrained mixture formulation [6] to predict growth and remodeling of collagen and elastin. More specifically, collagen production and degradation rates are calculated based on the activity levels of the corresponding genes, while elastin degradation is driven by excessive tissue deformation.

Pharmacological intervention

With this computational approach, we aim to detect new targets for pharmacological treatment. To that end, the simulation is run several times, each time fully inhibiting or fully activating one of the nodes in the cell-scale network model, setting the activity score to zero or one, respectively, for the duration of the simulation. To compare with existing treatments for other types of aortopathy, we virtually test the effects of pharmacological intervention with β-blockers by reducing the aortic pressure to 85% of its baseline level. Treatment by angiotensin-receptor blockers (ARBs) is simulated by also reducing the aortic pressure, and at the same time setting the activity level of the angiotensin-receptor AT1R node in the cell-scale network model to zero.

* Corresponding author. E-mail: lauranne.maes@kuleuven.be

RESULTS

Figure 2 shows the radius evolution for all possible perturbations, compared to the baseline, and treatment with β-blockers or ARBs. Note that the baseline model was calibrated and validated with results from our animal experiments [5]. The most promising intervention in terms of reduction of long-term autograft distension is the inhibition of the ETS1 transcription factor. Its beneficial effect is depicted in figure 3, showing that ETS1 inhibition has no negative impact on the transcription of fiber forming collagens (COL1 and COL3), compared to baseline level, while highly reducing the activation of MMP3, a potent collagenase. These beneficial effects for benign remodeling are not as pronounced with β-blockers and ARBs. However, ARBs are more effective at reducing inflammation levels, for example shown by the activity scores of cytokines IL6 and TNFα. Figure 3 also shows that after six months, most gene activities are back to their homeostatic levels.

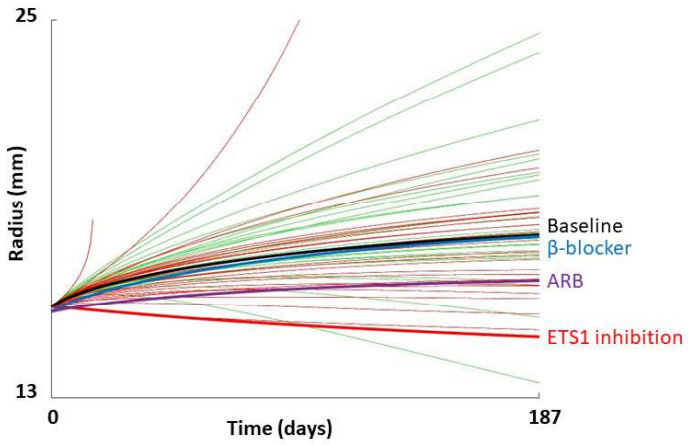

Figure 2. Predicted autograft radius over a remodeling period of 187 days. Black: baseline without pharmacological treatment, green and red: respectively all possible activation and inhibition perturbations in the cell-scale network model, of which ETS1 inhibition is indicated with a thicker line, blue and purple: results by virtual treatment with β-blockers or ARBs.

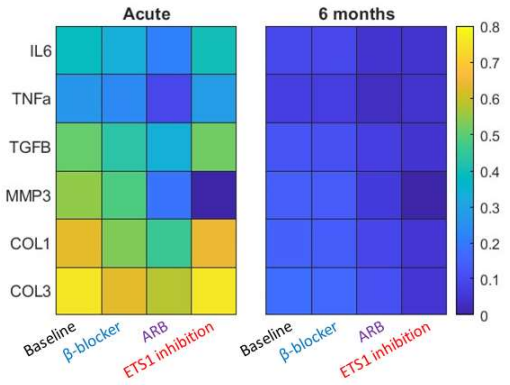

Figure 3. Predicted difference of activity scores of selected genes, acutely after surgery, and after six months, with respect to the homeostatic case before the surgery. Results are shown for the baseline case, virtual treatment with β-blockers or ARBs and inhibition of ETS1.

DISCUSSION AND CONCLUSIONS

An improved long-term outcome of the Ross procedure was predicted by treatment with β-blockers and ARBs, although the improvement is limited in the former case. An even better outcome in terms of diminished distension is predicted by inhibition of the ETS1 transcription factor, a currently unexplored target for pharmacological treatment in this context. This shows how *in silico* methods are promising tools that allow for refinement of ethically and economically more costly *in vivo* approaches in the exploration of novel treatment methods.

ACKNOWLEDGEMENTS

The authors would like to thank the **Research Foundation-Flanders (FWO)** for providing financial support to this project through a travel grant (K225123N) and two doctoral fellowships (1SE2123N and 1S70220N|1S70222N).

References

[1] Ross, D.N.: *Replacement of aortic and mitral valves with a pulmonary autograft*. The Lancet Vol. 290(7523), pp. 956-958, 1967.

[2] Sievers, H.H., Stierle, U., Petersen, M., Klotz, S., Richardt, D., Diwoky, M., Charitos, E.I.: *Valve performance classification in 630 subcoronary Ross patients over 22 years*. Journal of Thoracic and Cardiovascular Surgery Vol. 156, pp. 79-86, 2018.

[3] Van Hoof, L., Verbrugghe, P., Jones, E.A.V., Humphrey, J.D., Janssens, S., Famaey, N., Rega, F.: *Understanding Pulmonary Autograft Remodeling after the Ross Procedure: Stick to the Facts*. Frontiers in Cardiovascular Medicine Vol. 9, 2022.

[4] Maes, L., Vervenne, T., Van Hoof, L., Jones, E.A.V., Rega, F., Famaey, N.: *Computational modeling reveals inflammation-driven dilatation of the pulmonary autograft in aortic position*. Biomechanics and Modeling in Mechanobiology Vol. 22, pp. 1555-1568, 2023.

[5] Maes, L., Vervenne, T., Hendricks, A., Estrada A.C., Van Hoof, L., Verbrugghe, P., Rega, F., Jones, E.A.V., Humphrey, J., Famaey, N.: *Cell signaling and tissue remodeling in the pulmonary autograft after the Ross procedure: a computational study*. Under review at the Journal of Biomechanics.

[6] Cyron, C.J., Aydin, R.C., Humphrey, J.D.: *A homogenized constrained mixture (and mechanical analog) model for growth and remodeling of soft tissue*. Biomechanics and Modeling in Mechanobiology Vol. 15, pp. 1389-1403, 2016.

EMERGENT MORPHOLOGIES OF ACTIVE SURFACES

Alexander Mietke[1], Rui Ma[2]

1. Rudolf Peierls Centre for Theoretical Physics, University of Oxford, UK
2. Department of Physics, College of Physical Science and Technology, Xiamen University, China

Many force-generating structures in developing organisms, including the actomyosin cortex of cells and organ-lining epithelial tissues, are organised on effectively two-dimensional surfaces. A key challenge for the shape transformations such living materials are undergoing during morphogenesis is to organise locally generated active forces such that a desired global geometry robustly emerges. A popular theoretical framework that leads to the self-organisation of forces in an active material is mechano-chemical feedback, in which some "patterning agent", e.g. a concentration or order parameter field, tunes local active stress and is itself changing due to the generated flows or deformations. While this feedback ultimately leads to self-organised shape changes of an active surface, surprisingly little is known about the potential impact of active stresses that directly depend on the local curvature and, in particular, what role curvature-driven active stresses could play in guiding the robust generation of a desired surface geometry. Importantly, such a scenario eliminates the need for a separate patterning agent. Instead, surface curvature itself becomes the patterning agent and stationary states of curvature patterns correspond to emergent stationary surface geometries. Investigating this idea using a novel numerical approach to solve the force-and moment-balance equations of deforming active surfaces, we show in this work that the fully self-organized formation of stationary tubular, ellipsoidal and biconcave surfaces, as well as global shape transformations akin to cell division, can be controlled by homogeneous active processes that respond only to the local curvature.

EXPLORING THE EVOLUTIONARY MECHANISMS OF COLLAGEN AS A PROTEIN MATERIAL

Debora Monego[1,*]

1. Heidelberg Institute for Theoretical Studies, Germany

INTRODUCTION

Collagen, the predominant protein in connective tissues, plays a crucial role in maintaining structural integrity and biomechanical functionality, essential for tissue resilience and durability. Drawing parallels from enzymes, which evolve specific amino acid sequences to form precise structural folds for biochemical functions [1], we explore whether similar evolutionary principles apply to collagen. Just as enzymes have active sites stabilized by their protein scaffold, collagen may exhibit analogous regions formed by complex intermolecular interactions that contribute to its mechanical properties. By focusing on amino acid conservation and coevolution, we aim to extend the understanding of protein evolution from single protein chains to self-assembled protein materials like collagen.

MATERIALS AND METHODS

We start by employing hybrid Monte Carlo/Molecular Dynamics (KIMMDY) simulations to probe collagen's mechanical behavior under stress [2]. We perform detailed atomistic molecular dynamics simulations on a Type I collagen fibril subjected to a constant force to identify potential rupture sites. Our approach takes into account force distributions and bond dissociation energies within a reactive Monte Carlo framework, providing insights into the mechanical behavior of collagen at the molecular level.

Building on these findings, we further explore the role of collagen's structural evolution in defining its mechanochemical behavior. Using Direct Coupling Analysis (DCA) [3], we investigate evolutionary patterns including the conservation and coevolution of amino acid residues within collagen sequences. Specifically, we focus on identifying key interactions necessary for the protein's functionality and mechanical properties. By contrasting the mechanical insights gained from our simulations with evolutionary data from DCA, we aim to understand how molecular interactions and evolutionary pressures have shaped collagen's ability to withstand and respond to mechanical stresses.

RESULTS

Our simulations reveal that lysine-derived crosslinks, particularly trivalent ones, are the primary sites of micro-ruptures in collagen under mechanical stress. These crosslinks act as sacrificial bonds, rupturing before the backbone to preserve the overall integrity of the fibril (see Figure 1 for an overview of the structure of a collagen fibril). We present evidence supporting the theory that this rupture mechanism also limits chemical damage by producing exceptionally stable radical species, thereby mitigating uncontrolled degradation of the fibril.

Our evolutionary modelling allows us to identify coevolved residue pairs and map these onto the collagen structures from our molecular models. Although results on this front are in the preliminary stage, the focus is on discerning the relationship between collagen's evolutionary trajectory and its observed mechanochemical properties. We are particularly interested in investigating whether residues interacting across triple helices, crosslink sites (lysines), and redox active residues like Thy/Phe/Met - all known to be important for collagen's mechanochemistry - have coevolved. Out work will offer mechanistic insights into residue interactions, as well as a deeper understanding of how protein evolution translates to function in self-assembled protein materials.

* Corresponding author. E-mail: debora.monego@h-its.org

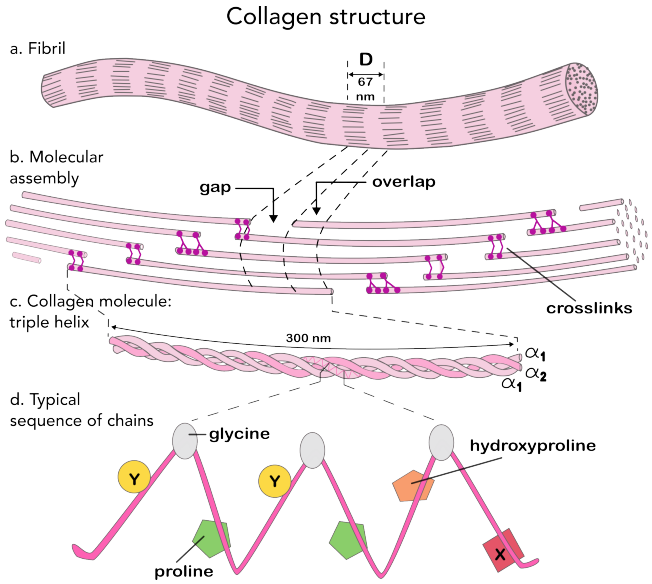

Figure 1. Collagen I hierarchical structure: Collagen fibrils (a) are formed by crosslinked bundles of assembled triple helices that are shifted relative to each other (b). There is hydrogen-bonding between the three chains (c), which have an amino acid sequence formed by the Gly-X-Y repeat, with X and Y being often proline and hydroxyproline (d).

DISCUSSION AND CONCLUSIONS

Our results suggest that collagen's crosslinks are evolutionarily adapted to enhance durability and prevent early onset of macroscopic failure, thus extending the material's functional lifespan. This behavior mirrors principles observed in high-performance synthetic polymers and highlights an evolutionary strategy in protein design that balances mechanical strength with chemical stability.

More generally, our study illustrates the applicability of evolutionary principles, typically associated with enzymes, to complex protein materials such as collagen. By demonstrating that collagen has evolved regions functionally similar to enzyme active sites, but involving multiple chains and intermolecular interactions, we provide a new perspective on how protein materials can be viewed through the lens of molecular evolution. These findings not only enhance our understanding of collagen's structural and mechanical properties but also suggest broader implications for the design of biomimetic materials and the therapeutic targeting of tissue repair and aging processes. Future work will further explore these evolutionary and functional analogies across different collagen types and species, informing both theoretical models and practical applications in biomedical engineering.

ACKNOWLEDGEMENTS

I thank Prof. Dr. Frauke Graeter and Prof. Dr. Debora Marks who collaborated with me in this work, as well as their respective research groups at the Heidelberg Institute for Theoretical Studies, Germany, and the Harvard Medical School, United states, respectively.

References

[1] Narayanan, C., Gagné, D., Reynolds, K.A. *et al.*: *Conserved amino acid networks modulate discrete functional properties in an enzyme superfamily*. Sci Rep 7, 3207, 2017.

[2] Rennekamp, B., Karfusehr, C., Kurth, M. *et al.*: *Collagen breaks at weak sacrificial bonds taming its mechanoradicals*. Nat Commun 14, 2075, 2023.

[3] Hopf, T.A., Green, A.G., Schubert, B., *et al.*: *The EVcouplings Python framework for coevolutionary sequence analysis*. Bioinformatics 9, pp. 1582–1584, 2019.

BIOMECHANICAL ALTERATIONS OF ENDOTHELIAL CELLS EXPOSED TO BACTERIALLY-INFECTED IMMUNE CELLS

Marie Muenkel[1,*], Erva Keskin[1], Aylin Balmes[2], Tilman Schäffer[2], Marco Lebtig[1], Dorothee Kretschmer[1], Kathryn Wright[3], Serge Mostowy[3], Effie Bastounis[1]

1. Interfaculty Institute of Microbiology and Infection Medicine, CMFI, University of Tübingen, Tübingen, Germany; 2. Institute of Applied Physics, University of Tübingen, Tübingen, Germany; 3. Department of Infection Biology, London School of Hygiene and Tropical Medicine, London, UK

INTRODUCTION

Infectious diseases are a significant cause of mortality worldwide and thereby pose a global health concern [1]. This is further exacerbated by the standing emergence of antibiotic resistant strains. Yet, we still do not fully understand how many pathogens can infect and spread throughout the human body. In particular, intracellular bacterial pathogens, like food-borne *Listeria monocytogenes* (LM), have developed a multitude of subtle strategies for manipulating their host cells without destroying host cell integrity, since they rely on it [2]. One of the ways LM can achieve systemic spread from the primary site of infection, the intestinal epithelium, is by being carried within macrophages (MΦs). These professional phagocytes are able to traverse the vasculature, a process known as transmigration, thus reaching distant organs such as the brain or the placenta, further spreading infection and causing fatalities [3]. How do infected MΦs manage to successfully transverse vascular endothelia breaching their barrier integrity? Have they developed mechanisms for (in)directly manipulating endothelial cell (EC) biomechanics?

MATERIALS AND METHODS

To explore changes in the biomechanics of ECs exposed to uninfected or LM-infected MΦs, we infected the monocyte-like cell line U937 with a green fluorescent strain of LM (JAT606) and exposed infected or non-infected U937 cells to human umbilical vein endothelial cells (HUVECs). We then measured HUVEC bulk stiffness using atomic force microscopy (AFM). Stiffening or softening might influence how well MΦs transmigrate across the endothelial monolayer. Traction force microscopy (TFM) was used to assess HUVECs´ ability to exert forces on their substrate via focal adhesions, a property that is needed to regulate the barrier function of the monolayer, and crucial, for example, to prevent pathogens to cross the blood-brain-barrier. The barrier integrity of a monolayer itself was directly measured using the transendothelial electric resistance (TEER) method.
We combined these measurements with immunostaining, videomicroscopy, transmigration-assays, and enzyme-linked immunosorbent assay (ELISA), and are complementing *in vitro* experiments with infection assays in zebra fish larvae to gain insights into the systemic spread of LM via infected MΦs.

RESULTS

When HUVECs were exposed to LM-infected or not U937 cells, they became more polarized and collectively aligned as compared to non-exposed HUVECs. At the same time their migration speed dropped 2-fold. In contrast, only when exposed to uninfected U937 cells, HUVECs displayed more F-actin stress fibers (data not shown) and higher bulk stiffness (from 1.5 to 2 kPa after 24 h exposure) (Fig. 1.A). Likewise, only during exposure (1-20 hours) to uninfected U937 cells HUVEC traction stresses (Fig. 1. C/D) as well as their electrical resistance increased (Fig. 1.E). The differential response of HUVECs to LM-infected. vs. uninfected U937 cells was also observed earlier during exposure. These findings suggest an altered response and lower barrier integrity in HUVECs exposed to LM infected U937 cells, which was further supported by a 50% increase in transmigration of infected U937 cells across HUVEC monolayers within a period of 24 h as compared to uninfected U937.

* Corresponding author. Email: **marie.muenkel@uni-tuebingen.de**

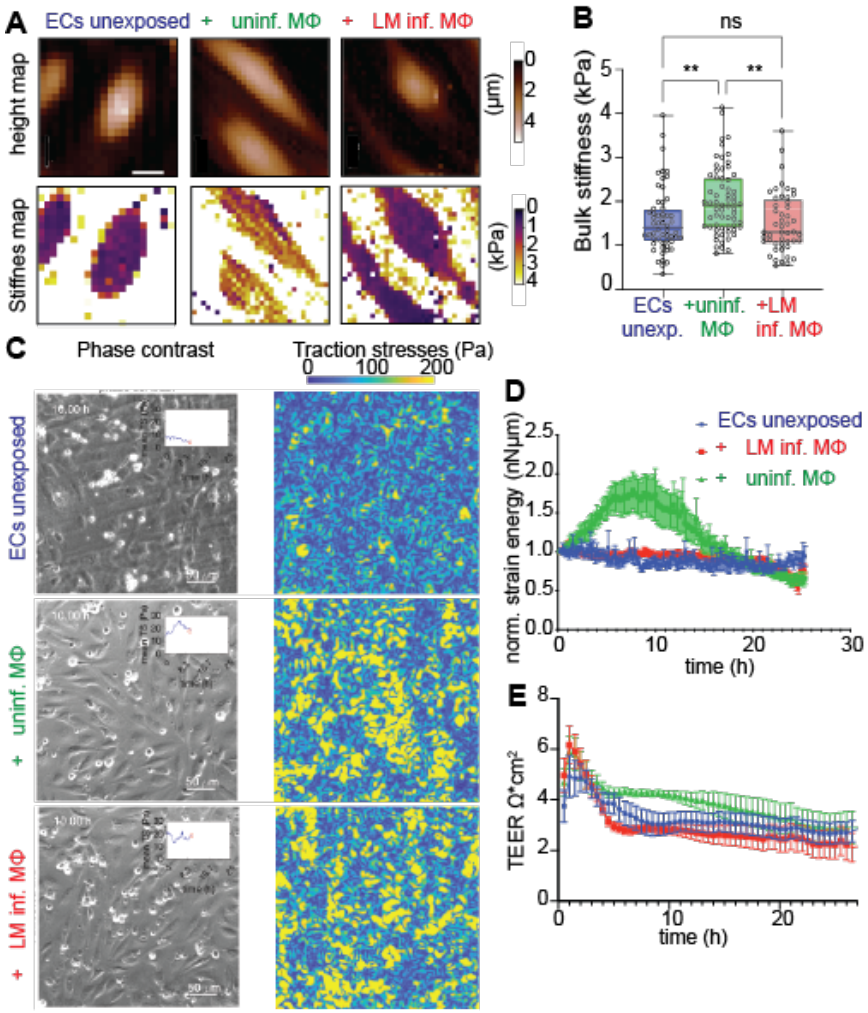

Figure 1 Stiffness, traction forces and monolayer barrier integrity are increased in HUVECs upon exposure to uninfected U937 cells but not to LM-infected U937 cells. A: representative height and stiffness maps of HUVECs exposed to differentiated U937 cells infected or not with *Listeria monocytogenes* (LM) as measured using atomic force microscopy. Scale bar 20 µm. **B**: Quantification of N=3 independent replicates of A. Boxplots showing mean +/- SEM. Dots represent mean value of one stiffness map. ANOVA with Kuskal-Wallis test. ns: non-significant. **:p=0.0021 **C**. Representative phase contrast images and traction force colour maps 10 h post exposure of HUVECs to differentiated U937 cells infected or not with LM. Mean traction force over time in subplot of the phase contrast images. **D**. Mean strain energy normalized to starting point of 3 independent replicates of C. Mean +/- SEM. **E**. Mean trans endothelial electrical resistance of HUVEC monolayers in the same conditions as in C. Mean +/- SEM.

DISCUSSION AND CONCLUSIONS

Alterations in EC biomechanics might underlie the ability of infected MΦs to breach EC barriers like the blood brain barrier. Understanding how infected MΦs modulate EC mechanotrasduction may help hinder LM spread in the brain. Here we show how EC cellular stiffness, traction forces and barrier resistance play a crucial role in facilitating systemic LM spread.

ACKNOWLEDGEMENTS

The authors would like to thank Libera Lo Presti for reviewing and discussing the project as well as Julie Theriot and Prathima Radhakrishnan for preliminary work and discussion. We thank the staff of FACs facility Uni Klinken Berg Tübingen for the assistance with the flow sorting. This project was funded by the Cluster of Excellence EXC 2124 'Controlling Microbes to Fight Infections' project ID 390838134 and an EMBO scientific exchange grant to MM.

References

[1] Balakrishnan, V. S. (2022) *WHO's first global infection prevention and control report*. Lancet Infect Dis, 22, 1122.

[2] Dowd, G. C., R. Mortuza, M. Bhalla, H. Van Ngo, Y. Li, L. A. Rigano & K. Ireton (2020) *Listeria monocytogenes exploits host exocytosis to promote cell-to-cell spread*. Proceedings of the National Academy of Sciences, 117, 3789.

[3] Birmingham, C., Canadien, V., Kaniuk, N. et al. *Listeriolysin O allows Listeria monocytogenes replication in macrophage vacuoles*. Nature 451, 350–354 (2008).

A COMBINATORIAL IN SILICO AND IN VITRO APPROACH TO STUDY CARTILAGE MECHANOBIOLOGY USING A CARTILAGE-ON-CHIP SETUP

Satanik Mukherjee[1*], Raphaelle Lesage[1], Laurens Spoelstra[3], Thanh Le[3], Carolina Serrano Larrea[3], Carlo Alberto Paggi[3], Jorge Barrasa Fano[1], Hans van Oosterwyck[1], Marcel Karperien[3], Liesbet Geris[1,2]

[1]KU Leuven, Belgium;[2]University of Liège, Belgium ;[3]University of Twente, the Netherlands

INTRODUCTION

Chondrocytes, the primary cells in articular cartilage require mechanical loading to maintain homeostasis. Understanding the mechanobiology of chondrocytes not only helps in unravelling factors that contribute to cartilage degeneration in Osteoarthritis (OA), but also in devising mechanical cues to stimulate chondrocytes to regenerate cartilage in a tissue engineering scenario. To support this, we have developed a multiscale *in silico - in vitro* approach using a combination of numerical modeling and a cartilage-on-chip microfluidic device [1] that mimics the mechanical environment of the chondrocyte in the knee joint. Using this approach, we investigated how mechanical loading might affect the synthesis of relevant matrix proteins by chondrocytes embedded in agarose hydrogel.

MATERIALS AND METHODS

Primary human chondrocytes were seeded in 2% w/v agarose hydrogel, together with fluorescent beads and injected in the cartilage-on-chip device (Fig 1a). The device was actuated for dynamic compression with a pressure of 300 mBar and a frequency of 0.5 Hz. An in-house algorithm [2] was used to track the beads to obtain mechanical strains across the hydrogel. Furthermore, image processing algorithms were used to calculate deformation of individual cells as obtained from brightfield microscopy images. Immunofluorescence staining was performed for Collagen 2 and 6, followed by confocal microscopy to obtain to obtain individual cells' matrix deposition. In parallel, a multiscale *in-silico* model of the setup was developed consisting of 3 different length scales as shown in figure 1.: i) **Gel-level finite element (FE) model**, containing the cell- and bead-laden hydrogel in the setup; ii) **Cell-level FE model**, containing individually segmented cells in hydrogel from the setup, and iii) **Intracellular gene/protein regulatory network**, which is an additive, semi-quantitative gene and protein regulatory network for chondrocyte mechanotransduction and inflammation developed using a combination of knowledge-based and inference-based approaches [3].

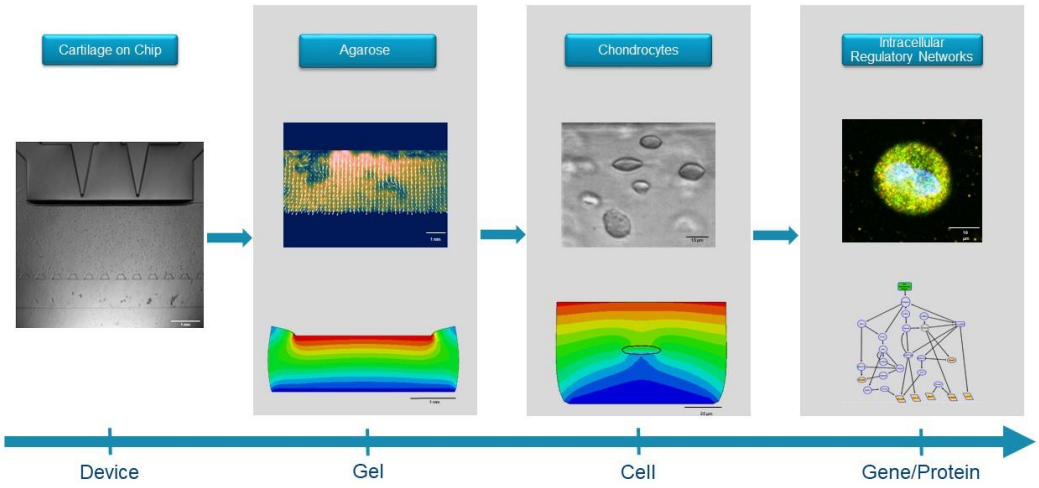

Figure 1: Overview of the multiscale model for the cartilage-on-chip setup

RESULTS

In the cartilage-on-chip device, a 36 µm membrane deformation was observed upon application of 300 mBar actuating pressure. By tracking the beads, a gradient in hydrogel deformation was observed, with the deformation decreasing on moving further away from the actuating membrane (Fig 2b). Furthermore, on zooming in to individual cells, and obtaining brightfield and fluorescent microscopy images, we were able to calculate both cellular deformations as well as deformations of the cellular microenvironment (Fig 2c). After a week of static

culture of the cells in the setup, immunofluorescent staining revealed deposition of Coll2 and Coll6 by the cells in their near vicinity, which was further increased following a week of dynamic mechanical stimulation with a frequency of 1Hz and amplitude of 300mBar (Fig 1d). This thereby indicates the influence of external mechanical stimulation in aiding the formation of a pericellular matrix by the cells.

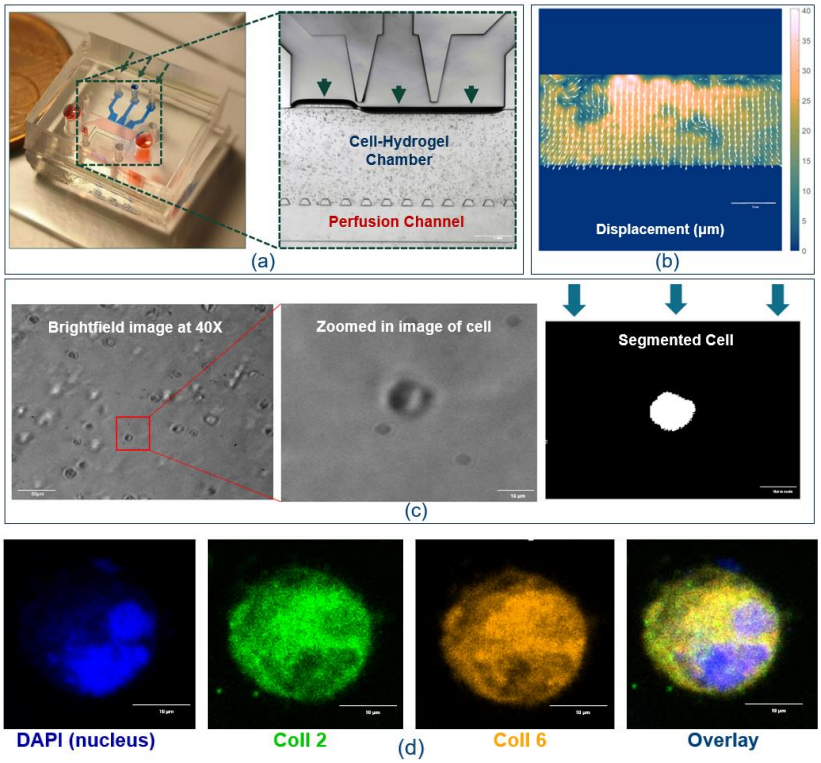

Figure 2. a) Cartilage-on-chip setup; b) Deformation field in the hydrogel by beads tracking; c) Single cell deformation; d) Immunofluorescence staining at 2 weeks

DISCUSSION AND CONCLUSIONS

Using the cartilage-on-chip device together with *in silico* modeling, we studied chondrocyte mechanobiology in a multiscale manner from an external mechanical stimulus to a measured cellular response. The established workflow not only allowed measuring cell-specific deformations, but also measuring local deposition of matrix constituents by the cells that represent the pericellular matrix. The workflow can be used in future to investigate specific mechanisms of chondrocyte mechanotransduction, as well as test efficacy of pharmaceutical drugs in arresting mechanically induced catabolic processes in chondrocytes.

ACKNOWLEDGEMENTS

We acknowledge funding from the EC (MSCA 721432, ERC CoG 772418 & 101088919), FWO and ESB Mobility Award.

References

[1] Paggi et.al. *Lab Chip*, 2022
[2] Barrasa-Fano et al. *SoftwareX*, 2021;
[3] Lesage et. al. *Bmc Biology*, 2022.

INFERENCE OF CYTOSKELETAL CONTRACTILITY FROM TFM DATA

Jose Muñoz[1,2,3,*], Shafaq Zahra[1], Andrea Malandrino[1,4]

1. Laboratori de Càlcul Numèric (LaCàN), Universitat Politècnica de Catalunya, Spain; 2. Centre Internacional de Mètodes Numèrics en Enginyeria (CIMNE), Spain; 3. Institut de Matemàtiques de la UPC-BarcelonaTech, Spain4. Biomaterials, Biomechanics and Tissue Engineering, UPC, Spain.

INTRODUCTION

Traction Force Microscopy (TFM) has revealed a very useful technique for retrieving the tractions that cell exert on a substrate. From the measurements of displacement field on the substrate, and solving an inverse problem, the tractions can be computed in two and three dimensions [2, 5]. This techniques has allowed researchers to deduce the mechanisms that cell employ during collective migration [4], or cell morphology in linear and non-linear gels [1]

We here aim at further estimate the cytoskeletal geometry and contractile state from the traction field computed from TFM. By constructing a set of mechanically compatible dipoles, we infer a geometrical distribution that exerts an equivalent traction field. In contrast to previous similar works [3], we do not require any constitutive law of the dipoles nor of the cell. We also present a similar methodology for computing the approximated intracellular stress state that is also compatible with the measured traction field.

MATERIALS AND METHODS

Cytoskeletal inference

We assume a flat domain $\Omega \in \mathbb{R}^2$ where a traction field $\boldsymbol{t}$ has been computed on a set of nodes i (or pixel images), $i = 1, \dots, n$. We aim at placing mechanical dipoles of length s between general nodes i and j, and with contractility c_{ij}, which must be in equilibrium with the set of nodal tractions $\boldsymbol{t}_i$. That is, at each pixel i, the following mechanical constraint needs to be satisfied:

$$\sum_j c_{ij} \boldsymbol{e}_{ij} = \boldsymbol{t}_i$$

with $\boldsymbol{e}_{ij}$ the unitary vector from i to j, i.e. $\boldsymbol{e}_{ij} = (\boldsymbol{x}_j - \boldsymbol{x}_i)/||\boldsymbol{x}_j - \boldsymbol{x}_i||$. This linear constrain can be written in a compact manner as

$$\mathbf{D}_s \mathbf{c} = \mathbf{t}$$

where matrix $\mathbf{D}$ gathers all the directions $\boldsymbol{e}_{ij}$ of the dipoles considered, and vector $\mathbf{c}$ includes all the contractilities. Consquently, finding an optimal set of compatible dipoles is tantamount to solving the following regularised minimisation problem

$$\begin{aligned} &\min_{\mathbf{D}_s, \mathbf{c}} ||\mathbf{D}_s \mathbf{c} - \mathbf{t}||^2 + \alpha ||\mathbf{c} - \mathbf{c}_{ref}||^2 \\ &\quad \mathbf{c} \geq -\boldsymbol{\delta} \end{aligned} \tag{1}$$

The regularisation parameter α allows to obtain a unique solution, while the reference values $\mathbf{c}_{ref}$, which is iteratively changing, allows to minimise the effect of the regularisation on the mechanical imbalance $\boldsymbol{\xi} = \mathbf{D}_s \mathbf{c} - \mathbf{t}$. The problem in (1) is linear on $\mathbf{c}$, but non-linear if $\mathbf{D}_s$ is also unknown. We solve on both variables in a staggered manner, where sequential linear problems are solved on $\mathbf{c}$, with a varying matrix $\mathbf{D}_s$. The latter is constructed by inspecting the dual problem to (1).

Current numerical experiments show that is computationally more effective to start with small dipoles lengths ($s = 1$) and solving a series of problems in (1) with increasing size s, until $\|\boldsymbol{\xi}\| < tol$. The constant vector $\boldsymbol{\delta}$ corresponds to the maximum amount of compression allowed, mimicking the presence of thicker elements such as microtubules.

Intracelular stresses inference

We have also developed a similar approach for inferring the internal stress field $\boldsymbol{\sigma}$ of the cell. A stress tensor is assumed at each quadrilateral elements formed by four nodes (or pixel images). Resorting to a finite element discretisation, the equilibrium condition of the stress field with a distributed traction field $\boldsymbol{t}$ reads

$$\nabla \cdot \boldsymbol{\sigma} + \boldsymbol{t} = \mathbf{0}$$

The finite elements discretisation of this equations may be written as $\mathbf{B}^T \boldsymbol{\sigma} = \mathbf{N}\mathbf{t}$, with $\boldsymbol{\sigma} = \{\boldsymbol{\sigma}_1, \dots \boldsymbol{\sigma}_n\}$ the set of elemental stress tensors, $\mathbf{B}$ a standard deformation matrix, and $\mathbf{t}$ the set of nodal tractions. Consequently, the optimal

* Corresponding author. E-mail: j.munoz@upc.edu

stress field may be computed as

$$\min_{\boldsymbol{\sigma}} ||\mathbf{B}^T\boldsymbol{\sigma} - \mathbf{t}||^2 + \alpha||\boldsymbol{\sigma} - \boldsymbol{\sigma}_{ref}||^2$$
$$s.t.\ \sigma_{xi}\sigma_{yi} - \tau_i^2 \geq -\delta,\ i = 1, \ldots, N_{elementos}$$
$$\sigma_{xi} + \sigma_{yi} \geq -\delta,\ i = 1, \ldots, N_{elementos}$$

The inequality constraints are equivalent to $\det(\boldsymbol{\sigma}_i) \geq 0$ and $trace(\boldsymbol{\sigma}_i) \geq 0$, that is, the principal stresses must be positive, indicating a tensile stress state. In order to solve this problem with the non-linear constraints, specific interior point methods have been adapted to the problem at hand.

RESULTS

We have tested the methodology described above on single MDCK cells adhered to hydrogel substrates with stiffness of 3.5 kPa. Figure 1 shows an example of a single cell, its corresponding dipoles distribution, up to $s = 6$, and a contour plot of the stress field $\boldsymbol{\sigma}$.

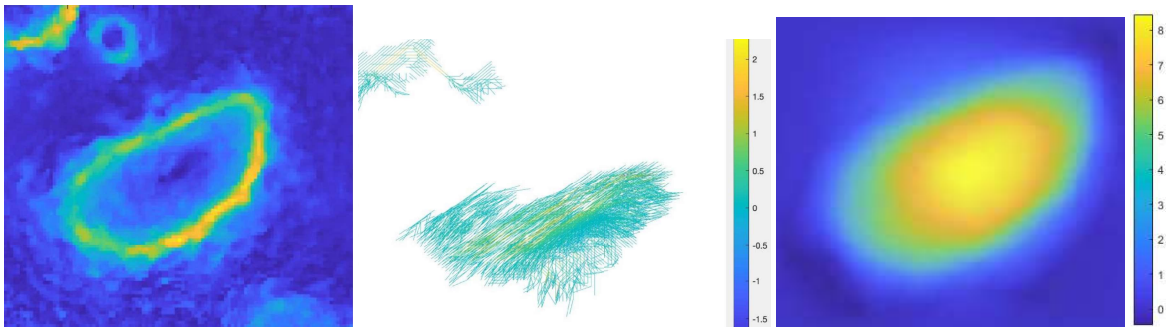

(a) (b) (c)

Figure 1. Example of application of cytoskeletal inference. (a) Traction field, contour plot of $\|\boldsymbol{t}\|$. (b) Set of compatible mechanical dipoles up to $s = 6$. Colour proportional to values of c_{ij}. (c) Internal stress field $\boldsymbol{\sigma}$. Showing $\sigma_x + \sigma_y$.

DISCUSSION AND CONCLUSIONS

The current approach will be validated with imaging of actin structures within the cell, and also relating this geometry with different conditions during cell migration. Importantly, we also aim at informing the minimisation process with the experimental imaging of relevant cellular properties, such as the location of the focal adhesions. By restricting the placement of the dipoles to these locations, an improvement of the accuracy is expected. Current research is being pursued to combine the results of the two minimisation problems, $\mathbf{c}$ and $\boldsymbol{\sigma}$, for generating more realistic cytoskeletal reconstructions.

ACKNOWLEDGEMENTS

The authors have been financially supported **Universitat Politècnica de Catalunya** through PhD grant program FPI-UPC, by the **Spanish Ministry of Science and Innovation** through grant PID2020-116141GB-I00, and the local government of **Generalitat de Catalunya**, with grant 2021 SGR 01049.

References

[1] A. Apolinar-Fernández, J. Barrasa-Fano, M. Cóndor, H. Van Oosterwyck, and J.A. Sanz-Herrera. Traction force reconstruction assessment on real three-dimensional matrices and cellular morphologies. *Int. J. Eng. Sci.*, 186:103828, May 2023.

[2] J.P. Butler, I.M. Tolić-Nørrelykke, B. Fabry, and J.J. Fredberg. Traction field, moments, and strain energy that cells exert on their surroundings. *Amer. J. Physiol. Cell Physiol.*, 282:C595–C605, 2002.

[3] J.R.D. Soiné, C.A. Brand, J. Stricker, P.W. Oakes, M.L. Gardel, and U.S. Schwarz. Model-based traction force microscopy reveals differential tension in cellular actin bundles. *PLOS Comp. Biol.*, 11(3):e1004076, 2015.

[4] R. Sunyer, V. Conte, J. Escribano, A. Elosegui-Artola, A. Labernadie, L. Valon, D. Navajas, J.M. García-Aznar, J.J. Muñoz, P. Roca-Cusachs, and X. Trepat. Collective cell durotaxis emerges from long-range intercellular force transmission. *Science*, 353(6304):1157–1161, 2016.

[5] G. Vitale, L. Preziosi, and D. Ambrosi. Force traction microscopy: An inverse problem with pointwise observations. *J. Math. Anal. Appl.*, 395:788–801, 2012.

QUANTUM-DOT BASED NANOSENSORS TO STUDY FOCAL ADHESION ASSEMBLY AND MECHANOSENSING

Audrey Ntadambanya[1], Julien Pernier[2], Violaine David[1], Kimihiro Susumu[3], Igor L. Medintz[3], Mayeul Collot [4], A. Klymchenko[4], I. Le Potier[5], Niko Hildebrandt [6], Christophe Le Clainche[1], Marcelina Cardoso Dos Santos[1*]

[1]Institute for Integrative Biology of the Cell (I2BC), France; [2] Gustave Roussy Institute, France; [3]Center for Bio/Molecular Science and Engineering U.S. Naval Research Laboratory, USA; [4]LBP, France; [5]C2N, France; [6] McMaster University, Canada

INTRODUCTION

Transmission of force between the cell and its environment is essential for the cell to accomplish adhesion and migration processes required for tissue building and repair. Transmission of force across the cell membrane is facilitated by focal adhesions (FAs) [1]. The mechanosensors that make up FAs are proteins sensing cytoskeletal tension. Talin is largely responsible for the mechanosensing of FA [2]. Filamentous actin binds to Talin and with myosin exerts a pulling force. However, the mechanism of mechanosensing still requires in-depth observation and due to lack of tools, how cells sense the cytoskeleton force remains unclear. To improve our comprehension of how Talin interacts with the membrane and its stretching, we have developed intra and inter molecular biosensors. This FRET (Förster Resonance Energy Transfer) nanosensor is made of Quantum Dot (QD) donor, able to measure distances greater than those from conventional FRET, and a dye acceptor.

In this study, we could deduce how Talin assemble according to the membrane and measure separating distances thanks to FRET efficiencies obtained using fluorescence spectroscopy and microscopy. Changes of Talin conformation with cytoskeleton tension were observed.

MATERIALS AND METHODS

Three Talin variants produced in E.Coli bacteria strain were used: AB-Ta (actin binding Talin) variant, composed of F_2-F_3-R_1-R_2-R_3-R_{13}, ΔABD-Ta (delta actin-binding domain Talin) composed of F_2-F_3-R_1-R_2-R_3-R_4-R_5-R_6 R_7-R_8 and mini ΔABD-Ta (mini delta actin-binding domain Talin) composed of F_2-F_3-R_1-R_2-R_3. CdSe/CdS/CdZnS/ZnS core/multishell QDs were prepared and coated with CL4 capping ligands [6]. FRET nanoprobes were prepared by mixing QD (λ_{em}=600nm) at 20 nM and Talin in a 1:2 concentration ratio in KCl 100mM/HEPES 20 mM buffer with 0.06% BSA for 1h at RT. Talin-QD conjugate was added on GUVs. Later, MemBright640 acceptor (λ_{em}=664nm) diluted at 400 nM was added for integration in GUV lipidic bilayer . GUVs made by PVA gel-assisted vesicle formation method. They are made of egg PC with 20% mole cholesterol, 10% mole PIP_2 and 3.5 % mole DSPE-(PEG2000)-biotin; in chloroform.

Spectroscopy experiments were conducted on FluoroMax-4 where emission spectra of donor alone (I_D) and donor in the presence of the acceptor (I_{DA}) were acquired using 625V gain, 2 nm slit range, and excitation 405 nm. For the microscopy experiments, we used Spinning-Disc microscopy to register I_D and I_{DA}. FRET efficiencies (η) were calculated as following: $\eta = 1 - \frac{I_{DA}}{I_D}$ (Eq. 1), since η varies proportionally with the inverse sixth power of the distance r between the donor and acceptor molecules, it was calculated as: $r = (\frac{1}{\eta} - 1)^{1/6} \times R_0$ (Eq. 2), with R_0 being the Förster distance.

RESULTS

To quantify intermolecular distances, spectroscopy was employed to study the interaction between Talin and the membrane. This interaction results in the quenching of the donor's emission (Fig 1 A, blue curve). For three Talin variants: AB-Ta, ΔABD-Ta and mini ΔABD-T, corresponding η values of 0.65, 0.38, and 0.51, were found from Eq.1. Eq. 2 was used to determine the distance between the QD donor and acceptor for AB-Ta, ΔABD-Ta and mini ΔABD-Ta as 6.3 ± 0.8, 7.3 ± 0.2 and 6.7 ± 0.2 nm respectively. This distance reflects the distance separating Talin from the membrane.

* Corresponding author. Email: marcelina.cardoso-dos-santos@i2bc.paris-saclay.fr

Single GUV measurements were made in microscopy with images in "donor channel. Mean I_D and I_{DA} were extracted before and after MemBright640 addition (Fig 1 B_1, B_2). We can see a difference in intensity between I_D and I_{DA} images. In fact, the intermolecular distance shortening makes the donor quenching more visible. The calculated η were of 0.35, 0.17 and 0.32 and the deduced intermolecular distances were $r_{AB\text{-}Ta}$=7.3 ± 1 nm, $r_{\Delta ABD\text{-}Ta}$=8.6 ± 1 nm and $r_{mini\Delta ABD\text{-}Ta}$=7.5 ± 1 nm, respectively for AB-Ta, ΔABD-Ta and mini ΔABD-Ta.

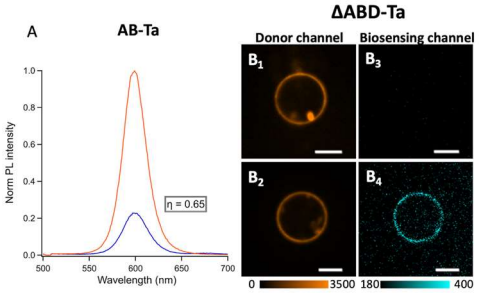

Figure 1. A) Talin-membrane interaction revealed by fluorescence spectroscopy. Normalized emission spectra of AB-Ta. B) Talin-membrane interaction revealed by fluorescence microscopy(ΔABD-Ta images). In donor channel PL intensity of QD donor before (B_1) and after acceptor addition (B_2) and in biosensing channel for donor alone (B_3) and donor+acceptor (B_4) Scale bars: 5 µm.

To mimic the tensile force of cytoskeleton, Actin and Myosin II (Two major microfilament components) have been used on the AB-Ta. The mechanosensing process happens when actin filaments contract and Talin stretches upon Myosin addition. As a result, Talin changes conformation. A slight variation of η is observed. Here, for the first time to our knowledge, Talin mechanosensing mechanism, as a consequence of actin-myosin activity, has been revealed and quantified at the nanometric scale.

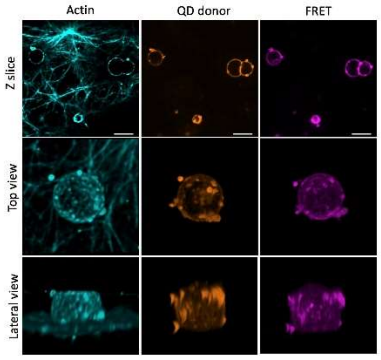

Figure 2. Talin mechanosensing. Talin AB-Ta stretched by actin-myosin: z slice of an area of few GUVs (top); 3D Visualization of top view (middle) and lateral view (bottom) on one GUV in Actin; QD nanosensor and FRET channels.

DISCUSSION AND CONCLUSIONS

Results of η for the Talin intermolecular distance explain the quenching decrease. Our findings were compared with theoretical models in Alphafold where we observed the orientation of domains interacting with the membrane relative to Talin. Talin interacts with various partners regulating the mechanical response of the adhesion. However, these interactions are complex and require further investigation. In our study, we could observe a distance shortening with actin-myosin. In conclusion, our QD-based FRET nanosensors have yielded quantitative insights into talin stretching dynamics. We will be able to elucidate emerging models for Talin assembly with different partners.

ACKNOWLEDGMENTS

This work was partially funded by the Interdisciplinary Object “OI Bioprobe”. Authors thank the Light Microscopy facility of Imagerie-Gif and Integrative Bioinformatics platform (BIOI2) @I2BC.

References

[1] P. Kanchanawong *et al.*, “Nanoscale architecture of integrin-based cell adhesions,” *Nature*, vol. 468, no. 7323, pp. 580–584, 2010.

[2] J. Liu *et al.*, “Talin determines the nanoscale architecture of focal adhesions,” *Proc. Natl. Acad. Sci.*, vol. 112, no. 35, 2015.

* Corresponding author. Email: marcelina.cardoso-dos-santos@i2bc.paris-saclay.fr

Hybrid Approach for In-Silico Modelling of Atherosclerosis: Combining Continuous and Agent-Based Methods

Ricardo Caballero[1]., Miguel A. Martínez [1,2] and Estefanía Peña [1,2]

Aragón Institute of Engineering Research (I3A). University of Zaragoza, Spain; 2. 2 Biomedical Research Networking Center in Bioengineering, Biomaterials and Nanomedicine (CIBER-BNN), Spain

INTRODUCTION

Cardiovascular diseases (CVDs) persist as a substantial threat to global health, remaining a primary cause of morbidity and mortality worldwide [1]. Of all cardiovascular conditions, atherosclerosis emerges as a central factor in the prevalence of CVDs. Atherosclerosis is a multifaceted and persistent inflammatory ailment marked by the buildup of fatty deposits, cholesterol, cellular debris, and various substances along the inner walls of arteries. Gradually, these accumulations form plaques, which can constrict and harden arteries, hindering proper blood circulation [1]

In this work, we present an in-silico model that combines a continuous convection-diffusion-reaction model and an agent-based model to predict atheroma plaque growth. We explore how hemodynamics affect the mechanics and transport properties in the arterial wall, triggering cellular events that are related to atheroma plaque growth.

The hybrid model has three modules coupled together: computational fluid dynamics (CFD), continuous module of continuous convection-reaction-diffusion (CRD) equations and agent-based model (ABM).

MATERIALS AND METHODS

Our hybrid model has three coupled modules: computational fluid dynamics (CFD), mass transport, and agent-based modelling (ABM). The CFD module starts from a 3D coronary artery geometry, in which hemodynamics are calculated using the Navier-Stokes equations. Then, several 2D cross-sectional surfaces are selected in the zone of least wall shear stress (WSS) of the 3D model, and the plasma filtration process is reproduced using Darcy's Law. The mass transport module models the transport of substances using the convection-diffusion-reaction equations. Low-density lipoprotein (LDL) leakage through the endothelium is evaluated using the three-pore model [2], which considers three pore sizes: small, normal, and large [3].

The ABM module imports both the 2D geometry and the WSS and LDL concentration values from the CFD and mass transport modules. This module is responsible for predicting arterial wall remodelling using conditional and stochastic behavioural rules, which calculate the probability of occurrence for each cellular process. The cellular processes included: mitosis and apoptosis of cells; production and degradation of extracellular matrix; production, phagocytosis, and necrosis of macrophages, becoming foam cells (FCs) due to excess LDL in the wall; and the change of phenotype of smooth muscle cells (SMCs) from contractile to synthetic.

To couple both models, a segmentation process is performed on the ABM output image, identifying the different layers that form the arterial wall. Then, with this information, the 3D geometry is reconstructed and the process is repeated.

RESULTS

The CFD module reveals wall shear stress (WSS) distribution along the artery. A pathological area with WSS > 0.5 Pa is observed after the bifurcation, as shown in Figure 1a. This region is anticipated to undergo significant growth due to plaque formation. The mass transport module provides LDL concentrations to the ABM, initiating macrophage action, and ultimately transforming into foam cells. Figure 1b illustrates the accumulation of foam cells in a necrotic core, surrounded by synthetic smooth muscle cells (sSMCs) forming the fibrous cap through migration and proliferation. A remarkable increase in the cellular density is observed in regions surrounding the necrotic core, as a result of the remodelling of the vessel, reproducing the dynamic nature of the arterial remodelling in response to plaque development.

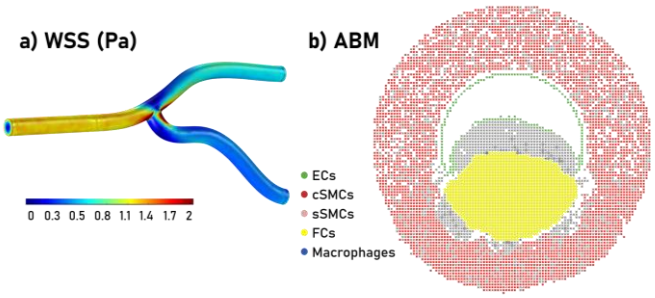

Figure 1. a) WSS (Pa) results on 3D CFD model. b) Plaque growth replication in the Agent-based model

DISCUSSION AND CONCLUSIONS

Our agent-based model (ABM) demonstrates promising capabilities in realistically predicting the growth of atheroma plaques, particularly in areas with lower wall shear stress (WSS). It is important to note that these findings are preliminary and require further validation. This work represents an early exploration of the complex dynamics involved in cardiovascular disease progression.

ACKNOWLEDGEMENTS

This work was supported by the Spanish Ministry of Science and Innovation through research projects PID2019-107517RB-I00 and PID2022-140219OB-I00 and the Instituto de Salud Carlos III (ISCIII) through the CIBER initiative.

References

[1] Roth G. et al., The Lancet, 392 (10159): 1736 – 1788, 2018.
[2] C. C.; CURRY, F. E. Microvascular permeability. Physiological Reviews, 1999
[3] Cilla M. et al. Annals of Biomedical Engineering, 43 7 1516 30 2015

GEOMETRIC CONTROL BY ACTIVE MECHANICS OF EPITHELIAL GAP CLOSURE

Giulia Pozzi[1,2], Pasquale Ciarletta[2]

1. Dipartimento di Scienze Matematiche (DISMA) - Politecnico di Torino, Italy; 2.MOX - Politecnico di Milano, Italy

INTRODUCTION

Living tissues possess intrinsic self-repair mechanisms to close wounds and restore tissue integrity post-injury. It is known that dysregulation of the physiological features of wound healing can result in severe infection and it can promote the onset of cancer. Experimental evidence [1] shows that the wound closure process is regulated by a dynamic interplay between cellular crawling and a supracellular purse-string mechanism due to the presence of an actomyosin cable. Several mathematical models, ranging from continuum [2] to discrete [3] approaches, have been proposed in the literature to unravel the complex biomechanical processes governing wound healing. In this work, for the first time we propose a novel diffuse interface model, integrating thermodynamic principles with mechano-biological dynamics, to simulate gap closure efficiently across various geometries. By means of formal analysis and finite element simulations, we demonstrate the model ability to capture key aspects of wound closure dynamics, shedding light on the underlying physics [4].

MATERIALS AND METHODS

In this study we investigate epithelial closure using a model of a confluent monolayer of epithelial cells immersed in a large bath, with a gap created by a PDMS stencil. The monolayer is modeled as a biphasic mixture with a diffuse interface separating the wound from the healthy tissue. The interface movement is governed by slow, coarse-grained variables partly driven by a gradient flow dependence with respect to a chemical potential, incorporating both local and non-local interactions. Following the thermodynamic arguments for extending the maximum dissipation principle accounting for active cellular phenomena and dissipation mechanisms and enforcing the momentum balance equation leads to a Darcy–Brinkman equation, balancing cell–cell forces, substrate friction, and Korteweg forces. Mechanical forces from actomyosin cables are represented as a surface tension at the wound edge. Cell crawling is accounted for by an extra chemical potential and a crawling rate term.

To elucidate how the interplay between crawling and purse-string forces are integrated into our model, we conduct a formal asymptotic analysis on the model as the interface thickness approaches zero. As so, we derive a sharp interface limit model for the wounded monolayer endowed by jump conditions at the interface, accounting for the normal crawling pressure and active purse-string tension.

Finally, Finite Element simulation are performed to assess the behavior of the proposed model and its ability to correctly predict different aspects of wound healing.

RESULTS

The sharp interface limit shows that the mixture behaves as an incompressible Darcy–Brinkman fluid, with interfacial forces representing crawling pressure and purse-string tension. The movement of the interface is governed by a Mullins–Sekerka problem, with crawling energy source defining the chemical potential. The purse-string mechanism introduces an active surface tension and substrate friction inversely proportional to the mobility parameter.

From the Finite Element simulations, we observe that the closure dynamics of the epithelial gap exhibit a consistent trend in local regulation, where regions with positive curvature advance faster than those with negative or flat curvature. Initially, purse-string tension regularizes the wound shape, leading to a rounded configuration. The in-silico healing times range from 40 to 60 minutes, showing a near-linear decrease in wound area over time regardless of the initial gap shape, see Figure 1. Parameter analysis reveals that lower crawling and motility parameters prolong healing times, while reducing substrate friction accelerates closure. Additionally, varying the purse-string force and crawling rate affects wound regularization and closure acceleration differently, as shown in Figure 2. Finally, we found that the predicted principal stress patterns indicate regions of compressive stress near convex borders and traction stress near concave borders, consistently with traction force microscopy measurements [5].

* Corresponding author. E-mail: giulia.pozzi@polito.it

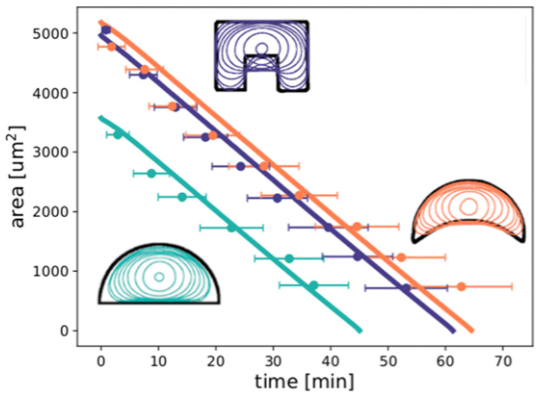

Figure 1. In silico simulated decrease of the area over time for three differently shaped wounds: *square inset* (blueline), *half circle* (greenline) and *half moon* (orangeline) with an initial area of 3500–5000 mm^2.The horizontal bars coincide with the error bars of the experimental data extracted from [1] for each geometry. The image shows also the overlay of outlines at different time points for each of the three wound shapes.

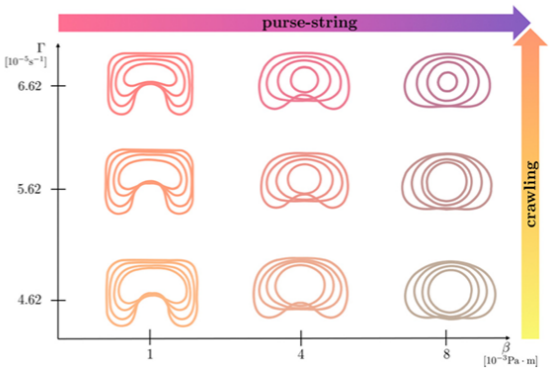

Figure 2. Phase diagram describing the evolution of the wound edge (*square inset* geometry) during the closure process by varying the purse-string intensity β and the crawling rate Γ. Each figure is obtained by overlapping the simulated wound edges at time t: 12 min, 24 min, 36 min, and 48 min.

DISCUSSION AND CONCLUSIONS

In this study, we introduce a novel diffuse interface model to characterize the mechano-biological dynamics of epithelial closure. Derived from thermodynamic principles within the mixture theory framework, our model integrates active phenomena and dissipation mechanisms. It describes the wounded epithelium as a viscous mixture akin to a Darcy–Brinkman–Korteweg fluid with volumetric mass sources and diffusive mass flux, guided by a chemical potential. The latter incorporates an active surface tension term simulating purse-string mechanisms and a short-range nonlocal interaction regulating interface width, while lamellipodia crawling is represented through an extra-pressure term and a crawling rate in the Cahn–Hilliard equation. The asymptotic analysis reveals the role of interfacial and frictional forces in leading the wound edge movements: Korteweg forces driven by the diffusive chemical potential and the crawling impose a pressure jump across the interface, while the diffusion of the chemical potential is governed by a Mullins–Sekerka system.

Finite element simulations align well with in-vitro experiments, capturing the quasi-linear decrease of wound area over time and morphological changes in the wound edge. Also the curvature-dependent regulation of closure dynamics and the related stress pattern in the monolayer are correctly predicted by our model. Besides these promising results, it is worth to notice that the proposed diffuse interface approach reduces numerical complexity compared to sharp interface models, offering a robust and computationally efficient alternative.

Future improvements will be devoted to the incorporation of the chemo-mechanical coupling to capture calcium wave dynamics and to explore effects of orientational order on cellular spreading.

ACKNOWLEDGEMENTS

The authors would like to thank the **Istituto Nazionale di Alta Matematica (INdAM - GNFM group)** and the **Italian Ministry for Universities and Research (MUR)** for providing financial support to this project.

References

[1] A. Ravasio, et al., *Gap geometry dictates epithelial closure efficiency*, Nat. commun., 2015, 6(1), 1–13.
[2] J. C. Arciero, et al., *Continuum model of collective cell migration in wound healing and colony expansion*, Biophys. J., 2011, 100(3), 535–543.
[3] S.-Z. Lin, et al., *Collective dynamics of coherent motile cells on curved surfaces*, Soft Matter, 2020, 16(12), 2941–2952
[4] Pozzi, G., Ciarletta, P., *Geometric control by active mechanics of epithelial gap closure*, Soft Matter, 20.4 (2024): 900-908.
[5] A. Brugues, et al.,*Forces driving epithelial wound healing*, Nat. Phys., 2014, 10(9), 683–690.

ENGINEERING CCM-ASSOCIATED MECHANICS ON A MICROFLUIDIC CHIP

Jyotsana Priyadarshani[1*], Apeksha Shapeti[1], Jorge Barrasa Fano[1], Eva Faurobert[2], Hans Van Oosterwyck[1,3*]

[1]KU Leuven, Biomechanics Section, BELGIUM, [2]University of Grenoble Alpes, Institute for Advanced Biosciences, FRANCE, [3]KU Leuven, Prometheus Division of Skeletal Tissue Engineering, BELGIUM

INTRODUCTION

Leveraging the advantages of microfluidics[1] and top-down microfabrication approach[2], we are presenting a novel *in vitro* model of a perfused microvascular network compatible with 3D traction force microscopy (TFM) to explore the mechanobiology of cerebral cavernous malformations (CCM). CCM results from the dysregulated homeostasis of venous capillary networks within the brain[3]. Upon losing one of the CCM genes, the mutated endothelial cells (ECs) in the capillaries adapt proangiogenic behavior and invade underlying ECM to form leaky mulberry-like lesions. Existing insights into CCM pathophysiology have been gleaned from *in vivo* models in worms, zebrafish, mice, and various in vitro 2D/3D cell-culture models[4]–[6]. However, the formation of CCM lesions and the interplay between intrinsic and extrinsic mechanical cues remain unexplored. A recent in vitro angiogenic invasion model from our research group revealed that CCM-mutated endothelial cells exhibit hyperangiogenic invasion by applying excessive forces on the surrounding ECM, as measured using 3D traction force microscopy (3D TFM)[7], [8]. The study highlights the significance of mechanical forces in vascular disease and paves the direction of developing a dynamic 3D TFM-compatible vessel on a chip.

MATERIALS AND METHODS

The study includes the microfabrication of vessel networks with comparable dimensions of the capillaries, which are prone to CCM lesion formation i.e., 5-20 µm in diameter, and are part of low flow venous regions of the brain. The fabrication process includes a top-down microfabrication approach to have a predefined vessel geometry within a hybrid Polydimethylsiloxane (PDMS)-Hydrogel construct where the PDMS layer provides mechanical robustness to the soft hydrogel (collagen type-1, Rat tail, Sigma Aldrich) to sustain hydrodynamic shear stresses. The entire vessel geometry comprises a parallel ladder-shaped closed-loop network, including two parallel channels fabricated within the hydrogel by casting needles, followed by generating multiple microcapillaries between the parallel channels using multiphoton laser photoablation as schematically represented in Fig. 1(a) and 1(b). The hydrogel is prepared by embedding uniform fluorescent nanobeads to make the device 3D TFM compatible. The fabricated device is further tested by manually perfusing green ink and capturing the microscopic images.

RESULTS

A perfusable microvasculature having channel dimensions of 120 µm is produced within a hybrid microfluidic device as shown in Fig. 1(c) after the needle casting method. Fig. 1(e) shows the generation of microcapillaries of 15 µm diameter between the needle-casted parallel channels. The selected region of interest for photoablation and cross-sections in the xy- & yz- planes of ablated capillaries are shown in the figure. The device provides precise control over hydrodynamic fluid perfusion and is suitable for probing cell suspensions as shown by introducing CCM-2 gene silenced endothelial cells and maintaining them for the next three days within the needle-casted channels (Fig. 1(e)).

* Corresponding author. Email: **jyotsana.priyadarshani@kuleuven.be; hans.vanoosterwyck@kuleuven.be**

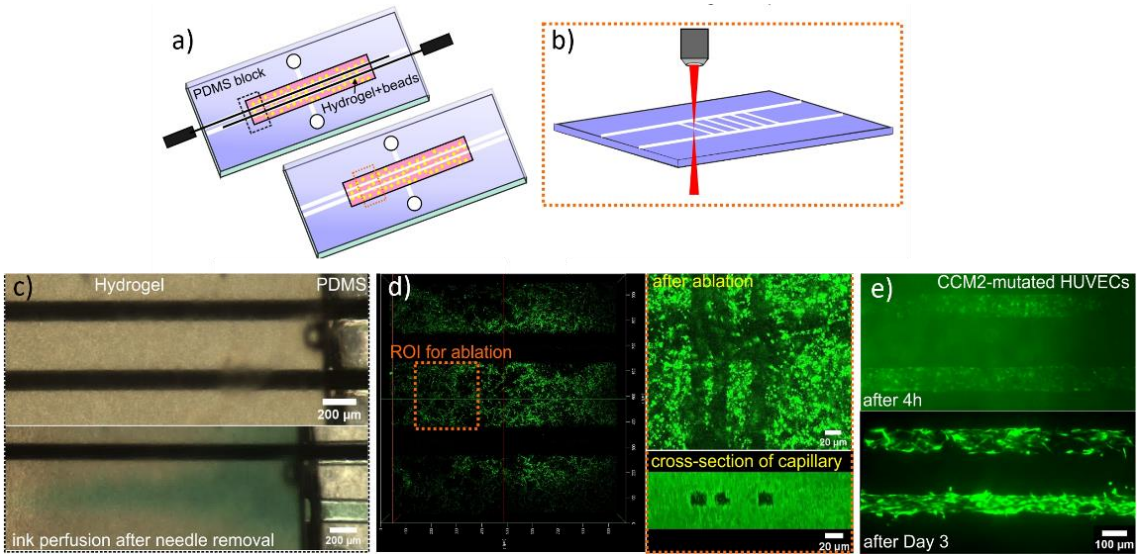

Figure 1: (a,b) Schematic showing microchannel fabrication using needle casting and photoablation respectively, (c) the optical image showing the perfusable channel after needle removal; green ink perfusion is shown for better visualization. (d) capillary generation after selecting the region of interest and ablating the hydrogel with a multiphoton laser. (e) three-day culture of CCM2 gene-mutated endothelial cells within needle-casted microchannels.

DISCUSSION AND CONCLUSIONS

This model addresses various structural and functional aspects of CCM disease by recapitulating the mechanobiology of CCM-associated capillaries through relevant geometrical dimensions, extracellular matrix (ECM) stiffness, physiological flow rates, and precise modulation of biochemical signaling factors. The ultimate aim of this innovative biochip is to enable the monitoring of cell-generated forces and vascular integrity under pathophysiological conditions, advancing the path toward therapy development.

ACKNOWLEDGEMENTS

The authors want to acknowledge KU Leuven Internal Funding (IDN/19/031, iBOF/21/083 C), FWO project G0C2422N, ERANET G0L1522N, and FWO junior postdoctoral fellowship, application number 12AZV24N.

References

[1] S. W. Chen, A. Blazeski, S. Zhang, S. E. Shelton, G. S. Offeddu, and R. D. Kamm, "Development of a perfusable, hierarchical microvasculature-on-a-chip model," *Lab Chip*, vol. 23, no. 20, pp. 4552–4564, Oct. 2023, doi: 10.1039/D3LC00512G.

[2] J. Priyadarshani, T. Roy, S. Das, and S. Chakraborty, "Frugal Approach toward Developing a Biomimetic, Microfluidic Network-on-a-Chip for in Vitro Analysis of Microvascular Physiology," *ACS Biomater. Sci. Eng.*, vol. 7, no. 3, pp. 1263–1277, Mar. 2021, doi: 10.1021/acsbiomaterials.1c00070.

[3] Y. Yamashiro and H. Yanagisawa, "The molecular mechanism of mechanotransduction in vascular homeostasis and disease," *Clin. Sci.*, vol. 134, no. 17, pp. 2399–2418, Sep. 2020, doi: 10.1042/CS20190488.

[4] C. M. Phillips, S. M. Stamatovic, R. F. Keep, and A. V. Andjelkovic, "Cerebral Cavernous Malformation Pathogenesis: Investigating Lesion Formation and Progression with Animal Models," *Int. J. Mol. Sci. 2022, Vol. 23, Page 5000*, vol. 23, no. 9, p. 5000, Apr. 2022, doi: 10.3390/IJMS23095000.

[5] D. R. Vannier *et al.*, "CCM2-deficient endothelial cells undergo a ROCK-dependent reprogramming into senescence-associated secretory phenotype," *Angiogenesis*, vol. 24, no. 4, pp. 843–860, Aug. 2021, doi: 10.1007/S10456-021-09809-2/FIGURES/7.

[6] J. Lisowska *et al.*, "The CCM1-CCM2 complex controls complementary functions of ROCK1 and ROCK2 that are required for endothelial integrity," *J. Cell Sci.*, vol. 131, no. 15, Aug. 2018, doi: 10.1242/JCS.216093/265578/AM/CEREBRAL-CAVERNOUS-MALFORMATION-1-2-COMPLEX.

[7] A. Shapeti *et al.*, "Force-mediated recruitment and reprogramming of healthy endothelial cells drive vascular lesion growth," *bioRxiv*, p. 2023.11.27.568780, Nov. 2023, doi: 10.1101/2023.11.27.568780.

[8] J. Barrasa-Fano, A. Shapeti, Á. Jorge-Peñas, M. Barzegari, J. A. Sanz-Herrera, and H. Van Oosterwyck, "TFMLAB: A MATLAB toolbox for 4D traction force microscopy," *SoftwareX*, vol. 15, Jul. 2021, doi: 10.1016/j.softx.2021.100723.

HYDROGELS WITH TUNEABLE COLLAGEN DENSITY REGULATE BREAST CANCER CELL MECHANICAL ACTIVITY

Raquel Ruiz-Mateos [1,2], Pablo Blázquez-Carmona [1,2], Jorge Barrasa-Fano [3], Apeksha Shapeti [3], José Enrique Martín-Alfonso [4], Jaime Domínguez [1,2], Hans Van Oosterwyck [3], Esther Reina-Romo [1,2], José Antonio Sanz-Herrera [1,2]

1. Escuela Técnica Superior de Ingeniería. Universidad de Sevilla, Spain; 2. Instituto de Biomedicina de Sevilla (IBIS), Spain; 3. Department of Mechanical Engineering, Biomechanics Section, KU Leuven, Belgium; 4. Chemical Product and Process Technology Research Center (Pro2TecS), Department of Chemical Engineering and Materials Science, ETSI, Universidad de Huelva, Spain.

INTRODUCTION

Increased density and stiffness of ECM fibres is observed during cancer progression and has been related to changes in the metabolism of breast cancer cells[1-2]. Furthermore, breast cancer cells proliferate rapidly as the substrate stiffens[3]. We asked whether steric hindrance, understood as micro-architectural barriers imposed by ECM pore size, influences the behaviour of human MDA-MB-231 breast cancer cells when embedded in type I collagen hydrogels from different natural sources. The hydrogels were mechanically tested by shear rheology and their microarchitectures characterised by focused ion beam scanning electron microscopy (FIB-SEM), while cellular forces and strain energies were reconstructed by 3D tensile force microscopy (TFM). The results obtained allowed us to investigate the influence of mechanical, physicochemical and microarchitectural matrix properties on the self-induced micromechanical environment of tumour cells.

MATERIALS AND METHODS

Cell culture and collagen hydrogel preparation

MDA-MB-231 cells were cultured in DMEM supplemented with fetal bovine serum (FBS) and penicillin-streptomycin. The cells were studied as a model of late-stage breast cancer and were embedded in several extracellular matrices for analysis of their mechanical behaviour. Nine different type I collagen hydrogels were selected based on their concentration (0.8 mg/ml, 1.5 mg/ml or 2.3 mg/ml) of pure bovine dermal collagen, pure rat tail collagen or a 1:1 mixture of both collagens. Polymerization of the hydrogels was induced by raising the pH to 7.4 and incubating at 37ºC for an hour.

Microenvironments' properties

Microarchitecture of the different collagen hydrogels was characterized by FIB-SEM ZEISS™ Crossbeam 550. Samples were fixed and treated with osmium impregnation treatment (OTO) to increase the back-scatter electron signal and the image contrast[4]. Images were acquired at a voxel size of 9.5x9.5x19 nm and analyzed using AVIZO™ software.

Elastic moduli of the different hydrogels were characterized by rheology tests using a stress-controlled rotational theometer MCR 301 at 37ºC with a standard steel cone geometry CP25-1 (25 mm of diameter and 1º). A frequency sweep was applied by increasing the oscillatory frequency from 0.1 to 10 Hz at a shear amplitude of 1% (10 Pt/dec). Then, the stored (G') and loss (G'') moduli were calculated as the average recorded in the plateau. Shear modulus (G) was calculated using Rubber's elasticity theory[5]. Finally, the elastic modulus (E) was derived from previous shear modulus (Eq 1):

$$E = 2G(1 + \nu) \qquad (1)$$

where ν is the Poisson's ratio, assumed equal to 0.34.

Traction Force Microscopy

MDA-MB-231 cells were labelled with commercially available fluorescent dye CellTracker™ and incubated for 1 hour prior to fluorescence microscopy. Cells were detached and resuspended in fresh DMEM before being added to the collagen mixture together with fluorescent microspheres (0.2 µm diameter). The hydrogels were allowed to polymerize in an incubator and covered with DMEM to promote spontaneous cell migration.

3D image stacks were acquired using a LEICA™ Stellaris 8 confocal microscope with a 20x glycerol objective. 7-9 Cells were imaged in parallel in a stressed state and then a permeable inhibitor of actin polymerization (Cyto-

D) was added to obtain comparative images of the cells in a non-stressed state. The displacement field of the microspheres and the traction force of the cells were calculated using the Matlab™ toolbox TFMLab[6].

RESULTS

Figure 1 shows some of the data obtained comparing the microstructure, morphology and cell tractions across each type of hydrogel. Fig. 1A shows that the mechanical properties (elastic modulus), is determined by the fibril organization (porosity), porosity consistently decreasing with the hydrogel stiffness for all three types of hydrogels. In addition of this, for each type of hydrogel both stiffness and traction increase approximately 11-fold between the lowest and highest concentration (Fig 1B) and notable differences were also found between collagen sources. It is also interesting that traction forces exerted by cells seem to reach a saturation plateau at a hydrogel stiffness of 70-80 Pa. Fig. 1C shows that the traction polarity remains stable in all fibrous structrures. The fiber density and pore size do not represent a barrier for the cell to interact with its ECM in a polarized manner. This supports the preference of the cells for an elongated morphology with two protusions without significant differences in its morphology and cell volume (Fig. 1D).

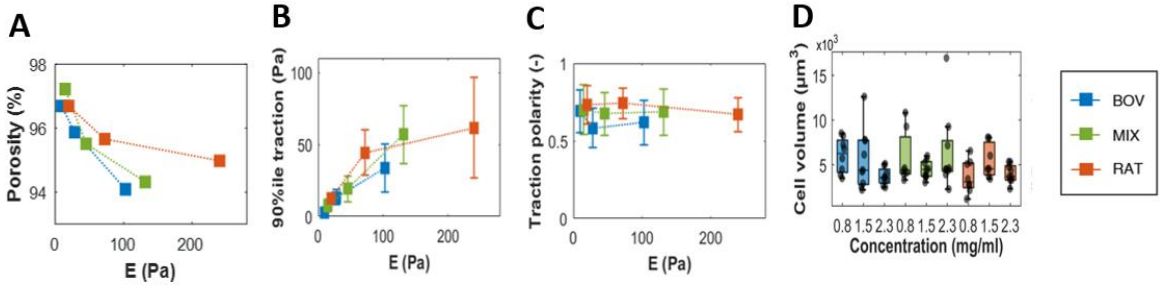

Figure 1. A) Relationship between porosity and the apparent elastic modulus (mean value) of the hydrogels. B-C) Relationship between the 90-percentile traction and the cellular specific strain energy with the hydrogel's apparent elastic modulus. D) Cell volume of the breast cancer cells reported as a boxplot per collagen source (bovine dermis-based, rat tail-based and mixed collagen) and concentration (0.8, 1.5 and 2.3 mg/ml).

DISCUSSION AND CONCLUSIONS

This study demonstrates that combining 3D TFM and FIB-SEM is a valuable method to better correlate cell mechanical behaviour with collagen ECM structural properties. We modelled several natural extracellular microenvironments with different mechanical properties and fibrillar microarchitectures using well-characterised tunable collagen-based hydrogels. Our results provide evidence that the mechanical and structural microenvironment does not influence cell morphology. In all cases, the cancer cells developed an elongated spindle-like shape without significant changes. The tractions and specific strain energy exerted by the cancer cells followed a linear response and plateaued with the stiffening of their ECM, reaching saturation in hydrogels with high apparent elastic moduli (> 200 Pa) due to the appearance of a cell's physico-mechanical limit. An increase in the porosity percentage or pore size of the collagenous substrate was also shown to affect the mechanical behaviour of the cancer cells, reducing the force and energy they exert to pull and deform the fibrous network. With all these results in hand, we hypothesise that the MDA-MB-231 breast cancer cells tune their mechanical state and the subsequent deformation of the hydrogel in order to maintain their ability to migrate and become invasive.

ACKNOWLEDGEMENTS

This publication is part of the R+D projects PID2020-113790RB-I00 and PID2021-126051OB-C42, financed by MCIN/ AEI/10.13039/501100011033.

References

[1] Lu, P., Weaver, V. M., & Werb, Z. *The extracellular matrix: a dynamic niche in cancer progression.* J. Cell Biol. 196, 395-406 (2012).

[2] Morris, B. A., Burkel, B., Ponik, S. M., Fan, J., Condeelis, J. S., Aguirre-Ghiso, J. A., Castracene, J., Denu, J. M., & Keely, P. J. *Collagen matrix density drives the metabolic shift in breast cancer cells.* EBioMedicine **13**, 146-156 (2016)

[3] Tilghman, R. W., Cowan, C. R., Mih, J. D., Koryakina, Y., Gioeli, D., Slack-Davis, J. K., Blackman, B. R., Tschumperlin, D. J., & Parsons, J. T. (2010). *Matrix rigidity regulates cancer cell growth and cellular phenotype*. PloS one 5, e12905 (2010).

[4] Guo, J., Wang, G., Tang, W., Song, D., Wang, X., Hong, J., Zhang, Z. *An optimized approach using cryofixation for high-resolution 3D analysis by FIB-SEM*. J Struct Biol, 212(1):107600 (2020).

[5] Garrido, C. A., Garske, D. S., Thiele, M., Amini, S., Real, S., Duda, G. N., Schmidt-Bleek, K., & Cipitria, A. *Hydrogels with stiffness-degradation spatial patterns control anisotropic 3D cell response.* Biomater. Adv. 151, 213423 (2023).

[6] Barrasa-Fano, J., Shapeti, A., Jorge-Penas, A., Barzegari, M., Sanz-Herrera, J. A., & Van Oosterwyck, H.. *TFMLAB: A MATLAB toolbox for 4D traction force microscopy*. SoftwareX 15, 100723 (2021).

APICAL SHEAR STRESS IMPACTS CELL DYNAMICS, KINEMATICS AND TRANSCRIPTOMIC PROFILE OF THREE DIFFERENT ENDOTHELIAL CELL TYPES

Julio César Sánchez-Rendón[1,2], Annalena Reuss[1], Effie E. Bastounis[1,2*]

1. Institute of Microbiology and Infection Medicine (IMIT), Eberhard Karls University of Tübingen, Germany. 2. Cluster of Excellence "Controlling Microbes to Fight Infections" EXC 2124, Eberhard Karls University of Tübingen, Germany.

INTRODUCTION

Endothelial cells (ECs) line the lumen of blood vessels, forming a single cell monolayer that acts as a protective barrier against different harms (i.e. pathogens). The barrier integrity is maintained through a synergy of several elements at the cell surface including focal adhesions, adherens junctions and surface receptors. In ECs, these components play a crucial role in the response to flow shear stresses (SS) and shear stress gradients (SSG), which vary in space, time and (patho)physiological conditions (e.g., arteriosclerosis). Although EC responses to unsteady SS magnitude have been studied to some extent, how SSGs modulate EC barrier function by impacting EC kinematics (i.e. speed, collective migration) and dynamics (i.e. traction forces and monolayer stresses) is relatively less understood. Whether such effects are universal or cell type specific is also unclear.

MATERIALS AND METHODS

Impinging flow device & live cell imaging

The impinging flow device shown in Fig. 1A was used to simulate SS magnitudes comparable with those experienced in the vascular capillaries [1]. This device has several advantages such as compatibility with standard 6-well plates, adjustable SS profiles, and the possibility of performing long-term live cell imaging. Three EC types from the microvascular (HMEC-1 & cMEC) and macrovascular (HUVEC) systems were exposed to a 3 mL/min flow (Fig. 1b) for a period of 20 hours.

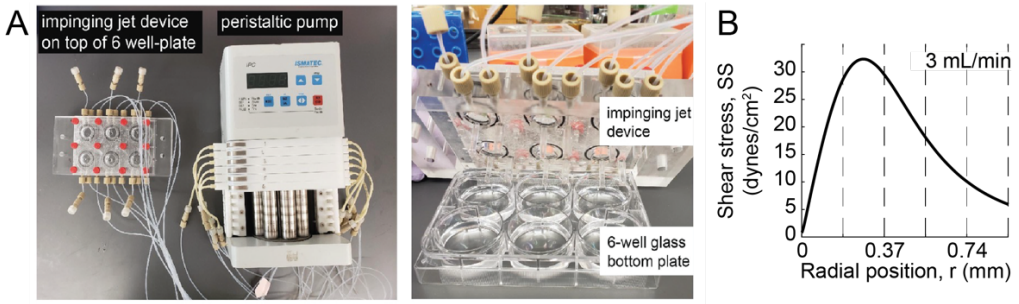

Figure 1. Impinging flow device basic setup (A) and SS magnitude profile (B) produced by a 3 mL/min flow with a maximum SS value comparable to those experienced in the capillaries.

Kinematic analysis

Cell motion was quantified by the method of Particle Image Velocimetry (PIV) implemented in a custom MATLAB® code. Briefly, the relative displacement between successive microscopy images was calculated as the correlation peak in the interrogation areas or sub-images [2]. Cell collective movement was quantified using the correlation length, or the longest distance in which displacement vectors are correlated [3].

Traction Force & Monolayer Stress Microscopy

Cell traction forces were quantified with the method of traction force microscopy (TFM). Briefly, cells were seeded on top of a hydrogel of specific stiffness (e.g. 3 kPa) with embedded fluorescent beads. Bead displacement due to cell motion was measured using PIV. Traction forces were inferred from bead displacements with a custom MATLAB® code that solves the elastostatic equation of equilibrium for a linear, homogeneous, isotropic, 3D body on a substrate of finite thickness. Monolayer stress microscopy (MSM) was used to calculate monolayer tensile stresses from the traction forces with a custom MATLAB® code that solves the force equilibrium on the plane of the monolayer [4].

* Corresponding author. Email: **effie.bastounis@uni-tuebingen.de**

RESULTS

Using a live-cell imaging-compatible impinging flow device, we found that exposure of three different EC types to flow led to an immediate, sustained, and reversible 2-fold decrease in EC migration speed. The three EC types exposed to flow also increased directional collective movement. Traction force and monolayer stress analysis for HMEC-1 revealed a 50% increase in the traction forces ECs exert on their matrix and a 20% increase in monolayer stresses - a proxy for EC barrier integrity - after 20h of flow exposure.

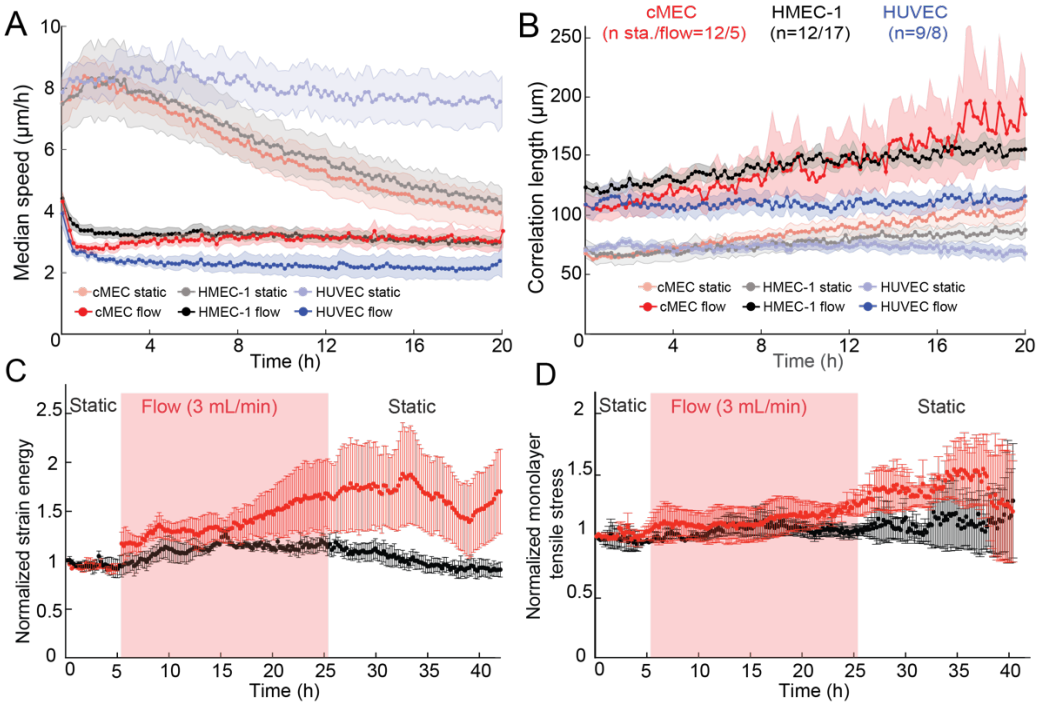

Figure 2. Kinematic and dynamic analysis of three ECs types under impinging flow. (A) Migration speed for control (static) and flow exposed cells. (B) Collective movement for control (static) and flow exposed cells. (C) Normalized strain energy as calculated with TFM for HMEC-1 cells (red: flow exposed, black: control) seeded on 3 kPa hydrogel (n = 3). (D) Normalized monolayer tensile stresses as calculated with MSM from (C).

DISCUSSION AND CONCLUSIONS

The results shown are consistent with the idea that enhanced actomyosin contractility and focal adhesion organization power the movement of ECs, in this case, against the flow gradient, which we confirmed by pharmacological treatment (data not shown). To identify the concurrent changes in biochemical signaling, we performed RNA sequencing in all EC types exposed or not to flow for 20 h and found that all three cell types upregulated *TGFB1* or genes related to this growth factor. We are investigating whether this is the common denominator regulating the increase in EC traction forces and the corresponding increase in monolayer stresses during flow. These results contribute to the understanding how SS modulate EC biomechanics, which may open avenues for the treatment of vascular pathological conditions.

ACKNOWLEGMENTS

The authors would like to thank the German Research Foundation (DFG) and the Cluster of Excellence - Controlling Microbes to Fight Infections (CMFI) for providing financial support to this project.

References

[1] Ostrowski, Maggie A., Huang, E. Y., Surya, V. N., Poplawski, C., Barakat, J. M., Lin, G. L., Fuller, G. G., Dunn, A. R.: *Multiplexed fluid flow device to study cellular response to tunable shear stress gradients*. Annals of biomedical engineering Vol. 44, pp. 2261-2272, Springer 2016.

[2] Gui, L., Wereley, S. T.: *A correlation-based continuous window-shift technique to reduce the peak-locking effect in digital PIV image evaluation.* Experiments in Fluids Vol. 32, pp. 506-517, Springer 2002.

[3] Angelini, T. E., Hannezo, E., Trepat, X., Fredberg, J. J., Weitz. D. A.: *Cell migration driven by cooperative substrate deformation patterns.* Physical review letters Vol. 104 (16), pp. 168104, The American Physical Society 2010.

[4] Bastounis, E., Meili, R., Álvarez-González, B., Francois, J., del Álamo, J. C., Firtel, R. A., Lasheras. J. C.: *Both contractile axial and lateral traction force dynamics drive amoeboid cell motility.* Journal of Cell Biology Vol. 204, pp. 1045-1061, Rockefeller University Press 2014.

* Corresponding author. Email: **effie.bastounis@uni-tuebingen.de**

MONITORING THE MECHANICAL ACTIVITY OF CANCER CELLS UNDER NORMAL, HYPOXIC AND CHEMOTHERAPEUTIC CONDITIONS

Pablo Blázquez-Carmona[1], Raquel Ruiz-Mateos[1], Alejandro Apolinar-Fernández[1], Jorge Barrasa-Fano[2], Apeksha Shapeti[2], Hans Van Oosterwyck[2] , Esther Reina-Romo[1], José A. Sanz-Herrera[1,*]
1. Universidad de Sevilla, Spain; 2. KU Leuven, Belgium

INTRODUCTION

Cells respond to mechanical stimuli by adapting their microenvironment through alteration of the extracellular matrix (ECM). In particular, increased ECM density and stiffness, caused primarily from increased collagen deposition, increased crosslinking and alignment of fibrillar proteins within the stroma, is observed during cancer progression [1]. Moreover, cancer cells proliferates rapidly as substrate stiffness increases [2]. To understand the in vivo complexity and discover new approaches of cancer therapies, cell culture plays an important role, from drugs development to modelling of cell–ECM interactions. In combination with traction force microscopy (TFM), forces exerted by cells and mechanical microenvironment can be characterized in these investigations.

In this work, we use state-of-the-art TFM methodologies to analyse and monitor the mechanical activity of different cancer cell lines under normal, hypoxic and chemotherapeutic conditions. It is seen that the mechanical activity of breast cancer cells MDA-MB-231 embedded in collagen I type hydrogels from different natural sources highly correlates with microarchitectural and mechanical characteristics of the hydrogels. On the other hand, our preliminary studies on A549 lung cancer cells show significant morphological and mechanical differences when subjected to cisplatin drug and hypoxia conditions, versus the control case. These results will allow to investigate further the mechanics of tumour cells and its impact in the treatment of cancer disease.

MATERIALS AND METHODS

Two different studies are carried out in this work. First, breast cancer cells MDA-MB-231 were cultured in nine different type I collagen hydrogels sourced from only bovine dermis (BOV), only rat tail (RAT), or a 1:1 combination of both (MIX); at concentrations of 0.8, 1.5, or 2.3 mg/ml. The shear moduli of the different hydrogels were characterized by rheology tests using a stress-controlled rotational rheometer MCR 301 (Anton Paar, Gratz, Austria). Furthermore, the morphology and micro/nano-architecture of all collagen hydrogels were characterized with focused ion beam milling and scanning electron microscope (FIB-SEM). This methodology allows for the segmentation of a 3D fibered network and subsequent quantification of structural parameters, thereby overcoming common limitations such as 2D aggregations and overlapping of adjacent fibrils. Image stacks were analyzed using Avizo (Thermo Scientific, Waltham, Massachusetts, USA).

On the other hand, A549 lung cancer cells were seeded in mixed BOV-RAT 1.5 mg/ml hydrogels. Four groups were analyzed: (i) Control, (ii) Senescence: 7 days with cisplatin (12 ug/ml), (iii) Conditioned media: 2 days with media of the senescence group, and (iv) Hypoxia: Culture in the hypoxic incubator (1.1% O_2).

For all cases, 3D image stacks were acquired 24 h after collagen polymerization using a Leica Stellaris 8 confocal microscope (Leica Microsystems, Wetzlar, Germany) with a 20x glycerol immersion objective (NA 1.5). TFMLAB [3] was used to compute the displacement field in the selected ROIs. Then, cellular tractions are recovered along the boundary of the cell using an inverse formulation [4], that computes a consistent solution of stresses that fulfills equilibrium conditions within the hydrogel domain. TFMLAB outputs (among other variables) displacement and traction fields along the cell boundary, as well as energy developed by the cells. (See schematics shown in Fig. 1A).

RESULTS

Fig. 1B,C,D shows the relationship of tractions and energies versus the mean elastic modulus for the different cases of hydrogels. As seen, the exerted tractions to achieve a given deformation in stiffer microenvironments should be higher. This hypothesis is consistent with our observed displacement fields, where not many quantitative differences were found between the analyzed cases. Further, the mesenchymal-like elongated morphology of the cells seen for all the analyzed cases suggests that cells maintain a consistent and optimal morphology to mechanosense the hydrogel.

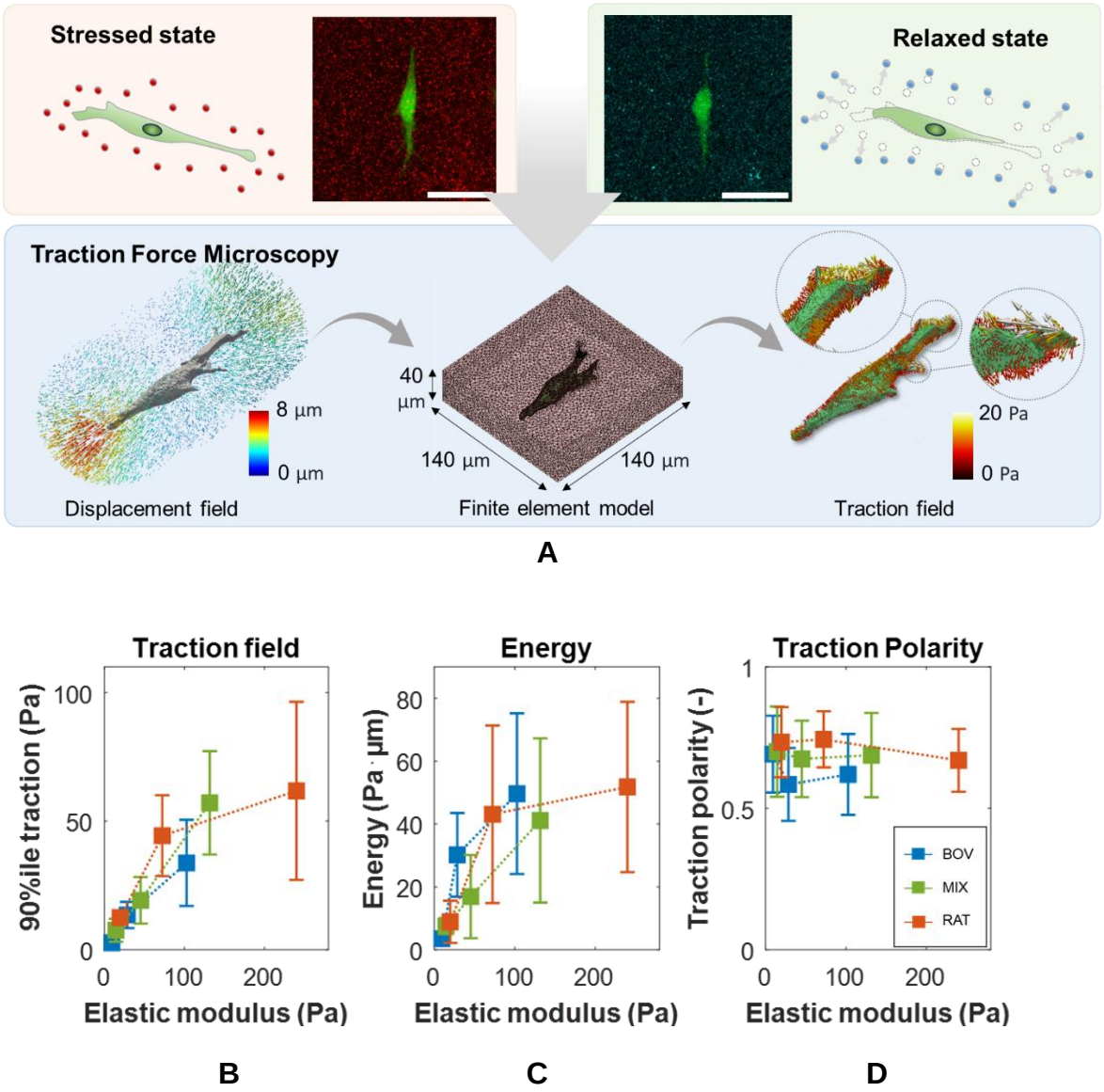

Figure 1. Traction Force Microscopy methodology to determine the mechanical state of cancer cells. A. Schematics of TFM methodology to analyze the mechanical state of cells embedded in collagen matrices. (B, C) Tractions and energy exerted by MDA-MB-231 cells for hydrogels of varying stiffness. D. Traction polarity of MDA-MB-231 cells for hydrogels of varying stiffness.

ACKNOWLEDGEMENTS

This work was supported by MCIN/AEI/10.13039/501100011033 [PID2020-113790RB-I00, PID2021-126051OB-C42].

References

[1] Lu, P., Weaver, V.M., Werb, Z.: *The extracellular matrix: a dynamic niche in cancer progression.* J. Cell Biol. Vol. 196, pp. 395-406, 2012. https://doi.org/10.1083/jcb.201102147

[2] Tilghman, R.W., Cowan, C.R., Mih, J.D., Koryakina, Y., Gioeli, D., Slack-Davis, J.K., Blackman, B.R., Tschumperlin, D.J., Parsons, J.T.: *Matrix rigidity regulates cancer cell growth and cellular phenotype.* PLoS One. 5, e12905, 2010.

[3] Barrasa-Fano, J., Shapeti, A., Jorge-Peñas, A., Barzegari, M., Sanz-Herrera, J.A., Van Oosterwyck, H.: *TFMLAB: A MATLAB toolbox for 4D traction force Microscopy.* SoftwareX Vol. 15, pp. 100723, 2021.

[4] Sanz-Herrera, J.A., Barrasa-Fano, J., Cóndor, M., Van Oosterwyck, H.: *Inverse method based on 3D nonlinear physically constrained minimisation in the framework of traction force microscopy.* Soft Matter Vol. 17, pp. 10210-10222, 2021.

A semi automatised pipeline to measure the nano mechanics of complex samples.

Yogesh Saravanan[1*], Sudiksha Mishra[2], Ramray Bhat[2], Claire Valotteau[1], Felix Rico[1]

1. Aix-Marseille Univ, INSERM, DyNaMo, Turing centre for living systems, Marseille, France ;
2. Indian Institute of Science, India

INTRODUCTION

Cells live in heterogeneous microenvironments as monolayers on a basal membrane or isolated cells on stroma. The mechanics of the surrounding extracellular matrix (ECM) play pivotal roles in the context of development, migration, and disease, specifically cancer. Palpation of a tumour reveals that it is stiff, but paradoxically the underlying individual cancer cells themselves are softer than their healthy counterparts. Stiffening of the tumour microenvironment (TME) is a leading hypothesis for this paradox [1,2]. To understand this process, it is important to grow cells on ECM mimicking substrates and uncouple cell from substrate mechanics. However, this is often difficult due to the heterogeneity of the samples. To tackle such a question, we need tools to mechanically characterize complex and heterogenous samples and allow discerning cells from the ECM. In this work, we propose a methodology to analyse and extract mechanical properties of both the cancer cell and its ECM from mechanical maps obtained by atomic force microscopy.

MATERIALS AND METHODS

Cell culture:

MDA-MB -231 triple negative mammalian breast cancer cells (ATCC) were cultured in Dulbecco's Modified Eagle Medium F12 (DMEM F12) supplied with 10 % Fetal Bovine Serum and antibiotics. The cells were split at 80% confluence (i.e. every 2-3 days). During cell splitting, 1.5 x 10^5 cells were seeded on top of Type 1 collagen for 48 hours in DMEM F12 supplemented with appropriate hormones and growth factors. Two different collagen concentrations, 1mg/ml and 2.5mg/ml, were used to physiological mimic healthy (soft) and cancerous (stiff) TME, respectively.

AFM Measurements:

AFM maps are arrays of force curves recorded over a region of interest. Large AFM maps covering cell and the surrounding collagen were recorded at room temperature using a Nanowizard4 AFM (JPK) mounted on top of an inverted optical microscope (NIKON eclipse TI). Force-indentation curves were acquired using a pre-calibrated hemispherical tip of size 1 μm with nominal spring constant of 0.25 N/m applied force between 0.15-0.3 nN of range resulting an indentation of range 300-1000 nm . This tip was passivated with 1% Pluronic for at least 15 minutes before experiment. The InvOLS (nm/V) of the optical beam deflection was calibrated from thermal response using the contactless SNAP procedure [3].

Data analysis:

The mechanical properties were extracted from the recorded AFM maps using a custom written Python script based on modules from PyFMLab [4]. The Young's modulus (YM) was extracted by fitting the Hertz model to an indentation range of 0-500 nm (green shaded region in fig 1b) .

RESULTS

The measured sample height from the AFM map were clustered to distinguish cell and ECM (collagen) using a K-means algorithm (fig 1a). This clustering results into two clusters of force curves labelled as 'cell' and 'col', respectively. The cell centre is defined as force curve with the maximum height (95^{th} quantile) within the cell cluster. These cells are spindled shaped and migrate along their major axis. The two cell edges of the major axis were manually annotated to define the cell polarity line in the AFM map (black dashed line on fig1a). For any given arbitrary force curve on the map, we can also obtain spatial information, Euclidean distance (R, dashed white line on fig 1a) and the orientation angle (θ) subtended with the cell polarity line.

* Corresponding author. Email: yogesh.saravanan@inserm.fr

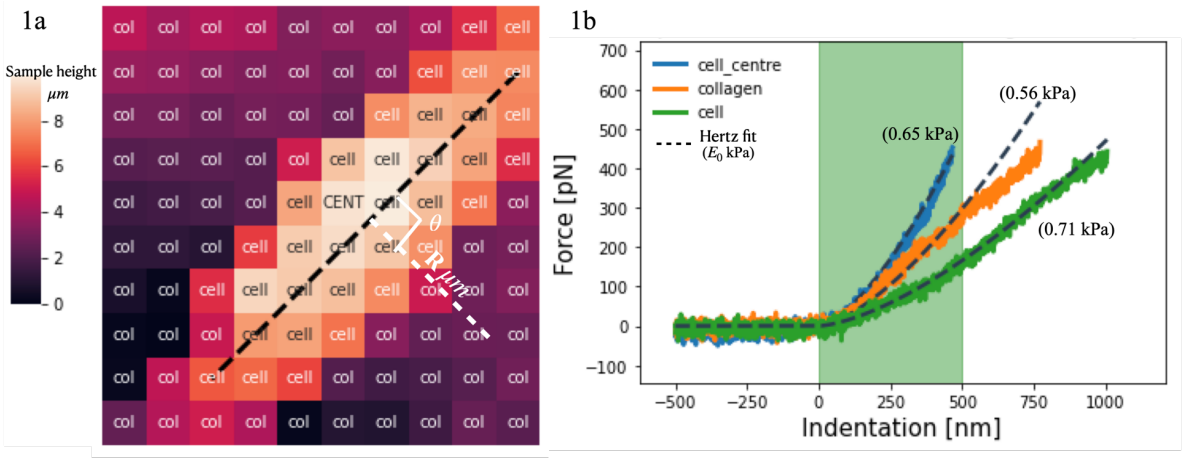

x

Figure 1 (a). Clustered large AFM map of a cell and collagen. The clustering helps us distinguishes the force curves recorded on the cells from the collagen and cell polarity line (black dashed line) can be defined. The Euclidean distance and orientation angle (R μm , θ) for any arbitrary force curve in the map (white dashed line). (b), Representative force curves fitted with hertz model acquired on cell and collagen.

The YM is extracted from the labelled force curves through a Hertz fitting (fig 1b). Our preliminary results show that the YM of collagen around the cell tends to a constant value, irrespective of collagen concentration (1mg/ml or 2.5mg/ml). This indicates a potential remodeling of the collagen.

DISCUSSION AND CONCLUSIONS

In this work we have developed a semi automatised analysis pipeline to classify and measure mechanical response of cells and ECM with additional spatial information. This pipeline was tested on AFM maps of cells growing on collagen of two different concentrations. This pipeline enables us to decouple the cell and ECM mechanics and mechanically study the ECM remodelling in TME. The spatial information can be further used to draw correlations with the mechanics and our first results suggest remodelling of the surrounding collagen. In the future, we plan to improve the clustering classification by correlating optical images of the sample with AFM maps.

ACKNOWLEDGEMENTS

The authors would like to thank INSERM and CNRS for providing financial support to this project through the ATIP-AVENIR and International Emerging Actions respectively.

References

[1] Alibert, Charlotte, et al.: *Are Cancer Cells Really Softer than Normal Cells?* , *Biology of the Cell*, vol. 109, no. 5, May 2017.

[2] Fuhs, Thomas, et al.: *Rigid Tumours Contain Soft Cancer Cells*. *Nature Physics*, Sept. 2022.

[3] Schillers, Hermann, et al.: *Standardized Nanomechanical Atomic Force Microscopy Procedure (SNAP) for Measuring Soft and Biological Samples*. *Scientific Reports*, vol. 7, no. 1, 1, July 2017.

[4] López-Alonso, Javier, et al.: *PyFMLab: Open-Source Software for Atomic Force Microscopy Microrheology Data Analysis*. *Open Research Europe*, vol. 3, Oct. 2023.

EFFICIENT NUMERICAL SOLUTION OF A MODEL FOR THE EVOLUTION OF GLIOBLASTOMA CELLS

J. Sarrate[1*], E. Sala–Lardies[1], M. Pérez–Aliacar[2,3], J. Ayensa–Jiménez[2,3], M. Doblaré[2,3,4]

1. Barcelona School of Civil Engineering, UPC, Spain; 2. Aragon Institute of Engineering Research (I3A), UZ, Spain; 3. School of Engineering and Architecture, Department of Mechanical Engineering, UZ, Spain; 4. Centro de Investigación Biomédica en Red, Bioingeniería, Biomateriales y Nanomedicina (ciber-bbn), Spain

INTRODUCTION

Glioblastoma multiforme (GBM) is the most common and aggressive of the brain tumours. Understanding its evolution is a crucial step for the development of new treatments that allows its prognosis. GBM cells are integrated in a very complex and dynamic environment. However, *in vitro* experiments allow controlling and isolating the effects of a particular phenomenon. In this scenario, microfluidic devices as the ones described in [2] are of particular interest, since they allow reproducing some three-dimensional effects and provide a view of the temporal evolution. These devices are composed of a central chamber, where the cancer cells are inserted, connected to two lateral channels that provide nutrients (oxygen), as shown in Figure 1(a). The experiments in these devices may be long and results depend on many different variables. Therefore, an *in silico* tool is needed to improve the design of new devices or experiments. In this work we use the mathematical model proposed in [1] to reproduce these experiments and propose an efficient methodology to obtain accurate solutions.

MATHEMATICAL MODEL

According to [1], our model considers two cell phenotypes (living and dead cells) and a main nutrient (oxygen). The central chamber of the microfluidic device is filled with a mixture of hydrogel and cancer cells, with a concentration c^1, while the oxygen is provided through the lateral channels at a concentration c^0.

The oxygen concentration varies due to the molecular diffusion and the interaction with living cells which use it as a nutrient. Thus, the evolution of oxygen concentration verifies

$$\frac{\partial c^0}{\partial t} - \nabla \cdot \left(\mathbf{A}^0 \nabla c^0 \right) = s^0 \left(c^0, c^1 \right). \tag{1}$$

The living cells concentration varies due to molecular diffusion, chemotaxis process that accounts for the cells motion due to nutrient shortage, and the interaction with oxygen. Therefore,

$$\frac{\partial c^1}{\partial t} - \nabla \cdot \left(\mathbf{A}^1 \nabla c^1 \right) + \nabla \cdot \left(c^1 \mathbf{B}^1 (c^0, c^1) \nabla c^0 \right) = s^1 \left(c^0, c^1 \right). \tag{2}$$

Note that the source terms s^0, s^1 and the chemotaxis matrix $\mathbf{B}^1$ are highly non-linear and, therefore, the model involves solving a system of two coupled non-linear partial differential equations. We consider that dead cells do not move or migrate. Hence, their concentration c^2 can be obtained solving an ordinary differential equation

$$\frac{\partial c^2}{\partial t} = s^2 \left(c^0, c^1 \right). \tag{3}$$

The solution of these coupled problems allows predicting the performance of microfluidic devices. For instance, Figure 1(b) shows the concentration of living cells after a simulation of one day in a 3D device.

NUMERICAL MODEL

The equations described above, with appropriate boundary and initial conditions, are solved using finite elements to discretize the space and a DIRK method to advance in time. This yields a system of non-linear equations that must be solved at each stage of each time step of the DIRK scheme. Due to the coupling between living cells concentration and oxygen concentration, the number of unknowns of these non-linear systems is, approximately, two times the number of nodes in the mesh when a monolithic approach is used.

In order to reduce the cpu time and the memory footprint needed to solve these systems a staggered approach is considered in this work. This leads to smaller and uncoupled non-linear problems. For instance, Figure 2 shows the matrix profile for the monolithic approach and the staggered one. It is clear that using a staggered approach the system dimension decreases. In addition, the fill-in for direct methods will be reduced improving the performance of the numerical simulation.

* Corresponding author. E-mail: jose.sarrate@upc.edu

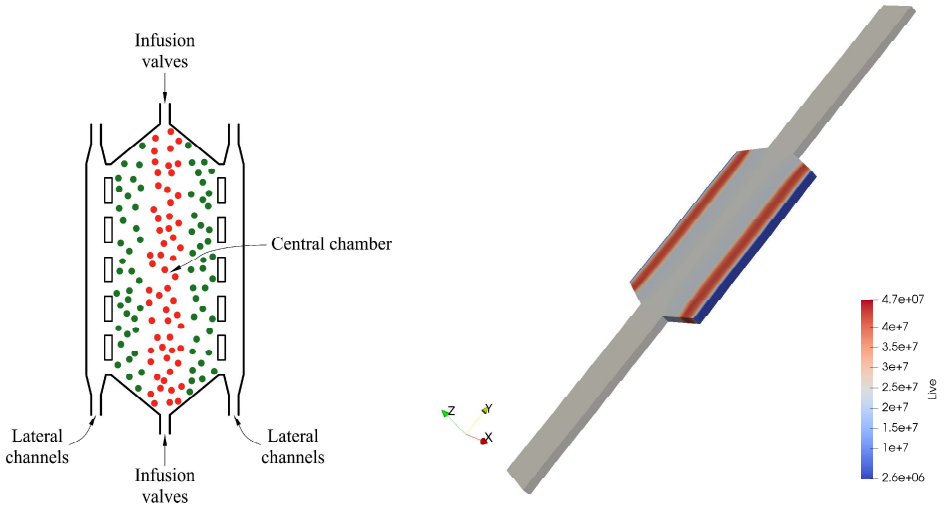

(a) (b)

Figure 1. (a) 2D sketch of a microfluidic device. (b) Simulation of living cells concentration in a 3D device.

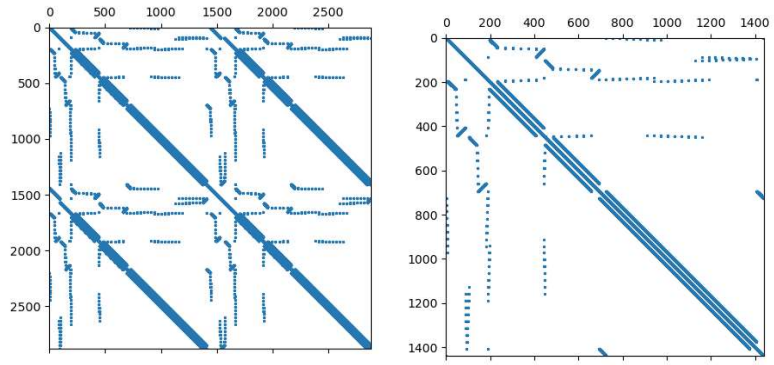

(a) (b)

Figure 2. Profile of the system matrix (a) using a monolithic approach and (b) a staggered formulation.

ACKNOWLEDGEMENTS

This work has been supported by FEDER and the Spanish Government, Ministerio de Ciencia e Innovación under grant project contract PID2021-126051OB-C44

References

[1] Ayensa-Jiménez J., Pérez-Aliacar M., Randelovic T., Sanz-Herrera J. A., Doweidar M. H and Doblaré M.: *Mathematical formulation and parametric analysis of in vitro cell models in microfluidic devices: application to different stages of glioblastoma evolution*. Scientific Reports, 10(1):1{21}, 2020.

[2] Ayuso J. M et al. *Development and characterization of a microfuidic model of the tumour microenvironment*. Scientific Reports, 6(1): 36086,2016.

CONTROLLING CELL CONTRACTION BY OPTOGENETICS

Ulrich Schwarz[1,*]

1. Institute of Theoretical Physics, University of Heidelberg, Heidelberg, Germany

ABSTRACT

Actomyosin contractility lies at the heart of many essential cellular processes, including cell adhesion, division and migration. Optogenetic activation of the Rho-pathway has emerged as a very powerful new tool to dissect the underlying mechanisms. Its high precision in space and time informs mathematical models, in particular when combined with micropatterning and traction force microscopy. We use a two-dimensional mathematical model for cells as thin and actively contracting material to demonstrate how cell size, shape and adhesion structure together determine how internally generated force is transmitted to the substrate [1] and to neighboring cells [2]. We also present a rigorous mathematical analysis of a one-dimensional active gel model that explains how cell migration can be controlled by optogenetic activation of contractility, including switches between sessile and motile states and reversals of the direction of migration [3].

References

[1] T. Andersen, D. Wörthmüller et al. "Cell size and actin architecture determine force generation in optogenetically activated cells." Biophysical Journal 122.4 (2023): 684-696.
[2] A. Ruppel, D. Wörthmüller et al. "Force propagation between epithelial cells depends on active coupling and mechano-structural polarization." Elife 12 (2023): e83588.
[3] O.M. Drozdowski, F. Ziebert and U.S. Schwarz. "Optogenetic control of migration of contractile cells predicted by an active gel model." Communications Physics 6.1 (2023): 158.

* Corresponding author. E-mail: schwarz@thphys.uni-heidelberg.de

ROLE OF CELL ADHESION AND CYTOSKELETON STRUCTURES IN THREE-DIMENSIONAL AGGREGATES OF SMALL CELL LUNG CACER CELLS

Beatrice Senigagliesi[1], Nassim Haffiane[1], Julien Sage[2], Pierre Nassoy[3], Rémi Galland[1], Grégory Giannone[1,*]

1. Bordeaux University-CNRS, Interdisciplinary Institute for Neuroscience, UMR5297, Bordeaux, France; 2. Stanford University, Palo Alto, CA, USA 3. Bordeaux University-CNRS, LP2N, Institut d'Optique Graduate School, UMR5298, Talence, France

INTRODUCTION

How biochemical and biomechanical signals synergize to control cell movement, shape, and tissue morphologies is a fundamental question in cell biology. Adhesive structures and actin structures, including the actin-based plasma membrane protrusions, have a key role in sensing the physical and chemical properties of the environment to trigger downstream signaling pathways that control essential cellular functions (e.g. proliferation, adhesion, and migration)[1,2]. Integrin-based adhesions (IAS) are involved in all these cellular events and mainly contact the surrounding extracellular matrix (ECM)[3]. Nonetheless, recent evidence has revealed the existence of integrin-dependent cell-cell adhesions that are important for tissue formation and mechanical cohesion[4,5]. Actin-based protrusions forming at the leading edge of cells drive their migration in the surrounding environment[6], while contractile actomyosin structures, such as actin stress fibers, exert mechanical forces on the surrounding ECM to move the cell forward[7]. Dysregulation of IAS (e.g. increased integrin-adhesion activity)[8,9], actin-based protrusions (e.g. invasive and matrix-degrading structures[6,10]), and the consequent mechanical perturbations of cells and tissues can contribute to tumor invasion and metastasis. The metastatic process requires several necessary steps: cancer cells first detach from the primary tumor site, break through the basement membrane and extracellular matrix, enter into the blood/lymphatic circulation, and finally move out from vessels to create secondary tumor sites[11,12]. During all these steps, the features that enable cancer cells to survive in circulation and form metastases are their ability to adapt their interaction with the ECM and adjacent cancer cells, as well as to adapt to different physical and mechanical cues of the environment. Cell adhesions, membrane protrusions, and actin skeleton could also play mechano-protective roles for cancer cells: they are instrumental in making circulating tumor cell clusters (CTCs) more resistant to shear stress than their non-transformed counterparts[13]. We hypothesize that the acquisition of a metastatic potential could be directly associated with the expression of a new panel of adhesive and cytoskeletal structures that promote the ability of cancer cells to migrate and survive in circulation in order to then metastasize to secondary sites. A highly metastatic cancer[14,15], Small Cell Lung Cancer (SCLC), will be used as clinically relevant model to test this hypothesis. SCLC is a highly aggressive neuroendocrine tumor that accounts for ~ 15% of lung cancers and causes more than 200,000 annual deaths[16]. A recent study revealed that mouse SCLC cells both in culture and in vivo are characterized by actin-based cellular protrusions that resemble axons (axon-like protrusions, ALPs) regulated by neuronal factors involved in axon guidance and neuroblast migration. Disruption of these ALPs impairs cell migration in culture and inhibits metastatic ability *in vivo*[17]. The stability and function of actin-based protrusions during cancer cell migration is regulated by the formation of IAS[18], which can contribute to tumor invasion and metastasis also in SCLC[19]. Integrins binding to laminin and to fibronectin are both expressed at the surface of metastatic SCLC cells[20,21].

Here, we aim to understand how the hijacking of IAS and actin structures (actin-based protrusions and actin membrane skeleton) by SCLC cells promotes their ability to invade surrounding tissues and survive in blood or lymphatic vessels as single or clustered cells to metastasize to other organs.

MATERIALS AND METHODS

The involvement of integrins in SCLC spreading was evaluated altering the expression of β1/β3 integrins via CRISPR/Cas 9 genome-editing in murine SCLC cells. The role of β1/β3 integrins in the cell-ECM (e.g. laminin, fibronectin) interactions and in the formation of ALPs in SCLC was quantified through spreading assay and immunostaining experiments on 2D substrates. Thereafter, we took advantage of the spontaneous ability of self-assemble of the SCLC cells to have 3D multicellular cancer assemblies, referred as spheroids, to reveal whether the IAS and cytoskeleton molecular architecture and dynamics are different compared to those forming on 2D substrates. The high spatial and temporal resolution of confocal, spinning-disk confocal microscopy, and single-objective selective-plane illumination microscopy (soSPIM)[22] were used to investigate IAS and actin cytoskeletal structures in 3D cell models. Next, we evaluated the β1/β3 integrin involvement in the SCLC cell-cell interactions by evaluating spheroid shape parameters (aspect ratio, roundness, circularity, and solidity) and indirect spheroid speed of fusion. To mimic and investigate the mechanical features of SCLC cell aggregates occurring *in vivo*, we will use an engineering 3D cell assemblies, the Cell Capsule Technology (CCT)[23,24]. In the CCT, cells are encapsulated and grown, using a microfluidic method, inside permeable, elastic, and hollow alginate microspheres

of controlled size. The CCT capsules, given their elastic properties, can be used as a tool to measure the pressure exerted by the cells growing inside them[25]. Conversely, by tuning the geometry (e.g. diameter and thickness) and mechanical properties of the capsule, it is possible to generate compressive forces exerted by the capsule and study the direct cellular reorganization within the spheroids[24].

RESULTS

RNA-seq studies revealed that β1/β3 integrins are highly expressed in human and mouse SCLC cell lines. Therefore, the β1/β3 integrin altered SCLC cell models (WT vs KnockOut clones) were used to explore the involvement of these specific integrins in the formation of actin protrusions. Spreading assay experiments demonstrated that β1 integrin (e.g. laminin-binding α3β1/α6β1 and fibronectin-binding αvβ3/α5β1 integrins) is fundamental in the formation of integrin-based adhesions, spreading, and axon-like protrusions in murine SCLC cells. Further immunostaining experiment revealed the presence of β1 integrin activated proteins inside the self-assemble SCLC spheroids. This result suggests an integrin involvement in cell-cell interactions within SCLC aggregates. Indeed, the shape parameters and indirect speed of fusion experiments revealed a higher cohesion and regularity in spheroid spherical shapes with the presence of β1 integrin expression in SCLC self-assembled aggregates. In addition, soSPIM experiments have shown the formation of long protrusions of the same scale as the the axon-like protrusions in SCLC 3D multicellular assemblies.

DISCUSSION AND CONCLUSIONS

All our experiments show that integrin-based adhesions can mediate cell-cell interactions between SCLC cells, the formation of cell protrusions, and as consequence the stability in 3D multicellular aggregates that could be crucial in survival in circulation and metastatic spreading.

As the biomechanical properties of single cells and cell aggregates have proven to be of utmost importance for many processes in cell biology, this study could be crucial to scientific advancement in this domain. Of most importance for societal impact as well as for the scientific advances, the study these structures in particular in the aggressive and metastatic SCLC turns out to be of great importance for the development of new therapeutic approaches and drugs against this cancer.

References

1. Parsons, J. T., Horwitz, A. R. & Schwartz, M. A. Cell adhesion: integrating cytoskeletal dynamics and cellular tension. *Nat Rev Mol Cell Biol* **11**, 633–643 (2010).
2. Iskratsch, T., Wolfenson, H. & Sheetz, M. P. Appreciating force and shape-the rise of mechanotransduction in cell biology. *Nat. Rev. Mol. Cell Biol.* **15**, 825–833 (2014).
3. Canel, M., Serrels, A., Frame, M. C. & Brunton, V. G. E-cadherin-integrin crosstalk in cancer invasion and metastasis. *J. Cell Sci.* **126**, 393–401 (2013).
4. Blandin, A.-F. *et al.* Glioma cell dispersion is driven by α5 integrin-mediated cell-matrix and cell-cell interactions. *Cancer Lett.* **376**, 328–338 (2016).
5. Klapholz, B. *et al.* Alternative mechanisms for talin to mediate integrin function. *Curr. Biol.* **25**, 847–857 (2015).
6. Yilmaz, M. & Christofori, G. EMT, the cytoskeleton, and cancer cell invasion. *Cancer Metastasis Rev.* **28**, 15–33 (2009).
7. Schaks, M., Giannone, G. & Rottner, K. Actin dynamics in cell migration. *Essays Biochem.* **63**, 483–495 (2019).
8. Paszek, M. J. *et al.* Tensional homeostasis and the malignant phenotype. *Cancer Cell* **8**, 241–254 (2005).
9. Levental, K. R. *et al.* Matrix crosslinking forces tumor progression by enhancing integrin signaling. *Cell* **139**, 891–906 (2009).
10. Mondal, C., Di Martino, J. S. & Bravo-Cordero, J. J. Actin dynamics during tumor cell dissemination. *Int. Rev. Cell Mol. Biol.* **360**, 65–98 (2021).
11. Shibue, T. & Weinberg, R. A. EMT, CSCs, and drug resistance: The mechanistic link and clinical implications. *Nature Reviews Clinical Oncology* vol. 14 611–629 at https://doi.org/10.1038/nrclinonc.2017.44 (2017).
12. Martin, T., Ye, L., Sanders, A., Lane, J. & Jiang, W. *Cancer Invasion and Metastasis: Molecular and Cellular Perspective*. *Metastatic Cancer: Clinical and Biological Perspectives* vol. 9 (2014).
13. Follain, G. *et al.* Fluids and their mechanics in tumour transit: shaping metastasis. *Nat. Rev. Cancer* **20**, 107–124 (2020).
14. Sabari, J. K., Lok, B. H., Laird, J. H., Poirier, J. T. & Rudin, C. M. Unravelling the biology of SCLC: implications for therapy. *Nat. Rev. Clin. Oncol.* **14**, 549–561 (2017).
15. Ko, J., Winslow, M. M. & Sage, J. Mechanisms of small cell lung cancer metastasis. *EMBO Mol. Med.* **13**, e13122 (2021).
16. Gazdar, A. F., Bunn, P. A. & Minna, J. D. Small-cell lung cancer: what we know, what we need to know and the path forward. *Nat. Rev. Cancer* **17**, 725–737 (2017).
17. Yang, D. *et al.* Axon-like protrusions promote small cell lung cancer migration and metastasis. *Elife* **8**, (2019).
18. Arjonen, A., Kaukonen, R. & Ivaska, J. Filopodia and adhesion in cancer cell motility. *Cell Adh. Migr.* **5**, 421–430 (2011).
19. Zhao, G. *et al.* Cullin5 deficiency promotes small-cell lung cancer metastasis by stabilizing integrin β1. *J. Clin. Invest.* **129**, 972–987 (2019).
20. Feldman, L. E., Shin, K. C., Natale, R. B. & Todd, R. F. 3rd. Beta 1 integrin expression on human small cell lung cancer cells. *Cancer Res.* **51**, 1065–1070 (1991).
21. Li, N. *et al.* Down-regulation of β3-integrin inhibits bone metastasis of small cell lung cancer. *Mol. Biol. Rep.* **39**, 3029–3035 (2012).
22. Galland, R. *et al.* 3D high-and super-resolution imaging using single-objective SPIM. *Nat. Methods* **12**, 641–644 (2015).
23. Alessandri, K. *et al.* A 3D printed microfluidic device for production of functionalized hydrogel microcapsules for culture and differentiation of human Neuronal Stem Cells (hNSC). *Lab Chip* **16**, 1593–1604 (2016).
24. Alessandri, K. *et al.* Cellular capsules as a tool for multicellular spheroid production and for investigating the mechanics of tumor progression in vitro. *Proc. Natl. Acad. Sci.* **110**, 14843–14848 (2013).
25. Ruiz-Herrero, T., Alessandri, K., Gurchenkov, B. V, Nassoy, P. & Mahadevan, L. Organ size control via hydraulically gated oscillations. *Development* **144**, 4422–4427 (2017).

FORCE-MEDIATED ANGIOGENESIS – A MECHANISM FOR VASCULAR LESION GROWTH

Apeksha Shapeti[1*], Jorge Barrasa-Fano[1], Abdel Rahman Abdel Fattah[1,2], Janne de Jong[1], José Antonio Sanz-Herrera[3], Mylène Pezet[4], Said Assou[5], Emilie de Vet[1], Seyed Ali Elahi[1,6], Adrian Ranga[1], Eva Faurobert[4], Hans Van Oosterwyck[1,7,*]

1. KU Leuven, Biomechanics Section, Belgium; 2. CeMM The Research Center for Molecular Medicine of the Austrian Academy of Sciences, Austria; 3. Escuela Técnica Superior de Ingeniería, Universidad de Sevilla, Spain; 4. University of Grenoble Alpes, Institute for Advanced Biosciences, France; 5. IRMB, University of Montpellier, INSERM, France; 6. KU Leuven, Human Movement Biomechanics Research Group, Belgium; 7. KU Leuven, Prometheus Division of Skeletal Tissue Engineering, Belgium

INTRODUCTION

Force-mediated cellular interactions have proven vital to the pathogenesis of cancer and cardiovascular diseases. However, their exploration in vascular abnormalities, such as cerebral cavernous malformation (CCM), remains limited due to limited experimental methods in vascular mechanobiology. There is therefore a huge gap in knowledge in how individual cells communicate and respond to perturbations within diseased vascular tissue. CCMs are lesions of leaky brain capillaries with a dysregulated actin cytoskeleton and cell-cell junctions[1],[2]. Recent in-vivo models of CCM have shown that mutant endothelial cells (ECs) incorporate wild-type (WT) ECs into malformations, promoting lesion genesis[3],[4]. The underlying mechanisms of this recruitment and its subsequent impact on healthy ECs, however, remain poorly understood. We address this gap by mimicking and imaging angiogenic sprouting in-vitro in a 3D hydrogel compatible with traction force microscopy (TFM). Combining this with molecular biology techniques enabled the multi-modal assessment of force-mediated, extracellular matrix (ECM)-mediated, morphological and transcriptomic phenotypes.

MATERIALS AND METHODS

We coupled 3D TFM with an early angiogenic invasion assay using ECM-mimicking PEG hydrogels. These PEGs were modular to mimic various stiffnesses, ligand binding, degradability and angiogenic cues. Hydrogels were mixed with either fluorescent beads or fluorescent gelatin for confocal image-based quantification of 3D ECM deformations or ECM degradation respectively. 3D tractions were inferred from ECM deformations around invading non-mosaic or mosaic (with WT-ECs) sprouts for control, CCM2, CCM2+ROCK1, and CCM2+ROCK2 siRNA silenced HUVEC conditions. Further, we extended our 3D TFM algorithms to develop a unique approach to quantify forces at the cell-cell interface in 3D encapsulated cell pairs. Live overnight imaging was used to visualize dynamics of non-mutant EC recruitment. Finally, immunostaining and scRNA sequencing were used to investigate the modified mechanotransductive machinery at the protein and gene expression levels.

RESULTS

During 3D angiogenic sprouting of silenced HUVEC in PEG hydrogel, we found that loss of CCM2 enhances angiogenic sprouting in a ROCKs-dependent way through elevated cell-ECM forces and hydrogel matrix degradation. Further, when exploring the influence of CCM2-silenced ECs on surrounding wild-type ECs, we found that CCM2-silenced ECs and ROCKs change the invasion modes of WT ECs modes into the hydrogel. Highly angiogenic CCM2-silenced ECs were capable of enhancing the invasion of neighboring wild-type ECs through force and extracellular matrix-guided mechanisms. Mechanically hyperactive CCM2-silenced tip cells guide wild-type cells by transmitting pulling forces and leaving degraded tunnels in the matrix in a ROCKs-dependent manner. This force transmission is associated with reinforced β1-integrin focal adhesions and actin cytoskeleton in wild-type cells. Single-cell RNA sequencing further revealed that mutant ECs reprogram the recruited wild-type ECs into a proliferative stalk cell identity.

DISCUSSION AND CONCLUSIONS

Taken together, our multi-modal approach, integrating biophysical computational methods with molecular techniques, unveils a novel mechanism by which CCM2 mutants hijack wild-type cells to drive lesion growth, suggesting a potential mechanically-driven cell reprogramming. Our study is the first to identify a role for contractile

* Corresponding authors. Email: **apeksha.shapeti@kuleuven.be**, **hans.vanoosterwyck@kuleuven.be**

forces in the progression of vascular malformations. Our unique approach to quantify cell-cell forces within 3D multicellular systems also represents a completely new methodology for mathematical modeling of physiological and pathological processes where these mechanical forces are critical players, and could find broad application in understanding the mechanical basis of disease initiation and progression.

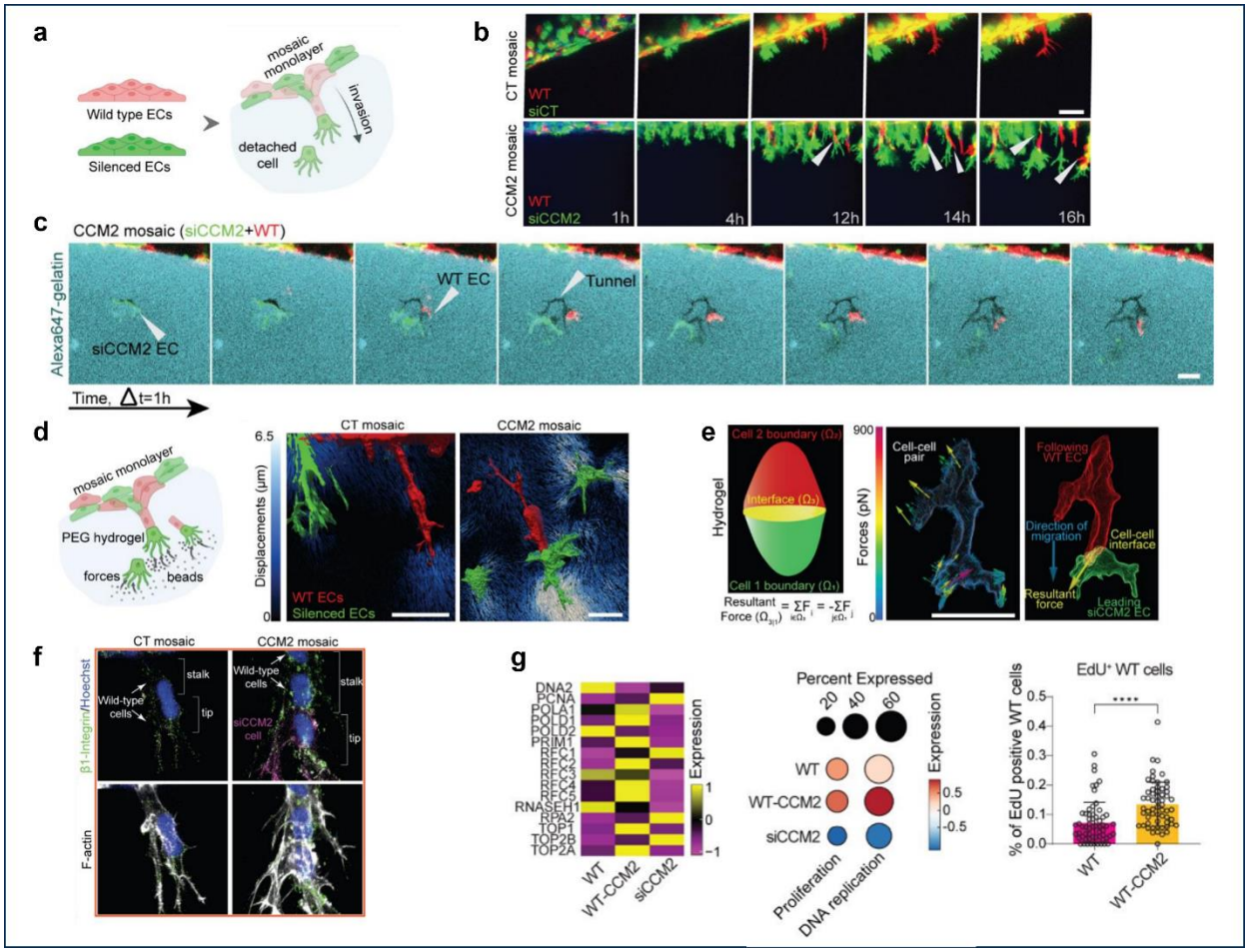

Figure 1. From [5] a) Schematic representation of mosaic invasion assay with wild-type ECs (red) and ECs siRNA silenced for Control or CCM2 (green). b) Maximally projected timelapse confocal images of 1:1 mix of WT ECs (in red) and siCT or siCCM2 ECs (in green). siCCM2 ECs lead WTs during invasion (arrows). c) Composite confocal images of a single z-plane of fluorescently labeled gelatin in the matrix. Follower WT EC (red) modifies direction of migration by sensing tunnels created by leading siCCM2 EC (green). d) 3D renders of displacements (in μm) computed around mosaic angiogenic sprouts. e) Two cell-hydrogel interfaces (green, Ω1; red, Ω2), the cell-cell interface (yellow, Ω3), forces exerted by the cells on the hydrogel. Non-zero force vector exerted by the leading siCCM2 cell on the cell-cell interface (yellow arrow) in the direction of migration (blue arrow). f) Immunofluorescence images of β1 integrin (green), Hoechst-labeled nuclei (blue), fluorescently labeled silenced EC (magenta) and F-actin (gray). g) Expression of genes associated with proliferation and EdU staining in WT ECs.

ACKNOWLEDGEMENTS

We acknowledge the Research Foundation of Flanders (FWO) for the following funding which made this work possible: PhD SB fellowship 1S68820N, postdoctoral fellowship 1259223N, projects G087018N, G0C2422N.

References

[1] J. Lisowska *et al.*, "The CCM1-CCM2 complex controls complementary functions of ROCK1 and ROCK2 that are required for endothelial integrity," *J Cell Sci*, vol. 131, no. 15, p. jcs.216093, Aug. 2018, doi: 10.1242/jcs.216093.

[2] D. R. Vannier *et al.*, "CCM2-deficient endothelial cells undergo a ROCK-dependent reprogramming into senescence-associated secretory phenotype," *Angiogenesis*, vol. 24, no. 4, pp. 843–860, Aug. 2021, doi: 10.1007/S10456-021-09809-2/FIGURES/7.

[3] M. R. Detter, D. A. Snellings, and D. A. Marchuk, "Cerebral cavernous malformations develop through clonal expansion of mutant endothelial cells," *Circ Res*, vol. 123, no. 10, pp. 1143–1151, 2018, doi: 10.1161/CIRCRESAHA.118.313970/FORMAT/EPUB.

[4] M. Malinverno *et al.*, "Endothelial cell clonal expansion in the development of cerebral cavernous malformations," *Nat Commun*, vol. 10, no. 1, p. 2761, Dec. 2019, doi: 10.1038/s41467-019-10707-x.

[5] A. Shapeti *et al.*, "Force-mediated recruitment and reprogramming of healthy endothelial cells drive vascular lesion growth", doi: 10.1101/2023.11.27.568780.

COMPUTATIONAL MODELING OF ACTIVE FOAM DYNAMICS IN 3D TISSUES

Jef Vangheel[1], Steven Ongenae[1], Tom Belpaire[1], Ioannis Papantoniou[2], Bart Smeets[1,2*]

1. MeBioS KU Leuven, Kasteelpark Arenberg 30, 3000 Leuven Belgium
2. Prometheus, Division of Skeletal Tissue Engineering, KU Leuven, Leuven, Belgium

INTRODUCTION

The jamming transition has been studied as a phenotypical transformation in various biological processes, notably in cancer progression and development. In two dimensions, vertex and Voronoi-type models have proven instrumental in elucidating how cortical tension and cellular activity influence the fluid-to-jamming transition [1]. However, a comprehensive theoretical framework addressing the dynamics of the jamming transition in 3D tissues is still missing. Here, we introduce a novel computational model designed specifically for dynamic, 3D tissues, treating individual cells as distinct, interacting entities and based on the analogy between tissue behaviour and bubble dynamics in foams [2]. Through combination of simulations and theoretical analysis, we derive universal scaling laws for tissue fluidity, based on measurable biophysical parameters including relative cortical tension, active traction dipole strength, and cell migration persistence time.

MATERIALS AND METHODS

Cells were modelled as pressurized bubbles characterized by a viscous shell with thickness t, viscosity η, and surface tension γ that represents the cell's acto-myosin cortex, see Figure 1 [3,4]. Cells may adhere to substrate and neighbouring cells with adhesive tension ω_s and ω_{cc}. Furthermore, contact interactions included wet friction with friction coefficient ξ. Cell migration was facilitated by an active protrusive pressure P_a, in the direction of the cell's polarization $\boldsymbol{p}$, which undergoes a persistent random walk with persistence time τ_a. First, we performed simulations of 3D cells adhered to a substrate in periodic boundary conditions. Varying cell-cell and cell-substrate adhesion, we obtained various characteristic epithelial architectures (squamous to columnar). After introducing active migration, we mapped the unjamming transition in function of cell-cell adhesion and cell-cell friction and compared to theoretical scaling limits. Next, we modelled cells in a small tissue spheroid, consisting of 100 cells, presenting a finite-sized system and a fully 3D environment for the cells. Here, we varied the tissue architecture by changing the relative cell-cell tension ω_{cc}/γ, and quantified the degree of fluidity in function of cell activity. Finally, we simulated the fusion of two spheroids. From these fusion simulations, we derived effective *macroscopic* continuum visco-elastic properties of the tissue material, and compared these to the *microscopic* cell mobility.

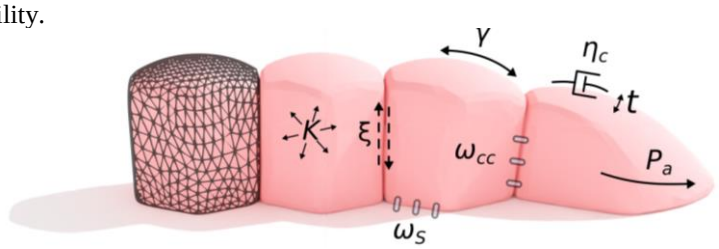

Figure 1. Schematic overview of the active foam model and its most important biophysical parameters

RESULTS

In simulations of active foams on a substrate, we identified two distinct regimes of the jamming transition. At low cell density and low cell-cell adhesion, increasing adhesion induces jamming by increasing the cell-cell pull-off force [2], similar to classical colloidal systems. In this regime, the *net* self-propulsion (rather than the force dipole) of a cell drives topological rearrangements. Conversely, at confluent cell densities and/or high levels of cell-cell adhesion (where cells are, at least locally, confluent in clusters), cell-cell adhesion promotes fluidity. In line with classical vertex model predictions [1], we found a critical shape index that delineates the unjamming transition. Here, topological rearrangements are governed by cell deformability, which arises from the balance between the active force dipole and relative cell-cell tension. Building upon this observation, we propose a theoretical scaling of the unjamming transition based on cell-scale biophysical properties. On the other hand, cell-cell friction, related to the bond turnover rate of cell-cell ligands [5], was not associated with traditional jamming physics. Rather, it reduces the frequency of topological rearrangements by increasing velocity correlation length, thereby increasing the apparent viscosity of the (fluid-like) tissue.

* Corresponding author. Email: **bart.smeets@kuleuven.be**

Extending these findings to confluent (or near-confluent) 3D tissue spheroids, we also observed that the ability of cells to deform governs tissue fluidity. Based on these simulations, we derive a universal scaling of the jamming transition that accounts for cell-cell tension, cortical viscosity, repolarization time and active pressure. This scaling also serves to parameterize changes in macroscopic material properties derived from spheroid-spheroid fusion dynamics. Consequently, arrested coalescence, the inability of spheroids to undergo complete fusion [6], is intricately linked with jammed configurations at the microscopic level, whereas complete fusion is associated with fluidized tissue material, with heightened levels of intermixing as cell activity increases further.

DISCUSSION AND CONCLUSIONS

The representation of tissues as a cellular foam has emerged as a powerful paradigm for force inference based on shape in 3D cell aggregates [7]. This work is the first to simulate the structural and dynamical properties of a 3D, active cellular foam with sliding interactions and intercellular pores. Based on simulations of this model, we were able to map the fluid-to-jammed phase transition in function of mechanical properties of the foam, which have been characterized as (coarse-grained) biophysical properties of the cell [8]. This bridges the gap between two contrasting models of fluidity in granular media: the colloidal model and the vertex model. Furthermore, our results suggest an important role of cell-cell friction in modulating topological rearrangements, which is distinct from the jamming transition. Further research is needed to clarify the role of cell-cell and cell-substrate friction in multicellular dynamics, also in relationship with continuum hydrodynamic models of tissues as active viscous materials.
Enriched with additional cell behaviours such as growth, cytokinesis [4], and cell-matrix interactions, the simulation platform for active foam dynamics could serve as a powerful tool for investigating multicellular behaviour across various applications, including embryonal development, tumour progression, and the fabrication of organoids and micro-tissues in biofabrication processes. However, these active foam simulations are currently computationally demanding, necessitating hundreds of degrees of freedom per cell, explicit time stepping, and adaptive remeshing. Consequently, our simulations are presently constrained to approximately 10^3 cells, which proves sufficient for certain biological systems, such as organoids or *C. elegans* embryos [4], but inadequate for others, such as tumours or large-scale developmental processes.

ACKNOWLEDGEMENTS

We acknowledge support from the Research Foundation Flanders (FWO), grants 11D9923N and 12Z6118N; and from KU Leuven internal funding C14/18/055.

References

[1] Bi, D., Lopez, J. H., Schwarz, J. M., & Manning, M. L. (2015). A density-independent rigidity transition in biological tissues. Nature Physics, 11(12), 1074-1079.

[2] Kim, S., Pochitaloff, M., Stooke-Vaughan, G. A., & Campàs, O. (2021). Embryonic tissues as active foams. Nature physics, 17(7), 859-866.

[3] Cuvelier, M., Pešek, J., Papantoniou, I., Ramon, H., & Smeets, B. (2021). Distribution and propagation of mechanical stress in simulated structurally heterogeneous tissue spheroids. Soft Matter, 17(27), 6603-6615.

[4] Cuvelier, M., Vangheel, J., Thiels, W., Ramon, H., Jelier, R., & Smeets, B. (2023). Stability of asymmetric cell division: A deformable cell model of cytokinesis applied to C. elegans. Biophysical Journal, 122(10), 1858-1867.

[5] Schwarz, U. S., & Safran, S. A. (2013). Physics of adherent cells. Reviews of Modern Physics, 85(3), 1327.

[6] Oriola, D., Marin-Riera, M., Anlaş, K., Gritti, N., Sanaki-Matsumiya, M., Aalderink, G., ... & Trivedi, V. (2022). Arrested coalescence of multicellular aggregates. Soft Matter, 18(19), 3771-3780.

[7] Ichbiah, S., Delbary, F., McDougall, A., Dumollard, R., & Turlier, H. (2023). Embryo mechanics cartography: inference of 3D force atlases from fluorescence microscopy. Nature Methods, 20(12), 1989-1999.

[8] Saha, A., Nishikawa, M., Behrndt, M., Heisenberg, C. P., Jülicher, F., & Grill, S. W. (2016). Determining physical properties of the cell cortex. Biophysical journal, 110(6), 1421-1429.

Tumor spheroid mechanics and invasion revealed by a microfluidic rheometer

Young Joon Suh[1], Mrinal Pandey[1], Alan T Li [1], Bangguo Zhu[2], Chung-Yuen Hui[2], Jeffrey E Segall[3], and Mingming Wu[1*]

[1]*Department of Biological and Environmental Engineering, Cornell University, Ithaca, NY. USA*
[2]*Sibley School of Mechanical and Aerospace Engineering, Cornell University, Ithaca, NY. USA.*
[3]*Department of Pathology, Albert Einstein College of Medicine, 1300 Morris Park Avenue, Bronx, NY. USA.*

INTRODUCTION

Clinically, the feel, touch, and shape of a solid tumor are important diagnostic methods for malignant state of a tumor. However, there are limited tools for quantifying the mechanics of the tumor and its relevancy to the malignant state. This is in part due to the lack of instruments where tumor mechanics can be examined quantitatively in a physiologically realistic setting. Here, we developed a microfluidic platform, where the tumor spheroids can be compressed either statically or dynamically in a high throughput way. The shape of the tumor spheroid, as well as single cell motility within each tumor spheroid can be imaged and followed in real time. From clinical point of view, this work allowed us to measure the instantaneous modulus of the tumor spheroid in a short time (less than a minute). We found that the spheroid modulus is correlated to the malignancy state of the tumor using cell lines that had various levels of malignancy. Scientifically, this tool enabled us to reveal the multi-time scale viscoelastic properties of the tumor spheroid for the first time. The microfluidic rheometer here can be easily extended to studies of mechanics of single cell and/or nucleus.

MATERIALS AND METHODS

A microfluidic rheometer [1]

The key components of the microfluidic device are the three layers (Fig. 1A), from bottom to top, the cell layer (L1), the PDMS piston layer (L2), and the pressure control chamber layer (L3). The tumor spheroid is placed within the cell chamber in the cell layer. The spheroids can be either surrounded by 3D ECM or media. When the pressure chamber is pressurized, the piston moves downward and press on the spheroid. The calibration curve of the device is shown in Fig.1B. We note that the compression distance Δh is controlled by the pressure, which can be controlled with a resolution at sub-micrometer size, which allows this device to press as small an object as a nucleus precisely.

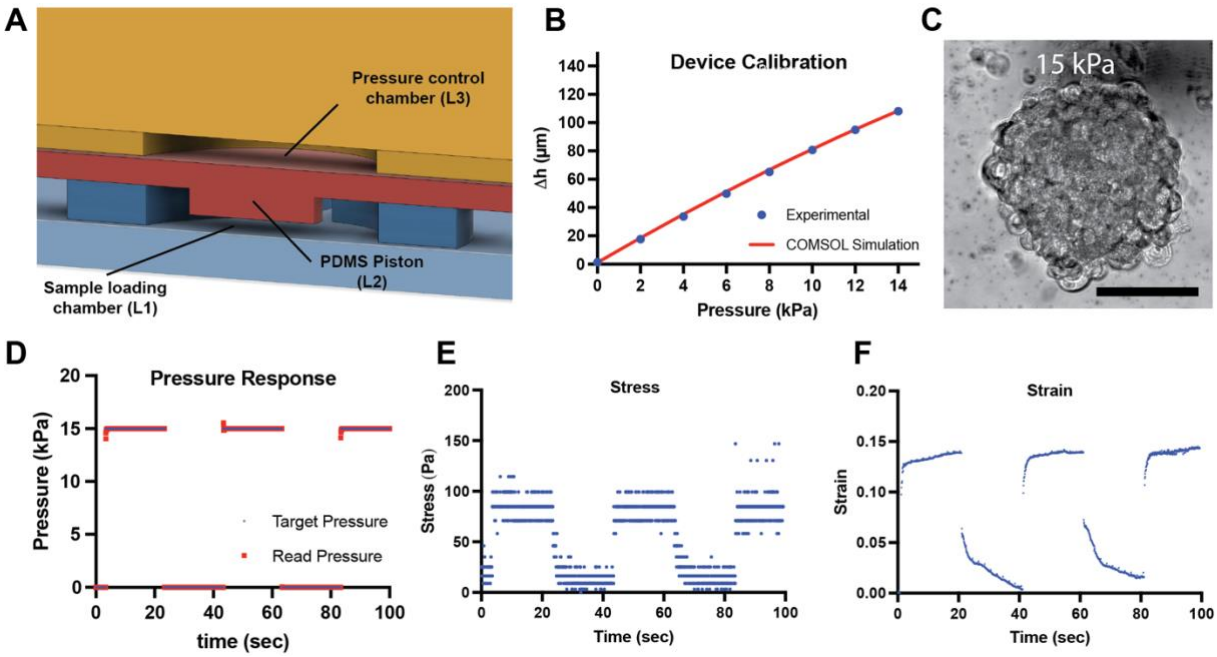

Figure 1: **Design of the Microrheometer, calibration and experiments** A. Schematic of the three-layer microrheometer, the cell chamber (L1), the PDMS piston (L2), and the pressure control chamber (L3). The pressure in the pressure chamber controls the vertical position of the piston, which subsequently compresses the spheroids [1]. B. Device calibration against COMSOL simulation. This calibration curve is obtained in the absence of the spheroids. C. An image of the tumor spheroid in the device.

Scale bar is 100 μm. D-F. Dynamic compression test of the tumor spheroids. D. The pressure applied to the pressure chamber. E. The stress experienced by the tumor spheroid. F. The strain experienced by the spheroid measured using the microrheometer.

Cells and spheroids

Three cell lines are used for this experiment. Since the formation of tumor spheroids depends sensitively on the level of E-cadherin, and tumor invasion within a 3D ECM depends primarily on the level of integrin. Consequently, in our current work we decided to use three different breast cancer cell lines (MCF-10A, MCF-7, and MDA-MB-231) with a diverse range of E-cadherin and integrin levels. MDA-MB-231 is a malignant and highly metastatic ER (estrogen receptor) negative cell line, while MCF-7 is a malignant and less metastatic ER positive cell line, and MCF-10A is a non-tumorigenic cell line. The levels of E-cadherin and integrin in these cell lines are tabulated below:

Cell Line	E-cadherin	Integrin
MDA-MB-231	0.04	278.8
MCF7	246.9	66.9
MCF10A	30.6	241.8

RESULTS AND DISCUSSION

We first tested the correlation between tumor spheroid mechanics and invasion using a modified Transwell assay [2] and the microfluidic rheometer. We found differential responses of malignant and non-tumorigenic spheroids to static compression. While the malignant (MDA-MB-231) spheroids became fluidized under compression and more invasive, the non-tumorigenic (MCF-10A) spheroids had no observable change in fluidization and were less invasive. Upon dynamic compression, we were able to measure the instantaneous modulus of the spheroids, corresponding to their molecular compositions. More interestingly, we found that the relaxation curve of the tumor spheroids follows a power law, an indication that the tumor spheroid is a multi-time scale viscoelastic material. Further work is needed to carefully correlate the relation of the tumor rheology with adhesion molecules E-cadherin and integrin.

* Corresponding author. Email: **mw272@cornell.edu**

ACKNOWLEDGEMENTS

This work was supported by a grant from the National Institute of Health (Grant No. 5R01CA221346-06). The authors would like to thank insightful discussions with Brian Cheung and Vivek Shenoy.

References

1. Suh, Y., Pandey, Mrinal, Wu, Mingming, *Microfluidic rheometer* Provisional patent application #: 63/452,881, 2023.
2. Pandey M, S.Y., Kim M, Davis HJ, Segall JE, Wu M. , *Mechanical compression regulates tumor spheroid invasion into a 3D collagen matrix.* ArXiv [Preprint]. 2023.

BMD EVOLUTION DURING BONE REGENERATION IN OSTEOPOROTIC BONE

Juan José Toscano-Angulo[1*], Juan Mora-Macías[2], Pablo Blázquez-Carmona[1], Juan Morgaz[3], Rocío Navarrete-Calvo[3], Jaime Domínguez[1], Esther Reina-Romo[1]

1. Escuela Técnica Superior de Ingeniería, Universidad de Sevilla, Spain; 2. Escuela Técnica Superior de Ingeniería, Universidad de Huelva, Spain; 3. Hospital Veterinario, Universidad de Córdoba, Spain;

INTRODUCTION

Osteoporosis (OP) is a systemic bone disorder characterized by a decrease in bone mineral density (BMD) and the degradation of the microarchitecture of trabecular tissue, which increases skeletal fragility and the risk of sudden fractures. 5 years after the first OP fracture, the risk of refracture in women increases by 24% and mortality rates by 39% [1]. In post-traumatic or surgical cases, *in vivo* studies have shown that bone remodelling occurs not only for the development and mineralization of the woven bone, but also for adjacent cortical tissue by decreasing its mineral density [2,3]. However, there is a lack of knowledge about the bone implications of fractures or surgical interventions in OP patients.

In this line, this *in vivo* study aims to characterize in terms of BMD variation, the influence of a bone surgical intervention in OP subjects. In particular, bone transport (BT) experiments will be performed to analyze the mineralization evolution during the consolidation phase of the woven bone and its adjacent regions.

MATERIALS AND METHODS

In vivo experiments were carried out in the right hind metatarsus of 11 female merino sheep, previously subjected to an OP induction procedure. The induction involved the performance of an ovariectomy (OVX), followed by 30 weeks of 0% Ca diet administration and periodic injections of glucocorticoids [4]. The BT experiments began with a standard surgical implantation of an external distractor-fixator and the performance of three osteotomies on the diaphysis, resulting in two central bone segments: a 25 mm proximal transportable fragment previously fixed to the distractor and a 15 mm distal fragment which is removed to generate a critical-size defect [5]. After a latency period of 7 days, the distraction phase started, in which the transportable fragment is distally displaced 1 mm/day for 15 days to fill progressively the induced large defect. Two ossification focuses appeared at the proximal and distal ends of the transported fragment, thus generating a distraction and docking calluses (see Figure 1A). Animals were randomly sacrificed at two different time points of this consolidation phase, at 40 (Sac40) or 100 (Sac100) days after BT surgery.

For each OP sheep, the BMD of the intervened metatarsus was assessed using computed tomography (CT) at 3 time points: on the OVX day (Control), on the BT surgery day (BT-CX, 30 weeks after OVX), and on the sacrifice day (Sac40 or Sac100). All CT measurements were processed using the open-source software ImageJ/FIJI®, calculating the BMD of each metatarsus cross-sectional slice along its length after a previous manual segmentation. Figure 1A shows the BMD along the metatarsus from CT evaluation in one of the ovariectomized sheep at three time points: OVX day, BT-CX day and 100 days after BT-CX. The evaluation was focused on five regions of interest: three different adjacent cortical fragments and two calluses. In this way, a mean ± standard deviation BMD value was obtained from the different cortical regions at each time point: proximal (PF), transport (TF) and distal (DF) fragments, 13%, 9% and 12% respectively of the metatarsus length. In addition, the apparent BMD of each callus was computed at the corresponding sacrifice time point of each pathologic animal: distraction (DiC) and docking (DoC) calluses, 5% and 1% respectively of the metatarsus length.

RESULTS

The mean and standard deviation values of BMD values measured in each cortical fragment and callus at each time point are shown in Figure 1B. Regarding the comparison between Control and BT-CX time points, no significant differences in cortical mineral density were reported over time for each analysed region. However, these differences are significant at both sacrifice time points (Sac40 and Sac100), reporting a trend of BMD reduction over time in the distal direction of the intervened bone. Regarding the analysis of the OP calluses, a significant increase in the BMD of the distraction callus was observed over the consolidation phase: 0.453 to 0.605 g/cm^3 at days 40 and 100 after BT-CX, respectively. By cons, no significant differences were reported in the docking callus (0.546 to 0.599 g/cm^3).

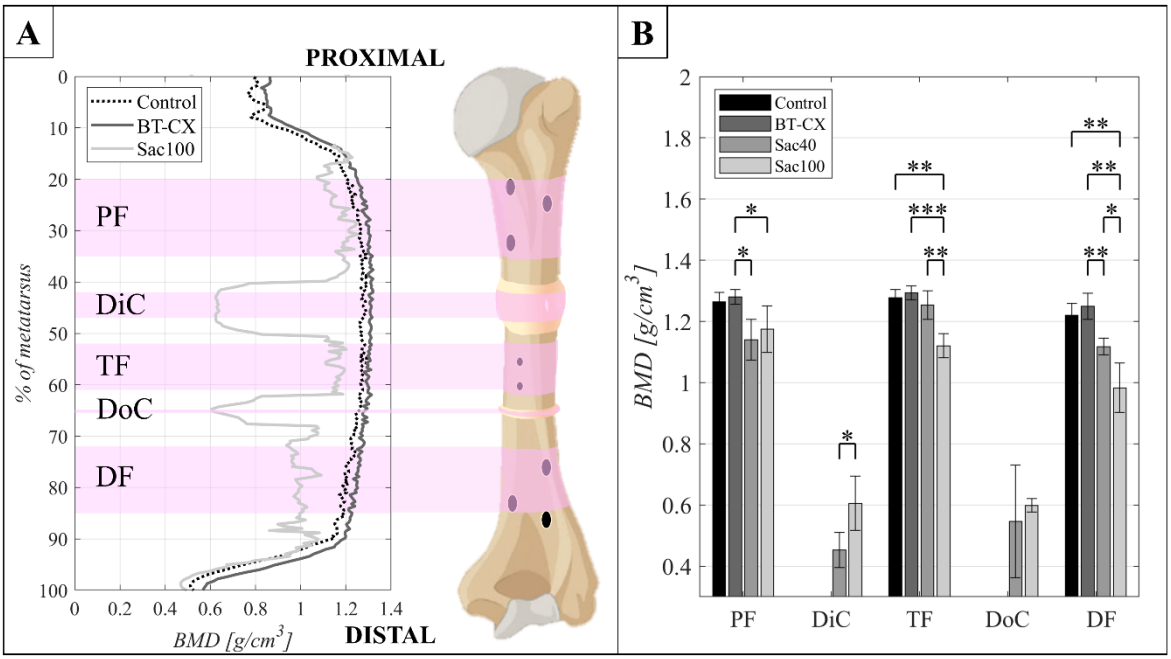

Figure 1. BMD evaluation of ovariectomized sheep intervened metatarsus at four CT-time points: Control (OVX day), BT-CX (30 weeks after OVX), Sac40 (40 days after BT-CX) and Sac100 (100 days after BT-CX). A) Apparent cross-sectional BMD throughout % of the intervened metatarsus length (0 % proximal, 100% distal) in an ovariectomized sheep. B) Mean ± standard deviation BMD evolution of fives ROIs of the intervened metatarsus: proximal fragment (PF), distraction callus (DiC), transport fragment (TF), docking callus (DoC) and distal fragment (DF).
* represents $p < 0.05$, ** represents $p < 0.01$ and *** represents $p < 0.001$.

DISCUSSION AND CONCLUSIONS

This study reports for the first time an evaluation of the BMD of an OP bone during a bone regeneration process. The results obtained seem to indicate two significant outcomes. First, osteoporosis does not alter the cortical mineral density, which is in line with studies reported in the literature [6]. Secondly, bone surgical interventions lead to a BMD reduction of the intervened bone which is more significant in the distal fragment of the bone, and over time, at least during the initial 100 days post-intervention. There are three main possible reasons for this decreased osteoblastic activity [2]: the lack of load bearing capacity in the operated limb during the first weeks after the intervention, the deficiency of distal blood supply due to the osteotomies and the critical-size defect [6], and the need for bone mineral to repair the induced defects, which is related to the increased level of ossification reported in both calluses. In this regard, it is concluded that bone fractures or surgical interventions weakens the mineral density of the operated bone more than osteoporosis itself. This side-effect could mechanically compromise the stabilizing function of the implanted fixator and requires more continuous clinical follow-up to minimize the risk of OP refractures.

ACKNOWLEDGEMENTS

This work is part of the R&D&i project PID2020-113790RB-I00, funded by MCIN/ AEI/10.13039/501100011033.

References

[1] Bliuc D., Nguyen N. D., Nguyen T.V., Eisman J.A., Center J.R..: *Compound risk of high mortality following osteoporotic fracture and refracture in elderly women and men.* Journal of Bone and Mineral Research. Vol 28, pp. 2317-2324, 2013

[2] Augat P., Claes L..: *Increased cortical remodeling after osteotomy causes posttraumatic osteopenia.* Bone. Vol 43, pp. 539-543, 2008

[3] Ren T., Klein K., Von Rechenberg B., Darwiche S., Dailey H.L..: *Image-based radiodensity profilometry measures early remodeling at the bone-callus interface in sheep.* Biomechanics and Modeling in Mechanobiology. Vol 21, pp. 615-626, 2022

[4] Zarrinkalam M.R., Beard H., Schultz C.G., Moore R.J..: *Validation of the sheep as a large animal model for the study of vertebral osteoporosis.* European Spine Journal. Vol 18, pp. 244-253, 2009

[5] Mora-Macías J., Reina-Romo E., Morgaz J., Domínguez J..: *In Vivo Gait Analysis During Bone Transport.* Annals of Biomedical Engineering. Vol 43 pp. 2090-2100, 2015

[6] Bisazza K.T., Nelson B.B., Sikes K.J., Nakamura L., Easley J.T..: *Computed Tomography Provides Improved Quantification of Trabecular Lumbar Spine Bone Loss Compared to Dual-Energy X-Ray Absorptiometry in Ovariectomized Sheep*. Journal of Bone and Mineral Research Plus. Vol 7, 2023

[7] Melnyk M., Henke T., Claes L., Augat P..: *Revascularisation during fracture healing with soft tissue injury.* Archives of Orthopaedic and Trauma Surgery. Vol 128 pp. 1159-1165, 2008

The ECM and tissue architecture are major determinants of early invasion mediated by E-cadherin dysfunction

Rui DM Travasso[1]
Soraia Melo[2], Pilar Guerrero[3], Maurício Moreira-Soares[4], José Rafael Bordin[5], Fátima Carneiro[2,6], João Carvalho[1], Joana Figueiredo[2], Raquel Seruca[2]

[1] CFisUC, Departamento de Física, Universidade de Coimbra, Coimbra, Portugal
[2] IPATIMUP, Instituto de Investigação e Inovação em Saúde, Universidade do Porto, Porto, Portugal
[3] Departamento de Matemáticas, Grupo Interdisciplinar de Sistemas Complejos (GISC), Universidad Carlos III de Madrid, Spain
[4] OCBE, Centre for Bioinformatics, University of Oslo, Norway
[5] Instituto de Física e Matemática, Departamento de Física, Pelotas, RS, Brazil
[6] Departamento de Patologia, Faculdade de Medicina, Universidade do Porto Portugal

Germline mutations of E-cadherin cause Hereditary Diffuse Gastric Cancer (HDGC), a highly invasive cancer syndrome characterised by the occurrence of diffuse-type gastric carcinoma and lobular breast cancer. In this disease, E-cadherin-defective cells are detected invading the adjacent stroma since very early stages. Although E-cadherin loss is well established as a triggering event, other determinants of the invasive process persist largely unknown. Herein, we develop an experimental strategy that comprises in vitro extrusion assays using E-cadherin mutants associated to HDGC, as well as mathematical models epitomising epithelial dynamics and its interaction with the extracellular matrix (ECM). In vitro, we verify that E-cadherin dysfunctional cells detach from the epithelial monolayer and extrude basally into the ECM. Through phase-field modelling we demonstrate that, aside from loss of cell-cell adhesion, increased ECM attachment further raises basal extrusion efficiency. Importantly, by combining phase-field and vertex model simulations, we show that the cylindrical structure of gastric glands strongly promotes the cell's invasive ability. Moreover, we validate our findings using a dissipative particle dynamics simulation of epithelial extrusion. Overall, we provide the first evidence that cancer cell invasion is the outcome of defective cell-cell linkages, abnormal interplay with the ECM, and a favourable 3D tissue structure.

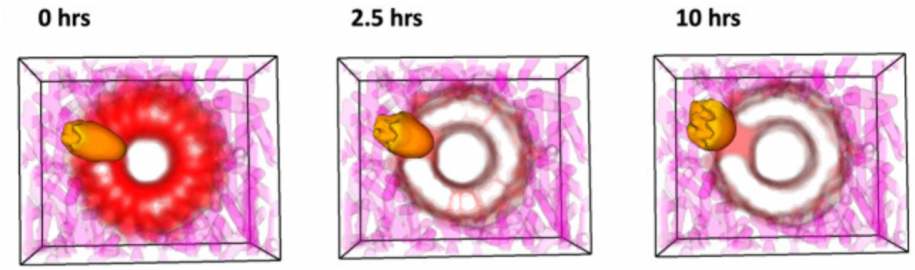

MODELING THE IMPACT OF CELL-MATRIX MECHANICS ON MIGRATORY HETEROGENEITY IN CANCER METASTASIS

Saber Shakibi[1], Erika Tsingos[1,*],

1. Computational Developmental Biology Group, Institute of Biodynamics and Biocomplexity, Utrecht University, Utrecht, Netherlands

INTRODUCTION

In early cancer metastasis, cells migrating away from the tumor core exhibit different migratory phenotypes (Figure 1 a). The balance between these modes of migration is controlled by several processes, including intercellular adhesion [2, 6], cytoskeletal activity [4, 6], and extracellular matrix (ECM) architecture [1, 2, 3]. Here, we will develop a computational model of cell migration in fibrous ECM to study the contribution of (combinations of) above-mentioned processes to these emergent phenotypes.

MATERIALS AND METHODS

Cells are modelled via a cellular Potts model (CPM), where each cell is represented as a collection of lattice sites on a grid. The lattice configuration changes dynamically based on an energy minimization algorithm. We will build on a recently developed CPM that was hybridized with a discrete coarse-grained ECM fiber model (Figure 1 b). The dynamics of the fiber model are solved in an overdamped environment using methods from molecular dynamics. ECM fibers are modeled in continuous space as bead-spring chains with harmonic potentials between consecutive beads and harmonic bending potentials between consecutive bead triplets. Fibers can be mechanically coupled via crosslinkers. The two model frameworks interact via discrete sites that model focal adhesions.

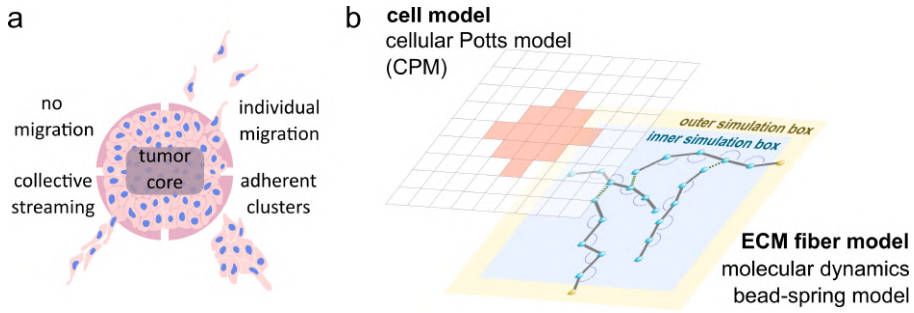

Figure 1. (a) Migratory heterogeneity in early metastasis. (b) Two different model formalisms are hybridized to model cell-ECM mechanics.

RESULTS

In previous work [5], the model's capabilities were demonstrated in a scenario mimicking a common experimental setup consisting of an isolated contractile cell embedded in an ECM fiber network. Due to the mechanical reciprocity between cell and ECM, the initially homogeneously shrinking cell equilibrated to inhomogeneous shapes (Figure 2 a). The model recapitulated the increase of bulk ECM stiffness with increasing crosslinker concentration, and demonstrated a transition from viscoplastic to viscoelastic bulk ECM behavior (Figure 2 b-c).

* Corresponding author. E-mail: e.tsingos@uu.nl

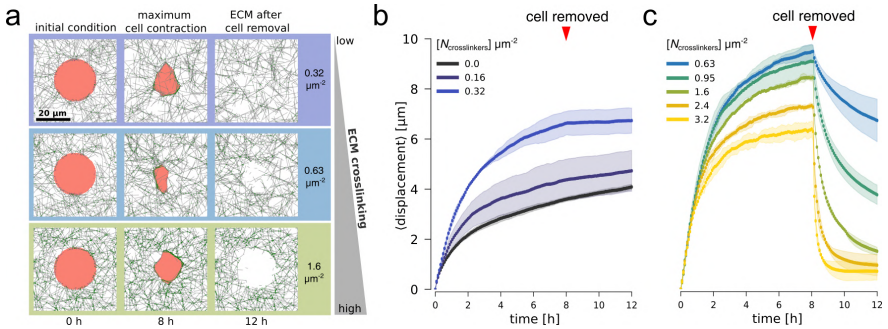

Figure 2. (a) Simulation screenshots showing initial state with uncontracted cell, fully contracted cell, and four hours after cell removal. (b-c) Bulk ECM displacement over time averaged in a circular radius around the contractile cell. (b) At low crosslinker densities, the bulk ECM exhibits viscoplastic behavior. (c) At high crosslinker densities, the bulk ECM exhibits viscoelastic behavior. Colored outlines in (a) correspond to legend in (b-c).

DISCUSSION AND CONCLUSIONS

Cell-based models such as the CPM excel at modeling how collective phenotypes emerge from cell behaviors due to their ability to simulate many individual cells interacting at the mesoscale, and the flexibility in tuning the level of model abstraction to the existing knowledge of biological detail. The hybrid model developed in [5] lays the foundation to investigate the role of cell-ECM mechanics in collective behavior. In ongoing work, we are extending this model to investigate the emergence of different modes of cell migration in cancer metastasis.

ACKNOWLEDGEMENTS

The authors thank NWO for providing financial support to this project under grant number VI.Veni.222.323.

References

[1] Haeger, A., Krause, M., Wolf, K., & Friedl, P.: *Cell jamming: collective invasion of mesenchymal tumor cells imposed by tissue confinement.* Biochimica et Biophysica Acta Vol. 1840(8), pp. 2386-2395, 2014.

[2] Ilina, O., Gritsenko, P. G., Syga, S., Lippoldt, J., La Porta, C. A., Chepizhko, O., ... & Friedl, P.: *Cell–cell adhesion and 3D matrix confinement determine jamming transitions in breast cancer invasion.* Nature Cell Biology Vol. 22(9), pp. 1103-1115, 2020.

[3] Kang, W., Ferruzzi, J., Spatarelu, C. P., Han, Y. L., Sharma, Y., Koehler, S. A., ... & Fredberg, J. J..: *A novel jamming phase diagram links tumor invasion to non-equilibrium phase separation.* iScience Vol. 24(11), 2021.

[4] Nieto, M. A., Huang, R. Y., Jackson, R. A., & Thiery, J. P..: *EMT.* Cell Vol. 166(1), pp. 21-45, 2016.

[5] Tsingos, E., Bakker, B. H., Keijzer, K. A., Hupkes, H. J., & Merks, R. M..: *Hybrid cellular Potts and bead-spring modeling of cells in fibrous extracellular matrix.* Biophysical Journal Vol. 122(13), pp. 2609-2622, 2023. Code: doi:10.5281/zenodo.7906972

[6] Yang, J., Antin, P., Berx, G., Blanpain, C., Brabletz, T., Bronner, M., ... & EMT International Association (TEMTIA).: *Guidelines and definitions for research on epithelial–mesenchymal transition.* Nature Reviews Molecular Cell Biology Vol. 21(6), pp. 341-352, 2020.

PHOTOPOLYMERIZATION OF 3D FIBER NETWORKS TO STUDY THE DYNAMICS OF CELL-MATRIX INTERACTION

Pierre Ucla [1,2], Xingming Ju [1,2], Joanne Le Chesnais [3], Henri Ver Hulst [1], Ludovic Leconte [4], Jean Salamero [4], Catherine Monnot [5], Hélène Moreau [6], Jessem Landoulsi [3], Vincent Semetey [2], Sylvie Coscoy [1]

[1] Institut Curie, Université PSL, Sorbonne Université, CNRS UMR168, Laboratoire Physico Chimie Curie, team Biology-inspired Physics at Mesoscales. [2] Chimie ParisTech, Université PSL, CNRS, Institut de Recherche de Chimie Paris, team Materials, Interfaces and Soft Matter. [3] Laboratoire de Réactivité de Surface, UMR 7197 Sorbonne Université - CNRS. [4] SERPICO/STED team, UMR144 CNRS Institut Curie, Université PSL, Sorbonne Université, 75005 Paris, and Inria Centre Rennes-Bretagne Atlantique, 35042, Rennes cedex. [5] Centre de Recherche des Cordeliers, INSERM, Sorbonne Université, Université de Paris Cité, team Inflammation, Complement and Cancer. [6] Immunité et Cancer, INSERM U932, Institut Curie, Université PSL, team Spatio-temporal dynamics of immune cells.

CONTEXT

The physical properties of the extracellular matrix play a decisive role in many processes of development or disease. During the tumor process, these physical properties are greatly altered by the action of chemical processes, but also mechanical ones, cells exerting traction forces. The tumor matrix typically exhibits increased stiffness, alignment of collagen fibers, and changes in porosity[1], playing a determining role in the initiation and progression of cancer, by controlling the behavior of cancerous and surrounding cells[2]. The characterization of forces exerted by cells within their microenvironment is the subject of intensive efforts and methods such as Traction Force Microscopy are commonly used to study the mechanobiological processes at work[3]. However, these methods have limitations resulting in particular from the non-linearities of the material considered, and the measurement of 3D cellular traction forces in contact with individual fibers requires the development of innovative approaches. While conventional approaches allow to adjust the macroscopic mechanical properties of gels, the control of local physical properties (stiffness of individual fibers, local density, geometry) calls for the development of new nano- and micro-fabrication techniques.

RESULTS

We propose an innovative technology to study interactions with the matrix of various cell types, with the development of fiber networks with fully controlled physical and chemical properties produced by two-photon polymerization. The produced fibers span a wide range of sizes and mechanical properties are characterized by means of force spectroscopy using Atomic Force Microscopy. We combine this approach with the development of an original method for measuring cellular traction forces in 3D, relying on automated 3D segmentation of the deformed fibers coupled with a Finite Element Modeling framework. We demonstrate that this technique is suitable to study traction forces in mesenchymal cells such as endothelial cells (HUVECs) and fibroblasts (NIH-3T3) but also in amoeboid-like cells such as dendritic cells, using fast volumetric imaging by Lattice Light-Sheet Microscopy to capture low intensity and short-lived traction forces.

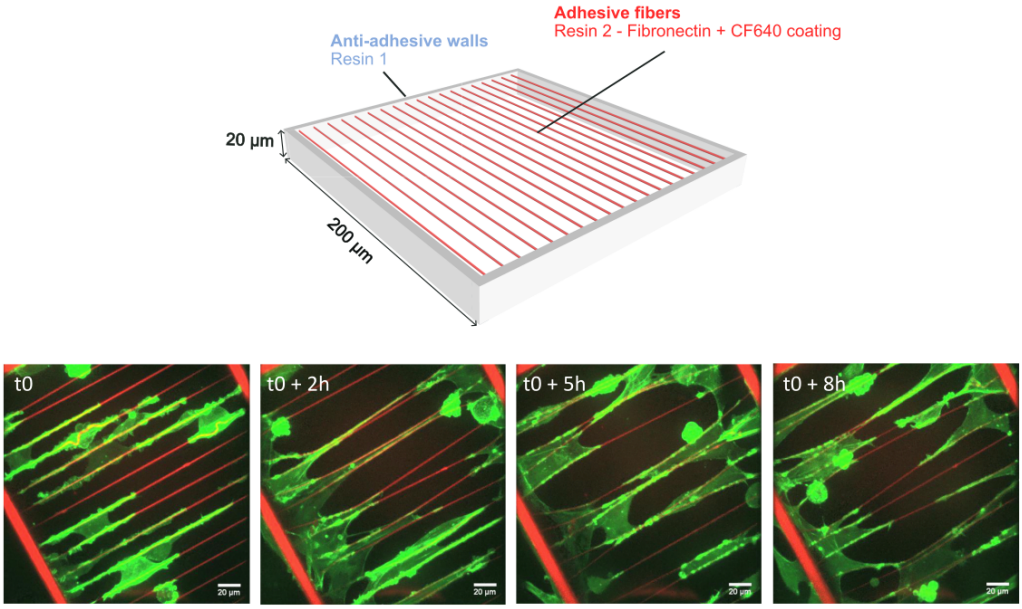

Figure 1. Deformable fiber arrays generated by two-photon polymerization. (Top) Design of a composite 3D microscaffold composed of anti-adhesive walls and an adhesive layer of fibers and (Bottom) spreading, traction force exertion and migration of HUVECs Lifeact-GFP on low stiffness photopolymerized fibers with a 10 µm spacing. Scale bar: 20 µm.

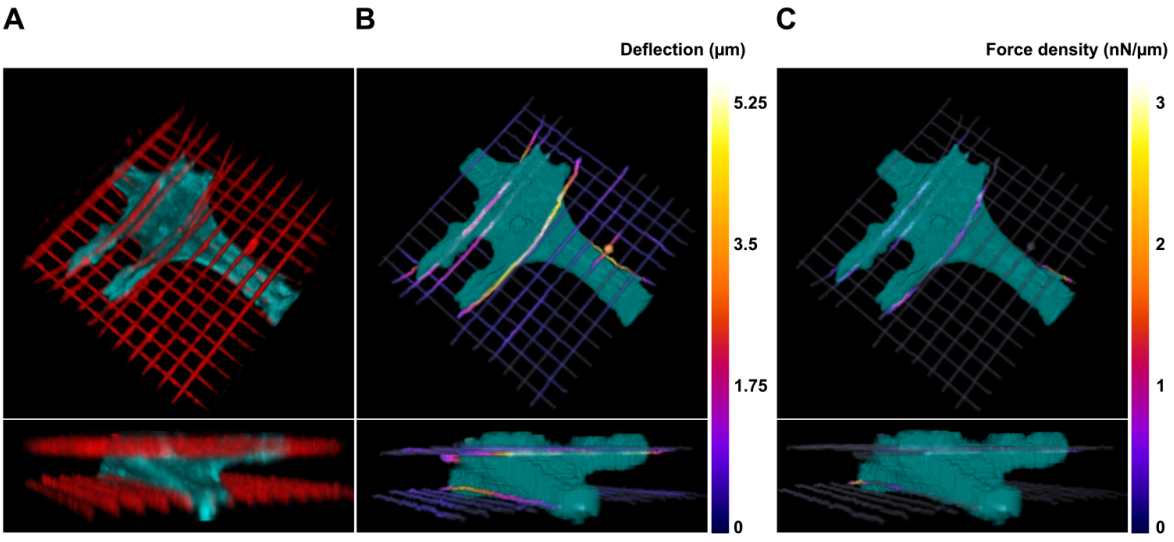

Figure 2. Automated traction force recovery analysis. (A) 3D reconstruction of a single HUVEC Lifeact-GFP cell in a 2-layer microscaffold. (B) Corresponding deflection map and (C) 3D Traction force map.

ACKNOWLEDGEMENTS

The authors would like to thank the '**Agence Nationale de la Recherche'** (ANR-23-CE19-0025-01), the **QLife** program (**université PSL**), the **LabEx Cell(n)Scale** (grants ANR-11-LABX-0038, ANR-10-IDEX-0001), the **Sorbonne Université** program "Interfaces pour le Vivant", **La Ligue contre le cancer,** the Oversea Study Program of Guangzhou Elite Project, **the Centre National de la Recherche Scientifique (CNRS), Inserm (Institut National de la Santé et de la Recherche Médicale), Chimie ParisTech and Institut Curie** for providing financial support to this project.

References

1. Provenzano E, Ulaner GA, Chin SF. Molecular Classification of Breast Cancer. PET Clin. 2018
2. Emon B, Bauer J, Jain Y, Jung B, Saif T. Biophysics of Tumor Microenvironment and Cancer Metastasis - A Mini Review. Comput Struct Biotechnol J. 2018
3. Koch TM, Münster S, Bonakdar N, Butler JP, Fabry B. 3D Traction forces in cancer cell invasion. PLoS One. 2012

UNRAVELING THE MECHANISMS OF TRACTION FORCE GENERATION BY CHONDROCYTES AND THE EFFECT OF OSTEOARTHRITIS

Nele Vaes[1], Maxim Vovchenko[1,2], Rocío Castro Viñuelas[3], Jorge Barrasa-Fano[1], Apeksha Shapeti[1], Ilse Jonkers[4], Hans Van Oosterwyck[1,5*]

1. Biomechanics Section, Dept. of Mechanical Engineering, KU Leuven, Belgium; 2. Laboratory for Soft Matter and Biophysics, Dept. of Physics and Astronomy, KU Leuven, Belgium 3. Human Movement Biomechanics Research Group, Dept. of Movement Sciences, KU Leuven, Belgium 4. Laboratory for Tissue Homeostasis and Disease, Dept. of Development and Regeneration, Skeletal Biology and Engineering Research Center 5. Prometheus Division of Skeletal Tissue Engineering, KU Leuven, Belgium

INTRODUCTION

Osteoarthritis (OA) is a degenerative joint disease affecting 57 million people in Europe alone. Cartilage breakdown is a hallmark of OA and reflects in joint pain and decreased joint mobility, which reduces life quality of patients. Despite the high prevalence and the symptoms, no treatment is available that can reverse the pathogenesis. Many studies have shown the importance of cell generated forces in cell processes such as differentiation, migration etc. [6]. Cell forces are generated via actomyosin contraction of the cytoskeleton and are transferred to the extracellular matrix via focal adhesions. Recent studies have shown alterations upon OA to components involved in force generation such as the cytoskeleton [3] and integrin receptor expression [4], indicating a potential role for traction forces in OA development. Moreover, the Wnt signalling pathway is upregulated in OA and has been suggested as a chemical model of OA [5]. Therefore, our aim is to investigate the mechanisms of cell force generation for healthy and osteoarthritic cells by looking at the cytoskeleton, integrin expression and cell forces.

MATERIALS AND METHODS

Traction forces were evaluated in 2D and 3D. In 2D, human articular chondrocytes (hACs) were seeded on a Polyacrylamide (PAA) hydrogel with a fibronectin coating that provides binding sites for the cells. In 3D, hACs were embedded in a non-degradable polyethylene glycol (PEG) hydrogel that is functionalized with Arg-Glys-Asp (RGD) to provide binding sites for the cells. Both the cytosol and the actin cytoskeleton were fluorescently stained to visualize cell morphology. Fluorescent beads were incorporated in the hydrogel to allow tracking of hydrogel deformations induced by cells. The effect of Wnt upregulation was studied by addition of the GSK3 inhibitor CHIR99021.

Cell induced deformations and tractions were recovered by means of a previously established TFM computational workflow, incorporated in the software tool TFMLAB [1]. Briefly, cell induced displacements are obtained by non-rigid image registration of deformed and undeformed bead image stacks. Subsequently, traction forces are inferred by solving a minimization problem under the imposition of mechanical equilibrium in the hydrogel [2].

RESULTS

When comparing mechanisms of traction force generation by chondrocytes in 2D, two important findings emerge. First, staining of the actin cytoskeleton shows long, thick actin stress fibers in healthy chondrocytes, while the actin cytoskeleton in osteoarthritic cells is disrupted and disorganized. Second, traction forces of osteoarthritic hACs are lower than those of healthy hACs. Preliminary results also show a trend towards lower tractions upon CHIR99021 treatment.

* Corresponding author. Email: **hans.vanoosterwyck@kuleuven.be**

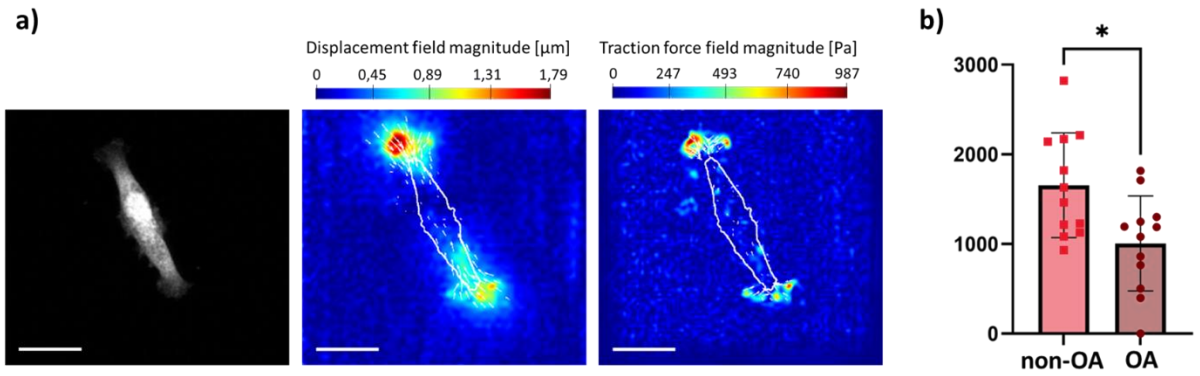

Figure 1: ***a)*** *Brightfield image of a hAC and the corresponding displacement field and the traction force field. Scalebar = 30µm ,* ***b)*** *Max traction force for non-OA and OA hAC on PAA, * $p<0.05$, $n_{non-OA} = 12$, $n_{OA} = 12$ (Unpublished data)*

Analysis of hACs in 3D shows a very distinct and round morphology, lacking protrusions as observed in 2D. The actin cytoskeleton lacks stress fibers and is mainly present as a cortex. Moreover, TFM shows both pulling (arrows pointing towards the cell) and pushing (arrows pointing outwards) traction force patterns.

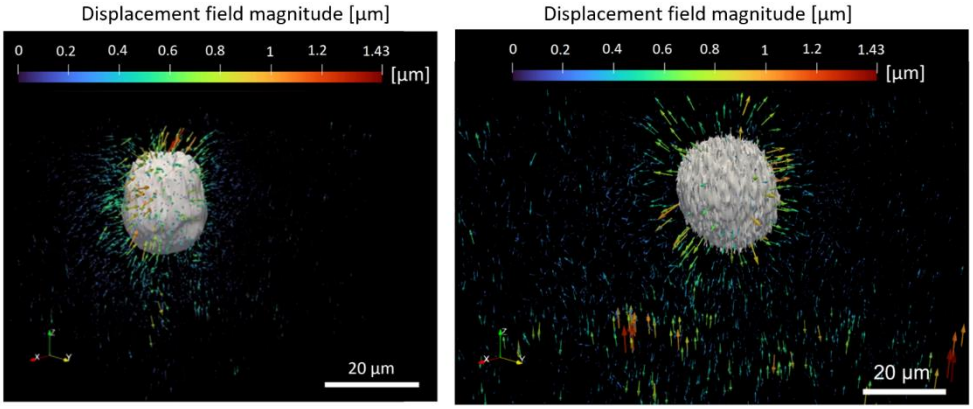

Figure 2: Displacement field of a pulling hAC and a pushing hAC in PEG (Unpublished data)

DISCUSSION AND CONCLUSIONS

Our hypothesis of lower traction forces upon OA was confirmed and might be caused by the disrupted actin cytoskeleton. Preliminary data of hACs treated with CHIR to upregulate Wnt signaling showed a similar decrease in traction forces. The distinct traction force patterns observed in 3D show a different traction force generation mechanism in 3D compared to 2D. We plan to further investigate traction forces in 3D and compare them for healthy and osteoarthritic hACs.

ACKNOWLEDGEMENTS

The authors would like to thank KU Leuven internal funding (IDN/20/019 Project-4-earlyOA, iBOF/21/083 C) for providing financial support to this project.

References

[1] Barrasa-Fano, J. et al.: *TFMLAB: A MATLAB toolbox for 4D traction force microscopy*. SoftwareX 15, 100723 (2021).

[2] Barrasa-Fano, J. et al. *Advanced in silico validation framework for three-dimensional traction force microscopy and application to an in vitro model of sprouting angiogenesis.* Acta Biomater 126, 326–338 (2021).

[3] Blain, E. J.: *Involvement of the cytoskeletal elements in articular cartilage homeostasis and pathology.* International Journal of Experimental Pathology vol. 90 1–15 (2009).

[4] Loeser, R. F.: *Integrins and chondrocyte–matrix interactions in articular cartilage.* Matrix Biology 39, 11–16 (2014).

[5] Luyten, F. P., Tylzanowski, P., Lories, R. J.: *Wnt signaling and osteoarthritis.* Bone 44, 522–527 (2009).

[6] Polacheck, W. J., Chen, C. S.: *Measuring cell-generated forces: a guide to the available tools.* Nature Methods 2016 13:5 13, 415–423 (2016).

MEASURING CELLULAR FORCES IN 3D AND APPLICATION TO MICROVASCULAR DISEASE

Hans Van Oosterwyck [1,2*]

1. KU Leuven, Department of Mechanical Engineering, Belgium; 2. KU Leuven, Prometheus Division of Skeletal Tissue Engineering, Belgium

ABSTRACT

3D Traction Force Microscopy (TFM) for the quantification of cell-generated forces in 3D has been introduced more than a decade ago [1] and has since then been extended and improved, such as towards its compatibility with nonlinear elastic, fibrillar hydrogels [2]. Still, it remains a technique that comes with many computational and experimental challenges, rendering its use for addressing mechanobiological research questions far from trivial. In an attempt to make 3D TFM more accurate, efficient and user-friendly, we recently introduced a novel inverse method that constrains solutions by imposing force equilibrium in the hydrogel domain [3], evaluated its accuracy under conditions that are representative for real 3D TFM experiments [4], and made it available to the scientific community as part of a MATLAB toolbox called TFMLAB [5]. By making 3D TFM compatible with an in vitro assay of sprouting angiogenesis, we were able to explore the role of aberrant cellular force exertion for the growth of cerebral cavernous malformations (CCMs), lesions that affect microcapillary function in the brain [6].

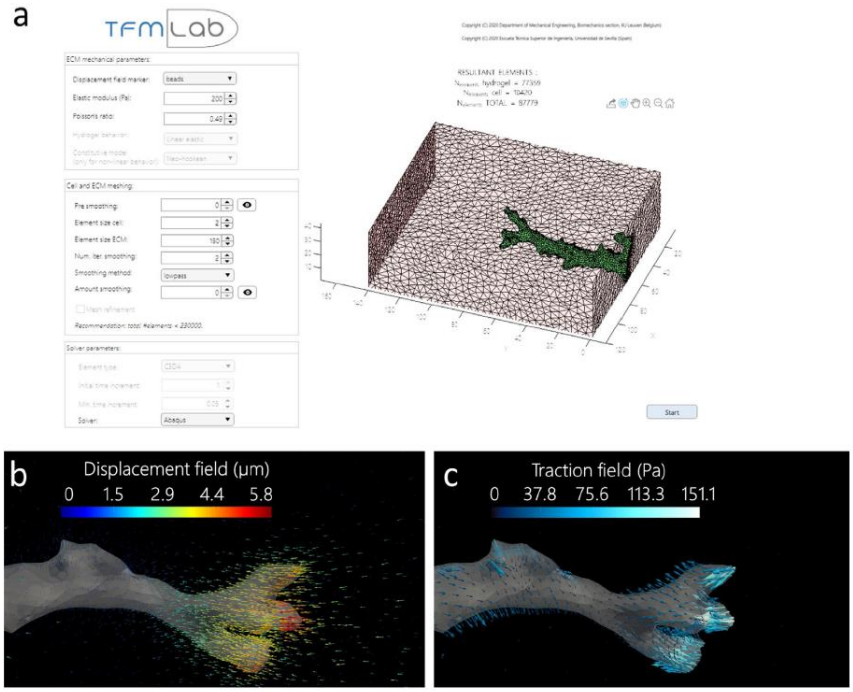

Figure 1. TFMLAB: A MATLAB toolbox for 3D traction force microscopy (a) GUI for FE meshing and force calculation. (b) 3D displacement field around an angiogenic sprout tip (c) corresponding 3D traction field (taken from [5]).

References

[1] Legant, W. R., Miller, J. S., Blakely, B. L., Cohen, D. M., Genin, G. M., Chen, C. S.: *Measurement of mechanical tractions exerted by cells in three-dimensional matrices*. Nature Methods Vol. 7, pp. 969-971, 2010

[2] Steinwachs, J., Metzner, C., Skodzek, K., Lang, N., Thievessen, I., Mark, C., Munster, S., Aifantis, K. E., Fabry, B.: *Three-dimensional force microscopy of cells in biopolymer networks*. Nature Methods Vol. 13, pp. 171-176, 2016.

[3] Sanz-Herrera, J.A., Barrasa Fano, J., Cóndor, M., Van Oosterwyck, H.: *Inverse method based on 3D nonlinear physically constrained minimisation in the framework of traction force microscopy*. Soft Matter Vol. 17, pp. 10210-10222, 2020.

[4] Barrasa Fano, J., Shapeti, A., de Jong, J., Ranga, A., Sanz-Herrera, J.A., Van Oosterwyck, H.: *Advanced in silico validation framework for three-dimensional Traction Force Microscopy and application to an in vitro model of sprouting angiogenesis*. Acta Biomaterialia, pp. 326-338, 2021

[5] Barrasa Fano, J., Shapeti, A., Jorge Peñas, A., Barzegari Shankil, M., Sanz-Herrera, J.A., Van Oosterwyck, H.: *TFMLAB: a MATLAB toolbox for 4D Traction Force Microscopy*. SoftwareX, Art.No. 100723, pp. 1-9, 2021.

[6] Shapeti, A., Barrasa Fano, J., Abdel Fattah, A.R., Sanz-Herrera, J.A., Pezet, M., Assou, S., de Vet, E., Elahi, S.A., Ranga, A., Faurobert, E., Van Oosterwyck, H.: *Force-mediated recruitment and reprogramming of healthy endothelial cells drive vascular lesion growth*. bioRxiv.

MODELLING THE INFLUENCE OF MECHANICAL LOADING ON THE DEVELOPMENT OF BONE METASTASES USING A HYBRID CELLULAR AUTOMATON

Claire C. Villette[1,*], Liesbet Geris[1,2]

1. KU Leuven, Belgium; 2. University of Liège, Belgium

INTRODUCTION

Bone metastases (BMs) are among the most debilitating complications for cancer patients. They are associated with poor prognosis and are often incurable. BMs develop through cancer-induced perturbation of the inherent bone remodelling process, which is responsible for healthy bone integrity through balanced resorption of old/damaged bone by osteoclasts and formation of new tissue by osteogenic cells. Osteolytic BMs interfere with this balance in a vicious cycle whereby cancer cells favour bone resorption. Growth factors are released from the degraded matrix and enhance tumour growth, which in turn intensifies bone resorption. Mechanical loading naturally induces an opposite shift to the remodelling balance by stimulating bone apposition. Early in-vitro and in-vivo experiments suggest a therapeutic potential for mechanical stimulation against metastases in bone [1].

The aim of this study was to develop a computational model of load-induced bone remodelling in the context of cancerous metastases, in order to support screening of loading regimens with potential therapeutic benefits.

MATERIALS AND METHODS

Overview

A 3D hybrid cellular automaton (HCA) model was implemented in FEniCSx [2]. Drawing from a published framework for modelling breast cancer chemotherapy [3], this novel HCA coupled three inter-connected modules based on different formalisms to recapitulate the following processes: (i) cellular events, (ii) extra-cellular matrix (ECM) deposition/degradation, (iii) osteogenic control over osteoclasts via RANKL/OPG ratio, (iv) influence of cancer cells on osteogenic/osteoclastic activity via PTHrP signalling, (v) influence of mechanical stimulation on cellular activity, and (vi) changes in material properties of the system associated with ECM modifications. As proof-of-concept, the model was applied to tri-culture tissue engineering systems on hydrogel-based carriers.

Cell module

Cellular events were modelled using a cellular automaton (CA) implemented on a regular 3D grid of 10 micrometer resolution. It described migration, proliferation, and death of three cell populations: osteogenic cells, osteoclasts, and cancer cells, as well as their activity in terms of ECM modification and biochemical signaling. Logistic function models were defined to represent the influence of mechanical stimulation and receptor occupancy on cellular activity.

Biochemical module

A partial differential equation (PDE) problem was implemented to represent the diffusion of osteoprotegerin (OPG) and receptor activator of NF- kB ligand (RANKL) produced by osteogenic cells, as well as binding of RANKL to OPG or to RANK receptors on osteoclast membrane. A separate PDE problem was implemented to represent diffusion of parathyroid hormone-related protein (PTHrP) produced by cancer cells and its binding to PTHrP receptors on osteogenic cell membrane. The general form of the equation governing the concentration of compound *i* followed Eq. (1) with *D* the diffusion constant, *r* the production rate, k_a and k_d the association and dissociation constants, and φ the decay rate .

$$\frac{\partial C_i}{\partial t} = D\nabla^2 C_i + r - k_a C_i C_j + k_d C_{ij} - \varphi C_i \quad (1)$$

Mechanics module

Another PDE problem was defined to solve for the local mechanical environment in response to external loading, based on a variational formulation of the equilibrium, constitutive, and stress-displacements equations. Hydrogel was considered as hyperelastic neohookenian material with Lamé constants dependent on ECM density and level of mineralization. The PDEs were solved using Finite Element solvers on linear tetrahedral elements with a mesh resolution of around 4.5 micrometers. Computed von Mises stress was used as mechanical stimulus modulating cellular activity.

Preliminary calibration and evaluation

As a first qualitative proof-of-concept, this model was tested for a sample of 20*20*20 cellular automaton grid

* Corresponding author. Email: claire.villette@kuleuven.be

cells, taken to represent an in-vitro experiment wherein cells would be seeded in a gel-type 3D carrier with no extra-cellular matrix (ECM) initially present. A 30% density of healthy cells was considered. Three scenarios were tested and compared: healthy bone (only healthy cells were seeded), metastatic bone (cancer cells were also seeded at a 20% density), and loaded metastatic bone (cancer cells were seeded at 20% density and sideway loading was applied to the carrier).

A preliminary calibration was then performed which aimed to capture a biofidelic ratio of RANKL/OPG, considered as key driver of osteoclast-mediated osteolysis. To this end, the ratio of predicted RANKL and OPG concentrations integrated over the model volume was compared to gene expression data from in vitro mineralised bone metastases constructs [4]. In this case, the model set-up mimicked the in-vitro system made of three stacked layers: osteogenic cells in mineralised hydrogel, osteogenic cells in non-mineralised hydrogel, and osteoclasts + cancer cells in non-mineralised hydrogel.

RESULTS

In the first proof of concept, the OPG/RANKL ratio (considered as an 'osteogenic signal') dropped in the presence of cancer cells (Figure 1). The signal was partially restored when loading was applied. Mirroring these observations, the level of ECM deposition in metastatic bone was lower than in a healthy culture but increased substantially when loading was applied.

As shown in Table 1, the preliminary calibration against in-vitro data captured the extent of the differences in RANKL/OPG ratios between healthy and metastatic bone, and between static and dynamic conditions. Predicted absolute orders of magnitude were also consistent with experimental reports.

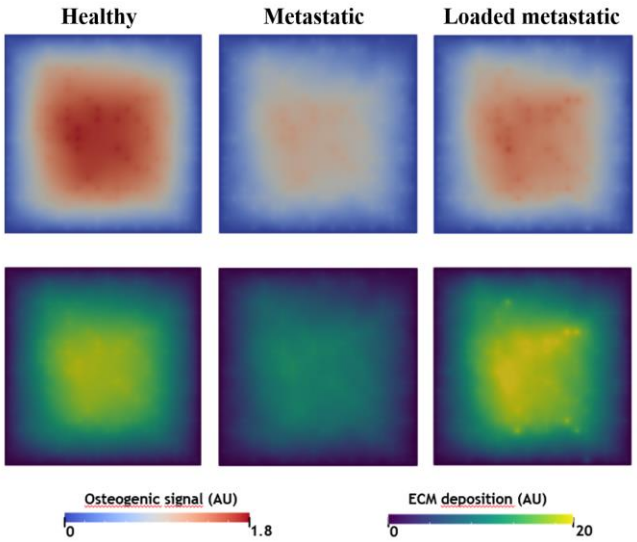

Figure 1. 2D slices of the model showing osteogenic signal shortly after loading (top) and ECM deposition after several cycles of loading (bottom). AU=arbitrary units.

Experimental	Static	Dynamic
Healthy bone	0.6	< 0.05
Metastatic bone	3	< 0.1
Predicted	Static	Dynamic
Healthy bone	0.17	0.013
Metastatic bone	1.7	0.013

Table 1. RANKL/OPG expression levels (experimental) and concentrations (predicted) in healthy and metastatic bone under static or dynamic conditions.

DISCUSSION AND CONCLUSIONS

An HCA model of load-induced remodelling of metastatic bone was implemented whose preliminary calibration captures the magnitude of cancer-induced perturbations of the main signal for osteoclast-mediated osteolysis reported in experimental studies.

Future work will involve parameter sensitivity study and comprehensive calibration. In-vitro protocols are being developed to support validation exercises. The validated model will be used to identify potential therapeutic regimens of loading.

ACKNOWLEDGEMENTS

The authors would like to thank **FWO** for providing financial support to this project.

References

[1] Lynch et al., 2013. Journal of Bone and Mineral Research, 28(11), pp.2357-2367.
[2] Logg and Wells, 2010. ACM Transactions on Mathematical Software, 37.2, 20:1-20:28
[3] Lai et al., 2022. International Journal for Numerical Methods in Biomedical Engineering 38.1, e3542.
[4] Kumar et al. 2023. bioRxiv. *Preprint.* DOI 10.1101/2022.09.19.508588.

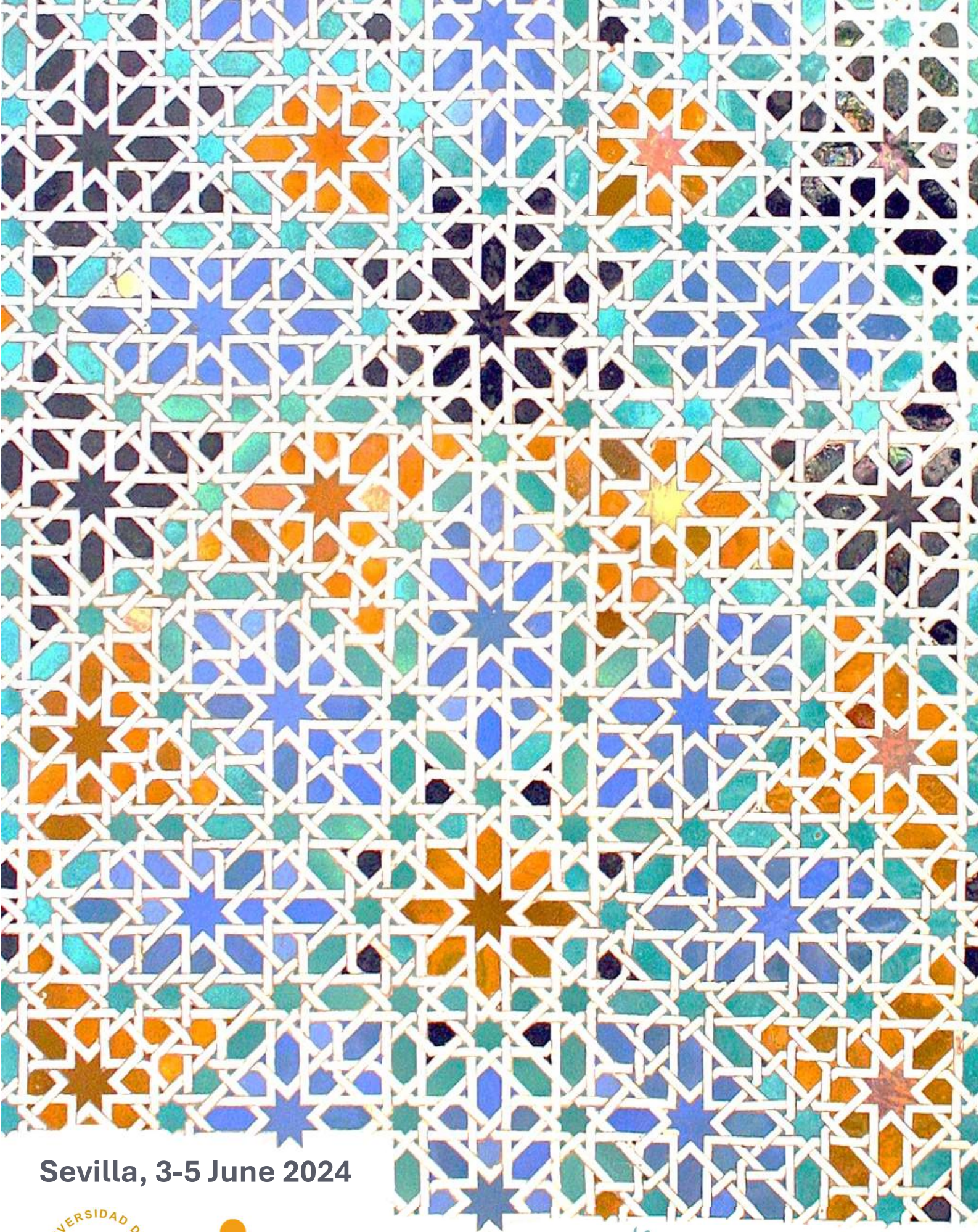

Sevilla, 3-5 June 2024

Escuela Técnica Superior de INGENIERÍA DE SEVILLA

MECBIOLAB

IUTAM

VII Plan Propio de Investigación y Transferencia –
Vicerrectorado de Investigación, Universidad de Sevilla